POLITECNICO DI MILANO

POLO TERRITORIALE DI LECCO

SCUOLA DI ARCHITETTURA URBANISTICA E INGEGNERIA DELLE COSTRUZIONI

MASTER DEGREE IN BUILDING AND ARCHITECTURAL ENGINEERING

Optimized Envelope Systems for Zero Carbon Architecture

Office Building - Zenith - MIND DISTRICT

Supervisor:
Prof. Gabriele Masera

Students:
Chiara Berti
Seyed Mohammad Seyedi

Accademic Year 2025 - 2026

ABSTRACT

The construction sector is responsible for approximately 40% of global CO_2 emissions. Within the European context, the transition toward Zero Carbon architecture is no longer optional but a regulatory and design imperative. The building envelope represents a critical interface in determining overall energy performance; however, current approaches often prioritize operational efficiency, overlooking the embodied carbon associated with materials and complex construction systems.

This thesis addresses this gap by using an existing office building under construction as a baseline case study. Starting from the current design, the research develops a set of progressively improved envelope and design scenarios aimed at enhancing energy performance, reducing environmental impact, and increasing daylight quality. Through the integration of dynamic energy simulations and life cycle assessment (LCA), each scenario is evaluated to highlight trade-offs and synergies between operational and embodied carbon.

The analysis evaluates progressive envelope configurations, incorporating high-performance glazing, optimized insulation assemblies, and solar shading, to map their cumulative impact on thermal loads, daylight metrics, and whole-life carbon. Contrary to the frequent assumption that added envelope materials produce prohibitive embodied carbon penalties, the findings demonstrate that the upfront material investment is rapidly offset by pronounced operational emission savings across the life cycle. Ultimately, this work provides practical decision-making criteria for architects and engineers, proving that targeted envelope intensification remains a decisive, carbon-positive strategy for commercial office decarbonization.

ABSTRACT - Lingua Italiana

Il settore delle costruzioni è responsabile di circa il 40% delle emissioni globali di CO_2. Nel contesto europeo, la transizione verso un'architettura a zero emissioni di carbonio (Zero Carbon) non è più un'opzione, ma un imperativo normativo e progettuale. L'involucro edilizio rappresenta un'interfaccia critica nel determinare le prestazioni energetiche complessive; tuttavia, gli approcci attuali privilegiano spesso l'efficienza operativa, trascurando il carbonio incorporato (embodied carbon) associato ai materiali e ai sistemi costruttivi complessi.

Questa tesi affronta tale lacuna assumendo come caso studio di riferimento un edificio per uffici esistente attualmente in costruzione. A partire dal progetto di partenza, la ricerca sviluppa una serie di scenari progettuali e d'involucro progressivamente migliorati, volti a potenziare le prestazioni energetiche, ridurre l'impatto ambientale e incrementare la qualità della luce naturale. Attraverso l'integrazione di simulazioni energetiche dinamiche e dell'analisi del ciclo di vita (LCA), ciascuno scenario viene valutato per evidenziare trade-off e sinergie tra carbonio operativo ed embodied carbon.

L'analisi valuta configurazioni progressive dell'involucro , integrando vetrate ad alte prestazioni, pacchetti di isolamento ottimizzati e schermature solari , per mapparne l'impatto cumulativo sui carichi termici, sulle metriche di daylight e sulle emissioni di carbonio lungo l'intero ciclo di vita (whole-life carbon). Contrariamente all'ipotesi comune secondo cui l'aggiunta di materiali d'involucro comporti penalizzazioni insostenibili in termini di carbonio incorporato, i risultati dimostrano che l'investimento iniziale di materiale viene rapidamente compensato da marcati risparmi di emissioni operative lungo l'intero ciclo di vita dell'edificio. Infine, questo lavoro fornisce criteri decisionali pratici per progettisti e ingegneri, dimostrando come un'intensificazione mirata delle prestazioni dell'involucro rimanga una strategia decisiva e vantaggiosa in termini di carbonio netto per la decarbonizzazione degli uffici terziari.

TABLE OF CONTENTS

1. RESEARCH FRAMEWORK

1.1 The construction sector in the climate crisis p. 2
1.2 The dual nature of carbon: Operational vs. Embodied emissions p. 3
1.3 Research gap: Integrating LCA and Operational Energy p. 4
1.4 Thesis objectives p. 5
1.5 Thesis roadmap p. 6

2. BACKGROUND AND THEORETICAL FRAMEWORK

2.1 Life-Cycle Stages and the Modular Nature of Carbon p. 9
2.2 Low-Carbon Design Strategies p. 11
2.3 Trade-offs between Energy, Carbon, and Daylighting p. 12

3. METHODOLOGY

3.1 Case study: Zenith; MIND – Milano Innovation District p. 14
3.2 Baseline building: Analysis of the current executive project p. 15
3.3 Scenario-based approach: from Baseline to optimized Configurations p. 16
3.4 Multi-domain simulation workflow: p. 17
- 3.4.1 Energy modeling
- 3.4.2 Life Cycle Assessment (LCA) setup

3.5 Limitations and assumptions p. 19
3.6 Daylight-Driven alternatives for Shading and Glazing p. 21
3.7 Nomenclature and Scenario Classification Logic p. 37
3.8 The Carbon Rating: Benchmarks adopted p. 38

4. DESIGN SCENARIOS

The MIND District p. 43
PV Panels: Layout and Generation Modeling p. 45

4.1 Baseline: The building as currently under construction p. 47
- 4.1.1 Building's plans
- 4.1.2 Building's zones and schedules
- 4.1.3 Building's stratigraphies
- 4.1.4 Baseline Results: Operational and Embodied Carbon

4.2 Scenario 1: Material improvement strategy p. 64
- 4.2.1 Structural stratigraphies improvement
- 4.2.2 Façade stratigraphy improvement

4.3 Scenario 2: Baseline with Active Renewable Integration p. 68
- 4.3.1 Parametric Envelope Assessment: Glazing and Shading Variants on Baseline Geometry

4.4 Scenario 3: Horizon-Driven Envelope Strategies p. 79
- 4.4.1 Glazing and Shading Variants on Horizon Geometry

4.5 Scenario 4: Daylight Optimization-Driven Envelope Strategies p. 87
- 4.5.1 Glazing and Shading Variants on Daylight optimization Geometry

5. RESULTS AND CONCLUSIONS

5.1 Results p. 101
- 5.1.1 Elaboration of the results
- 5.1.2 Comparative matrix between the Scenarios

5.2 Cross-Scenario Synthesis p. 124
5.3 Key-findings and Strategic Optimization Sequence p. 131
5.4 Future Developement p. 132
- 5.4.1 The Shifting Balance of Embodied and Operational Carbon
- 5.4.2 Dynamic Carbon Modeling and the Paradigm Shift in Desing

REFERENCES

ANNEX A: Daylight Optimization Data

ANNEX B: Energy and Carbon Simulations Results

LIST OF FIGURES

fig. 1: *Thesis Roadmap. Diagram created for the Thesis with Illustrator*
fig. 2: *Brute Force Method. Diagram created for the Thesis with Illustrator*
fig. 3: *Genetic Algorithms. Diagram created for the Thesis with Illustrator*
fig. 4: *Machine Learning Method. Diagram created for the Thesis with Illustrator*
fig. 5: *Proposed Method. Diagram created for the Thesis with Illustrator*
fig. 6: *Diagram to for which building typologies this research can be applied. Diagram created for the Thesis with Illustrator*
fig. 7: *The "Horizon" building. Image taken from the MIND official website, post-produced with Photoshop and Illustrator*
fig. 8: *Configurations analyzed along with the research to achieve the best Daylight-Driven option. Images exported from Rhino + Grasshopper*
fig. 9: *Final configuration as the best Daylight-Driven option. The meshes show the daylight benefits. Images exported from Rhino + Grasshopper*
fig. 10: *The "Zenith" building. Image taken from the MIND official website, post-produced with Photoshop and Illustrator*
fig. 11: *The "Zenith" building plan. Image taken from the MIND official website, post-produced with Photoshop and Illustrator*
fig. 12: *Configurations analyzed along with the research to achieve the best Daylight-Driven Optimized Static Shadings. Images exported from Rhino + Grasshopper*
fig. 13: *Configurations analyzed along with the research to achieve the best Daylight-Driven Optimized Static Shadings – Second Phase. Images exported from Rhino + Grasshopper*
fig. 14: *Configurations analyzed along with the research to achieve the best Daylight-Driven Optimized Static Shadings – Third Phase. Images exported from Rhino + Grasshopper*
fig. 15: *Final configuration as the best Daylight-Driven Optimized Static Shadings. The meshes show the daylight benefits. Images exported from Rhino + Grasshopper*
fig. 16: *Configurations analyzed along with the research to achieve the Visible Transmittance Optimization Images exported from Rhino + Grasshopper*
fig. 17: *Final configuration as the best Transmittance Optimization. The meshes show the daylight benefits. Images exported from Rhino + Grasshopper*
fig. 18: *Organization of the "Combinatorial matrix for the design alternatives". Diagram created for the Thesis with Illustrator*
fig. 19: *Genotypes identified along with research. Diagram created for the Thesis with Illustrator*
fig. 20: *30 Phenotypes identified along with research. Diagram created for the Thesis with Illustrator*
fig. 21: *Carbon HEROES Benchmark diagram. Image taken from the official website of OneClick LCA*
fig. 22: *LETI Benchmark diagram. Image taken from the official website of LETI Benchmark*
fig. 23: *LETI Benchmark for Embodied Carbon. Image taken from the official website of LETI Benchmark*
fig. 24: *RIBA Benchmark for Operational Energy. Image taken from the official website of RIBA Benchmark*
fig. 25: *Diagrammatic image of Lombardy Region. Diagram created for the Thesis with Illustrator*
fig. 26: *Diagrammatic image of Milan Province. Diagram created for the Thesis with Illustrator*
fig. 27: *Diagrammatic image of the MIND District site. Image taken from the MIND official website, post-produced with Illustrator*
fig. 28: *Rendered view of the MIND District site, highlighting the "Zenith" building. Image created for the Thesis with Rhino and post-produced with Photoshop*
fig. 29: *"Zenith" building's surroundings heatmap. Image exported from Rhino + Grasshopper*
fig. 30: *"Zenith" building heatmap, facing North. Image exported from Rhino + Grasshopper*
fig. 31: *"Zenith" building heatmap, facing South. Image exported from Rhino + Grasshopper*
fig. 32: *"Zenith" building view study, facing North. Image exported from Rhino + Grasshopper*
fig. 33: *"Zenith" building view study, facing South. Image exported from Rhino + Grasshopper*
fig. 34: *Typical floor plan for Monotenant type in "Zenith" building. Image taken from the MIND official website, post-produced with Photoshop*
fig. 35: *Typical floor plan for Bitenenat type in "Zenith" building. Image taken from the MIND official website, post-produced with Photoshop*
fig. 36: *"Coffee Shop" area in "Zenith" building. Image exported from Rhino + Grasshopper*
fig. 37: *"Lobby" area in "Zenith" building. Image exported from Rhino + Grasshopper*
fig. 38: *"Bookshop" area in "Zenith" building. Image exported from Rhino + Grasshopper*
fig. 39: *"Perimeter Office" area in "Zenith" building. Image exported from Rhino + Grasshopper*
fig. 40: *"Core" area in "Zenith" building. Image exported from Rhino + Grasshopper*
fig. 41: *"Parking" area in "Zenith" building. Image exported from Rhino + Grasshopper*
fig. 42: *"Restroom" area in "Zenith" building. Image exported from Rhino + Grasshopper*

fig. 43: *"Interior Office" area in "Zenith" building. Image exported from Rhino + Grasshopper*
fig. 44: *Typical slab's stratigraphy used in "Zenith" building. Image created for the Thesis with Rhino and post-produced with Photoshop*
fig. 45: *Roof's stratigraphy used in "Zenith" building. Image created for the Thesis with Rhino and post-produced with Photoshop*
fig. 46: *Ground floor slab's stratigraphy used in "Zenith" building. Image created for the Thesis with Rhino and post-produced with Photoshop*
fig. 47: *Basement slab's stratigraphy used in "Zenith" building. Image created for the Thesis with Rhino and post-produced with Photoshop*
fig. 48: *Façade's stratigraphy used in "Zenith" building. Image created for the Thesis with Rhino and post-produced with Photoshop*
fig. 49: *Opaque partition's stratigraphy used in "Zenith" building. Image created for the Thesis with Rhino and post-produced with Photoshop*
fig. 50: *Transparent partition's stratigraphy used in "Zenith" building. Image created for the Thesis with Rhino and post-produced with Photoshop*
fig. 51: *Basement wall's stratigraphy used in "Zenith" building. Image created for the Thesis with Rhino and post-produced with Photoshop*
fig. 52: *Core wall's stratigraphy used in "Zenith" building. Image created for the Thesis with Rhino and post-produced with Photoshop*
fig. 53: *Oblique view for Configuration 1, Scenario 2. Image exported from Rhino + Grasshopper*
fig. 54: *Oblique view for Configuration 2, Scenario 2. Image exported from Rhino + Grasshopper*
fig. 55: *Oblique view for Configuration 3, Scenario 2. Image exported from Rhino + Grasshopper*
fig. 56: *Oblique view for Configuration 1, Scenario 3. Image exported from Rhino + Grasshopper*
fig. 57: *Oblique view for Configuration 2, Scenario 3. Image exported from Rhino + Grasshopper*
fig. 58: *Oblique view for Configuration 3, Scenario 3. Image exported from Rhino + Grasshopper*
fig. 59: *Oblique view for Configuration 1, Scenario 4. Image exported from Rhino + Grasshopper*
fig. 60: *Oblique view for Configuration 2, Scenario 4. Image exported from Rhino + Grasshopper*
fig. 61: *Oblique view for Configuration 3, Scenario 4. Image exported from Rhino + Grasshopper*
fig. 62: *Identifying which phenotypes were used for the Final Conclusions. Diagram created for the Thesis with Illustrator*
fig. 63: *North view of the Best performing Configuration S_35 H 3G OS for the Total GWP*
fig. 64: *South view of the Best performing Configuration S_35 H 3G OS for the Total GWP*
fig. 65: *North view of the Worst performing Configuration S_28 B 2G VT for the Total GWP*
fig. 66: *South view of the Worst performing Configuration S_28 B 2G VT for the Total GWP*
fig. 67: *North view of the Best performing Configuration S_35 H 3G OS for the Operational GWP*
fig. 68: *South view of the Best performing Configuration S_35 H 3G OS for the Operational GWP*
fig. 69: *North view of the Worst performing Configuration S_28 B 2G VT for the Operational GWP*
fig. 70: *South view of the Worst performing Configuration S_28 B 2G VT for the Operational GWP*
fig. 71: *North view of the Best performing Configuration S_20 B 2G NS for the Embodied GWP*
fig. 72: *South view of the Best performing Configuration S_20 B 2G NS for the Embodied GWP*
fig. 73: *North view of the Worst performing Configuration S_34 H 3G BL for the Embodied GWP*
fig. 74: *South view of the Worst performing Configuration S_34 H 3G BL for the Embodied GWP*
fig. 75: *North view of the Best performing Configuration S_23 B 3G NS for the Heating EUI*
fig. 76: *South view of the Best performing Configuration S_23 B 3G NS for the Heating EUI*
fig. 77: *North view of the Worst performing Configuration S_22 B 2G OS for the Heating EUI*
fig. 78: *South view of the Worst performing Configuration S_22 B 2G OS for the Heating EUI*
fig. 79: *North view of the Best performing Configuration S_35 H 3G OS for the Cooling EUI*
fig. 80: *South view of the Best performing Configuration S_35 H 3G OS for the Cooling EUI*
fig. 81: *North view of the Worst performing Configuration S_20 B 2G NS for the Cooling EUI*
fig. 82: *South view of the Worst performing Configuration S_20 B 2G NS for the Cooling EUI*
fig. 83: *North view of the Best performing Configuration S_22 B 2G OS for the NUDA*
fig. 84: *South view of the Best performing Configuration S_22 B 2G OS for the NUDA*
fig. 85: *North view of the Worst performing Configuration S_30 H 2G NS for the NUDA*
fig. 86: *South view of the Worst performing Configuration S_30 H 2G NS for the NUDA*

fig. 87: *North view of the Best performing Configuration S_32 H 2G OS for the ASE*
fig. 88: *South view of the Best performing Configuration S_32 H 2G OS for the ASE*
fig. 89: *North view of the Worst performing Configuration S_20 B 2G NS for the ASE*
fig. 90: *South view of the Worst performing Configuration S_20 B 2G NS for the ASE*
fig. 91: *North view of the Best performing Configuration S_20 B 2G NS for the sDA*
fig. 92: *South view of the Best performing Configuration S_20 B 2G NS for the sDA*
fig. 93: *North view of the Worst performing Configuration S_35 H 3G OS for the sDA*
fig. 94: *South view of the Worst performing Configuration S_35 H 3G OS for the sDA*
fig. 95: *North view of the most effective trade-off Configuration S_45 D 3G OS, among all Configurations considering Tot GWP and NUDA.*
fig. 96: *South view of the most effective trade-off Configuration S_45 D 3G OS, among all configurations considering Tot GWP and NUDA.*
fig. 97: *Strategic Optimization sequence. Diagram created for the Thesis with Illustrator*

LIST OF CHARTS

chart 1: *Optimization chart for the best Daylight-Driven option. Chart exported from Rhino + Grasshopper and post-produced with Illustrator*
chart 2: *Optimization chart for the best Daylight-Driven Optimized Static Shadings – Left side shadings – First Phase. Image exported from Rhino + Grasshopper and post-produced with Illustrator*
chart 3: *Optimization chart for the best Daylight-Driven Optimized Static Shadings – Right side shadings – First Phase. Image exported from Rhino + Grasshopper and post-produced with Illustrator*
chart 4: *Optimization chart for the best Daylight-Driven Optimized Static Shadings – Top side shadings – First Phase. Image exported from Rhino + Grasshopper and post-produced with Illustrator*
chart 5: *Optimization chart for the best Daylight-Driven Optimized Static Shadings – Left side shadings – Second Phase. Image exported from Rhino + Grasshopper and post-produced with Illustrator*
chart 6: *Optimization chart for the best Daylight-Driven Optimized Static Shadings – Right side shadings – Third Phase. Image exported from Rhino + Grasshopper and post-produced with Illustrator*
chart 7: *Optimization chart for the best Visible Transmittance optimization. Image exported from Rhino + Grasshopper and post-produced with Illustrator*
chart 8: *Annual Solar Exposure (aSe), Spacial Daylight Autonomy (SDA) and the resultant Net Useful Daylight Area (NUDA). mage exported from Rhino + Grasshopper and post-produced with Illustrator*
chart 9: *“Coffee Shop” schedules in “Zenith” building. Image exported from Rhino + Grasshopper*
chart 10: *Lobby” schedules in “Zenith” building. Image exported from Rhino + Grasshopper*
chart 11: *“Bookshop” and “Perimeter Office” schedules in “Zenith” building. Image exported from Rhino + Grasshopper*
chart 12: *“Core” and “Parking” schedules in “Zenith” building. Image exported from Rhino + Grasshopper*
chart 13: *“Restroom” schedules in “Zenith” building. Image exported from Rhino + Grasshopper*
chart 14: *“Interior Office” schedules in “Zenith” building. Image exported from Rhino + Grasshopper*
chart 15: *Baseline Energy Balance, before any improvements. Image exported from Rhino + Grasshopper*
chart 16: *Baseline GWP comparison. Chart created for the Thesis with Excel*
chart 17: *Baseline Embodied Carbon breakdown. Chart created for the Thesis with Excel*
chart 18: *Embodied Carbon comparison before Structural and Façade materials improvement and after them. Chart created for the Thesis with Excel*

chart 19: *Embodied Carbon breakdown after structural materials improvement. Chart created for the Thesis with Excel*
chart 20: *Embodied Carbon breakdown after façade materials improvement. Chart created for the Thesis with Excel*
chart 21: *Insulation Thickness optimization chart for S_20; S_23. Image exported from Rhino + Grasshopper and post-produced with Illustrator*
chart 22: *Insulation Thickness optimization chart for S_51; S_61. Image exported from Rhino + Grasshopper and post-produced with Illustrator*
chart 23: *Diagram about the behavior of all the Scenarios against Total GWP (60y). Diagram exported from Rhino + Grasshopper and post-produced with Illustrator*
chart 24: *Diagram about the behavior of all the Scenarios against Operational GWP (60y). Diagram exported from Rhino + Grasshopper and post-produced with Illustrator*
chart 25: *Diagram about the behavior of all the Scenarios against Embodied GWP (60y) . Diagram exported from Rhino + Grasshopper and post-produced with Illustrator*
chart 26: *Diagram about the behavior of all the Scenarios against Heating EUI. Diagram exported from Rhino + Grasshopper and post-produced with Illustrator*

chart 27: *Diagram about the behavior of all the Scenarios against Cooling EUI. Diagram exported from Rhino + Grasshopper and post-produced with Illustrator*
chart 28: *Diagram about the behavior of all the Scenarios against NUDA. Diagram export-ed from Rhino + Grasshopper and post-produced with Illustrator*
chart 29: *Diagram about the behavior of all the Scenarios against ASE. Diagram exported from Rhino + Grasshopper and post-produced with Illustrator*
chart 30: *Diagram about the behavior of all the Scenarios against sDA. Diagram exported from Rhino + Grasshopper and post-produced with Illustrator*
chart 31: *Comparative Matrix for all the configurations studied along with the research. Di-agram exported from Rhino + Grasshopper and post-produced with Illustrator*
chart 32: *Diagram about the Carbon Payback from 2G configurations to 3G configurations. Diagram exported from Rhino + Grasshopper and post-produced with Illustrator*
chart 33: *Diagram about the Cost-Benefits of 2G to 3G transformation. Diagram exported from Rhino + Grasshopper and post-produced with Illustrator*
chart 34: *Diagram about the Impact of Minimizing the Glazing Ratio. Diagram exported from Rhino + Grasshopper and post-produced with Illustrator*
chart 35: *Diagram about the Daylight-Driven Glazing Configuration. Diagram exported from Rhino + Grasshopper and post-produced with Illustrator*
chart 36: *Diagram about the Impact of Generalized Shading System. Diagram exported from Rhino + Grasshopper and post-produced with Illustrator*
chart 37: *Diagram about the Impact of Optimized Shading System. Diagram exported from Rhino + Grasshopper and post-produced with Illustrator*
chart 38: *Diagram about the Impact of modifying Visual Trasmittance. Diagram exported from Rhino + Grasshopper and post-produced with Illustrator*
chart 39: *Average Total GWP, Operational GWP and Embodied GWP among all the Simulations + Ratio. Diagram exported from Rhino + Grasshopper and post-produced with Illustra-tor*
chart 40: *Total GWP, Operational GWP and Embodied GWP for all the Sim ulations + Ratio. Diagram exported from Rhino + Grasshopper and post-produced with Illustrator*
chart 41: *LETI Benchmark for Offices. Diagram taken from the official LETI Benchmark website*
chart 42: *LETI Benchmark compared with the Average calculated for Opera tional GWP and Embodied GWP among all the Simulations. Diagram taken from the official LETI Bench-mark website and post-produced with Illustrator*
chart 43: *Diagram about the future behavior forecasted for all the Configurations, across a spectrum of the grid carbon intensity. Diagram exported from Rhino + Grasshopper and post-produced with Illustrator*

LIST OF TABLES

tab. 1: *"Coffee Shop" setpoints in "Zenith" building. Table created with Excel*
tab. 2: *"Coffee Shop" settings in "Zenith" building. Table created with Illustrator*
tab. 3: *"Lobby" setpoints in "Zenith" building. Table created with Excel*
tab. 4: *"Lobby" settings in "Zenith" building. Table created with Illustrator*
tab. 5: *"Bookshop" and "Perimeter Office" setpoints in "Zenith" building. Table created with Excel*
tab. 6: *"Bookshop" and "Perimeter Office" settings in "Zenith" building. Table created with Illustrator*
tab. 7: *"Core" and "Parking" setpoints in "Zenith" building. Table created with Excel*
tab. 8: *"Core" and "Parking" settings in "Zenith" building. Table created with Illustrator*
tab. 9: *"Restroom" setpoints in "Zenith" building. Table created with Excel*
tab. 10: *"Restroom" settings in "Zenith" building. Table created with Illustrator*
tab. 11: *"Interior Office" setpoints in "Zenith" building. Table created with Excel*
tab. 12: *"Interior Office" settings in "Zenith" building. Table created with Illustrator*
tab. 13: *Results highlights for S_20 B 2G NS*
tab. 14: *Results highlights for S_23 B 3G NS*
tab. 15: *Results highlights for S_21 B 2G BL*
tab. 16: *Results highlights for S_24 B 3G BL*
tab. 17: *Results highlights for S_22 B 2G OS*
tab. 18: *Results highlights for S_25 B 3G OS*
tab. 19: *Results highlights for S_28 B 2G VT*
tab. 20: *Results highlights for S_29 B 3G VT*
tab. 21: *Results highlights for S_30 H 2G NS*
tab. 22: *Results highlights for S_33 H 3G NS*
tab. 23: *Results highlights for S_31 H 2G BL*
tab. 24: *Results highlights for S_34 H 3G BL*
tab. 25: *Results highlights for S_32 H 2G OS*
tab. 26: *Results highlights for S_35 H 3G OS*
tab. 27: *Results highlights for S_38 H 2G VT*
tab. 28: *Results highlights for S_39 H 3G VT*
tab. 29: *Results highlights for S_40 D 2G NS*
tab. 30: *Results highlights for S_43 D 3G NS*
tab. 31: *Results highlights for S_41 D 2G BL*
tab. 32: *Results highlights for S_44 D 3G BL*
tab. 33: *Results highlights for S_42 D 2G OS*
tab. 34: *Results highlights for S_45 D 3G OS*
tab. 35: *Results highlights for S_48 D 2G VT*
tab. 36: *Results highlights for S_49 D 3G VT*
tab. 37: *Results highlights for S_51 B 2G OS VT*
tab. 38: *Results highlights for S_61 B 3G OS VT*
tab. 39: *Results highlights for S_52 B 2G VT OS*
tab. 40: *Results highlights for S_62 B 3G VT OS*
tab. 41: *Results highlights for S_53 D 2G OS VT*
tab. 42: *Results highlights for S_63 D 3G OS VT*
tab. 43: *Results highlights for S_54 H 2G OS VT*
tab. 44: *Results highlights for S_64 H 3G OS VT*
tab. 45: *Cumulative table with all the Simulations and their Results. Table created with Excel*

1

RESEARCH FRAMEWORK

1.1 The construction sector in the climate crisis
1.2 The dual nature of carbon: operational vs. embodied emissions
1.3 Research gap: Integrating LCA and operational energy
1.4 Thesis objectives
1.5 Thesis roadmap

1.1 The construction sector in the climate crisis

The built environment is one of the primary sources of global emissions, pressuring the global climate emergency. According to the UNEP and Global ABC's most recent Global Status Report for Buildings and Construction, published in March 2025, buildings currently account for 32% of global energy use and contribute 34% of global CO_2 emissions, making it a sector where significant emissions reductions must happen.[1][2]

Despite some policy successes, CO_2 emissions from building operations have actually risen by 5.5% since the Paris Agreement of 2015, rather than falling.
The urgency of this challenge is amplified by the pace of urban growth, the cities are raising, yet less than 1% of buildings have their carbon footprints assessed.[3]
Despite growing awareness and some policy progress, particularly in the deployment of mandatory building energy codes and renewable energy targets, few national strategies align with net-zero operational emissions, and many countries' building energy codes remain outdated. [4]

Office buildings occupy a particularly important position in this matter. As high-intensity, long-lifespan structures located predominantly in urban areas, they combine high operational energy demand with substantial embodied carbon from materials and construction. Their design decisions, made at the beginning of a project, largely determine their environmental performance for decades to come. A lack of standardized data on material usage and embodied carbon for non-residential buildings makes it challenging to accurately assess and compare their environmental impacts; a gap this thesis directly addresses through a real case study of an office building currently under construction. [5]
This gap is confirmed at the national scale: a 2025 study analyzing mandatory energy assessment of hundreds of Italian office buildings reveals a sector with highly variable performance and limited systematic benchmarking, pointing to the urgent need for evidence-based design frameworks. [10]

1.2 The dual nature of carbon: operational vs. embodied emissions

Reducing the carbon footprint of buildings requires distinguishing between two different types of emissions. Operational carbon refers to the CO_2 produced by the energy consumed during a building's active life such as heating, cooling, ventilation, and lighting. Embodied carbon considers all emissions tied to the materials and processes that go into constructing, maintaining, and eventually demolishing a building: extraction, manufacturing, transport, and on-site assembly.
Within the total share of emissions from the building and construction sector, the majority currently derive from indirect operational emissions. However, the share of embodied carbon is projected to jump from 25% to nearly half of all building related emissions by 2050 , as electricity grids progressively transition to renewables and operational performance improves. [6]
In other words, as decarbonization of the grid gradually eliminates operational carbon, embodied carbon will remain, unless actively addressed through material choices and design strategy.
This shift has critical implications for how buildings are designed and evaluated. Embodied carbon is a lost cost: once spent during construction, it cannot be recovered or reduced after building completion; timber is one of the few exceptions, since it has a negative carbon storage, therefore the embodied carbon in this case can be deducted. [3][9]
This makes early-stage design decisions impacting, including envelope configuration, structural systems, and material specifications; which are not equally significant, in terms of carbon content. For new buildings, embodied carbon can represent more than 50% of total life-cycle carbon, and its optimization together with operational performance is technically feasible and necessary too, to achieve net-zero over the full life cycle. [7]

Despite this, research and policy have historically focused almost exclusively on operational energy efficiency. Environmental policies have traditionally prioritized improving energy efficiency and renewable energies in the use phase while neglecting material efficiency in construction; a policy approach that, if maintained, may miss important opportunities to reduce overall carbon emissions. [8]

1.3 Research gap: Integrating LCA and operational energy

Life Cycle Assessment (LCA) is one of the main methodological framework for quantifying the full environmental impact of buildings across all phases of their existence: from material extraction to end of life. While operational carbon emissions have declined through energy efficiency advancements, embodied carbon emissions remain challenging to address due to their complexity across multiple building lifecycle stages. Still nowadays LCA faces limitations in dynamic scenarios, regional variability for databases, system boundary inconsistencies and lack of accurate material to fulfill the assessment (e.g., proxy data instead of actual ones). [11]

A further complication is that optimizing for carbon alone is not enough. Buildings are not designed with the purpose to minimize emissions; they are environments in which people live and work. Daylighting, governed largely by window-to-wall ratio, glazing selection, and floor plan depth, represents a critical dimension of building performance, and it is frequently in tension with carbon reduction and energy efficiency strategies.

For these reasons, a series of trade-offs often needs to be resolved to respond to targets of energy efficiency and daylight availability. For example, highly insulated envelopes with reduced glazed areas that lower heating and cooling demand may simultaneously compromise daylight autonomy and increase reliance on artificial lighting; deep floor plans that maximize occupancy density may reduce daylight penetration to interior zones; increasing WWR to improve visual comfort and daylight access may in turn raise solar heat gains and cooling loads, particularly in unshaded configurations [12].

The convergence of daylighting and energy efficiency is not an absolute compromise, but rather a mutual relationship: studies on window-to-wall ratio optimization show that appropriately calibrated glazing configurations can meet daylight autonomy targets while simultaneously reducing operational energy demand; yet achieving this balance in practice requires careful, multi-domain simulation and evidence-based design [29].

The research gap addressed by this thesis lies at the intersection of these three domains: operational energy performance, embodied carbon (via LCA), and daylighting performance. Most existing studies treat these as separate lines of inquiry. Integrated, scenario-based frameworks that evaluate all three simultaneously, in a parametric way, applied to a real, under-construction building and its further development, are proposed in this thesis as well.

1.4 Thesis objectives

This thesis aims to bridge the gap identified above through a multi-domain, scenario based study of an office building within the MIND (Milano Innovation District). The following objectives structure the research:

- Quantify the baseline carbon profile of an under-construction office building in terms of both operational energy demand, using energy simulation tools, and embodied carbon, using LCA methodology from cradle to grave.

- Develop and validate an integrated simulation workflow that combines energy modeling and LCA within a single multi-domain framework, applicable to real projects in the early and detailed design phases.

- Optimization of design scenarios; ranging from structural materials and façade optimization to shading and roof systems, this study identifies the necessary upgrades for a transition from simple system improvements to full façade reconfiguration between windows and shadings, measured against energy and carbon benchmarks.

- Derive design recommendations that are transferable beyond the specific case study, offering guidance for future low-carbon, daylight-optimized office development in comparable urban and climatic contexts.

The research question is:
Among all the existing strategies to reduce the Operational Energy, to what extent these strategies can be truly useful when considering Embodied Carbon footprint, moreover to what extent can parametric design and multi-objective optimization of the building envelope effectively balance the trade-offs between embodied carbon reduction and operational energy efficiency in a commercial office building?

1.5 Thesis Roadmap

PHASE 1: FOUNDATION & SETUP
Chapters 1, 2, 3

PHASE 2: BASELINE DEFINITION
Chapter 4 (4.1 - 4.2)

PHASE 3: PARAMETRIC EXPLORATION
Chapter 4 (4.3, 4.4, 4.5)

PHASE 4: SYNTHESIS & IMPACT
Chapters 5, 6

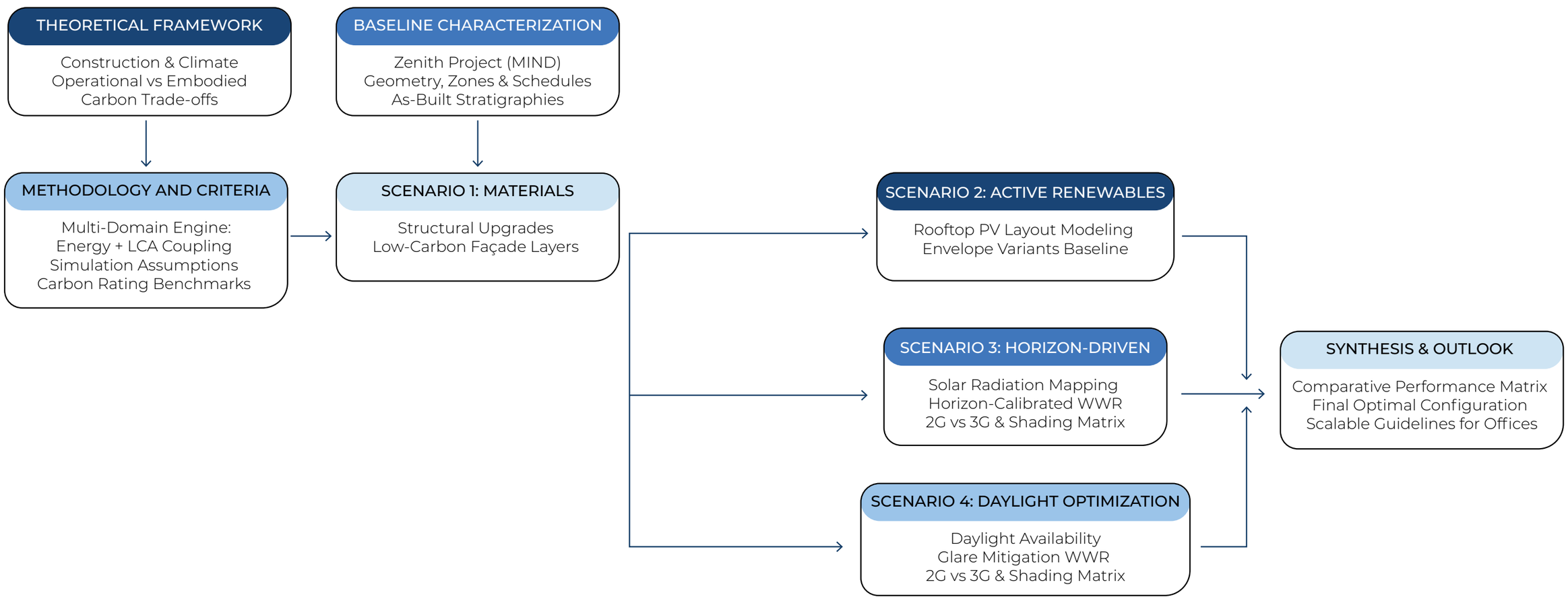

DATA STREAM & TOOLS:
Case Study Geometry → Ladybug / Honeybee / EnergyPlus → LCA Database / Embodied Carbon → Carbon Rating Benchmark

fig. 1

2

2. BACKGROUND AND THEORETICAL FRAMEWORK

2.1 Life-Cycle Stages and the Modular Nature of Carbon
2.2 Low-carbon design strategies
2.3 Trade-offs between energy, carbon, and daylighting

2.1 Life-Cycle Stages and the Modular Nature of Carbon

While chapter 1 established the scale of emissions, a deeper understanding requires examining how buildings generate carbon across their full life cycle and examine the mechanisms through which buildings generate carbon across their full existence. This requires adopting a life-cycle perspective: one that traces carbon flows from the extraction of raw materials through construction, operation, maintenance and eventual demolition.
The analytical process used to quantify these flows follows a standardized four-phase iterative approach, as defined by ISO 14040/14044 [14]:

- Goal and scope: defining the system boundaries (e.g., cradle-to-grave) and the functional unit (e.g., 1kg of material or 1m² of floor area).

-Life cycle inventory (LCI): the “accounting” phase, where all inputs (energy, raw materials) and outputs (emissions, waste) are compiled.

- Impact assessment (LCIA): converting inventory data into environmental indicators, such as global warming potential (GWP), or acidification potential (AP)

- Interpretation: evaluating results to identify “hotspots” and inform design decisions.
This is an iterative process where findings in one phase often lead to refinements in the goals or inventory.

Within this methodological process, the dominant framework for this analysis is the european standard EN 15978, which structures building carbon emissions into a sequence of modules organized across four life-cycle stages. This is the foundamental structure of the LCA process.

- Stage A: it covers the product and the construction phase; from raw material supply (A1), transport (A2) and manufacturing (A3) unti reaching the transportation to site (A4) and the construction and installation (A5).

- Stage B: this stage is about the “in use phase”, including maintenance, repair, replacement and refurbishment (from B1 to B5), eventually the operational energy use (B6) and finally the operational water use (B7).

- Stage C: it is related to the end-of-life of the element in consideration; considering the deconstruction (C1), the transportation of the residuals (C2), the waste processing (C3) and the final disposal (C4).

- Stage D: this last module is often consider as optional, but it accounts for potential benefits from the reuse of materials, the recovery and the recycling beyond the system boundary. It is mostly used when the material in consideration is timber.

Together, from module A1 to module C4 define what is known as a “cradle-to-grave” assessment; the most comprehensive rapresentation of a building’s carbon footprint nowadays. [13]
This modular structure is analytically important because it makes visible a distinction that policy and practice have been ignored for long: the difference

between upfront carbon (A1–A5), which is emitted before a building is ever occupied, and operational carbon (B6), which accumulates over decades of use. Whole life carbon emissions are the sum total of all asset-related greenhouse gas emissions and removals (both operational and embodied) over the full life cycle, including disposal. The term “embodied carbon” refers broadly to all non-operational emission, as developed in the paragraph 1.2: Those locked into materials and processes at every stage outside of B6 and it is this component that has received the least systematic attention in both research and regulation.

Embodied carbon emissions make up a progressively larger share of total life-cycle emissions as building operational carbon decreases, a structural shift driven by the progressive decarbonization of electricity grids and the tightening of operational energy codes. As grids transition to renewables, the carbon intensity of each kilowatt/hour of energy consumed by a building falls, reducing B6 emissions. But the carbon embodied in the concrete, steel, insulation, and glazing remains fixed at the moment of manufacture. This means that the relative weight of initial embodied carbon in total life-cycle carbon grows over time and that design decisions made before a building breaks ground carry consequences that no amount of operational efficiency can subsequently reverse.

Optimizing the relationship between operational and embodied emissions requires looking not only at the thermal performance of materials, such as the U-value of insulation, but also at the carbon cost of their manufacture and installation. This principle directly informs the analytical approach of this thesis: each design scenario is evaluated not only for its energy demand reduction, but for the embodied carbon cost required to achieve it.

The whole-life carbon balance which is the net outcome across all life-cycle stages is, therefore, the primary metric against which the design scenarios in this thesis are compared in chapters 4 and 5. How that balance can be shifted through deliberate design choices is the subject of the sections that follow.

2.2 Low-carbon design strategies

At the design stage, two broad and complementary categories of intervention are available: passive strategies, which minimize energy demand through the building’s physical form and active systems, which supply the remaining demand as efficiently and cleanly as possible.

Passive strategies operate without mechanical or electrical input. They include building orientation to optimize solar gain and natural ventilation, high-performance insulation to limit thermal losses, shading devices to reduce cooling loads, thermal mass to buffer temperature fluctuations, and envelope airtightness to eliminate uncontrolled infiltration. Evidence from the literature shows that advanced envelope materials can reduce heating and cooling loads signficantely. The efficacy of these strategies is perhaps best exemplified by the Passivhaus standard; developed in Germany and now widely adopted across Europe, it codifies these principles into a rigorous design methodology that has proven effective across diverse climates and building types.[15]

Active strategies consider efficient mechanical, electrical, and plumbing systems, such as heat pumps, mechanical ventilation with heat recovery (MVHR), LED lighting and on-site renewable energy generation. Comparative analysis of pioneering zero-carbon buildings demonstrates that context-specific integration of passive design and active technologies can achieve energy generation exceeding consumption by up to 200%, with carbon emission reductions reaching 90%. [16]

The most effective low-carbon outcomes arise not from passive or active strategies in isolation, but from their integration from the earliest design stages. The interaction between passive methods such as building orientation and natural ventilation, and active systems such as renewable energy integration and HVAC automation, identifies emerging pathways for smart, climate-resilient buildings. In practice, this means that the building envelope and the mechanical systems must be co-designed: while passive strategies drastically reduce operational demand, their implementation must be balanced against the embodied carbon of the high-performance materials used, ensuring a net-positive impact across the full life cycle. [17]

2.3 Trade-offs between energy, carbon, and daylighting

The three domains at the heart of this thesis, energy performance, embodied carbon, and daylighting performance, do not always point in the same direction.
Understanding the nature of their interactions, and the conditions under which they conflict or align, is essential theoretical grounding before entering the scenario analysis.
The most fundamental tension is between glazed surface area and thermal performance.
High window-to-wall ratios improve daylight autonomy and reduce reliance on artificial lighting, but larger glazed areas also increase heat loss in winter and solar heat gain in summer, raising both heating and cooling loads.
In practice, this tension is typically resolved through high-performance glazing systems, low-emissivity coatings, inert gas fills, or triple-pane assemblies, which recover much of the thermal performance lost to a larger window area.
However, the embodied carbon of these more complex glazing systems must then be factored into the life-cycle balance. [20]

A second trade-off exists between thermal performance and light transmittance in glazing selection. High-performance coatings and additional panes that reduce heat loss and solar gain typically also reduce visible light transmittance (VLT), lowering the daylight potential of a given glazed area.
Achieving the same daylight autonomy target with a lower-VLT, higher-performance glass therefore requires either a larger glazed surface or greater reliance on artificial lighting, partially offsetting the operational energy savings gained from improved thermal performance.

A third tension concerns the timing of daylighting carbon cost:
Shading devices reduce solar heat gain and glare while preserving usable daylight, improving operational performance from day one.
Yet their embodied carbon is paid entirely upfront, recovered, if at all, only over years of operational savings.

A holistic approach is needed that expands research, currently focused largely on residential buildings, to include non-residential ones, and that considers more carefully the variables related to occupancy and building form: orientation, envelope, windows, materials, and insulation. This thesis responds directly to this call by applying an integrated, multi-domain framework to a non-residential case study, treating energy, LCA, and daylighting not as separate performance targets but as interdependent variables within a single design decision space. [21]
Ultimately, the theoretical framework of this chapter leads to a single central proposition: achieving genuine low-carbon performance in an office building requires moving beyond single-metric optimization, but embracing the full complexity of whole-life carbon, operational efficiency, and daylighting simultaneously, from the earliest stages of design. This proposition structures the scenario-based methodology presented in the following chapter.

3

3. METHODOLOGY

3.1 Case study: Zenith; MIND – Milano Innovation District
3.2 Baseline building: Analysis of the current executive project
3.3 Scenario-based approach: from baseline to optimized configurations
3.4 Multi-domain simulation workflow:
    3.4.1 Energy modeling
    3.4.2 Life Cycle Assessment (LCA) setup
3.5 Limitations and assumptions
3.6 Daylight-Driven alternatives for Shading and Glazing
3.7 Nomenclature and Scenario Classification Logic
3.8 The Carbon Rating: Benchmarks adopted

This chapter presents the methodological framework employed to investigate the environmental performance and spatial quality of a representative office building within the MIND – Milano Innovation District. The research is structured around a multi-domain simulation workflow that integrates dynamic energy modelling, with Ladybug Tools, including Honeybee, and Life Cycle Assessment (LCA), adressed with Bombyx, from ETH Zürich, to evaluate a progression of design scenarios, ranging from the current baseline to a speculative high-performance future configuration.
The methodological approach is designed to be both rigorous and replicable, contributing to the overall thinking on low-carbon, human-centric design strategies in the commercial built environment.

3.1 Case Study: Zenith; MIND - Milano Innovation District

The selected case study is an office building located within MIND – Milano Innovation District, a large-scale urban regeneration project developed on the former site of the 2015 World Expo in Milan, Italy.
MIND represents one of the most ambitious innovation hubs in Southern Europe, with a programmatic focus on research, life sciences, and knowledge-based enterprises. Its urban vision emphasizes sustainability and digital infrastructure, making it a contextually appropriate site for investigating integrated low-carbon design strategies.[22]

The specific building selected for analysis is a recently designed multi-storey office block, currently in the executive project phase. Zenith was chosen due to the representativeness of its typology within the broader hub, and the explicit sustainability ambitions embodied in its design brief.
The building serves as both a concrete object of investigation and a proxy for a wider class of commercial office buildings seeking to align with European climate targets.
The contextual relevance of MIND is diverse. On one hand, the district operates under a comprehensive sustainability framework that imposes performance benchmarks across energy, carbon, and daylighting dimensions.
On the other hand, its ongoing development phase affords a rare opportunity to assess design decisions at a critical point, one at which interventions can still meaningfully influence long-term environmental outcomes. This temporal positioning is central to the research purpose.

3.2 Baseline building: Analysis of the current executive project

The baseline configuration presented here does not correspond to a fully documented executive project, but rather to a reconstructed representation of the building derived from limited available information. The primary sources consisted of two architectural plans provided through the MIND project platform, which were not dimensioned and did not include detailed technical specifications regarding structural systems, envelope composition, or building services. One pdf was available online, providing few renders and a stratigraphy for the slabs used.
As a consequence, the development of the baseline model required a process of informed assumption-making. Geometric proportions, floor-to-floor heights, and overall building dimensions were approximated based on typical office building standards and internal consistency between the available drawings. The ground floor, lacking of any information, was entirely assumed. Similarly, key performance-related parameters, including envelope thermal properties, glazing ratios, internal heat gains, occupancy densities, and HVAC system characteristics, were not directly available and were therefore defined using a combination of normative references, standard practice values, and reasonable engineering judgement.

Rather than representing a precise digital twin of the actual building, the baseline should be understood as a plausible and internally consistent approximation, constructed to enable comparative simulation across multiple design scenarios. Its role within the research is therefore not to provide absolute performance predictions, but to establish a controlled reference model against which the relative impact of design modifications can be evaluated. This perspective is critical: the validity of the analysis lies not in the exactness of the baseline itself, but in the consistency of assumptions across all scenarios, ensuring that performance differences can be attributed to the implemented design changes rather than to variations in input data quality.

The baseline model serves a dual function in this research. First, it provides absolute performance benchmarks against which all subsequent scenarios are measured. Second, it enables the identification of specific envelope and system components whose modification results in the significant improvements in operational energy and embodied carbon. This diagnostic function is essential for formulating meaningful and targeted design scenarios.

3.3 Scenario-based approach: from baseline to optimized configurations.

The methodological core of this research is a scenario-based comparative analysis. Four different design configurations are defined and evaluated, each representing a distinct area of intervention along the building's envelope and structural system. This approach enables a systematic examination of the trade-offs and synergies between energy performance, embodied carbon, and daylighting, without reducing the complexity of these interactions to a single-objective optimization problem. The baseline constitutes the reference condition, as described in Section 3.2. It is evaluated without modification to establish reference values across all performance domains.

Scenario 1: Material improvement strategy; targets the embodied carbon of the building's structural and façade stratigraphies by substituting or optimizing constituent materials, without altering geometry or envelope configuration, isolating the carbon impact attributable to material choice alone.

Scenario 2: Roof strategies; evaluates the roof as an independent performance domain, incorporating photovoltaic generation to assess its contribution to offsetting operational energy demand against the embodied carbon of the additional system.

Scenario 3: ? mohammad
Scenario 4 : ? mohammad

Each scenario is defined through a structured parameter matrix that specifies the relevant modifications across the domain of intervention: materials, roof system, envelope elements and shading devices, respectively. This matrix ensures comparability across scenarios and prevents the merging of distinct design decisions, while maintaining a clear progression from the baseline condition toward increasingly performance-oriented configurations.

3.4 Multi-domain simulation workflow

The environmental performance of each scenario is evaluated through a coordinated simulation workflow covering two complementary analytical methods: dynamic energy modelling and Life Cycle Assessment (LCA). Both analyses are conducted within the parametric environment of Rhinoceros 3D and Grasshopper, which serves as the shared computational and parametric core of the workflow. This integration within a single modelling platform ensures that geometry, material assignments, and simulation inputs remain consistent across both analyses, minimising the risk of data transfer errors and enabling real-time feedback as design parameters are adjusted across scenarios.

3.4.1 Energy modelling

Dynamic energy simulation is performed using Honeybee, a Grasshopper plugin that serves as the primary tool for operational performance assessment in this research. Honeybee integrates the EnergyPlus simulation engine with a Grasshopper-native parametric interface, enabling fully scripted model generation, sensitivity analysis, and automated scenario comparison without leaving the design environment.
This connection between geometry and simulation is particularly beneficial for a scenario-based study such as this one, in which envelope configurations and spatial layouts vary across multiple design alternatives.
The energy model was developed from the reconstructed baseline described in Section 3.2, combining available architectural information with assumed parameters derived from normative standards and literature references. Boundary conditions were defined using the EPW (EnergyPlus Weather) climate file for Milan, sourced from the EnergyPlus climate data repository. Occupancy patterns, equipment loads, and lighting power densities were assigned in accordance with EN 16798-1. Key performance indicators extracted from the model include: annual heating and cooling energy demand (kWh⁄m²⁄year), peak thermal loads (kW) and CO_2-equivalent operational emissions calculated using national grid emission factors.
Parametric simulation runs were scripted directly in Grasshopper, with each scenario defined as a distinct script.
This structure allows the contribution of individual modifications to be isolated by selectively activating and deactivating envelope or system parameters, supporting a causal rather than purely comparative interpretation of performance differences across scenarios.

3.4.2 Life Cycle Assessment (LCA) setup

The embodied carbon assessment is conducted using Bombyx, an open-source Grasshopper plugin for parametric LCA developed at ETH Zürich's Chair of Sustainable Construction [23]. Bombyx operates directly on the Rhinoceros 3D geometry, reading surface areas and volumes from the parametric model and mapping them to a SQL material database that stores environmental impact data, including Global Warming Potential (GWP) per unit of material. This geometry-driven approach ensures that embodied carbon calculations update automatically as design parameters are modified, enabling real-time LCA feedback within the same Grasshopper workflow used for energy modelling.
The plugin was chosen for several reasons specific to this research context. First, its direct integration with Grasshopper eliminates the need to export geometry to a separate LCA platform, preserving the parametric coherence of the simulation workflow and reducing the risk of differences between the energy model geometry and the LCA material BOQ. Second, Bombyx supports both top-down and bottom-up modelling approaches: in the top-down mode, the building is characteried using aggregated component categories, while the bottom-up mode allows individual material layers to be specified, a flexibility that is well-suited to the varying levels of design resolution across Scenarios 0 through 4. Third, the tool has been validated and applied in peer-reviewed research on office and residential building typologies [23], providing a credible methodological basis for its adoption in this thesis.
The LCA is conducted in accordance with EN 15978, encompassing life cycle stages A1–A5 (product and construction), B4–B6 (replacement and operational energy), and C3–C4 (end-of-life waste processing), with module D reported separately as supplementary information. Material quantities are extracted directly from the Grasshopper model geometry and cross-referenced with the KBOB database. Environmental impact data is drawn from the Ecoinvent background database integrated within Bombyx, supplemented by Environmental Product Declarations (EPDs).
The primary impact category assessed is GWP, expressed in $kgCO_2eq/m^2$ of gross floor area over a 60-year reference study period. Secondary categories, including Biogenic Carbon, are reported to identify potential environmental burden-shifting across scenarios.

3.5 Limitations and assumptions

The methodological framework described in this chapter is subject to a number of limitations that must be acknowledged in order to contextualise the research findings appropriately. These limitations arise from data availability, modelling conventions, and the related simplifications required to present a complex physical and material system suitable for computational analysis.

- A significant limitation of this study concerns the restricted availability of project data. The baseline model was developed using only partial architectural information, consisting of two non-dimensioned plans without accompanying technical documentation, one pdf explaining briefly the project and a render to show the façade. As a result, several key inputs required for both energy simulation and LCA were not directly available and had to be assumed.

- Geometric parameters, including overall building dimensions, floor heights, and facade articulation, were reconstructed based on proportional interpretation of the drawings and reference to typical office building configurations.
For these reasons the building is assumed as a rigid block, despite from the available renders its clearly visible an offset for one of the buildings corners.

- Envelope properties (U-values, glazing performance), internal loads (occupancy, equipment, lighting), characteristics were defined using standard values derived from relevant norms (e.g., EN 16798-1) and literature benchmarks.

- With regard to energy modelling, the simulation adopts a static occupancy schedule derived from normative standards rather than measured data, which may not fully capture the variability of actual occupancy patterns in innovation district workplaces. Furthermore, the energy model does not account for the potential contribution of district-level energy systems, which are under development at MIND and may significantly alter the operational carbon profile of the building in its final operational context.
For sake of simplicity and uncertainty the model has been calculated on an Idea AirLoad system.

- Material specifications for the LCA were similarly approximated, relying on generic assemblies representative of contemporary office construction in a Milanese context. While this introduces a degree of uncertainty in absolute impact values, the assumptions were applied consistently across all scenarios.

- In the LCA domain, the material database embodied in Bombyx is primarily calibrated to the Swiss construction context and uses the Swiss KBOB dataset as its primary data source.

This methodological choice implies that the results should be interpreted primarily in relative terms, focusing on the comparative performance between scenarios rather than on the absolute magnitude of energy use or carbon emissions. The study therefore prioritizes internal coherence and parametric sensitivity over empirical precision. Nevertheless, registered data are plausi-

ble with similar buildings.

The spatial quality assessment, while informing the definition of design scenarios, remains qualitative in nature and is not integrated into the quantitative simulation framework. This reflects the current limitations of computational tools in capturing the full complexity of spatial experience and livability, and represents a productive direction for future methodological development.

Internal Loads and Thermal Setpoint Schedules Modeling Strategy:
To streamline the dynamic energy simulation and ensure methodological consistency across functional macro-zones, operational schedules were aggregated based on shared occupancy patterns and boundary requirements.
Specifically, internal sensible loads, as occupancy (People), artificial lighting (Lighting), and plug loads (Equipment), were synchronized under uniform hourly fraction profiles, reflecting direct user-driven operation.
Furthermore, spaces exhibiting equivalent diurnal utilization cycles were paired under identical operational schedules and HVAC setpoints:
The Bookshop and External Office zones share identical daily comfort hours (20.0 °C heating / 26.0 °C cooling) and setback regimes.
Similarly, auxiliary circulation and service zones, namely the building Core and the Parking areas, share unified operational schedules, free-floating and setback thresholds.
This standardized grouping minimizes localized scheduling biases while preserving the realistic global energy demand of the non-conditioned and conditioned building volumes.
To maintain model conciseness while accurately representing non-habitable service volumes, common input parameters were adopted for the building core and parking areas.
Specifically, representative volume- and area-weighted averages were established for both occupant metabolic rates (Met) and mechanical air exchange rates (ACH).
The metabolic rate reflects a hybrid active-transient state combining walking circulation, transient physical effort, and vehicle parking activity. Concurrently, an equivalent baseline ventilation rate was assigned to capture the dual requirements of baseline circulation hygiene and diluted mechanical extraction. This unified approach simplifies zoning complexity while avoiding localized overestimation of auxiliary building loads

3.6 Daylight-Driven alternatives in Shading and Glazing

While façade variations can be driven by a multitude of design factors, ranging from formal aesthetic intent to material constraints and fabrication costs, this research deliberately isolates daylighting performance as the primary generative driver.
The rationale for this prioritization is twofold. First, indoor daylight availability directly governs qualitative environmental conditions, influencing occupant circadian health, visual comfort, and cognitive well-being. Second, a daylight-optimized envelope acts as an essential regulator of a building's operational energy balance: it curtails artificial lighting loads while simultaneously acting as the first barrier against undesirable peak solar heat gains.
To ensure that optimizing for natural light does not create secondary environmental burdens, the parametric envelope configurations generated through this workflow are subsequently evaluated against operational energy demands and whole-life embodied carbon footprints.

Definition of the Optimization Problem: From Discrete Standards to a Single Fitness Function

Dynamic, Climate-Based Daylight Modeling (CBDM) relies on spatial and temporal metrics to quantify daylight sufficiency and visual comfort simultaneously. Two foundational benchmarks established by the Illuminating Engineering Society (IES) in the IES LM-83 standard are [31]:

- Spatial Daylight Autonomy (sDA 300/50%): Measures the percentage of the analyzed work plane that receives at least 300 lux of horizontal illuminance from daylight for at least 50% of operating hours (8:00 to 18:00).
It acts as an indicator of daylight sufficiency and penetration depth.
- Annual Sunlight Exposure (ASE 1000, 250h): Quantifies the percentage of the floor area exposed to direct solar illuminance exceeding 1000 lux for more than 250 occupied hours per year, computed without interior dynamic window attachments.

It serves as an indicator of potential glare and localized thermal discomfort. In standard regulatory frameworks, sDA and ASE are treated as independent, decoupled constraints. However, evolutionary optimization solvers require a consolidated, continuous scalar objective to evaluate geometric fitness effectively. [32] To operationalize these two competing phenomena within a single-objective parametric workflow, this research employs a composite objective function termed Net Useful Daylight Area (NUDA):

$$NUDA = sDA\ 300/50\% - ASE\ 1000, 250h$$

Rather than treating solar overexposure as a secondary filter, this formulation utilizes ASE as a direct spatial penalty on daylight sufficiency, an approach aligned with multi-parameter performance aggregation in algorithmic building design [33].

By maximizing NUDA, the evolutionary solver is mathematically incentivized to push diffuse daylight deep into the interior core while concurrently evolving geometric features (such as self-shading profiles, reveal depths, or louver angles) to suppress direct solar penetration.

Methodological Comparison with Industry Standards

The formulation of NUDA bridges the operational gap between rigid green building certification thresholds and bin-based temporal metrics:

Translation of Rating Checklists (LEED v4 / LM-83): Green building rating systems such as LEED v4 award points based on a stepped, binary logic: spaces must clear discrete thresholds (e.g., sDA ≥ 55% for 2 points, ≥ 75% for 3 points) provided that ASE remains below a fixed limit ≤ 10%).

For algorithmic optimization, discontinuous step functions create flat fitness landscapes, stalling gradient and genetic solvers. Subtracting ASE converts this dual pass/fail requirement into a continuous gradient, rewarding incremental improvements in envelope geometry.

Spatial Analogy to Useful Daylight Illuminance (UDI) [34]: Categorizes annual hourly illuminance into discrete bins, specifically prioritizing the range between 100 and 2,000 lux while penalizing values above 2,000 lux as prone to visual and thermal discomfort.

While UDI is inherently a temporal evaluation per grid point, the proposed sDA - ASE composite operates as its macroscopic spatial equivalent, effectively delineating the floor zone where illuminance is adequate without risking direct solar overload.

While the formulation of the Net Useful Daylight Area (NUDA) provides a rigorous, single-objective fitness metric for evolutionary solvers, applying this dynamic evaluation across a large-scale architectural model introduces a critical new challenge: computational feasibility. Defining the optimization goal is only the first step; computing it efficiently at scale requires a specialized methodological workflow to prevent simulation stalling.

Definition of the Optimization Methodology: Decoupled Parametric Sweep with Local Regression

The building contains 267 rooms and 716 windows.

To address the computational bottlenecks inherent in high-dimensional architectural optimization, this research employs a method defined as a Decoupled Parametric Sweep with Local Regression. In complex building systems, optimizing hundreds of independent spatial zones simultaneously creates an exponentially large design space. Rather than treating the building as a single, highly-coupled organism, this methodology decomposes the global optimization problem into a series of localized, one-dimensional problems.

The workflow is executed in three primary phases:

- Uniform Parametric Sweeping: A discrete set of parameter variations is established.

A global simulation is run for each discrete step, applying the parametric change uniformly across all subsystems simultaneously.

- Localized Data Mapping: The performance metrics are extracted not at the global level, but at the localized subsystem level. This yields a dedicated dataset for each individual zone across the tested parameter domain.

- Regression and Interpolation: A regression curve is fitted to the localized dataset of each subsystem. By mathematically mapping the relationship between the parameter and the performance metric, the exact theoretical optimum for each isolated zone can be interpolated without the need for further simulation.

Comparative Analysis with Standard Optimization Algorithms

When contextualizing this methodology within the broader landscape of computational design, its primary advantage lies in how it manages computational time complexity in high-variable environments.

Traditional optimization workflows generally struggle as the number of independent subsystems increases.

1. An Exhaustive Search (Brute Force) approach seeks the absolute global optimum by evaluating every possible parametric permutation within the design space. If a system contains *N* independent subsystems that can each adopt *V* parametric states, the total number of required simulations scales exponentially as *O(V^N)*.

For complex architectural systems featuring hundreds of independent spatial zones, this combinatorial explosion renders brute-force methods computationally impossible within practical design timelines.

2. Evolutionary and Genetic Algorithms (GAs) address this combinatorial challenge through meta-heuristic strategies, such as selection, cross-over, mutation, and generational convergence, to sample the design space without evaluating every permutation.

While GAs excel at finding near-optimal solutions in complex, non-linear scenarios, they still require thousands of sequential simulations to achieve convergence. When applied to multi-variable architectural models where individual physics-based simulation runs are computationally intensive, standard GAs become an unsustainable bottleneck unless the geometric model is drastically simplified or variables are aggregated into broad clusters.

3. More recently, Machine Learning and Artificial Neural Network (ANN) Surrogate Models have emerged as an alternative to circumvent the speed limitations of physics-based solvers. In this paradigm, an algorithm is trained on an initial dataset of simulation results to learn the mapping between geometric parameters and performance outcomes, effectively acting as an instant “surrogate” evaluator. Once trained, the model evaluates designs in fractions of a second, enabling genetic algorithms or real-time solvers to test tens of thousands of permutations and capture complex inter-zone dependencies. However, surrogate modeling shifts rather than eliminates the computational burden: assembling an adequate ground-truth training dataset typically demands hundreds or thousands of high-fidelity simulations upfront. When

individual simulation runs require significant processing time, the data generation phase alone presents an enormous computational and temporal hurdle, often necessitating distributed cloud infrastructure or advanced active-learning protocols.

4. In contrast, the Decoupled Parametric Sweep with Local Regression offers a lightweight, deterministic alternative that avoids both the iterative overhead of genetic algorithms and the heavy training cost of machine learning. By decoupling the subsystems and applying mathematical regression locally, the required simulation overhead is governed strictly by the number of uniform parametric steps analyzed *(V)*, completely independent of the number of subsystems *(N)*. The computational complexity is reduced to *O(V)*, requiring only a minimal baseline of discrete simulations to derive continuous, localized mathematical models for hundreds of zones simultaneously.
Provided that localized cross-interference remains minimal, this methodology delivers high-resolution, customized optimization at a fraction of the computational expense required by traditional evolutionary searches or data-intensive machine learning pipelines.

1. Brute Force Method

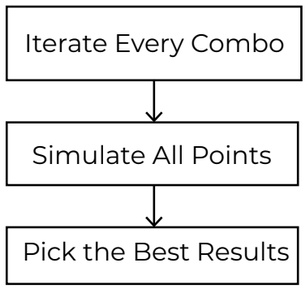

fig. 2

2. Genetic Algorithms

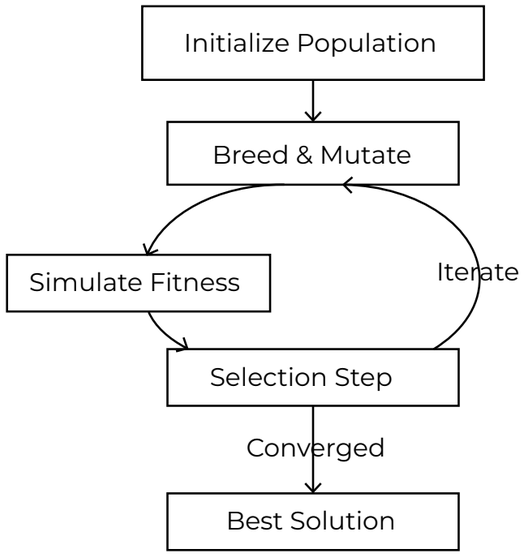

fig. 3

3. Machine Learning Method

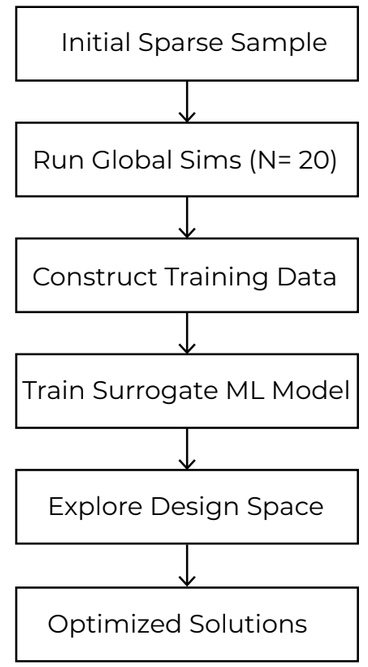

fig. 4

4. Proposed Method

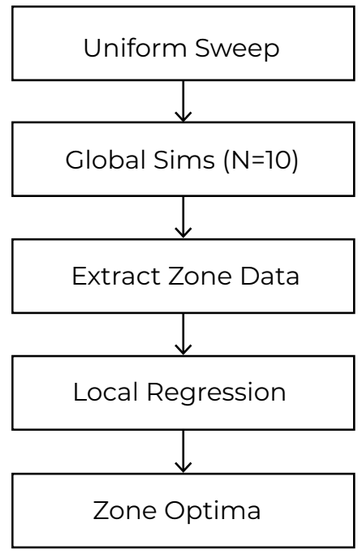

fig. 5

Limitations and The Assumption of Variable Independence

While this methodology maximizes computational efficiency, its mathematical validity relies on the critical assumption of Variable Independence.

Because the initial parametric sweep modifies all subsystems uniformly, the resulting regression models implicitly assume that the parameter state of Subsystem A has no physical or environmental impact on the performance of Subsystem B.
The methodology calculates the optimum for each zone in isolation, but those optima are derived from global simulations where all zones were acting in unison.
If the system contains localized cross-interference, where a geometric or parametric change in one zone directly alters the boundary conditions of an adjacent zone, the individual regression curves will contain a margin of error.
In highly complex, self-intersecting geometries, the optimized state of one variable may inadvertently degrade the performance of a neighboring subsystem.
To mitigate this, the methodology requires a final, global verification simulation. Once all local optima are calculated via regression and applied to their respective subsystems, a single comprehensive simulation must be run to confirm that no severe negative interference has occurred across the localized boundaries.



fig. 6

Façade Alternatives and Parametric Strategies

To evaluate the impact of the envelope on daylight performance, the parametric strategies were established across three primary categories: window proportions, external shading systems, and glazing optical properties.

Group 1: Window Size (Height Variation)

This category explores three different glazing configurations, representing maximum, minimum, and optimally balanced glazing ratios. Across all three iterations, the width and placement of the modular perimetral windows remain strictly constant; the overall Window-to-Wall Ratio (WWR) is modulated exclusively by altering the window height.

Baseline Configuration (Zenith type): Represents the existing state of the building. It features modular windows set to their maximum height, yielding the highest possible glazing ratio for the given width.

Minimum Configuration (Horizon type): Derived from the architectural language of a neighboring building with identical functionality. It features windows reduced to a minimum height, representing the lowest glazing ratio alternative.

Daylight-Driven Optimized Configuration: The result of the algorithmic solver, where the window height is parametrically modified to discover the exact dimension that maximizes the Net Useful Daylight Area (NUDA).

Group 2: External Shading Systems

This category investigates the geometric impact of external obstructions on direct solar penetration.

Blades Shading (Zenith type): Considers the building's existing façade articulation, where a series of vertical elements extruded outward act as an implicit shading system.

Optimized Static Shading: Introduces a parametrically generated system comprising both horizontal overhangs extending from the top of the window and vertical fins on the sides. The depths of these extrusions are mathematically optimized to maximize the NUDA score.

Group 3: Glazing Optical Properties

Rather than altering the physical geometry of the façade, this strategy evaluates the application of applied window treatments.

Optimized Visible Transmittance (VT): This approach assumes the installation of advanced thin films on the existing window glass to restrict excessive sunlight exposure.

Since these films are available in various shading coefficients, the optimization solver parametrically modulates the Visible Transmittance (VT) level of each specific window to maximize the overall Net Useful Daylight Area.

Group 1: Minimum Configuration (Horizon type)



fig. 7

Group 1: **Daylight-Driven Optimized Configuration:**

To determine the optimal window size for each room, the window height was parametrically varied from 0.5 to 3.0 meters. Throughout this process, spatial Daylight Autonomy (sDA) and Annual Sunlight Exposure (ASE) values were recorded for each iteration. These metrics were then used to calculate the Net Useful Daylight Availability (NUDA), serving as a single fitness value. By plotting the NUDA trendline and identifying its peak, the optimal window height was determined. In this example, the optimum height on the axis is 2.27 meters.

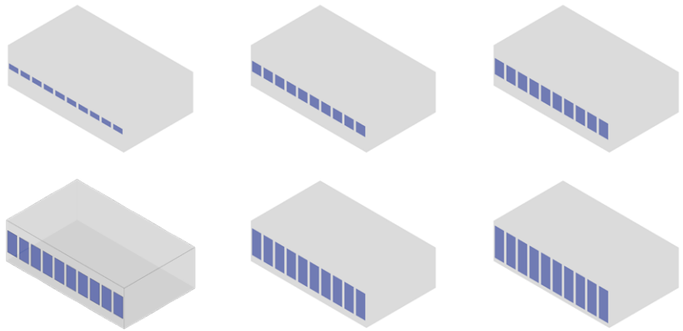

fig. 8

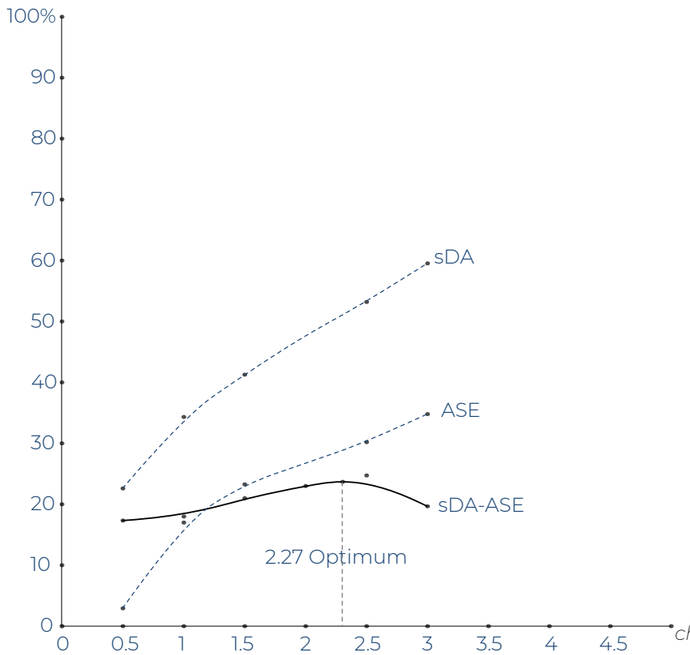

chart 1

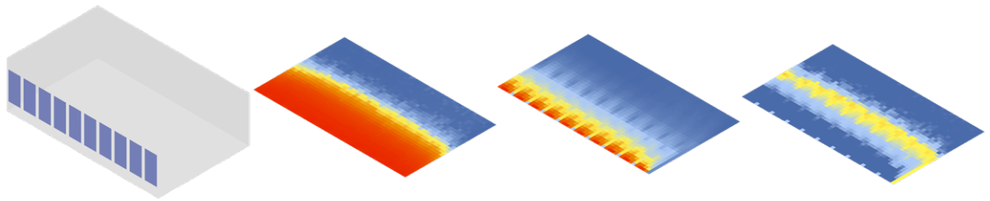

fig. 9

Group 2: **Blades Shading (Zenith type)**



fig. 10

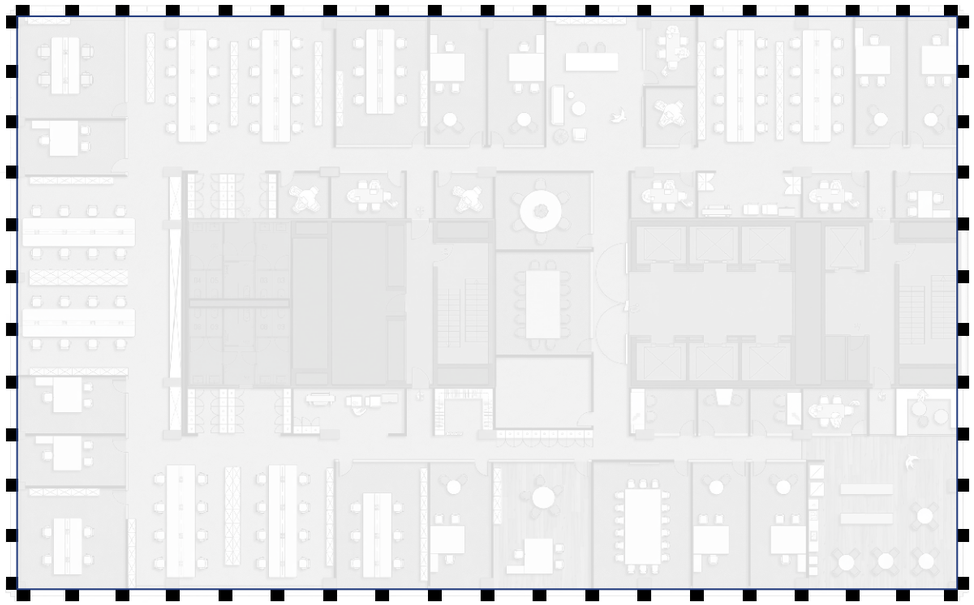

fig. 11

Optimized Static Shading:

To identify the most effective shading configuration, a sequential optimization process was conducted. First, the top, left, and right sides of the window frames were individually extruded outward from 0 to 100 cm. The NUDA trendline was plotted for each to determine the maximum impact. In this specific case, the top shading yielded the best results, with an optimal width of 83.63 cm.

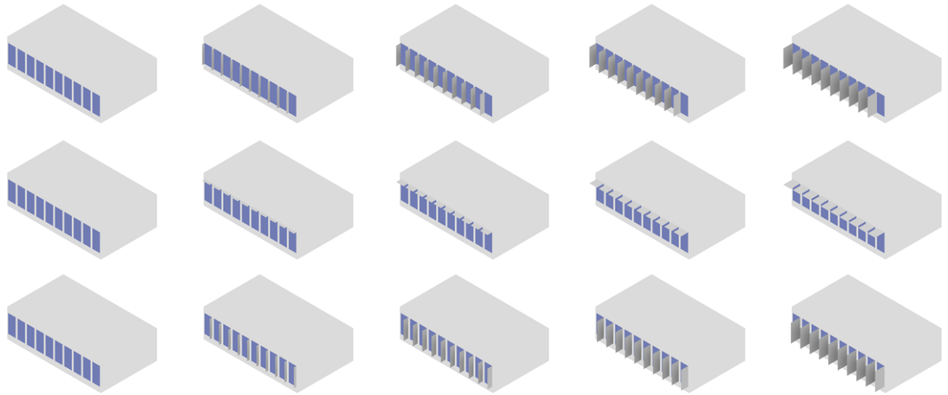

fig. 12

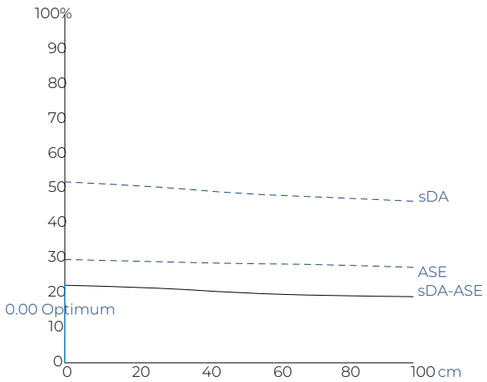

Left side , First

chart 2

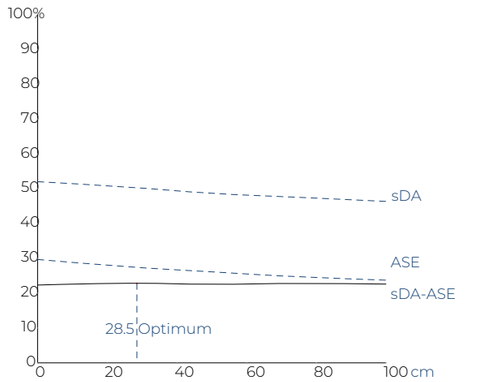

Right side , First

chart 3

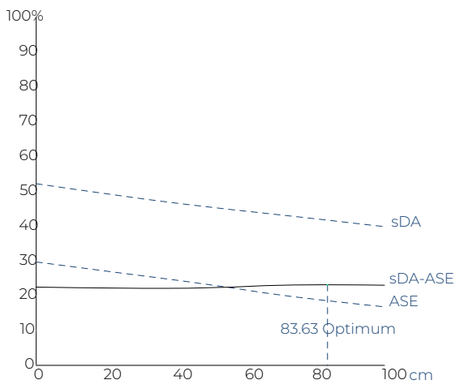

Top side , First

chart 4

The second optimization phase evaluated the next most impactful side, the left side of the window, while keeping the optimal top shading in place. The peak of the NUDA graph indicated an optimal left-side width of 56.20 cm.

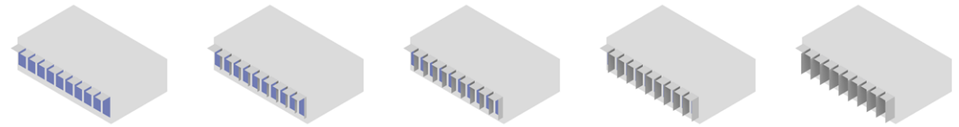

fig. 13

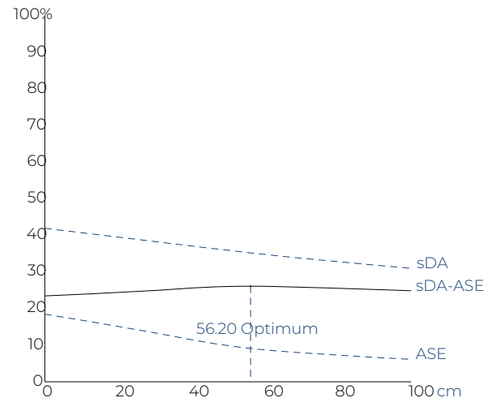

Left side , Second

chart 5

The third and final phase analyzed the right side of the window, which proved to be the least impactful element. With the top (83.63 cm) and left (56.20 cm) shadings already applied, the NUDA trendline peaked at the very beginning of the chart (0 cm). This suggests that implementing shading on the right side actively carries a negative impact on overall daylight performance.

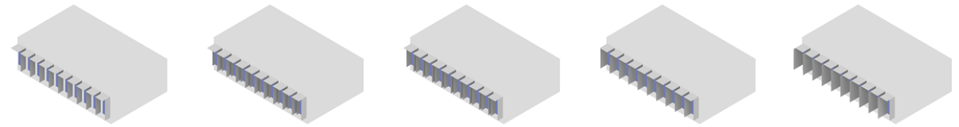

fig. 14

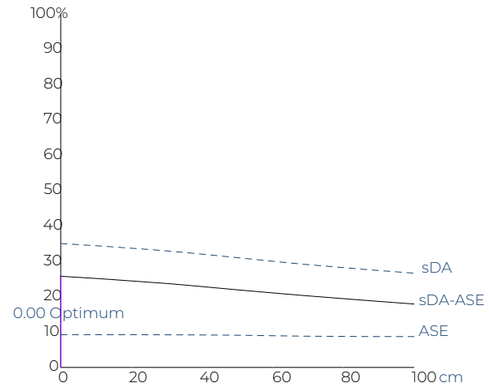

Right side , Second

chart 6

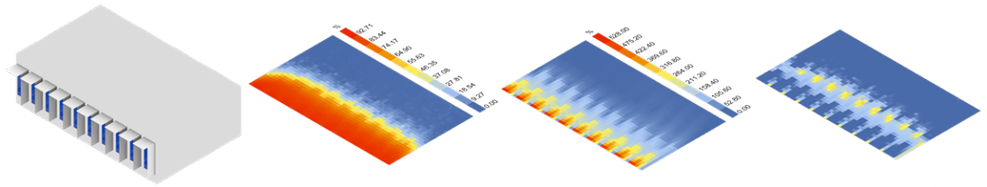

fig. 15

Visible Transmittance Optimization:

To determine the ideal visible transmittance (VT) for the windows, a similar optimization process was applied. Instead of altering the physical dimensions of the window or shading, the VT of the glazing, a critical physical characteristic, was varied from 0% (totally opaque) to 100% (completely transparent). This theoretical maximum of 100% was used for the sake of simplicity, keeping in mind that the clearest market-available glazings typically reach only around 85%. Identifying the maximum NUDA on the resulting graph suggests an optimal visible transmittance of 35.6%.

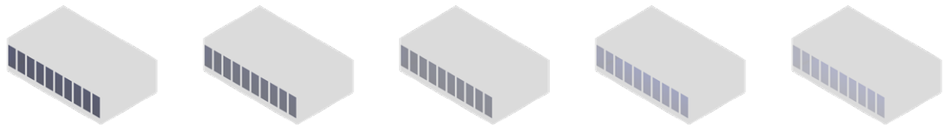

fig. 16

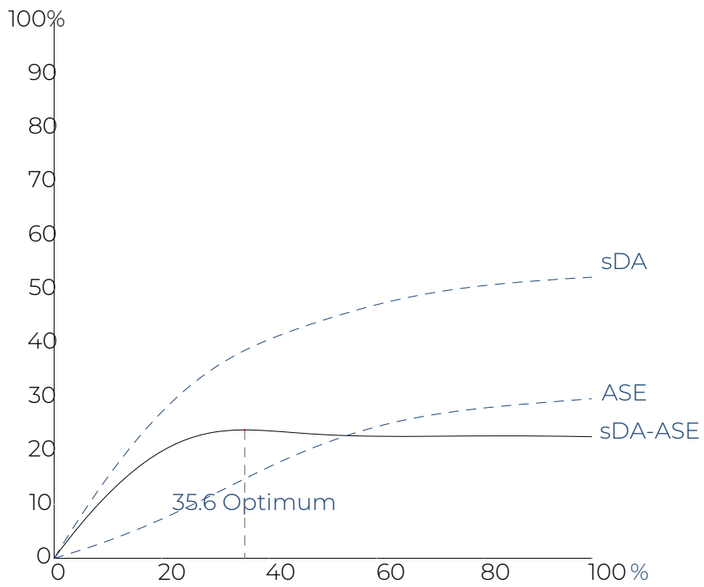

chart 7

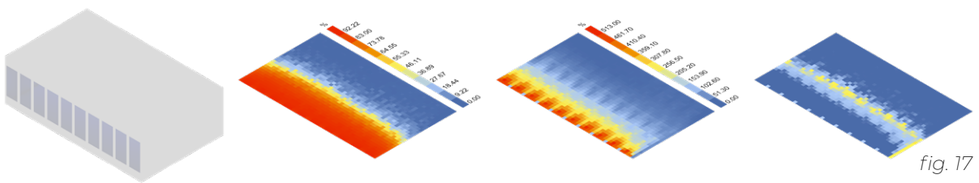

fig. 17

Combinatorial Matrix of Design Alternatives

To maximize the number of alternatives and systematically explore the design space, elements from the three groups were selectively combined. The three Window Size configurations (Group 1) were established as the base geometric "environments," while the shading variations (Group 2) and glazing optical properties (Group 3) functioned as the variable "genotypes."
Running these combinations yielded a numerous set of resultant "phenotypes," classified as follows:

NS - Baseline: No external shading and baseline glass transparency.

BL - Zenith Existing Shading: Application of the building's original vertical elements.

OS - Daylight-Driven Optimized Shading: Application of the algorithmically generated horizontal and vertical fins.

VT - Optimized VT: Application of the optimized optical thin films only.

BL- OS - Zenith Existing Shading + Optimized Shading: A combination of the existing vertical elements with the newly generated shading extrusions.

BL - VT - Zenith Existing Shading + Optimized VT: The existing physical shading coupled with optimized glass properties.

BL - OS - VT - Zenith Existing Shading + Optimized Shading + Optimized VT: The sequential overlay of existing physical shading, generated optimized shading, and optimized glass transparency.

BL - VT - OS - Zenith Existing Shading + Optimized VT + Optimized Shading: The sequential overlay of existing physical shading, followed by optimized glass transparency, and finally the generated optimized shading.

OS - VT - Optimized Shading + Optimized VT: An intervention calculating the custom physical geometry first, followed by the custom optical films.

VT - OS: An intervention calculating the custom optical films first, followed by the custom physical geometry.

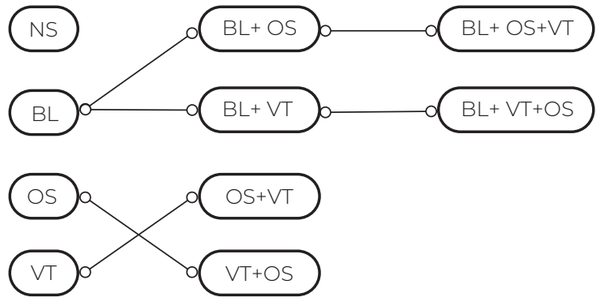

fig. 18

These genotypes would be applied on three environments which are as follows:

B - Baseline Configuration
H - Horizon Configuration
D - Daylight-Driven Optimized Configuration

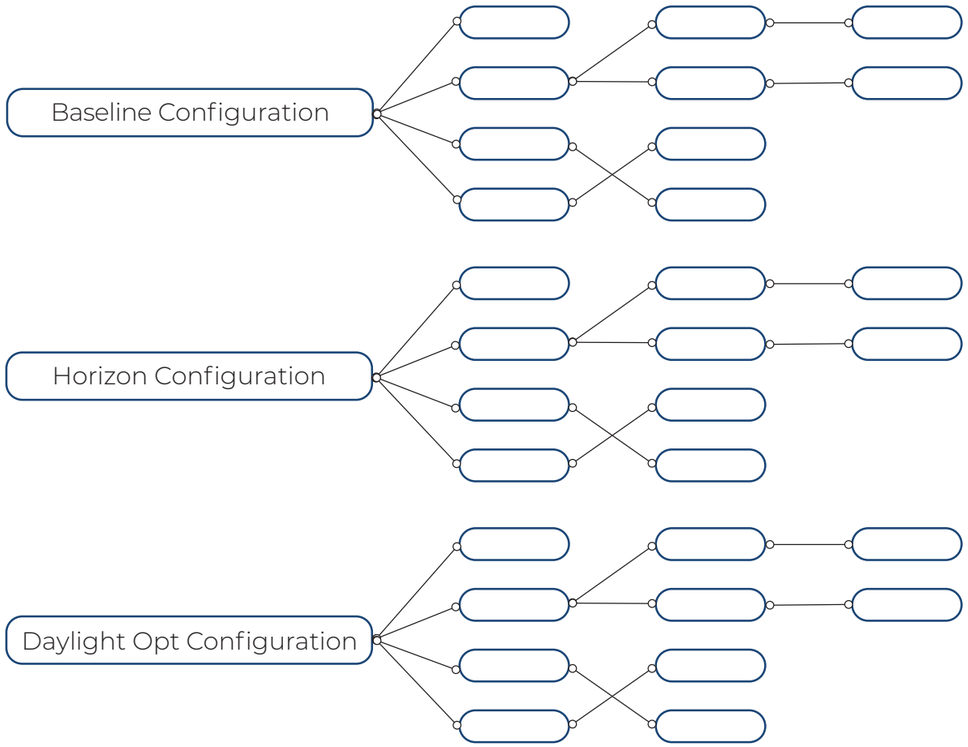

fig. 19

All the 30 phenotypes are being assessed considering Double glazing (2G) systems and Triple Glazing (3G) systems for operational and embodied energy and carbon foorprint.
Worths mentioning that changing the glazing system as long as visible light transmmitance remains constant, is not affecting the daylight analysis.
Therefore, for daylight seems to be enough simulating only once and assume that it would perform the same for both systems.

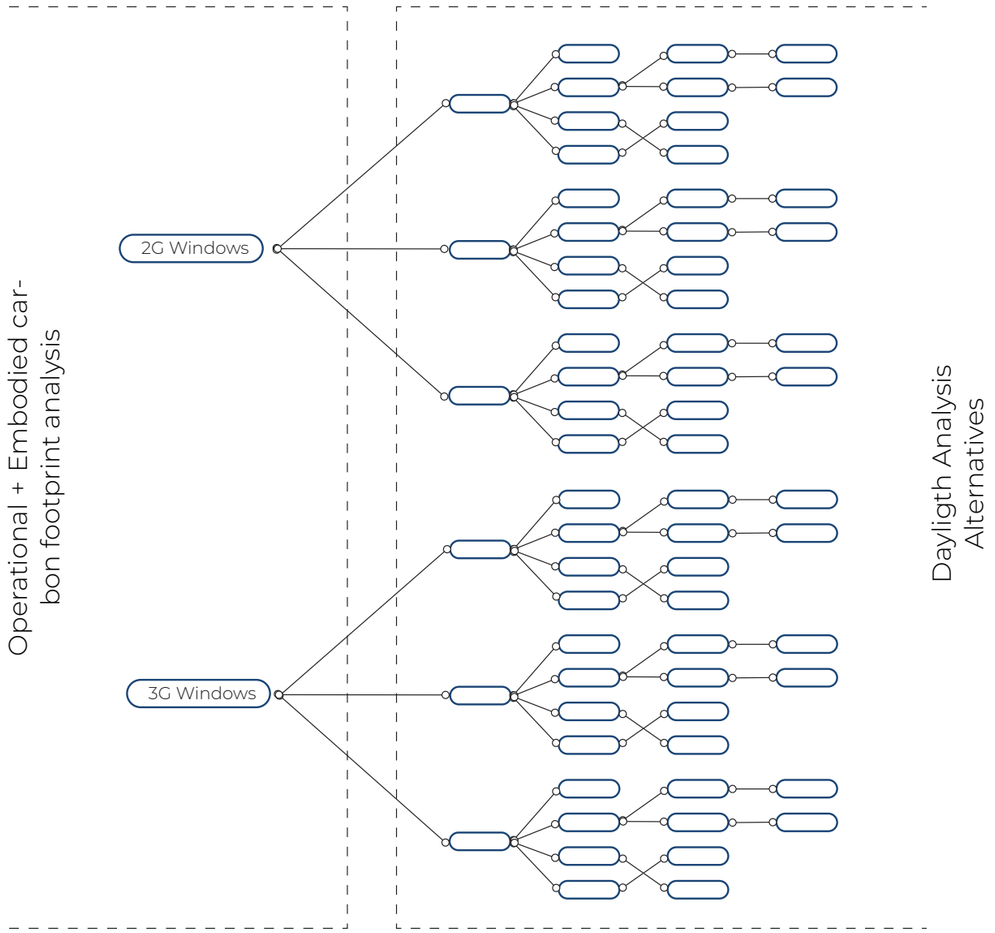

fig. 20

Annual Solar Exposure (aSe), Spacial Daylight Autonomy (SDA) and the resultant Net Useful Daylight Area (NUDA)

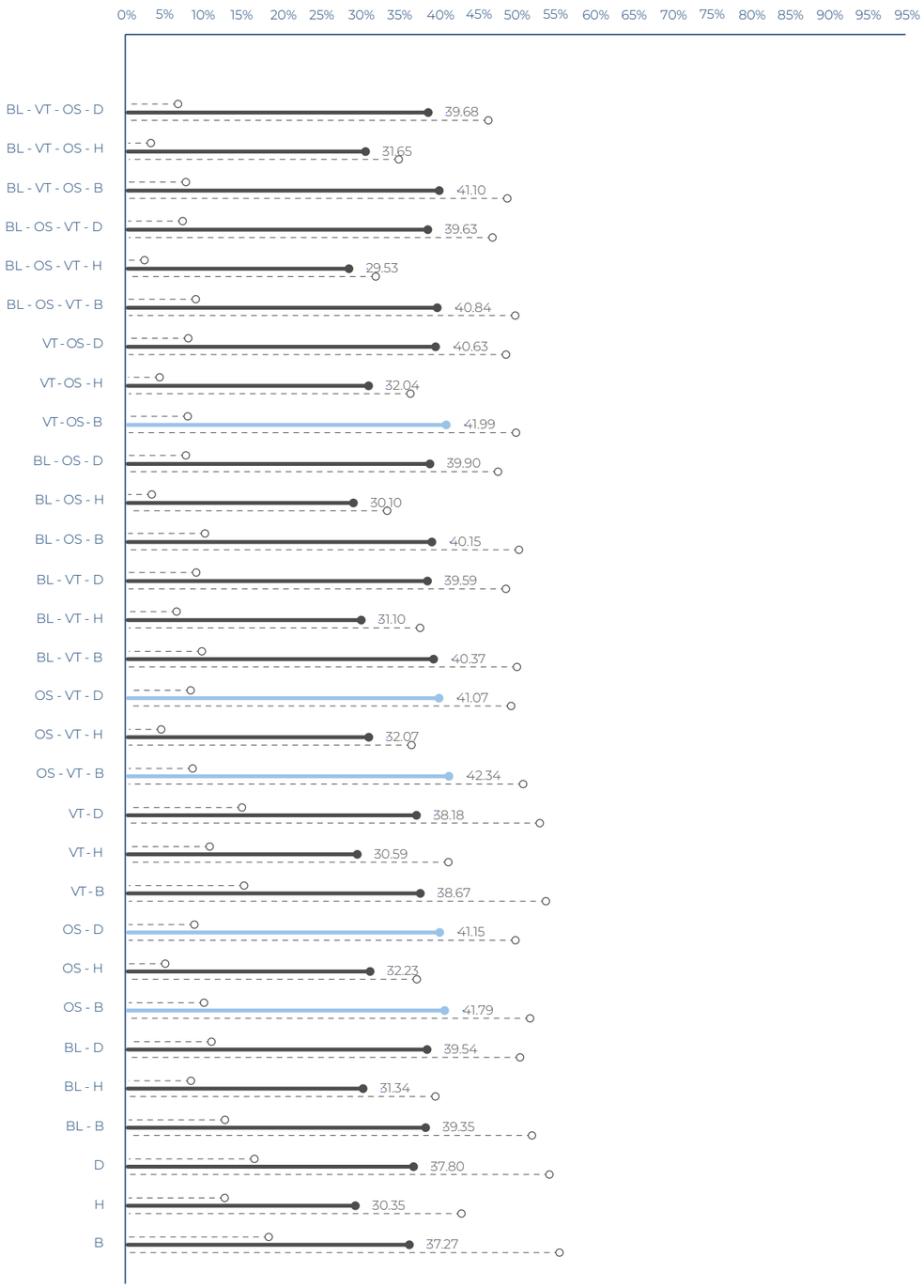

chart 8

3.7 Nomenclature and Scenario Classification Logic

The simulation framework is organized into two sequential methodological stages: an initial reference benchmark followed by material retrofits (Baseline and Scenario 1), and a parametric multi-objective envelope optimization matrix with active on-site generation (Scenarios 2, 3, and 4).

1. Reference Benchmark and Material Upgrades (S_10 Series)
The S_10 series evaluates static building modifications prior to the deployment of active renewable systems and parametric envelope variations:
S_10 (Baseline): The unoptimized reference model reflecting the building as currently under construction, lacking both on-site renewable energy systems and upgraded material selections (addressed in Section 4.1).
S_10A (Structure Improvement): Baseline envelope combined with low-carbon structural material optimizations (addressed in Section 4.2.1).
S_10B (Façade Improvement): Baseline geometry incorporating optimized opaque façade stratigraphies (addressed in Section 4.2.2).

2. Parametric Envelope Matrix with PV Integration (S_20 to S_64)
Starting from Scenario 2 (S_20), rooftop PV panels are permanently integrated across all subsequent configurations to establish an active renewable generation baseline.
Consequently, variations within the S_20, S_30, and S_40 series isolate the combined passive performance of window-to-wall ratios (WWR), glazing technologies, and solar shading strategies.
Each parametric configuration is identified by a standardized compound label:

S[X][Y]-[WWR]-[Glazing]-[Shading]

Macro-Scenario and WWR Strategy (X): The tens digit directly identifies the chapter scenario and its corresponding aperture configuration:

2: Scenario 2, Baseline WWR with integrated rooftop PV panels
3: Scenario 3, Horizon-driven WWR (S_30 series).
4: Scenario 4, Daylight-driven WWR (S_40 series)
The simulations reporting 8 and 9 are concerning the Visible Trasmittance (VT).

Envelope Permutation Index (Y): The units digit systematically denotes the six permutations of glazing systems and solar shading typologies:

0: Double Glazing without shading (2G NS)
1: Double Glazing with fixed blades (2G BL)
2: Double Glazing with optimized shading (2G OS)
3: Triple Glazing without shading (3G NS)
4: Triple Glazing with fixed blades (3G BL)
5: Triple Glazing with optimized shading (3G OS)

Explicit Suffix ([WWR] [Glazing] [Shading]):
Appended to ensure direct readability across performance charts and comparative tables without requiring cross-referencing:

WWR: B (Baseline), H (Horizon-driven), D (Daylight-driven)

Glazing: 2G (Double Glazing), 3G (Triple Glazing)

Shading: NS (No Shading), BL (Original Blades), OS (Optimized Shading)

Example: S_32 H 2G OS denotes Scenario 3 (Horizon-driven WWR with rooftop PV), envelope permutation 2 (Double Glazing 2G with Optimized Shading OS).

3.8 The Carbon Rating: Benchmarks adopted

Carbon HEROES Benchmark

While these isolated reductions in both the structural and façade stratigraphies confirm the effectiveness of individual component optimization, understanding their true impact requires evaluating the building as a holistic system against established industry standards. To achieve this, the cumulative whole-life carbon performance of both sub-scenarios was mapped against the Carbon Heroes Benchmark.

This tool is a widely adopted rating framework in the built environment, born as a global collaborative initiative managed by One Click LCA. It classifies buildings across a spectrum of performance band based on their total annual GWP expressed in $kgCO_2eq/m^2/year$.
The Carbon Heroes Benchmark goes from G, representing the highest carbon intensity, to A+, indicating near-zero or net-negative carbon.
It provides a standardized reference point for comparing design variations against industry norms, allowing design teams to track the tangible effect of carbon reduction decisions throughout the optimization process.

The framework evaluates embodied carbon only, completely excluding operational emissions (modules B6–B7). Its scope spans life cycle stages A1 through C4, covering material production (A1–A3), transport to site (A4), maintenance and replacements over the building's lifetime (B4–B5), and end-of-life processing (C1–C4). Two boundary conditions are worth noting: construction site emissions (A5) are excluded, as they remain inconsistently tracked at a global scale, and any benefits occurring beyond the system boundary, such as material recovery or energy export, fall outside the framework's scope (Module D).

This defined scope makes the benchmark particularly suited to evaluating the impact of material substitution strategies, as the carbon reductions achieved through the choices described in Sections 4.2.1 and 4.2.2 fall squarely within the life cycle stages it measures.
When plotted against this framework, the sequential effect of the material substitutions described in Sections 4.2.1 and 4.2.2 becomes clear:

Structural Phase: In the baseline configuration, the building sits within Band B. The structural stratigraphy optimization alone proves sufficient to cross the threshold into Band A, a significant result that confirms the primary role of structural material choices in driving whole-life carbon performance. Beyond the rating improvement itself, this step also creates additional headroom within Band A, positioning the building favorably for the subsequent façade optimization.

Façade Phase: The subsequent façade material substitutions, specifically targeting high-GWP components, further reduce the annual embodied GWP, consolidating and strengthening the Band A rating achieved in the previous phase.
This progression illustrates a critical reality in carbon accounting: while cumulative marginal gains are often what separate performance tiers, the structural phase here demonstrates that targeted, high-impact substitutions can independently shift a building's rating. The façade optimization then reinforces this outcome, ensuring the Band A classification is not merely reached but held with a comfortable margin, setting a strong foundation for the strategies explored in the scenarios that follow.

The methodology adopts the framework established by One Click LCA The methodology adopts the framework established by One Click LCA. Among the available datasets, the "Italy office 2025" Carbon Heroes Benchmark [28] was selected as the guideline for this thesis, as it re the most current and contextually appropriate data for the scope of this research.

Embodied Carbon Benchmark [3]

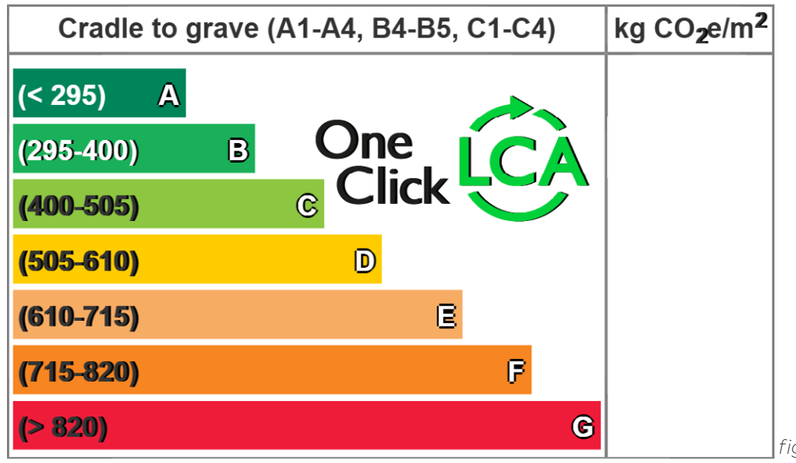

fig. 21

RIBA 2030 Benchmark

Alongside embodied carbon benchmarks, the RIBA 2030 Climate Challenge establishes a dedicated trajectory for operational energy, measured as Energy Use Intensity (EUI) in kWh/m²/year. While embodied carbon quantifies emissions tied to materials, construction, and end-of-life processing, the EUI evaluates continuous energy consumption throughout the building's operational life. Within a whole-life carbon framework, these two metrics are inherently complementary. [37]

The EUI metric is normalized by the building's Gross Internal Area (GIA) and encompasses both regulated loads (heating, cooling, ventilation, and lighting) and unregulated loads (plug-in equipment and IT appliances). Furthermore, on-site renewable generation directly offsets total consumption within the net EUI calculation. By accounting for total operational demand rather than standard regulatory baselines, this benchmark bridges the conventional 'performance gap', aligning projected figures with actual metered energy use rather than purely theoretical compliance models.

The RIBA operational trajectory for non-domestic office buildings is structured around two two phased threshold:

- 2025 Milestone: establishes an operational cap of 75 kWh/m²/year, serving as the minimum acceptable baseline for current design practice;
- 2030 Target: imposes a definitive requirement of 55 kWh/m²/year, necessary to achieve full alignment with long-term net-zero operational standards.

LETI Benchmark

Complementing the operational decarbonisation pathway set out by the RIBA 2030 Climate Challenge, the LETI framework evaluates embodied impacts across a graduated, letter-banded rating scale, functionally akin to the empirical Carbon Heroes classification. Rather than restricting the evaluation to initial construction stages, the assessment framework defines whole-life embodied carbon boundaries across a 60-year reference study period, capturing upfront material production and construction (modules A1–A5), recurring component replacements (module B4), and end-of-life disposal and processing (modules C3–C4), while excluding operational energy consumption (module B6) and external recovery credits (module D).

For the commercial office typology, this whole-life trajectory establishes an overarching 2030 design target of below 600 kgCO²eq⁄m² of GIA, which serves as the threshold for LETI Band A (aligned with the ultimate RIBA 2030 Climate Challenge ambitions). Progressive bands delineate higher levels of circularity and decarbonisation down to exemplary performance tiers (Band A+ at < 340\kgCO²eq⁄m² and Band A++ at < 150kgCO²eq⁄m²), while higher bands reflect intermediate transition baselines.

Because this scope covers the complete cradle-to-grave embodied cycle, the life-cycle results derived from the Bombyx model can be mapped directly onto the LETI Whole Life scale without requiring arbitrary disaggregation of upfront stages. [35] [36]

Proposed rating 'badge' [35]

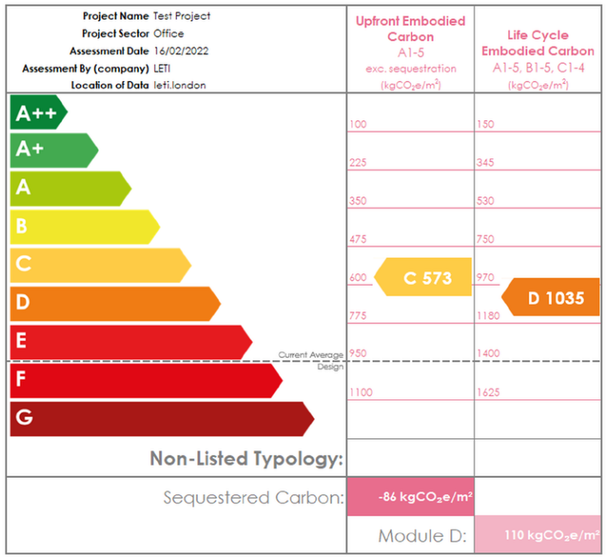

fig. 22

Life Cycle Embodied Carbon, A1-5, B1-5, C1-4 [35]

Band	Office	Residential (6+ storeys)	Education	Retail
A++	<150	<150	<125	<125
A+	<345	<300	<260	<250
A	<530	<450	<400	<380
B	<750	<625	<540	<535
C	<970	<800	<675	<690
D	<1180	<1000	<835	<870
E	<1400	<1200	<1000	<1050
F	<1625	<1400	<1175	<1250
G	<1900	<1600	<1350	<1450

fig. 23

RIBA 2030 Climate Challenge target metrics for non-domestic (new build offices) [37]

RIBA Sustainable Outcome Metrics	Business as usual (new build, compliance approach)	2025 Targets	2030 Targets	Notes
Operational Energy kWh/m²/y	130 kWh/m²/y DEC D (90)	< 75 kWh/m²/y DEC B (50) and/or NABERS Base build 5	< 55 kWh/m²/y DEC B (40) and/or NABERS Base build 6	Targets based on GIA. Figures include regulated & unregulated energy consumption irrespective of source (grid/renewables). 1. Use a 'Fabric First' approach 2. Minimise energy demand. Use efficient services and low carbon heat 3. Maximise onsite renewables
Embodied Carbon kgCO₂e/m²	1400 kgCO₂e/m²	< 970 kgCO₂e/m²	< 750 kgCO₂e/m²	Use RICS Whole Life Carbon (modules A1-A5, B1-B5, C1-C4 incl sequestration). Analysis should include minimum of 95% of cost, include substructure, superstructure, finishes, fixed FF&E, building services and associated refrigerant leakage. 1. Whole Life Carbon Analysis 2. Use circular economy strategies 3. Minimise offsetting & use as last resort. Use accredited, verifiable schemes (see checklist). BAU aligned with LETI band E; 2025 target aligned with LETI band C and 2030 target aligned with LETI band B.
Potable Water Use Litres/person/day	16 l/p/day (CIRA W11 benchmark)	< 13 l/p/day	< 10 l/p/day	CIBSE Guide G.

fig. 24

4

4. DESIGN SCENARIOS

The MIND District
PV Panels: Layout and Generation Modeling

4.1 Baseline: The building as currently under construction
- 4.1.1 Building's plans
- 4.1.2 Building's zones and schedules
- 4.1.3 Building's stratigraphies
- 4.1.4 Baseline Results: Operational and Embodied Carbon

4.2 Scenario 1: Material improvement strategy
- 4.2.1 Structural stratigraphies improvement
- 4.2.2 Façade stratigraphy improvement

4.3 Scenario 2: Baseline with Active Renewable Integration
- 4.3.1 Parametric Envelope Assessment: Glazing and Shading Variants on Baseline Geometry

4.4 Scenario 3: Horizon-Driven Envelope Strategies
- 4.4.1 Glazing and Shading Variants on Horizon Geometry

4.5 Scenario 4: Daylight optimization-Driven Envelope Strategies
- 4.5.1 Glazing and Shading Variants on Daylight optimization Geometry



fig. 25

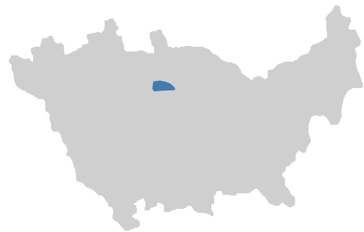

fig. 26

The study area is located within MIND - Milano Innovation District, developed on the former Expo 2015 site between the municipality of Milan and the north-western metropolitan belt (Rho-Pero).
At the macro scale, the district is situated within the north-western sector of the Metropolitan City of Milan and the Lombardy region, supported by transport infrastructure that connects the area to the regional and national networks. At the district and plot scale, the site is positioned within the western sector of the masterplan, embedded in an urban fabric composed of mixed-use blocks, pedestrian spaces, and green corridors. Within this context, the highlighted volume represents the specific building considered as the case study for the purposes of this thesis.



fig. 27

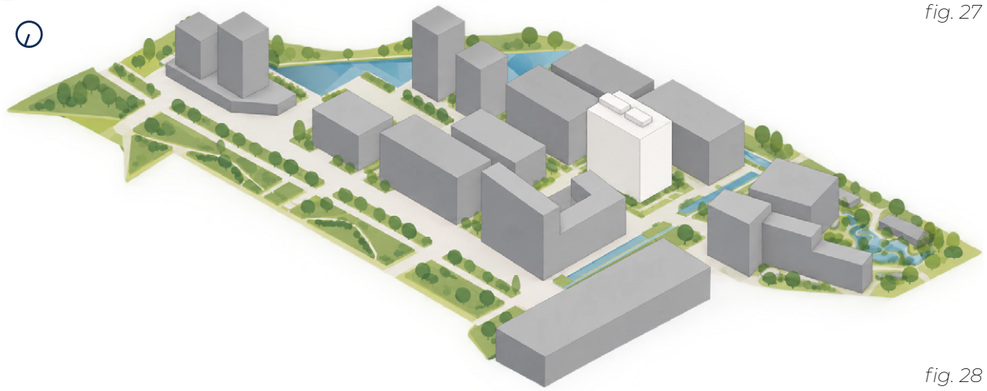

fig. 28

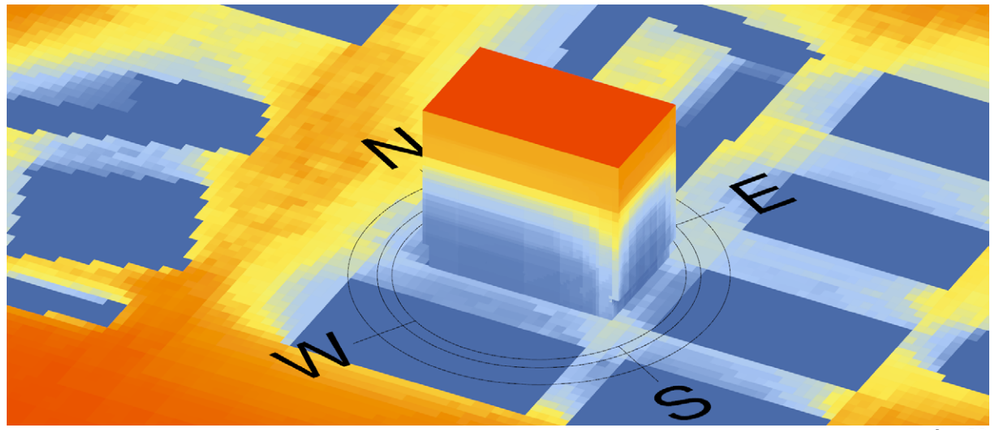

fig. 29

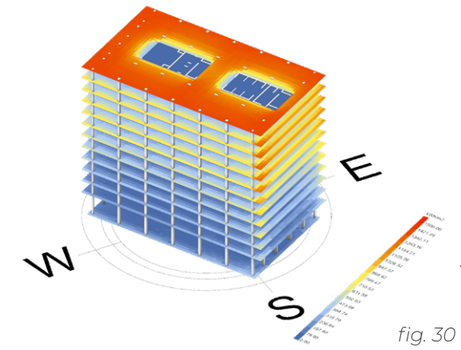

fig. 30

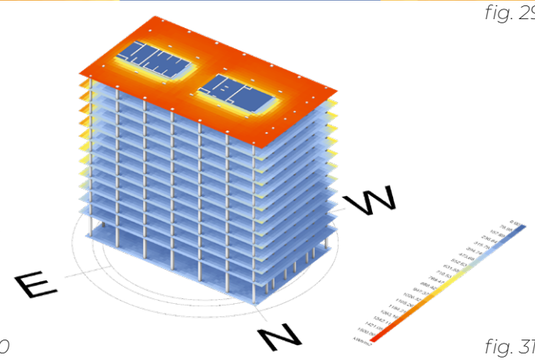

fig. 31

To evaluate the environmental conditions of the site, a solar radiation analysis was carried out, taking into account the obstruction caused by neighboring buildings.
As illustrated in the simulation, the surrounding urban massing significantly influences the lower portions of the building, casting substantial shadows across the ground level and lower storeys (indicated by the blue, low-exposure zones). Conversely, the upper levels and the roof surface remain entirely unobstructed, receiving direct and intense solar radiation throughout the year (represented by the warmer yellow-to-red gradients).
Furthermore, the orientation along the cardinal axes results in a pronounced differentiation between the facades: the southern and western exposures receive higher cumulative radiation during peak daylight hours, while the northern elevation remains predominantly shaded, highlighting distinct microclimatic conditions that directly inform facade design, daylighting potential, and thermal loads.

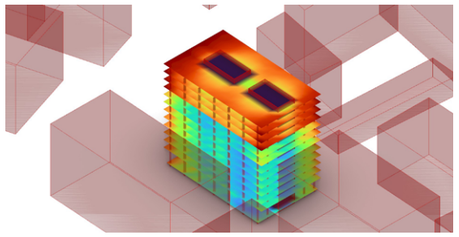

fig. 32

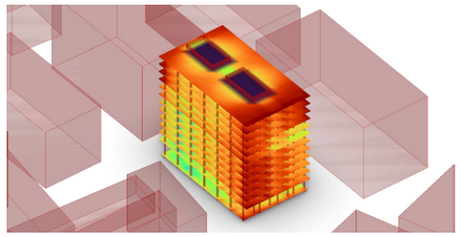

fig. 33

PV Panels: Layout and Generation Modeling

The integration of photovoltaic generation into the baseline configuration was treated not as the addition of a fixed technical component but as a geometric optimization problem, in which the productive capacity of the array is inseparable from the way the array occupies the surface available to it. The procedure was implemented in Grasshopper, coupling a parametric definition of the array geometry to an annual radiation simulation and to an evolutionary solver, so that layout and yield were resolved simultaneously rather than sequentially.
The first step consisted in isolating the surfaces of the envelope genuinely available for installation. The roof plane of the Zenith building was extracted from the executive model and reduced to a net usable area by subtracting the footprint of technical volumes and the perimeter setback required for access and safety. This distinction between gross and net surface is not merely bookkeeping: it fixes the upper bound of the entire scenario, and any generation figure reported downstream is conditioned by it. The resulting usable polygon of 1243.65 m² became the boundary within which all subsequent configurations were generated.
Three variables were then exposed as the genome of the parametric definition. The **tilt angle** of the modules, allowed to vary between 0° and 90°, governs the incidence of direct radiation across the year and, in the Milanese context, mediates between a steeper winter-favouring inclination and a shallower profile that privileges summer gains. The **azimuth orientation**, varied within ±90° of the system south, permits the array to start from the optimal orientation where the building geometry and the surrounding context makes such-start advantageous. With true north rotated by 55° relative to the building grid, true south corresponds to an orientation of 235° in model coordinates.
Finally the centre-to-centre **spacing** between consecutive module rows governs the density of occupation of the roof, with a spacing ranging between 0.8 m and 2.2 m.
These three parameters are not independent: any increase in tilt lengthens the shadow cast by each row and therefore demands a wider pitch to avoid mutual obstruction, so that the gain in per-module incidence is paid for in the number of modules the surface can accommodate. It is precisely this coupling that justifies treating the layout as an optimization problem rather than a design decision.

Annual incident radiation was computed through the Ladybug Tools environment, using the same site-specific EPW adopted for the energy model of the baseline so that the radiative assumptions underlying generation and those underlying the building's thermal behaviour remain consistent. Each module surface was discretized into an analysis mesh with a grid resolution of 0.50 m, and cumulative annual irradiation was calculated for each mesh face in kWh/m².
The simulation was run against the full context geometry rather than the isolated roof plane. The surrounding buildings of the MIND masterplan, together with the technical volumes and parapets of the Zenith building itself, were

included as shading context, allowing obstruction from the urban fabric to be resolved explicitly rather than approximated through a reduction coefficient. Row-to-row self-shading was captured by the same mechanism, since each modelled row acts as an obstruction for those behind it. This is the step that gives the pitch variable its physical meaning: without explicit self-shading, a denser array would always appear more productive, and the optimization would collapse to a trivial solution.
The search was conducted with the Galapagos evolutionary solver. The fitness function was defined as the total annual irradiation incident on the array, expressed in kWh rather than kWh/m², and set to be maximized. The choice of an absolute rather than a specific metric is deliberate and determines the character of the result: a per-square-metre objective would drive the solver toward a sparse array of individually well-oriented modules, whereas the cumulative formulation forces a balance between the performance of the single module and the number of modules the surface can host. The optimum goal is therefore the point at which the marginal irradiation lost to self-shading by adding one further row exceeds the irradiation that row itself contributes.
To accommodate variations in roof geometry and contextual exposure, the available roof surface was partitioned into distinct zones, with layout parameters optimized locally for each area. From the converged solutions, an aggregate total of 331 monocrystalline modules (1.3 m x1.1 m, ~320 Wp) was accommodated across the entire roof, corresponding to an overall active surface of 473.3 m² and a total installed capacity of 105.9 kWp.
Annual electricity generation was derived from the cumulative incident irradiation 784.6 MWh/yr by applying a module conversion efficiency of 22.5% and a performance ratio of 0.82, yielding an overall annual output of 144.8 MWh. [30]

This figure informs the subsequent performance assessments across two key domains. In the operational energy balance, on-site solar generation directly offsets the building's gross demand to establish the net delivered energy (reducing the operational EUI) from Scenario 2 onward.
In the Life Cycle Assessment, evaluated over the 60-year reference study period across the 25,705 m² gross floor area, the operational benefits were balanced directly against the system's embodied burdens:

- Operational Carbon Savings: The specific generation of 5.63 kWh/m²y avoids 1.13 kg CO_2-eq/m²y of operational emissions.
- Embodied Carbon Burden: The cradle-to-grave impact of the photovoltaic panels accounts for 0.112 kg CO_2-eq/m²y, representing less than 2% of the building's total embodied footprint.

The annual operational carbon savings exceed the annualized embodied carbon investment by an order of magnitude ~10:1. Consequently, the array fully offsets its cumulative life-cycle emissions in approximately 6 years (or under 2 years when considering the initial manufacturing phase alone), confirming an indisputable, net-positive whole-life carbon contribution.

4.1 Baseline: The building as currently under construction

The baseline represents the building as currently designed and under construction at the MIND . The case study is a 13-storey office building with a total conditioned floor area of 25,969.02 m². For the purposes of this study, the building is divided into eight thermal zones reflecting its functional organization:
two office zones (internal office, and external office), two service zones (core and underground), a lobby, a coffee shop, a bookshop and a bathroom block. The lobby and coffee shop share identical boundary conditions, with the exception that the lobby does not have domestic hot water demand. All zones operate on a common schedule, running from 07:00 to 19:00 on weekdays, each zone with specific variations, with no occupancy on weekends.
Each zone is assigned specific internal load profiles, including occupancy density, lighting, and equipment, which remain consistent across all subsequent scenarios and will be detailed in the following subsections.

To align the simulation with local socio-economic conditions, a 50% occupancy attenuation factor was applied during the month of August, reflecting the systemic reduction in building utilization associated with national summer holidays.
This approach avoids over-parameterizing the weekly schedule definitions while maintaining representativeness of real-world occupancy patterns.
The occupancy schedule is based on a typical occupancy in a building office in Milan.

Heating and cooling system schedules were defined in compliance with Italian regulation DPR 74/2013, which governs the activation periods of HVAC systems across climatic zones. Milan falls within Zone E, for which the permitted heating period runs from October 15th to April 15th.
Outside this window, the heating system operates exclusively in setback mode, maintaining a minimum indoor temperature of 12°C to prevent plant freezing, a standard threshold for the Milan climate and consistent with common practice in Italian building simulation.
On the other hand the cooling system does not have strict rules, but this thesis assumes the window to activate it between May 1st and September 30th.

The simulation findings are presented graphically through Energy Use Intensity (EUI) profiles, comprehensive energy balance diagrams, and GWP pie charts. The latter provide a detailed breakdown across individual building elements, enabling a direct comparative analysis of their respective lifecycle carbon contributions, and the comparison between the Operational carbon and the Embodied carbon.

4.1.2 Building’s plans

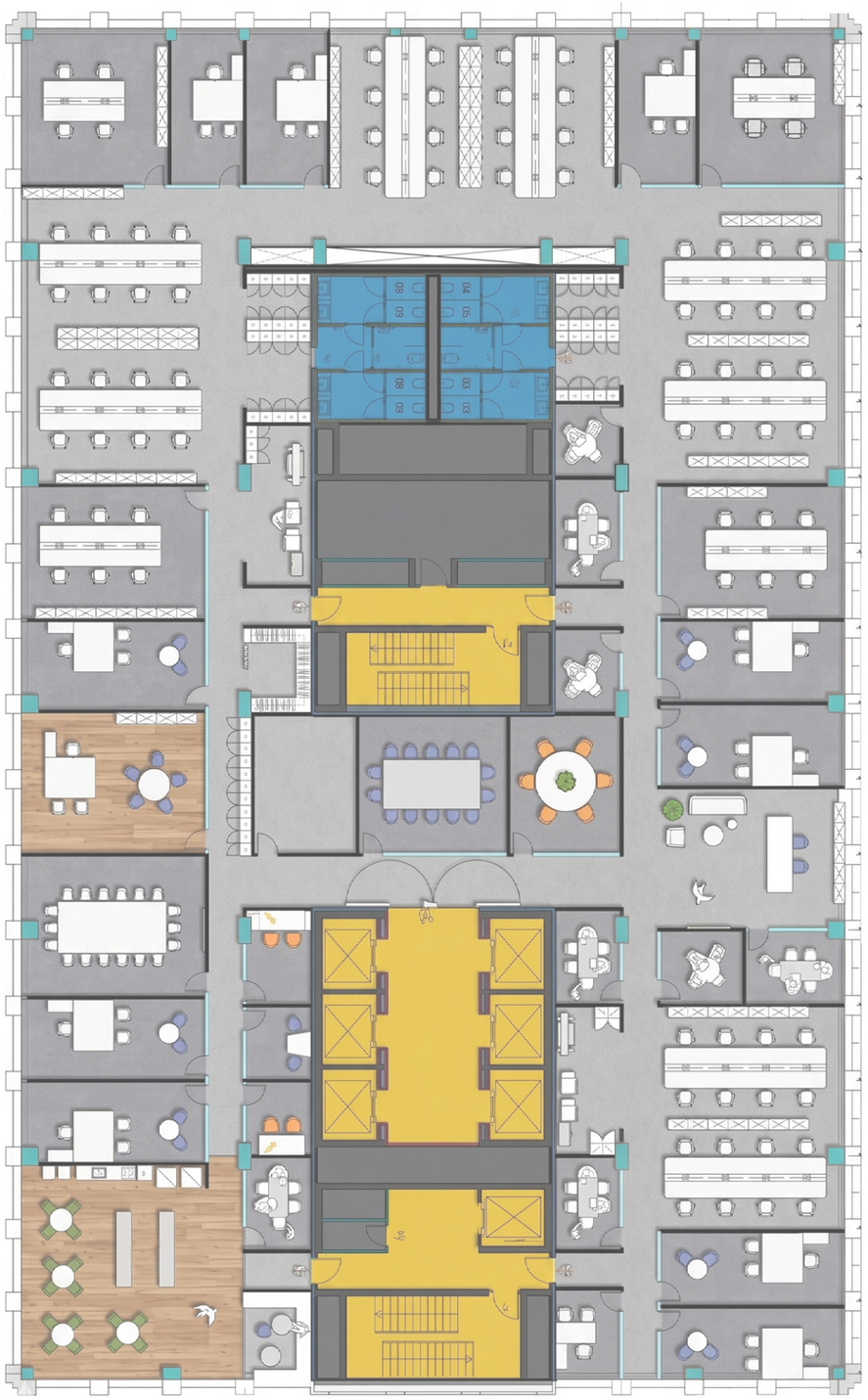

Monotenant

fig. 34



Bitenant

fig. 35

4.1.1 Building’s zones and schedules

The following subsections and graphical profiles detail the specific schedules, occupancy factors, and environmental settings assigned to each individual thermal zone.

Coffee Shop

The “Coffee Shop”, located at the groundfloor occupies an area of 720.26 m².

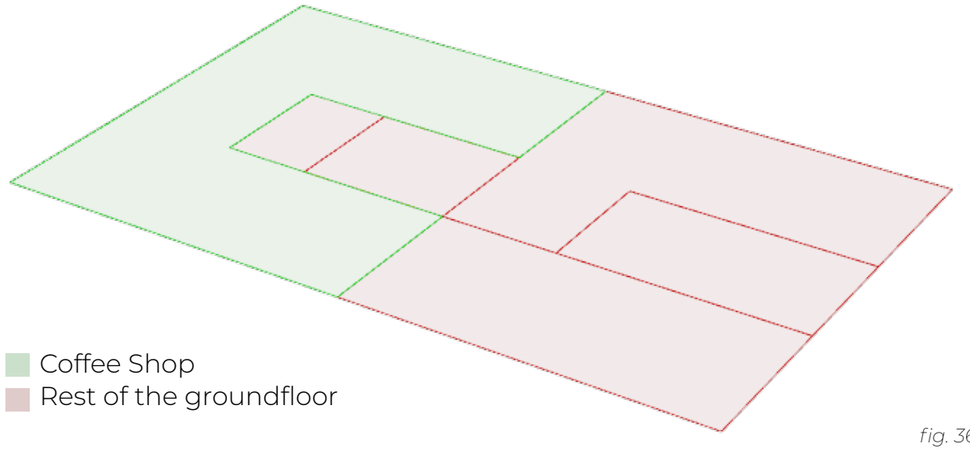

fig. 36

Coffee Shop’s Schedules

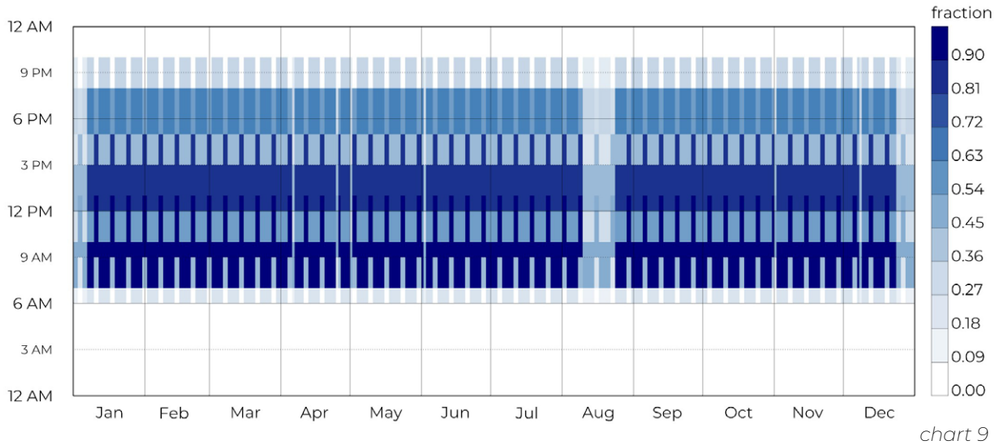

chart 9

Coffee Shop’s Setpoints

HVAC Parameter	Day Regime (07:00 – 22:00)	Night Regime (22:00 – 07:00)	Active Season
Heating Setpoint	20.0 °C	12.0 °C	Oct 15 – Apr 15
Cooling Setpoint	26.0 °C	38.0 °C (Off)	Jun 01 – Sep 15
Comfort Deadband	6.0 K	—	—

tab. 1

Coffee Shop’s Settings

people density	0.3	P/m²
metabolic rate	150	W/Person
equipment power density	15	W/m²
lighting power density	6	W/m²
H_2O flow rate per area	0.3	L/hm²
mechanical ventilation	3.5	ACH
Infiltration	0.0001	m³/sm²

tab. 2

Lobby

The “Lobby”, located at the groundfloor, occupies an area of 394 m²

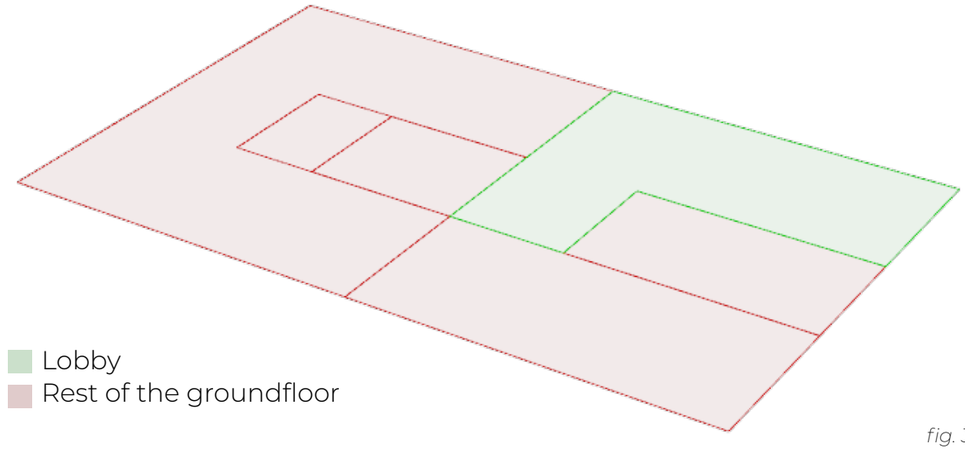

fig. 37

Lobby’s Schedules

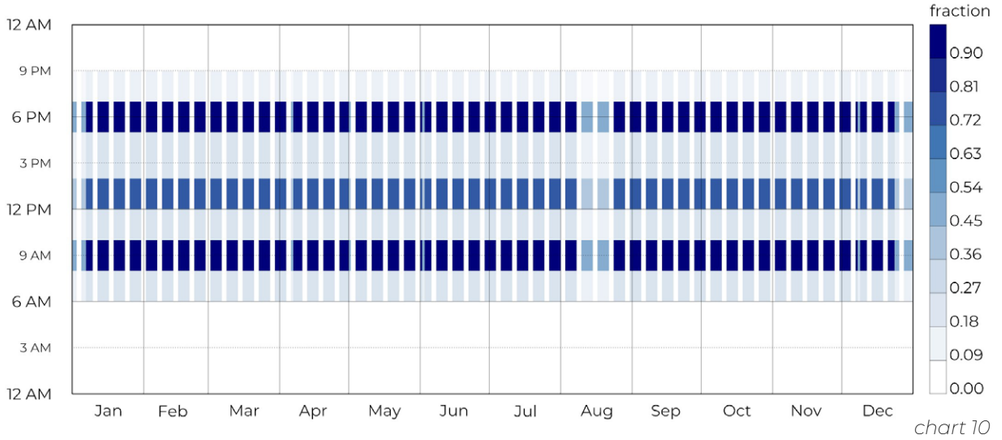

chart 10

Lobby's Setpoints

HVAC Parameter	Day Regime (06:00 – 21:00)	Night and Weekend Regime	Active Season
Heating Setpoint	20.0 °C	12.0 °C	Oct 15 – Apr 15
Cooling Setpoint	26.0 °C	38.0 °C (Off)	Jun 01 – Sep 15
Comfort Deadband	6.0 K	—	—

tab. 3

Lobby's Settings

people density	0.3	P/m²
metabolic rate	150	W/Person
equipment power density	11	W/m²
lighting power density	6	W/m²
mechanical ventilation	0.8	ACH
Infiltration	0.0001	m³/sm²

tab. 4

Bookshop and Perimeter Office

The "Bookshop", located at the groundfloor, occupies an area of 312.22 m²

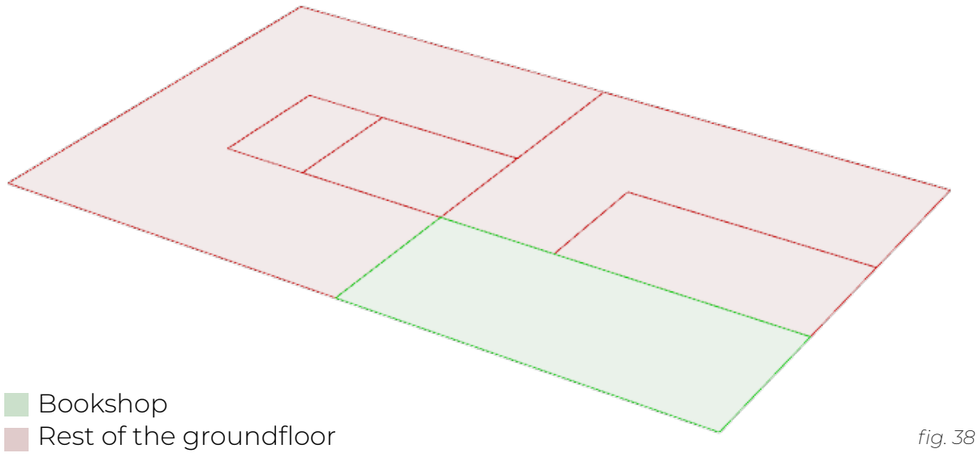

fig. 38

The "Perimeter Office" zone consolidates multiple individual office spaces that share the common feature of exterior glazing. For simulation simplicity, these spaces are aggregated into a single thermal zone due to their similarities.
The area of this zone is 1024.3 m².

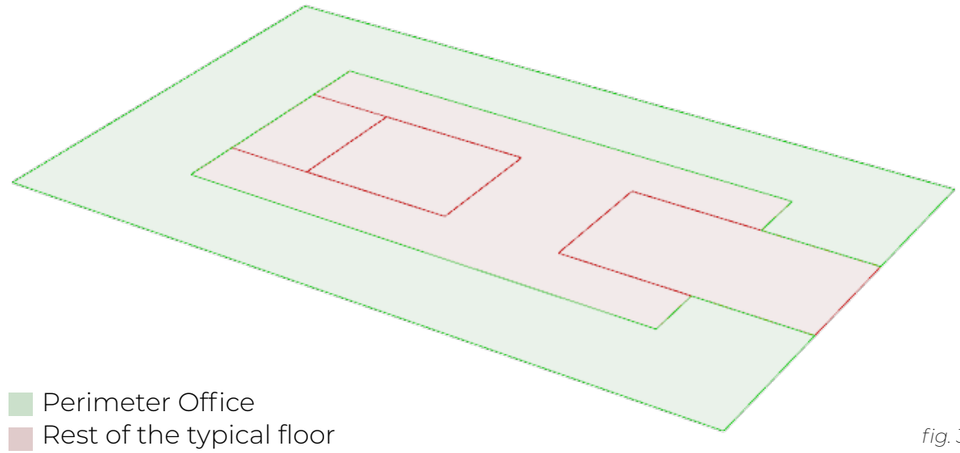

fig. 39

Bookshop and Perimeter Office's Schedules

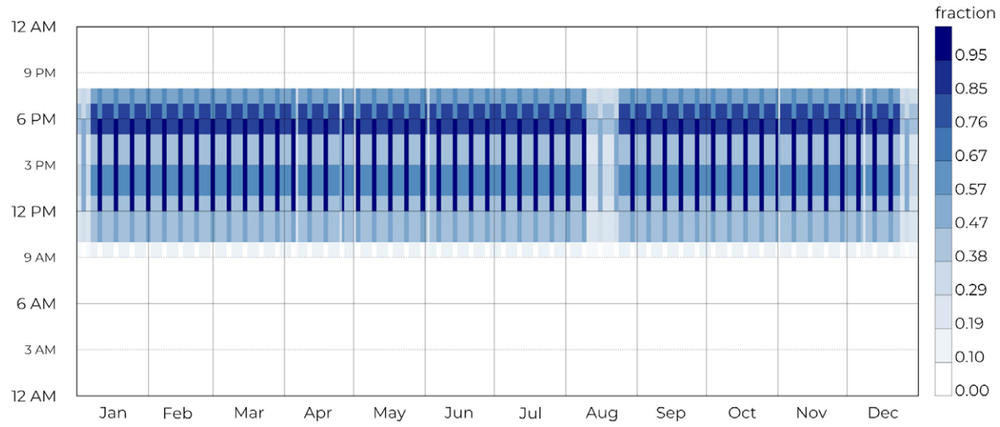

chart 11

Bookshop and Perimeter Office's Setpoints

HVAC Parameter	Day Regime (09:00 – 18:00)	Night and Weekend Regime	Active Season
Heating Setpoint	20.0 °C	12.0 °C	Oct 15 – Apr 15
Cooling Setpoint	26.0 °C	38.0 °C (Off)	Jun 01 – Sep 15
Comfort Deadband	6.0 K	—	—

tab. 5

Bookshop and Perimeter Office's Settings

people density	0.1	P/m²
metabolic rate	120	W/Person
equipment power density	11	W/m²
lighting power density	6	W/m²
mechanical ventilation	1.5	ACH
Infiltration	0.0001	m³/sm²

tab. 6

Core and Parking

The "Core" occupies a total area of 275.89 m². This zone will be the same for each type of floors: Groundfloor, Monotenant, Bitentant.

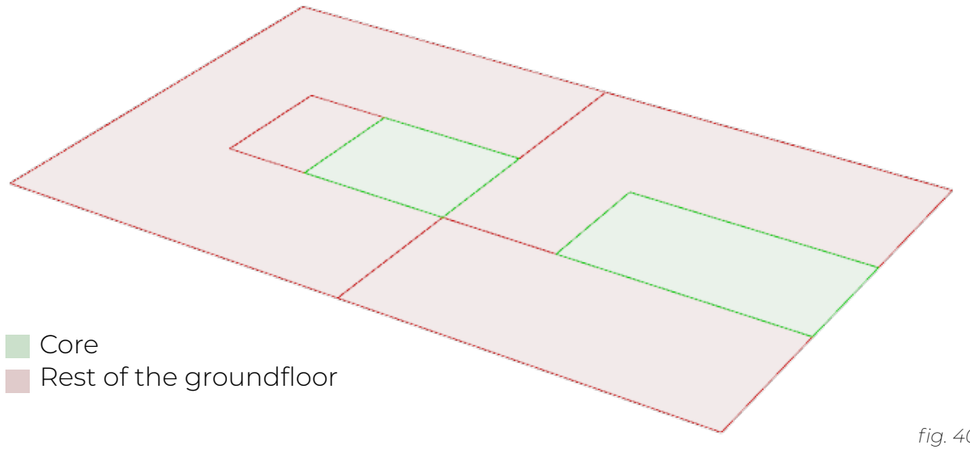

fig. 40

The "Parking" zone of the Zenith building consists of a 2,409.33 m² (estimated) underground space shared with neighboring constructions. This area is modeled as a single, unheated thermal zone.

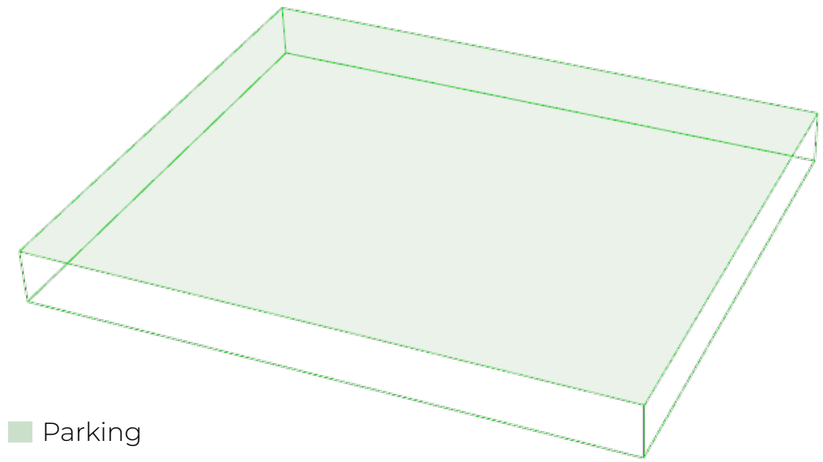

fig. 41

Reflecting the lack of mechanical conditioning and equipment appliances in these functional areas, the cooling availability matrix and equipment load schedules for the "Core adn Parking" zones are configured as "all off" across the entire simulation period.

Core and Parking's Schedules

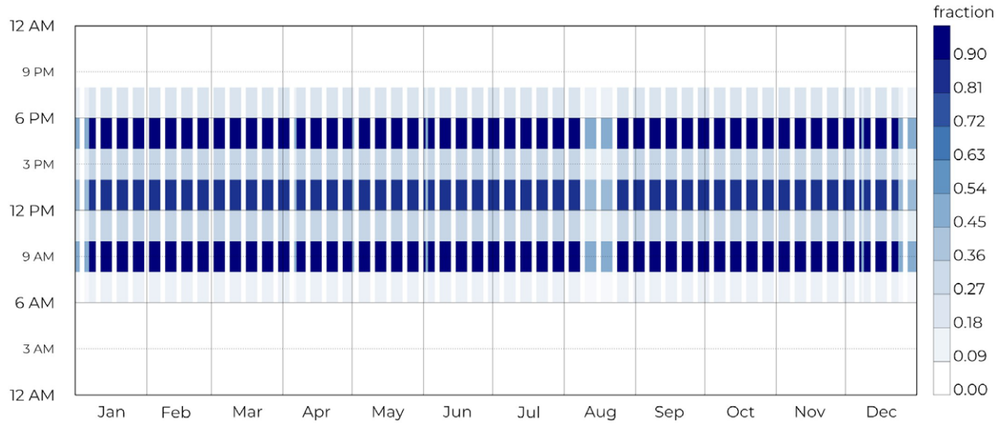

chart 12

Core and Parking's Setpoints

HVAC Parameter	Year-Round Regime (24/7)	Operational Status
Heating Setpoint	12.0 °C	Freeze Protection Only
Cooling Setpoint	free floating	Unconditioned
Comfort Deadband	—	No Active Conditioning

tab. 7

Core and Parking's Settings

people density	0.02	P/m²
metabolic rate	180	W/Person
equipment power density	0	W/m²
lighting power density	3	W/m²
mechanical ventilation	1.2	ACH
Infiltration	0.0001	m³/sm²

tab. 8

Restroom

The “Restroom” occupies an area of 60.16 m².
This zone will be the same for each type of floors: Groundfloor, Monotenant, Bitentant.

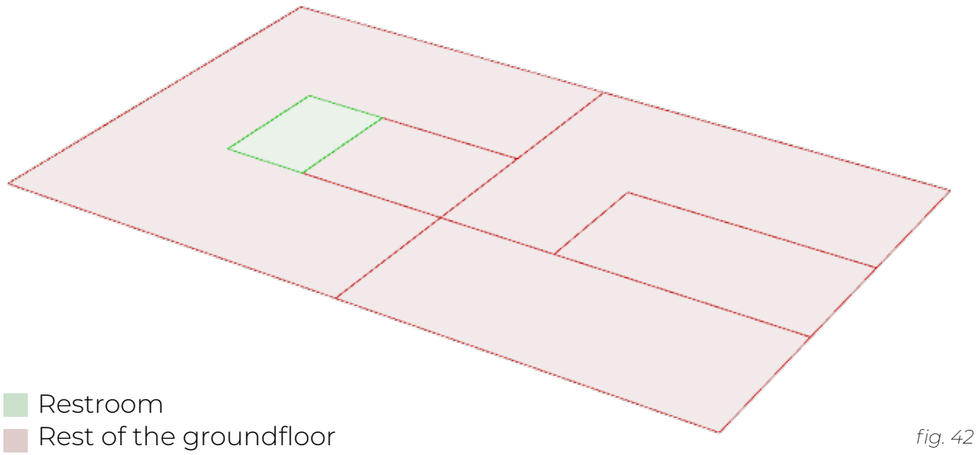

fig. 42

Restroom’s Schedules

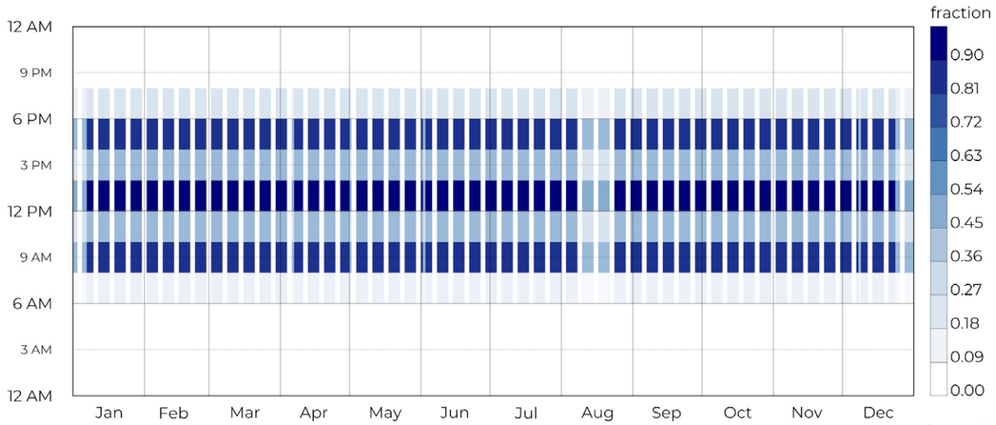

chart 13

Restroom’s Setpoints

HVAC Parameter	Day Regime (07:00 – 20:00)	Night / Weekend Regime	Active Season
Heating Setpoint	20.0 °C	12.0 °C	Oct 15 – Apr 15
Cooling Setpoint	26.0 °C	38.0 °C (Off)	Jun 01 – Sep 15
Comfort Deadband	6.0 K	—	—

tab. 9

Restroom’s Settings

people density	0.1	P/m²
metabolic rate	150	W/Person
equipment power density	2	W/m²
lighting power density	4	W/m²
H_2O flow rate per area	0.1	L/hm²
mechanical ventilation	4	ACH
Infiltration	0.0001	m³/sm²

tab. 10

Interior Office

The “Interior Office” zone consolidates multiple core office spaces that lack direct contact with the building envelope. For simulation simplicity, these deep-plan spaces are aggregated into a single thermal zone since they are entirely isolated from solar gains and outdoor weather variations, experiencing purely internal load dynamics.
The area of this zone is 402.18 m².

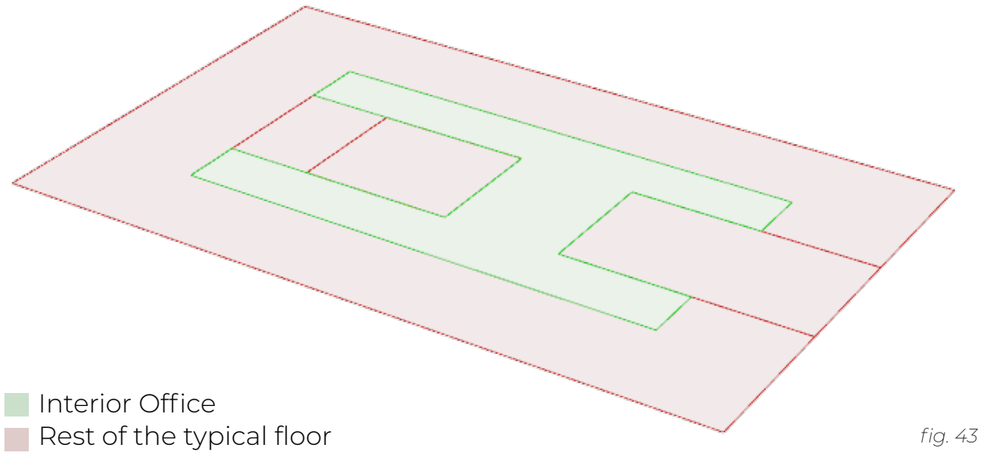

fig. 43

Interior Office's Schedules

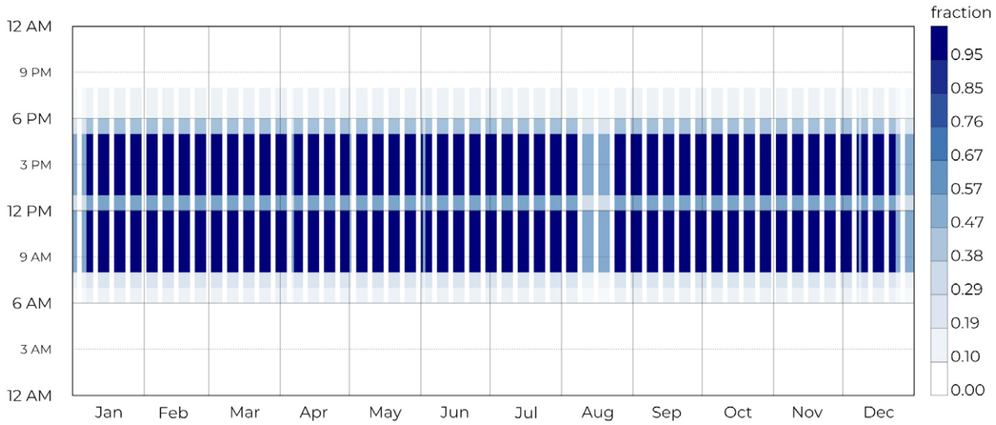

chart 14

Interior Office's Setpoints

HVAC Parameter	Day Regime (07:00 – 20:00)	Night / Weekend Regime	Active Season
Heating Setpoint	20.0 °C	12.0 °C	Oct 15 – Apr 15
Cooling Setpoint	26.0 °C	38.0 °C (Off)	Jun 01 – Sep 15
Comfort Deadband	6.0 K	—	—

tab. 11

Interior Office's Settings

people density	0.15	P/m²
metabolic rate	120	W/Person
equipment power density	22	W/m²
lighting power density	8	W/m²
mechanical ventilation	4.5	ACH
Infiltration	0.0001	m³/sm²

tab. 12

4.1.1 Building's stratigraphies

Alongside the scheduling assumptions, the thermal performance of the building envelope is governed by its stratigraphic composition. The U-values of walls, roof, floor slab and glazing, derived directly from the construction layers, constitute the key boundary condition linking energy demand to material choices, and are therefore presented in the following section before to the simulation results

LEGEND

1. Linoleum - 2.5mm
2. Glass wool - 2cm
3. Precast concrete - 5cm
4. Plywood - 2cm
5. Glulam - 6cm
6. Concrete tiles - 5cm
7. Precast concrete - 6cm
8. Bitumen waterproof membrane 5mm
9. XPS - 15cm
10. Structural RC - 20cm
11. XPS 10cm
12. Flax fibres (fireproof)- 2cm
13. Gypsum plasterboard- 2cm
14. Precast concrete - 10cm
15. Glassfibre reinforced concrete - 1.5cm
16. Glulam studs
17. XPS 5cm
18. Gypsum plasterboard - 1.6cm
19. Glass wool - 6.8cm
20. Window frame wood 1cm
21. Insulating glass, Double, U value 1.1 W/m2K - 9mm
22. Precast screed - 2 cm

TYPICAL SLAB



fig. 44

ROOF



fig. 45

GROUNDFLOOR SLAB

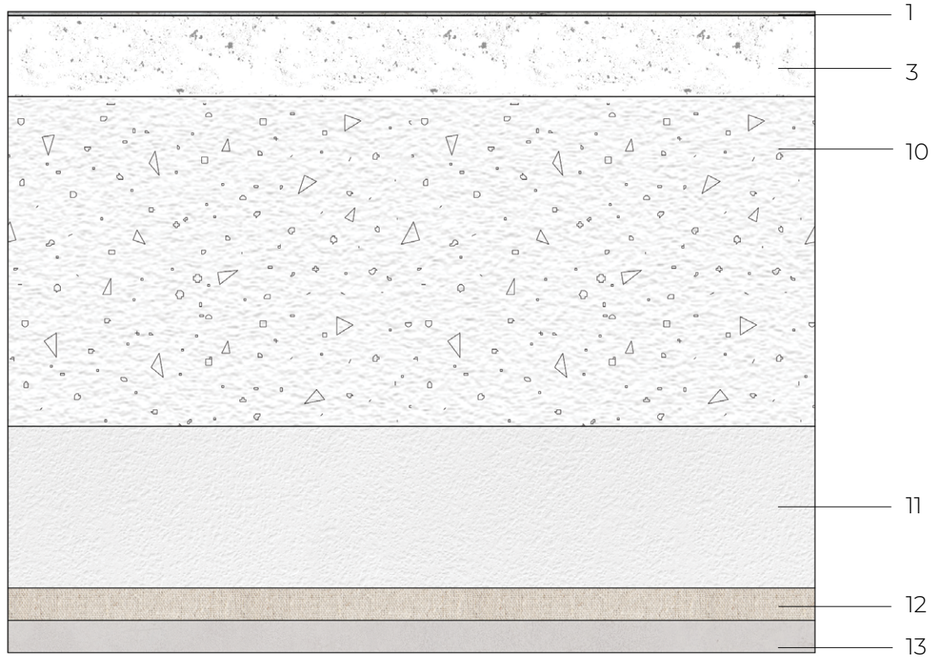

fig. 46

BASEMENT SLAB



fig. 47

FAÇADE

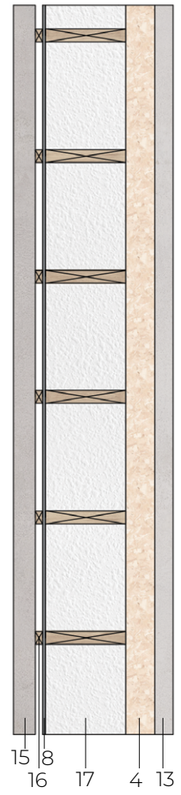

fig. 48

OPAQUE PARTITION

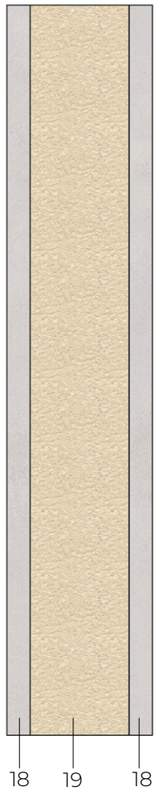

fig. 49

TRANSPARENT PARTITION

fig. 50

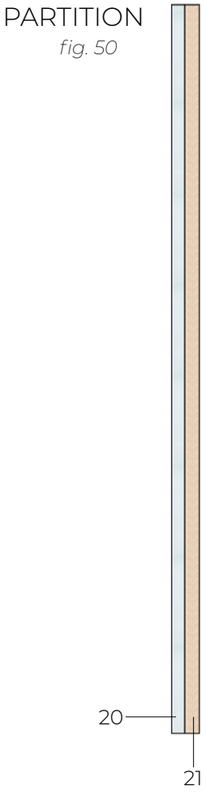

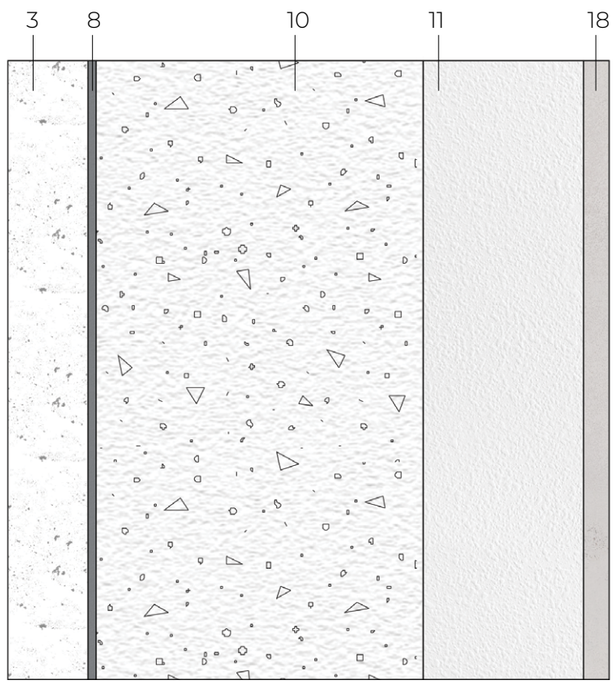

BASEMENT WALL

fig. 51

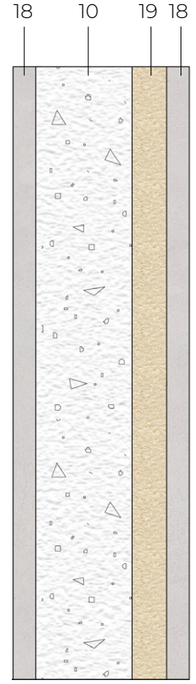

fig. 52

CORE WALL

4.1.4 Baseline Results: Operational and Embodied Carbon (S_00)

The preceding sections have described the building as it stands: its geometry, its occupancy regime, and the assemblies through which it exchanges heat with the Milanese climate.
This section closes the baseline by converting that description into the two quantities against which every subsequent scenario will be judged: the energy the building consumes in operation and the carbon embedded in the matter it is made of.

The distinction matters because the two behave differently in time.
Operational carbon accrues continuously and remains open to correction throughout the service life; embodied carbon is, for the most part, settled at the moment of construction and can only be influenced before the fact. Reporting both on a common annualised basis over the 60-year reference study period allows them to be read against one another, though the equivalence is one of accounting rather than of agency.

Read together, the results establish the terms of the optimisation that follows. The building is cooling-dominated, and its embodied burden is concentrated in elements largely fixed by the structural scheme, a configuration that narrows where meaningful reductions can be sought, and that the material and envelope strategies of Sections 4.2 and 4.3 are constructed to address.

S_00 Baseline Energy Balance

Before quantifying the baseline's carbon impact, the following figure presents the monthly energy balance across all load terms, establishing the seasonal drivers, a short heating season and a sharply peaked summer cooling load, that produce the 74.62 kWh/m²y EUI from which the operational carbon figure follows.

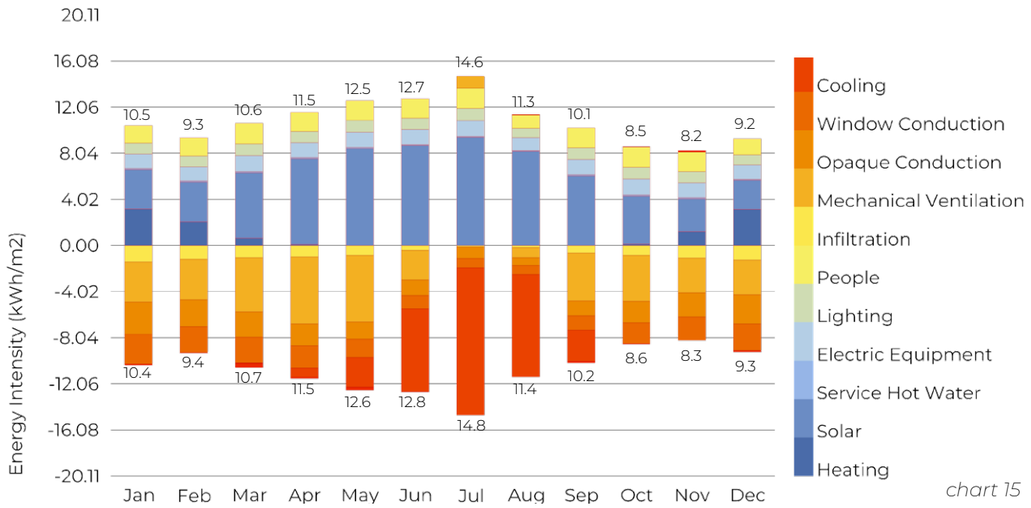

chart 15

S_00 Baseline GWP comparison

Building on that operational profile, these charts situate the baseline's total impact of 21.192 kgCO_2eq/m²y within its two constituent parts, establishing the operational–embodied split, both annually and in the life-expectancy of 60 years

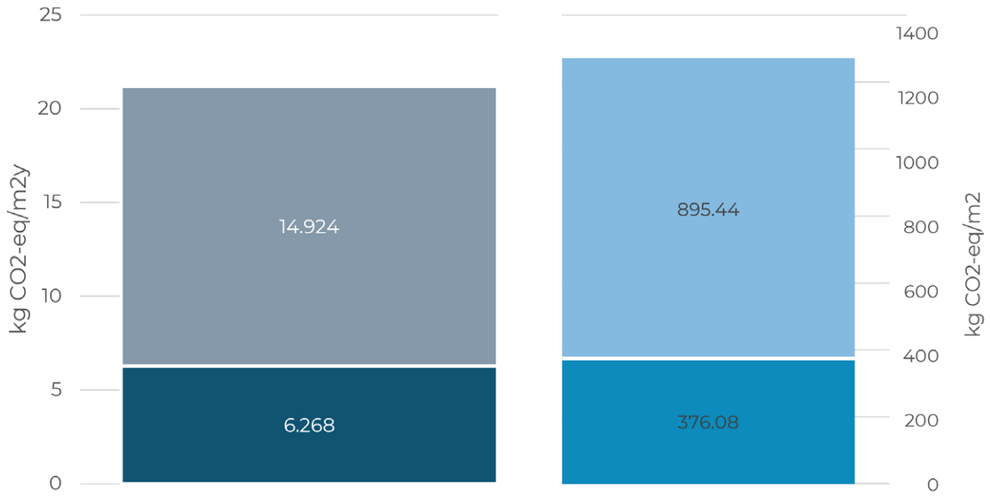

chart 16

Over a 60-year lifecycle, the S_00 Baseline registers 376.08 kg CO2-eq/m², slightly exceeding the 360 kg CO2-eq/m² limit for a Rank A rating in the Carbon HEROES benchmark and resulting in a Rank B classification.

S_00 Baseline Embodied Carbon breakdown

Having established the embodied share of the total, the following figures disaggregates that 6.268 kgCO_2eq/m²y across building elements, identifying where within the baseline's material composition the greatest reduction potential lies. The values are expressed in kg CO²-eq/m²y.

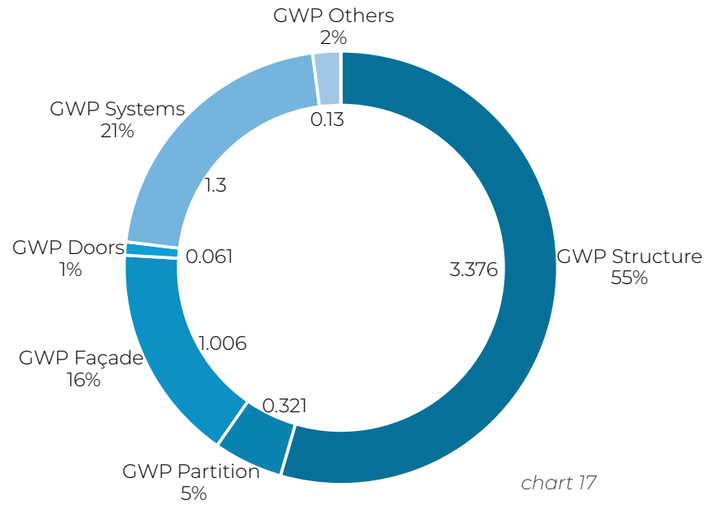

chart 17

4.2 Scenario 1: Material improvement strategy

Scenario 1 investigates the potential for whole-life carbon reduction through the targeted substitution of high-impact materials across the building assembly. The selection of components for substitution was informed by a preliminary sensitivity analysis conducted in Bombyx.
The substitution strategy focused on the material assemblies of the structural elements (which accounted for 55% of the baseline impact), the façade (16%), and the internal partitions (representing only 5% of the total embodied carbon). Collectively, these systems represent the most viable targets for embodied carbon reduction within the design.
In accordance with the GWP ranking provided in the baseline, the building systems (heat pump, mechanical ventilation, sanitary facilities and electrical system) were identified as significant contributors to operational and embodied carbon for 21% of the entire embodied carbon. However, given their functional constraints and the scope of this scenario, they were excluded from the material substitution exercise.
The scenario was structured as a cumulative, sequential process: material substitutions were first applied to the structural elements, and the resulting modified structural assembly then served as the baseline for the façade substitutions.
This layered approach allows the marginal carbon savings given by each building system to be isolated and evaluated independently, while simultaneously capturing the aggregate effect of the comprehensive material strategy.

4.2.1 Structural stratigraphies S_00A

The structural elements, such as the core shear walls, concrete columns and beams, timber beams and columns, floor and roof slabs, foundations, and basement slabs, were identified as the primary sources of embodied carbon within the baseline design.
This finding aligns with the broader literature on reinforced concrete and mass-timber hybrid constructions.
Consequently, the substitution strategy for this sub-scenario centered on the three material categories that dominate the structural assembly by mass and GWP impact: concrete, steel, and glulam as well as the high-impact insulation layers embodied within these structural stratigraphies.

Conventional ready-mix concrete was replaced with a low-carbon alternative: the *"Recycled concrete mixtures"* by *"Beton Lana GmbH/S.r.l."* [24].
This specific product was selected due to its high recycled aggregate content and geographic proximity to the MIND site in Milan, thereby minimizing potential transport-related emissions.
This approach represents a well-established strategy for reducing the carbon intensity of concrete without compromising structural performance.

Similarly, standard structural steel sections were substituted with recycled steel products, specifically *"Recycled Rebars"* from the *"Pittini Group"* [25], influencing substantially the GWP associated with electric arc furnace (EAF) production routes and the recycling of the steel.

For the timber components, the baseline glulam specification was substituted with *"RUBNER glulam"* from *"Rubner Holding AG - S.p.A."* [26]. This product was selected based on its lower declared GWP, as evidenced by its product-specific EPD. This type of optimization, replacing a material with a functionally equivalent alternative from a manufacturer with superior environmental credentials, reflects the growing differentiation within timber product markets; it highlights how early stage decisions can yield measurable carbon reductions without requiring modifications to the structural design. The biogenic carbon sequestration associated with the timber elements was accounted for in accordance with EN 15978 standards.
Finally, the baseline OSB panels were substituted with *"SWISS KRONO OSB-Platten"* by the "*SWISS KRONO Group"* [27], a choice driven by both its declared GWP and the logistics optimization regarding the MIND site.

Beyond the primary load-bearing materials, the optimization was extended to the thermal insulation layers integrated within the structural assemblies, specifically targeting the basement and roof stratigraphies. The baseline extruded polystyrene (XPS), characterized by a high embodied carbon footprint due to its manufacturing intensity, was substituted with an eco-efficient alternative, the *"Foam Glass"* provided by the KBOB database linked by Bombyx.
This material maintains the high insulating properties of the XPS, but introducing a significant improvement in the sustainability, since its composition is 100% from recycled glass pieces. This choice allowed for a meaningful reduction in the upfront emissions of the thermal envelope component without altering the required thermal resistance or the overall thickness of the structural build-ups.
In addition to the XPS, also the Glass Wool has been adapted to an even more sustainable material, once again provided by KBOB: "*Glass Wool, Isover, vegetable binder*" which consists of sand and recycled glass, with a binder combining organic and vegetable components.
Collectively, these strategic material substitutions successfully mitigate the high upfront carbon impacts typically associated with synthetic or conventional insulation assemblies, satisfying both thermal and acoustic performance requirements without compromising structural integrity.

Evaluated over the 60-year reference study period, the cumulative embodied carbon reaches 333.12 kg CO_2-eq/m². This reduction of 42.96 kg CO_2-eq/m² successfully brings the building below the 360 kg CO_2-eq/m² ceiling, elevating the structural baseline to Rank A in the Carbon Heroes benchmark.
In adherence to EN 15804+A2 and EN 15978 standards, biogenic carbon is accounted for separately and is not deducted from the fossil embodied GWP values reported above.
The engineered timber members introduce a permanent structural carbon

reservoir, storing 2.25 kg CO2-eq/m2y. This permanent biogenic storage further enhances the lifecycle performance of Scenario S_00A without masking upfront material manufacturing impacts.

4.2.2 Façade stratigraphy S_00B

Building upon the modified structural assembly established in the previous sub-scenario, material substitutions were subsequently applied to the façade elements.
The façade assembly represents a significant embodied carbon contribution owing to the high GWP of its insulation and cladding components, which were targeted in this phase. To maximize the GWP reduction, also the window frames were changed into a “PVC/PVC window frame” from the KBOB database.
Following this intervention, the embodied GWP decreased further to 323.04 kg CO_2-eq/m², bringing the total annual GWP to approximately 5.4 kg CO_2-eq/m²y. The relative share of the façade within the embodied breakdown lowers down to 15% and the values decreases from 1.006 kg CO_2-eq/m²y to 0.769 kg CO_2-eq/m²y.

chart 18

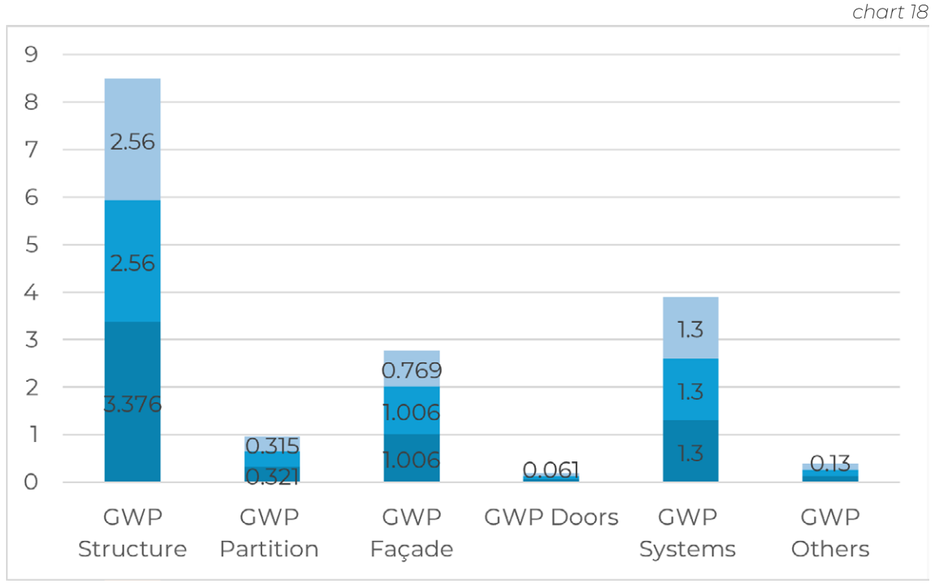

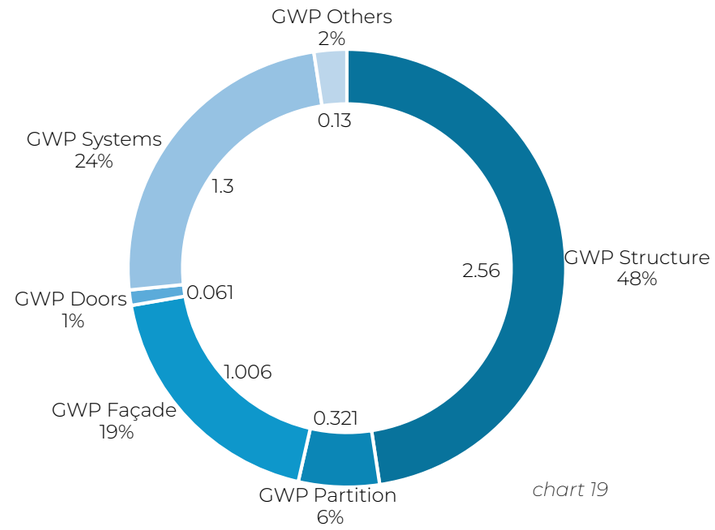

chart 19

From 6.194 kg CO_2-eq/m²y the GWP went down to 5.378 kg CO_2-eq/m²y

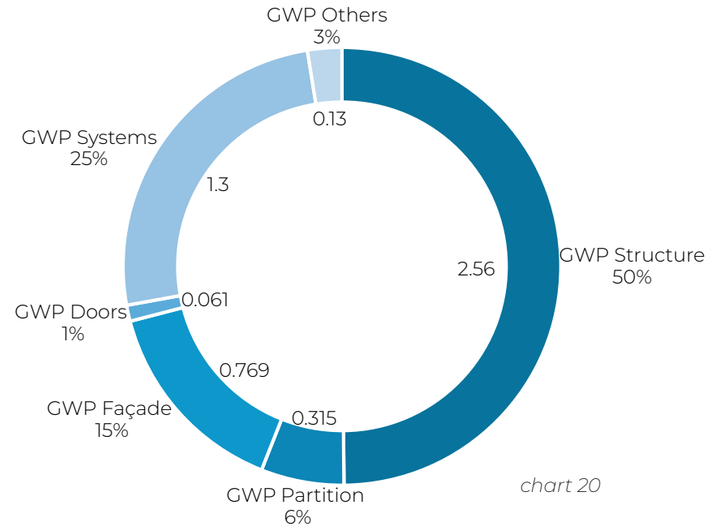

chart 20

From 5.378 kg CO_2-eq/m²y the GWP reduced even further, to 5.135 kg CO_2-eq/m²y

4.3 Scenario 2: Baseline with Active Reneweable Integrations

The computational workflow adopts a two-stage sequential optimization framework, resolving the photovoltaic (PV) array layout prior to conducting parametric envelope simulations (shading depths, glazing configurations, and WWR variations). This decoupling is justified by three technical principles:

- Physical Decoupling and Absence of Feedback Loops:
Rooftop solar generation is governed exclusively by astronomical vectors, local weather data, and inter-row shading geometries. It remains physically independent of vertical envelope thermophysical properties (e.g., U-values, SHGC, glazing assembly). Because envelope iterations exert zero feedback on rooftop solar yield, solving the PV geometry independently avoids redundant cross-coupling.
- Establishment of the On-Site Renewable Energy Budget:
Optimizing the PV layout first quantifies the maximum achievable on-site renewable generation potential (kWh/year) under site-specific geometric constraints. This value establishes a rigid renewable energy threshold, shifting subsequent parametric envelope variations from isolated demand-reduction exercises into a target-driven balancing process aimed at Net-Zero and operational carbon offset.
- Mitigation of the Curse of Dimensionality and Computational Overhead:
Combining array geometric variables (tilt, azimuth, pitch) with multi-variable façade iterations (shading geometry, double vs. triple glazing, WWR increments) within a single optimization solver would trigger a severe combinatorial explosion. Furthermore, PV incident radiation analysis relies on fast surface-based solar ray-tracing, whereas envelope evaluation requires computationally intensive dynamic thermal and daylighting engines. Decoupling these phases isolates the search spaces, accelerates algorithmic convergence in Galapagos, and ensures clear parametric attribution without noise from interrelated variables.

4.3.1 Parametric Envelope Assessment: Glazing and Shading Variants on Baseline Geometry

With the renewable contribution fixed at the beginning of this chapter, the geometry of Zenith is held at its baseline configuration: window-to-wall ratio unchanged from Section 4.1, no redistribution or resizing of openings.
What varies here is not the aperture itself but what governs the aperture's behavior, whether it is shaded, how, and to what degree it transmits. Four configurations test this space.

Configuration 1 retains the baseline glazing with no shading device, serving as the reference against which the following three are read.

Configuration 2 activates the horizontal blades already present on the façade as an architectural feature, treating them for the first time as a functioning solar control element rather than a decorative one.

Configuration 3 departs from a fixed shading geometry altogether, parameterizing the devices and optimizing their form against daylight performance rather than assuming a shape in advance.

Configuration 4 removes shading from the equation entirely and instead modifies the glazing's own transparency, testing whether the same control can be achieved through the assembly rather than an external device.

Read together, the four configurations separate three physically distinct strategies for managing solar gain at an unchanged opening, passive geometry already on the building, an optimized geometry designed for the purpose, and a change to the glass itself, allowing the results that follow to attribute performance differences to the control mechanism rather than to the aperture size, which Sections 4.4 and 4.5 hold as their own variable.
Each configuration consists in two different options: double glazing (2G) and triple glazing (3G).
The two options are presented together, so that they are directly comparable.

The difference between the 2G and the 3G options lies in the Uvalue and the SHGC considerated; for each configuration following along all the scenarios the Uvalue for 2G has been considered as 1 W/(m²K) and for the 3G 0.5 W/(m²K).
Similarly, the SHGC has a value of 0.5 for 2G and 0.25 for 3G.
Lastly, every configuration has a Benchmark evaluation, both for LETI/RIBA and for Carbon HEROES.
Reference Benchmarks:
RIBA 2030 Target: < 55 kWh/m²/yr
RIBA 2025 Target: < 110 kWh/m²/yr
LETI Target: 340 < Band A < 600
Carbon HEROES: Rank A <360

Detailed outputs and extended performance matrices for each simulated configuration are available in Annex II

Configuration 1: No shadings

Configuration 1 establishes the reference condition for Scenario 2: the baseline glazing left unshaded, with insulation thickness re-optimized independently of the façade improvements explored in Section 4.2. This isolates what insulation alone can achieve once the building's active generation is fixed and no solar control is introduced at the aperture, setting the term against which Configurations 2 through 4 will be read.

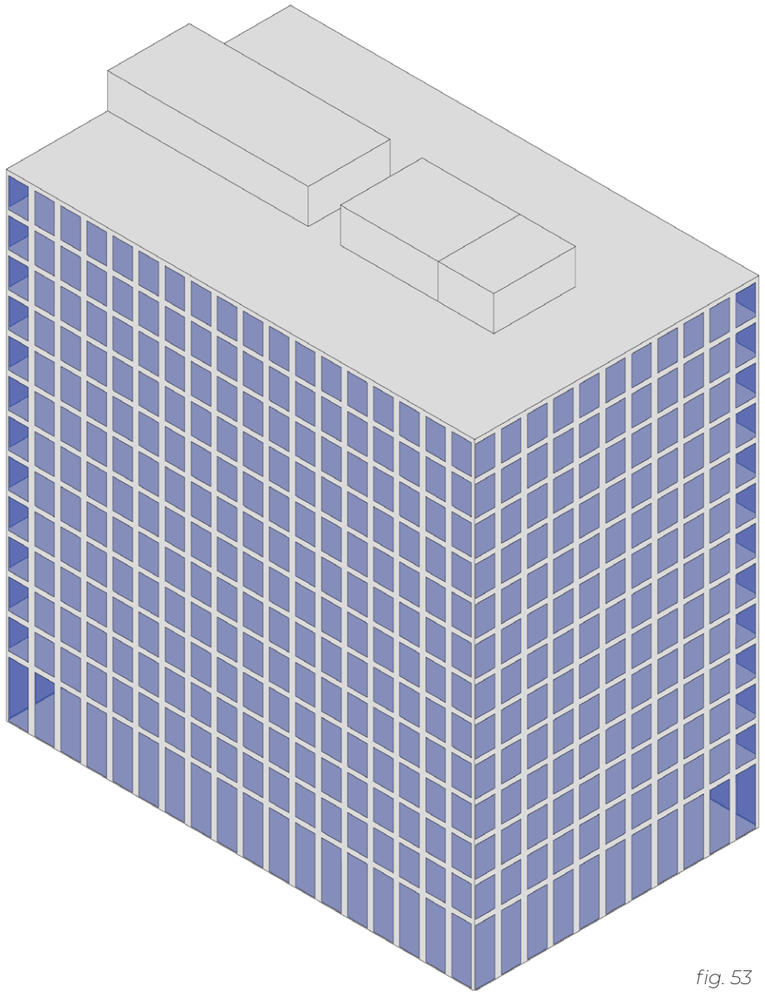

fig. 53

S_20 B 2G NS

With an optimal insulation thickness of 0.259 m, S_20 reaches an EUI of 59.178 kWh/m²y, a clear improvement on the 74.62 kWh/m²y of S_00 B. Two effects compound here: the re-optimized insulation reduces the building's own heating and cooling demand, while the photovoltaic array described at the beginning of this chapter is netted off the energy balance before the EUI is computed.

Over the 60-year reference period, embodied and operational GWP settle at 339.54 and 710.139 $kgCO_2$-eq/m² respectively. The façade's embodied contribution rises from 0.769 to 0.93 $kgCO_2$-eq/m²y, a increase that comes from the insulation build-up and the PV panel materials, and one that the operational savings easily offset.

Parameters	Operational Energy	Embodied Carbon
Design Value	59.178	339.54
RIBA/LETI	Compliant 2025 Target	Band A+
Carbon HEROES	N/A	Rank A

tab. 13

S_23 B 3G NS

Triple glazing with a thicker optimum (0.295 m) lowers the EUI to 50.286 kWh/m²y, 15% below S_20, and brings the design under the LETI/RIBA 2030 threshold. The gain stems from the lower U-value combined with a much lower solar heat gain coefficient, which trims peak cooling loads even without external shading. The embodied price is modest: façade-related GWP rises to 1.166 $kgCO_2$-eq/m²y and the 60-year embodied total to 353.76 $kgCO_2$-eq/m², yet whole-life GWP falls to 957.193 $kgCO_2$-eq/m², about 8.8% below S_20, with Carbon HEROES Rank A retained.

Parameters	Operational Energy	Embodied Carbon
Design Value	50.286	353.76
RIBA/LETI	Compliant 2030 Target	Band A
Carbon HEROES	N/A	Rank A

tab. 14

With Operational Energy in kWh/m²y, Embodied Carbon in $kgCO_2$-eq/m²y
N/A stands for Non Applicable

These two Scenarios share the sDa-ASE*Area/Total Area of 37.27%

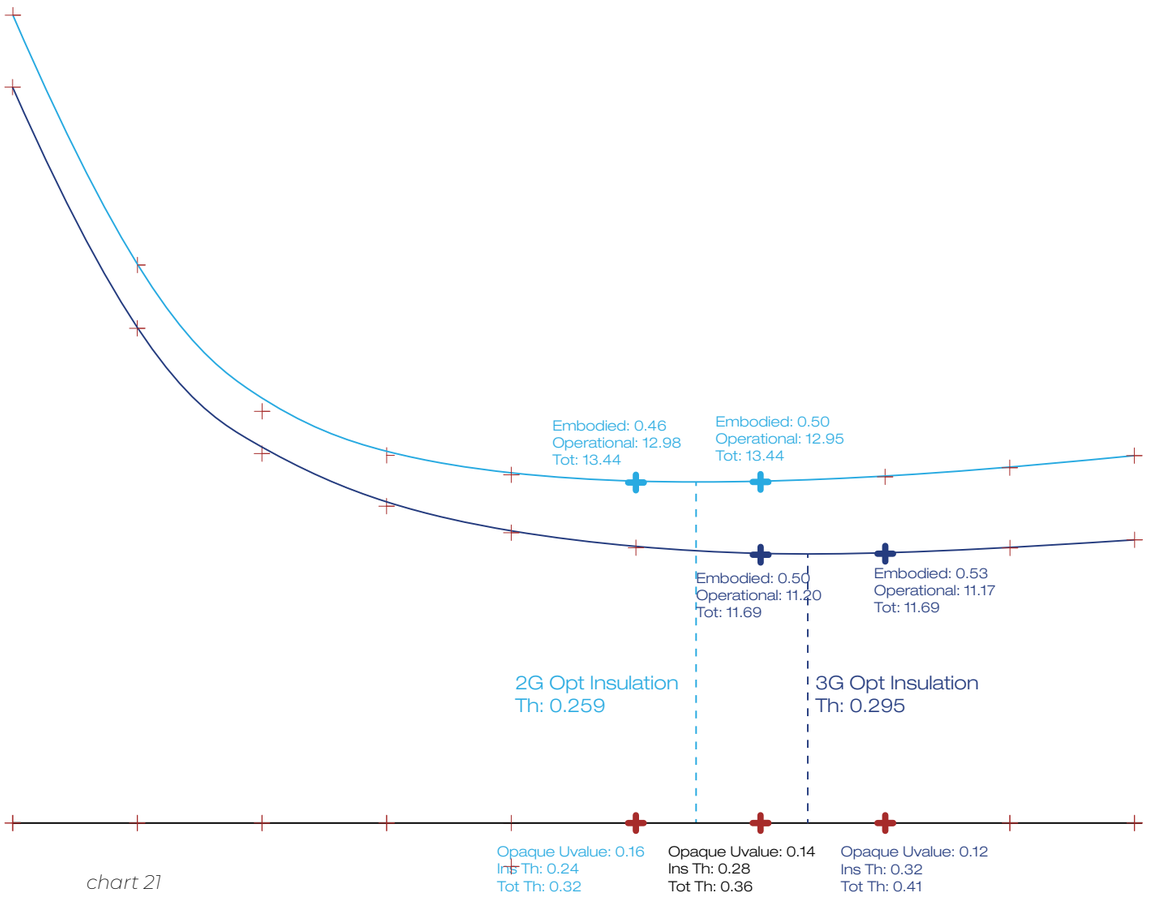

chart 21

Comparing the life-cycle GWP optimization curves, the move from double to triple glazing shifts the optimal insulation thickness from 0.259 m (U-value 0.15 W/m²K) to 0.295 m (U-value 0.13 W/m²K).

Better glazing would seem to call for less opaque insulation, but the outcomes of this research show that the shift runs the other way because of how the envelope's thermal balance interacts with whole-life carbon:

In a 2G configuration, the glazing is the dominant path for heat loss, so beyond 0.259 m the extra wall insulation saves too little operational energy to repay its own embodied carbon. Triple glazing closes that path, and the opaque envelope becomes an effective lever again, able to justify the embodied carbon of a further 3.6 cm of insulation.

The optimization trajectories show the same logic at the level of total emissions: the 3G curve is flatter and sits at a much lower level, 11.69 kgCO_2-eq/m²y against 13.44 for 2G. Its inflection point, where the linear growth of embodied carbon overtakes the diminishing operational savings, moves toward a thicker, higher-performing opaque assembly.

Configuration 2: Existing Façade Blades as Shading Devices

Configuration 2 tests an opportunistic retrofit strategy by functionally activating the building's existing horizontal blades. Rather than introducing new external shading elements or altering the original envelope geometry, this scenario investigates how much solar protection can be harvested directly from components already present as architectural features on the façade. By re-evaluating these elements as active passive-control devices rather than purely decorative accents, the analysis establishes whether baseline geometries can meaningfully mitigate cooling loads and reduce thermal stress at the aperture before resorting to bespoke or parametric interventions.

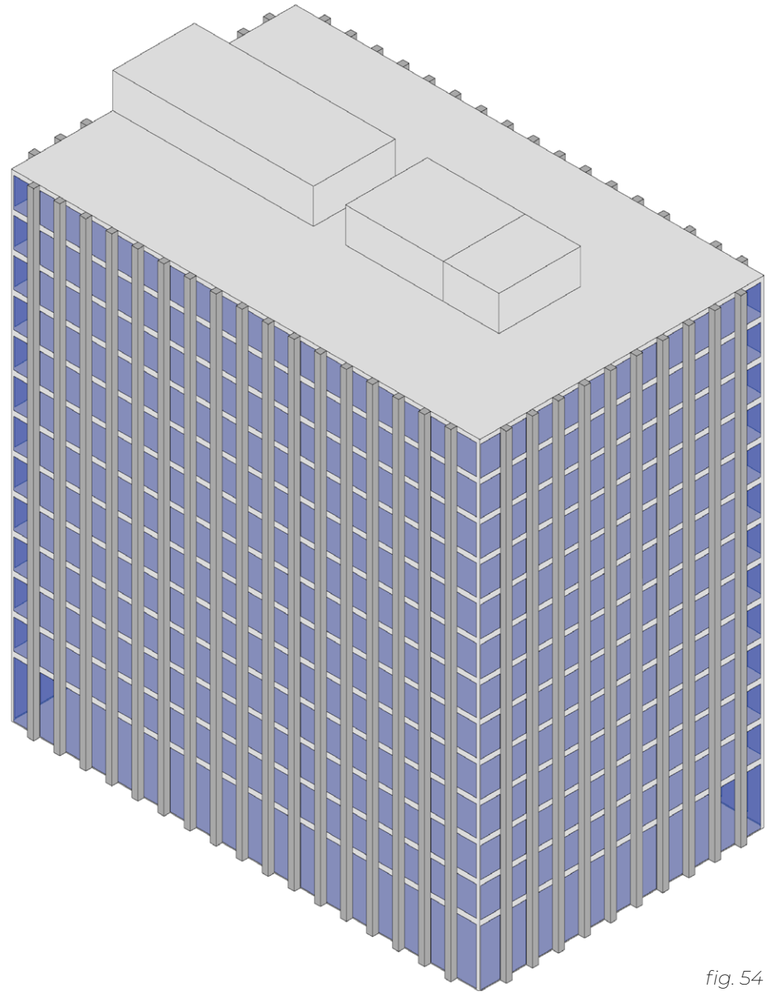

fig. 54

S_21 B 2G BL

With an optimal insulation thickness of 0.268 m, S_21 reaches an EUI of 56.222 kWh/m²y, which satisfies the LETI/RIBA 2025 target but stays just outside the stricter 2030 threshold. The result is about 3 kWh/m²y below S_20, a gain shared between the blades and a slightly thicker optimum. It also suggests that passive insulation is approaching diminishing returns at this aperture ratio (WWR 0.54).

Parameters	Operational Energy	Embodied Carbon
Design Value	56.222	358.02
RIBA/LETI	Compliant 2025 Target	Band A
Carbon HEROES	N/A	Rank A

tab. 15

S_24 B 3G BL

Triple glazing moves the carbon-optimal insulation to 0.295 m and the EUI to 48.593 kWh/m²y, 13.6% below S_21 and within the 2030 target. Lower conduction losses and tempered solar gains let the thicker opaque assembly work at full effect across the constant 0.54 WWR.

The cost is upfront. Façade-related emissions rise to 1.467 $kgCO_2$-eq/m²y and the 60-year embodied total to 371.82 $kgCO_2$-eq/m², dropping Carbon HEROES to Rank B while LETI Band A holds. Operational savings still dominate: whole-life GWP falls to 954.937 $kgCO_2$-eq/m² (15.916 $kgCO_2$-eq/m²y), 7.5% below S_21, with 2.29 $kgCO_2$-eq/m²y of biogenic carbon storage. Against the unshaded S_23, however, the blades buy very little: 957.193 versus 954.937 $kgCO_2$-eq/m², in exchange for roughly 18 $kgCO_2$-eq/m² of additional embodied carbon.

Parameters	Operational Energy	Embodied Carbon
Design Value	48.593	371.82
RIBA/LETI	Compliant 2030 Target	Band A
Carbon HEROES	N/A	Rank B

tab. 16

With Operational Energy in kWh/m²y, Embodied Carbon in $kgCO_2$-eq/m²y
N/A stands for Non Applicable

These two Scenarios share the sDa-ASE*Area/Total Area of 39.35%

For brevity, the optimization curves of the remaining configurations are deferred to Annex II. They behave as in Configuration 1, with triple glazing systematically pushing the carbon-optimal insulation to a greater thickness.

Configuration 3: Aperture-Specific Parametric Shading Optimization

Configuration 3 departs from uniform envelope treatments by introducing a computational, aperture-specific optimization of the shading devices. Recognizing that solar radiation and daylight accessibility vary significantly across floor levels and orientations, the geometry of each device is independently calibrated to balance internal illuminance against cooling load mitigation while strictly minimizing the added material mass. By tailoring the depth, profile, and placement of each louvre to the precise physical exposure of its corresponding opening, this scenario explores whether non-standardized, highly differentiated envelope assemblies can yield substantial operational savings without incurring a disproportionate embodied carbon penalty.

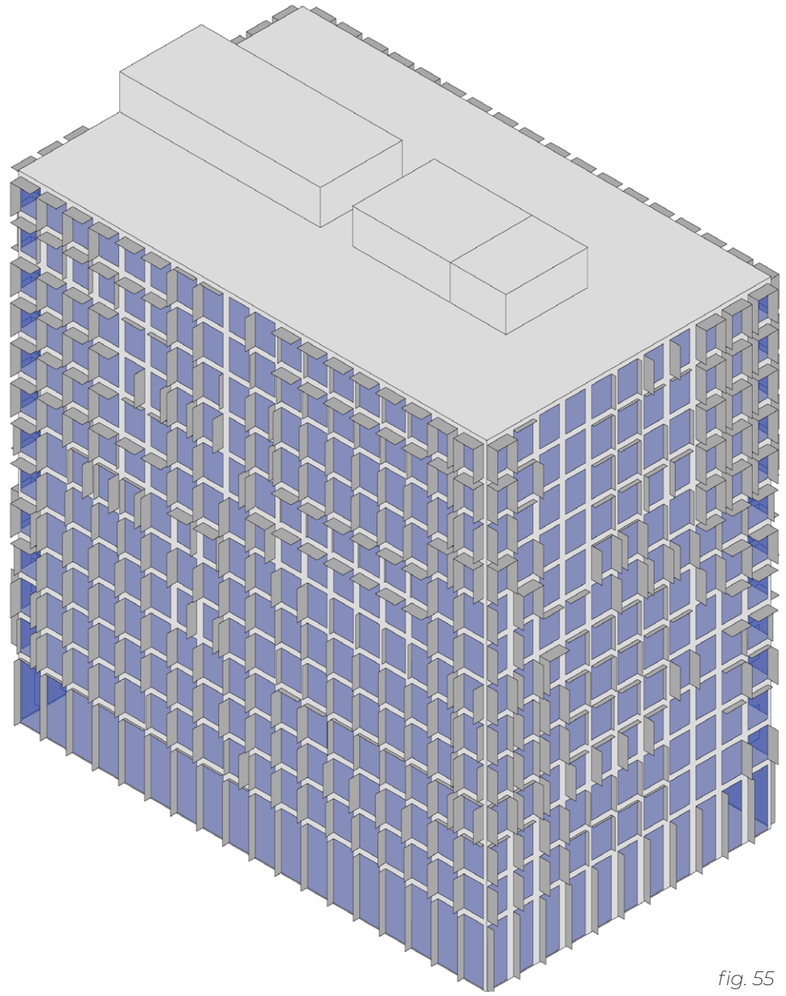

fig. 55

S_22 B 2G OS

S_22 reaches an operational demand of 54.078 kWh/m²y at an optimal insulation thickness of 0.288 m, entering the LETI/RIBA 2030 compliance domain, which neither S_20 nor S_21 managed. It stays 2.1 kWh/m²y below the blades of S_21 with only a moderate thickening of the opaque layer. The façade contributes 1.088 $kgCO_2$-eq/m²y and the 60-year embodied footprint is 349.02 $kgCO_2$-eq/m², enough for LETI Band A and Carbon HEROES Rank A. With an operational GWP of 648.939 $kgCO_2$-eq/m², whole-life impact totals 997.959 $kgCO_2$-eq/m² (16.633 $kgCO_2$-eq/m²y), about 5% below S_20, with 2.29 $kgCO_2$-eq/m²y of biogenic storage.

Parameters	Operational Energy	Embodied Carbon
Design Value	54.078	349.02
RIBA/LETI	Compliant 2030 Target	Band A
Carbon HEROES	N/A	Rank A

tab. 17

S_25 B 3G OS

Triple glazing pushes the carbon-optimal insulation past thirty centimeters (0.302 m) and lowers the EUI to 47.543 kWh/m²y, 12.1% below S_22.

The third pane and the extra insulation raise the façade's contribution to 1.307 $kgCO_2$-eq/m²y and the embodied footprint to 362.22 $kgCO_2$-eq/m², moving Carbon HEROES to Rank B with LETI Band A intact. The whole-life balance still improves, to 932.736 $kgCO_2$-eq/m² (15.546 $kgCO_2$-eq/m²y), 6.5% below S_22. Compared with the blades of S_24, the optimized shading reaches a lower whole-life total (932.736 versus 954.937) while carrying about 9.6 $kgCO_2$-eq/m² less embodied carbon.

Parameters	Operational Energy	Embodied Carbon
Design Value	47.543	362.22
RIBA/LETI	Compliant 2030 Target	Band A
Carbon HEROES	N/A	Rank B

tab. 18

With Operational Energy in kWh/m²y, Embodied Carbon in $kgCO_2$-eq/m²y
N/A stands for Non Applicable

These two Scenarios share the sDa-ASE*Area/Total Area of 41.79%

Configuration 4: Modified Visual Transmittance

The Modified Visual Transmittance configuration explores a streamlined envelope strategy where physical solar shading devices are intentionally omitted in favor of an optically recalibrated glazing assembly.
By altering the visual transmittance and associated solar optical properties of the glass panes, this design seeks to control excessive interior illuminance and solar heat gains at the envelope surface without adding exterior louvers or overhangs. From a whole-life carbon perspective, this setup isolates the pure energetic trade-off of transparent assemblies: it eliminates the upfront embodied carbon, bracketry materials, and maintenance requirements associated with exterior shading infrastructure, relying entirely on the selective solar filtering of the glazing paired with an optimized opaque insulation layer to manage thermal comfort and operational demand.
Unlike the previous configurations, a dedicated visual render is omitted here, as the geometric layout and external appearance are identical to Configuration 1 (No shadings).

S_28 B 2G VT

Without solar control elements, S_28 records an EUI of 64.548 kWh/m²y at an optimal insulation thickness of 0.260 m, the highest demand among the double-glazed variants of Scenario 2, though still within the LETI/RIBA 2025 target. It also sits about 9% above S_20, so the optical modification does not improve on the original glazing when nothing shades it. The light envelope keeps the façade at 0.931 $kgCO_2$-eq/m²y and the 60-year embodied carbon at 339.54 $kgCO_2$-eq/m², matching S_20 and earning LETI Band A+ and Carbon HEROES Rank A. Whole-life emissions reach 1114.12 $kgCO_2$-eq/m² (18.569 $kgCO_2$-eq/m²y).

Parameters	Operational Energy	Embodied Carbon
Design Value	64.548	339.54
RIBA/LETI	Compliant 2025 Target	Band A+
Carbon HEROES	N/A	Rank A

tab. 19

S_29 B 3G VT

With triple glazing, the optimum moves to 0.295 m and the EUI falls to 50.282 kWh/m²y, a 22.1% reduction that brings full LETI/RIBA 2030 compliance despite the absence of shading. Façade emissions rise to 1.165 $kgCO_2$-eq/m²y and embodied carbon to 353.70 $kgCO_2$-eq/m², with Rank A and Band A preserved. Whole-life GWP falls to 957.081 $kgCO_2$-eq/m² (15.951 $kgCO_2$-eq/m²y), 14.1% below S_28. The result is practically indistinguishable from S_23 (50.286 kWh/m²y; 957.193 $kgCO_2$-eq/m²): once the glazing is triple, the modified transmittance leaves energy and carbon performance essentially unchanged.

Parameters	Operational Energy	Embodied Carbon
Design Value	50.282	353.7
RIBA/LETI	Compliant 2030 Target	Band A
Carbon HEROES	N/A	Rank A

tab. 20

With Operational Energy in kWh/m²y, Embodied Carbon in $kgCO_2$-eq/m²y
N/A stands for Non Applicable

These two Scenarios share the sDa-ASE*Area/Total Area of 38.67%

4.4 Scenario 3: Horizon-Driven Envelope Strategies

While preceding investigations evaluated envelope interventions applied to Zenith's baseline geometry, Scenario 3 pivots the assessment to the opposite side of the urban setting by adopting the architectural morphology of Horizon as a design testbed. In contrast to the expansive glazing fields and continuous vertical divisions of Zenith, Horizon is defined by a more solid, disciplined envelope rhythm characterized by compact horizontal windows and an inherently lower window-to-wall ratio of 0.24.
This morphological shift reshapes the building's passive dynamics at its source. Increasing the proportion of opaque assemblies enhances the overall thermal resistance of the envelope and suppresses peak solar heat gains before they enter the interior, potentially mitigating the operational need for extensive external shading infrastructure. Concurrently, lower ribbon openings introduce tighter constraints on daylight penetration depth and internal illuminance uniformity across office floorplates.
Scenario 3 systematically examines this balance, determining whether a more compact, solid-dominated envelope can reduce façade-related embodied carbon and operational demand.
As mentioned above, this scenario is organized as the previous one; the same 4 configurations are explored, both for double glazing and for triple glazing, maintaing the Uvalues and SHGC previously stated.
The Benchmarks are, once again, the same with the same boundaries as scenario 2.

Configuration 1: No shadings

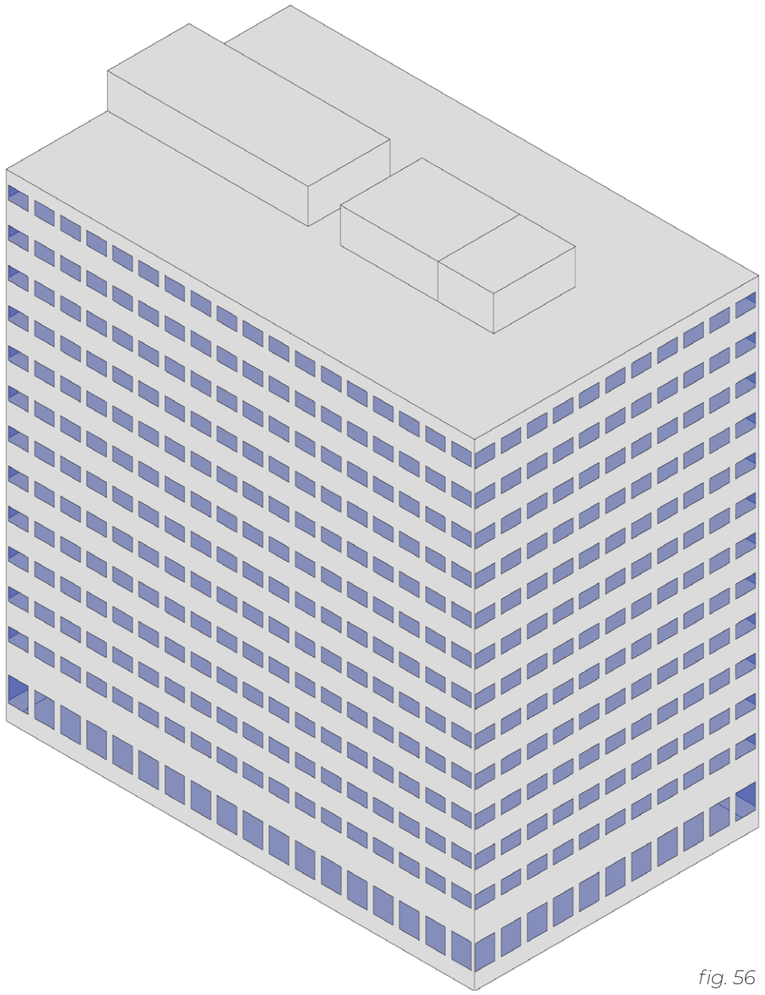

fig. 56

S_30 H 2G NS

Reducing the window-to-wall ratio to 0.24 brings an immediate efficiency gain. S_30 reaches an EUI of 49.406 kWh/m²y at an optimal insulation depth of 0.238 m, about 16.5% below its Zenith counterpart S_20, and meets the LETI/RIBA 2030 threshold without any aperture treatment. The embodied side moves the other way: the larger opaque surface carries a heavier load, with façade emissions of 1.130 $kgCO_2$-eq/m²y and a 60-year embodied total of 351.48 $kgCO_2$-eq/m², against 0.93 and 339.54 at Zenith. LETI Band A and Carbon HEROES Rank A are nonetheless secured, and whole-life emissions of 944.352 $kgCO_2$-eq/m² (15.739 $kgCO_2$-eq/m²y) sit about 10% below S_20.

Parameters	Operational Energy	Embodied Carbon
Design Value	49.406	351.48
RIBA/LETI	Compliant 2030 Target	Band A
Carbon HEROES	N/A	Rank A

tab. 21

S_33 H 3G NS

Triple glazing lowers the EUI to 45.290 kWh/m²y, 8.3% less than S_30, and thickens the optimum only slightly, to 0.247 m. This is a smaller return than the 15% seen at Zenith, as one would expect with a fraction of the glazed area. Façade carbon rises to 1.236 $kgCO_2$-eq/m²y and embodied carbon to 357.84 $kgCO_2$-eq/m², a penalty small enough to leave both ratings untouched. Whole-life GWP falls to 901.322 $kgCO_2$-eq/m² (15.022 $kgCO_2$-eq/m²y), 4.6% below S_30.

Parameters	Operational Energy	Embodied Carbon
Design Value	45.29	357.84
RIBA/LETI	Compliant 2030 Target	Band A
Carbon HEROES	N/A	Rank A

tab. 22

With Operational Energy in kWh/m²y, Embodied Carbon in $kgCO_2$-eq/m²y
N/A stands for Non Applicable

These two Scenarios share the sDa-ASE*Area/Total Area of 30.35%

Configuration 2: Existing Façade Blades as Shading Devices

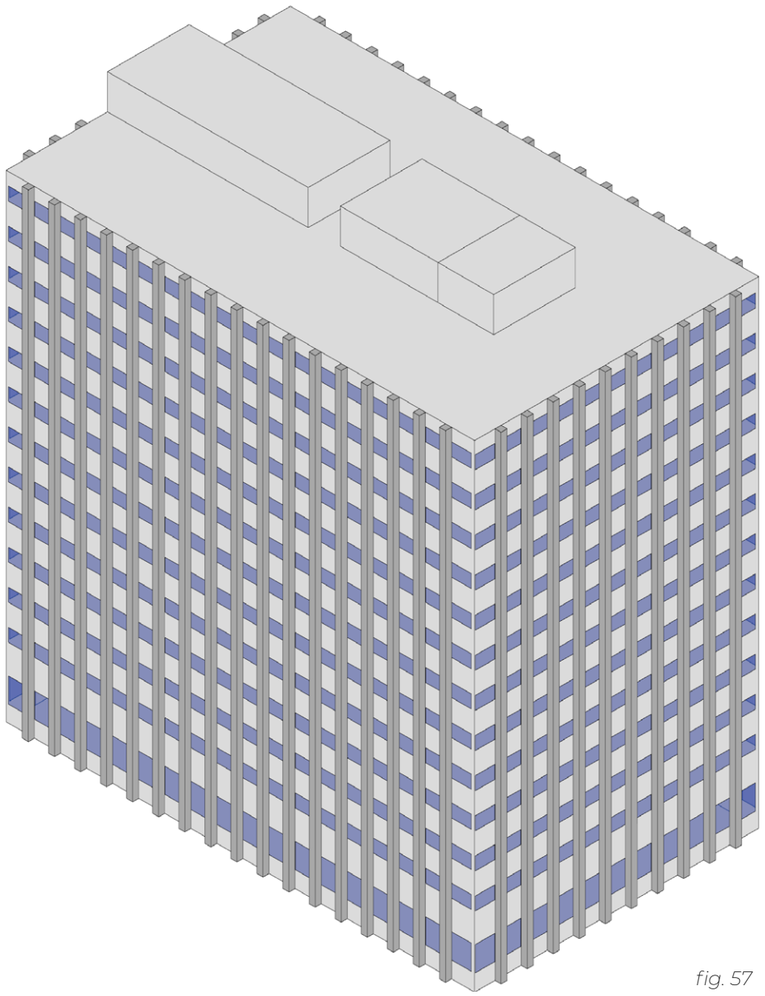

fig. 57

S_31 H 2G BL

With double glazing and blades, S_31 reaches an EUI of 48.120 kWh/m²y at 0.238 m, still within the 2030 target but only 2.6% below unshaded S_30: at this aperture ratio there is little solar exposure left to intercept. The blade substructure raises façade carbon to 1.432 $kgCO_2$-eq/m²y and embodied carbon to 369.60 $kgCO_2$-eq/m², which drops Carbon HEROES to Rank B (LETI Band A held). Whole-life emissions total 947.037 $kgCO_2$-eq/m² (15.784 $kgCO_2$-eq/m²y), marginally above S_30's 944.352, so under a low WWR the embodied cost of solar control slightly exceeds the cooling benefit.

Parameters	Operational Energy	Embodied Carbon
Design Value	48.12	369.6
RIBA/LETI	Compliant 2030 Target	Band A
Carbon HEROES	N/A	Rank B

tab. 23

S_34 H 3G BL

Triple glazing with blades brings the EUI to 44.592 kWh/m²y and the optimum to 0.248 m. Façade emissions of 1.539 $kgCO_2$-eq/m²y and embodied carbon of 376.02 $kgCO_2$-eq/m², the heaviest of the scenario, keep the design at Rank B with Band A. Whole-life GWP falls to 911.119 $kgCO_2$-eq/m² (15.185 $kgCO_2$-eq/m²y), 3.8% below S_31, though still above the unshaded S_33 (901.322).

Parameters	Operational Energy	Embodied Carbon
Design Value	44.592	376.02
RIBA/LETI	Compliant 2030 Target	Band A
Carbon HEROES	N/A	Rank B

tab. 24

With Operational Energy in kWh/m²y, Embodied Carbon in $kgCO_2$-eq/m²y
N/A stands for Non Applicable

These two Scenarios share the sDa-ASE*Area/Total Area of 31.34%

Configuration 3: Aperture-Specific Parametric Shading Optimization

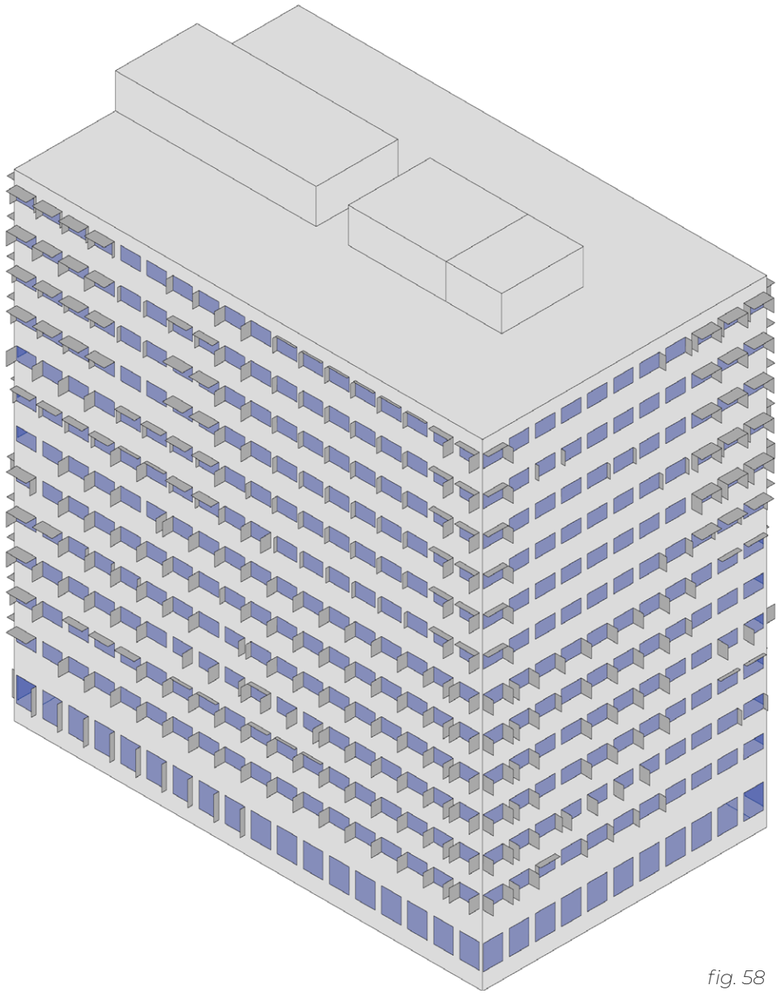

fig. 58

S_32 H 2G OS

With optimized shading, S_32 reaches 46.914 kWh/m²y at 0.249 m, outperforming the blades of S_31 (48.120) under the same 0.24 aperture ratio and meeting the 2030 target. The geometric rationalization also trims material: façade emissions of 1.208 $kgCO_2$-eq/m²y and embodied carbon of 356.16 $kgCO_2$-eq/m², well below the blades' 369.60, restore Carbon HEROES Rank A alongside LETI Band A. Whole-life emissions decrease to 919.124 $kgCO_2$-eq/m² (15.319 $kgCO_2$-eq/m²y), 2.7% below S_30.

Parameters	Operational Energy	Embodied Carbon
Design Value	46.914	356.16
RIBA/LETI	Compliant 2030 Target	Band A
Carbon HEROES	N/A	Rank A

tab. 25

S_35 H 3G OS

Triple glazing takes the EUI to 44.017 kWh/m²y, the lowest operational demand of the four configurations, with the optimal insulation at 0.257 m. The third pane and shaped shading lift façade carbon to 1.312 $kgCO_2$-eq/m²y and embodied carbon to 362.40 $kgCO_2$-eq/m², moving Carbon HEROES to Rank B while Band A stands. With operational GWP down to 528.203 $kgCO_2$-eq/m², whole-life emissions reach 890.603 $kgCO_2$-eq/m² (14.843 $kgCO_2$-eq/m²y), the lowest of Scenario 3 and 3.1% below S_32.

Parameters	Operational Energy	Embodied Carbon
Design Value	44.017	362.4
RIBA/LETI	Compliant 2030 Target	Band A
Carbon HEROES	N/A	Rank B

tab. 26

With Operational Energy in kWh/m²y, Embodied Carbon in $kgCO_2$-eq/m²y
N/A stands for Non Applicable

These two Scenarios share the sDa-ASE*Area/Total Area of 32.23%

Configuration 4: Modified Visual Transmittance

S_38 H 2G VT

S_38 (unshaded, modified transmittance, WWR 0.24) has an EUI of 51.120 kWh/m²y at 0.238 m, meeting the 2030 target because the reduced glazed area already limits radiative gains. It is nonetheless 3.5% above S_30, so, as at Zenith, the modified glazing does worse than the original when no shading accompanies it. Façade emissions of 1.131 $kgCO_2$-eq/m²y and embodied carbon of 351.54 $kgCO_2$-eq/m² are essentially those of S_30, with Band A and Rank A retained. Whole-life emissions total 964.979 $kgCO_2$-eq/m² (16.083 $kgCO_2$-eq/m²y).

Parameters	Operational Energy	Embodied Carbon
Design Value	51.12	351.54
RIBA/LETI	Compliant 2030 Target	Band A
Carbon HEROES	N/A	Rank A

tab. 27

S_39 H 3G VT

Triple glazing shifts the optimum to 0.245 m and cuts the EUI to 45.296 kWh/m²y, 11.4% below S_38. Façade carbon rises to 1.233 $kgCO_2$-eq/m²y and embodied carbon to 357.72 $kgCO_2$-eq/m², without altering either rating. Whole-life GWP falls to 901.272 $kgCO_2$-eq/m² (15.021 $kgCO_2$-eq/m²y), 6.6% below S_38 and again level with S_33.

Parameters	Operational Energy	Embodied Carbon
Design Value	51.12	351.54
RIBA/LETI	Compliant 2030 Target	Band A
Carbon HEROES	N/A	Rank A

tab. 28

With Operational Energy in kWh/m²y, Embodied Carbon in $kgCO_2$-eq/m²y
N/A stands for Non Applicable

These two Scenarios share the sDa-ASE*Area/Total Area of 30.59%

4.5 Scenario 4: Daylight optimization-Driven Envelope Strategies

This scenario pivots the assessment toward an envelope configuration explicitly calibrated around indoor natural lighting requirements, establishing an intermediate window-to-wall ratio of 0.46.
This morphological shift recalibrates the building's passive dynamics between the two previously tested extremes. By moving away from both the excessive solar gain risks inherent to broad glazing fields (WWR 0.54) and the daylight penetration depth constraints imposed by Horizon's low ribbon apertures, the daylight-driven geometry seeks an optimal balance: maximizing indoor visual autonomy to suppress artificial lighting electricity demand, while controlling summer solar heat intake to mitigate cooling loads. Concurrently, this moderate glazed area maintains an ample opaque perimeter capable of accommodating optimized thermal insulation layers.
This scenario systematically examines this balance, assessing whether a daylight-optimized aperture sizing can deliver superior whole-life carbon efficiency by reconciling façade-related embodied burdens with long-term operational performance.
As established in the previous sections, this scenario follows an identical methodological organization: the same 4 configurations are explored for both double and triple glazing, retaining the thermal transmittance (U-values) and solar heat gain coefficients (SHGC) defined earlier. The evaluation benchmarks and system boundaries likewise remain identical to those implemented in the preceding scenarios.

Configuration 1: No shadings

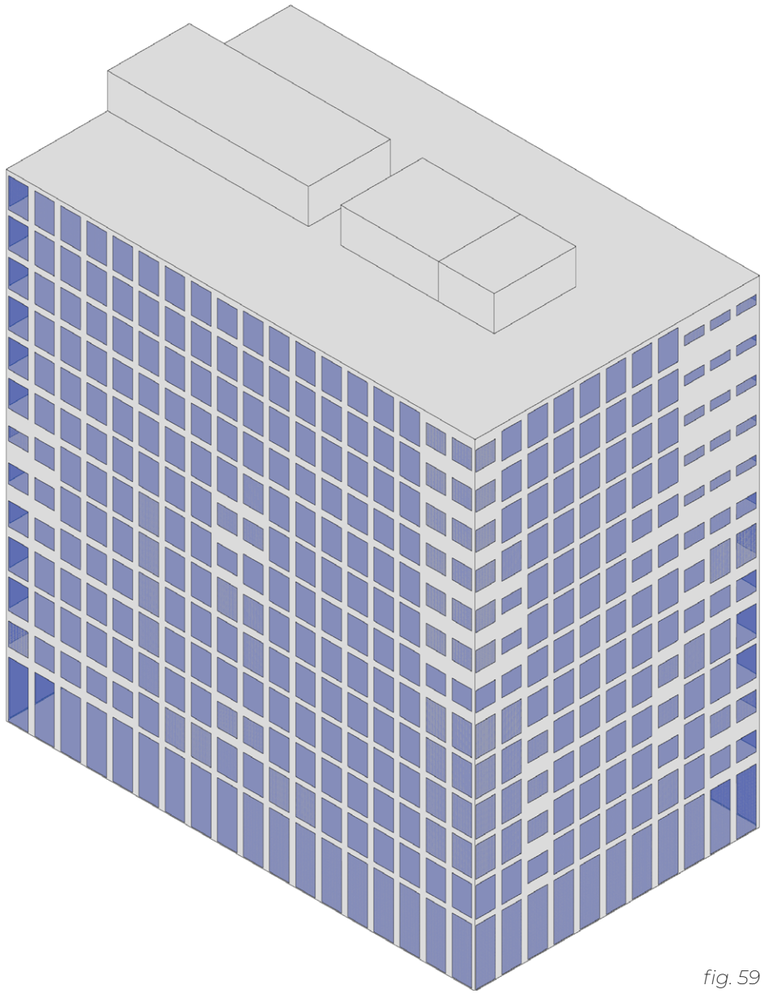

fig. 59

S_40 D 2G NS

S_40 sets the reference for the unshaded daylight-driven scenario, with an EUI of 56.183 kWh/m²y at an optimal insulation thickness of 0.243 m. With openings calibrated to daylight needs rather than to a broad glazing field, it lands between Zenith's S_20 (59.178) and Horizon's S_30 (49.406). Carbon follows the same ordering: façade emissions of 0.982 $kgCO_2$-eq/m²y and 342.60 $kgCO_2$-eq/m² of embodied carbon (LETI Band A, Rank A), and whole-life emissions of 1016.80 $kgCO_2$-eq/m² (16.947 $kgCO_2$-eq/m²y), again intermediate between S_20 (1049.679) and S_30 (944.352).

Parameters	Operational Energy	Embodied Carbon
Design Value	56.183	342.6
RIBA/LETI	Compliant 2025 Target	Band A
Carbon HEROES	N/A	Rank A

tab. 29

S_43 D 3G NS

With triple glazing the optimum rises to 0.271 m and the EUI falls to 48.814 kWh/m²y, 13.1% below S_40 and within the 2030 target, a return that tracks the glazed fraction. Façade emissions climb to 1.183 $kgCO_2$-eq/m²y and embodied carbon to 354.72 $kgCO_2$-eq/m², with both ratings retained. Whole-life GWP declines to 940.49 $kgCO_2$-eq/m² (15.675 $kgCO_2$-eq/m²y), 7.5% below S_40.

Parameters	Operational Energy	Embodied Carbon
Design Value	48.814	354.72
RIBA/LETI	Compliant 2030 Target	Band A
Carbon HEROES	N/A	Rank A

tab. 30

With Operational Energy in kWh/m²y, Embodied Carbon in $kgCO_2$-eq/m²y
N/A stands for Non Applicable

These two Scenarios share the sDa-ASE*Area/Total Area of 37.80%

Configuration 2: Existing Façade Blades as Shading Devices

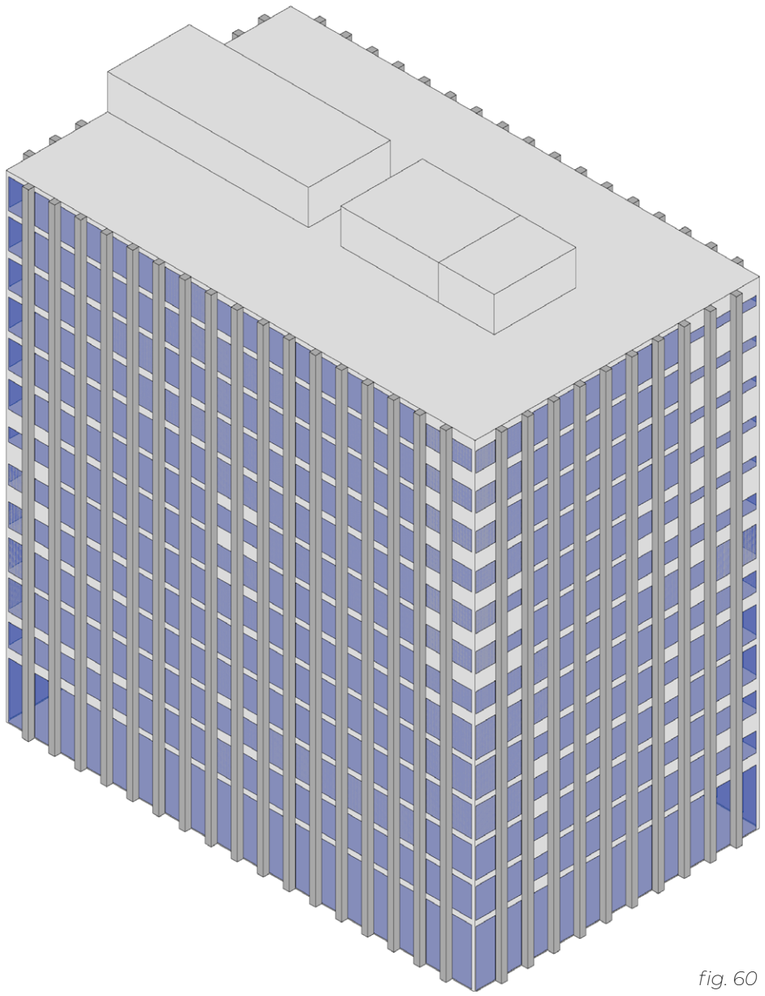

fig. 60

S_41 D 2G BL

The blades bring the EUI to 53.685 kWh/m²y with a carbon-optimal insulation of 0.255 m, enough for the 2030 target, and they lift the sDA–ASE ratio from 37.80% to 39.54%. The added hardware pushes façade emissions to 1.296 kg-CO_2-eq/m²y and embodied carbon to 361.50 kgCO_2-eq/m², shifting Carbon HEROES to Rank B (Band A intact). Whole-life emissions total 1005.724 kg-CO_2-eq/m² (16.762 kgCO_2-eq/m²y), only 1.1% below unshaded S_40.

Parameters	Operational Energy	Embodied Carbon
Design Value	53.685	361.5
RIBA/LETI	Compliant 2030 Target	Band A
Carbon HEROES	N/A	Rank B

tab. 31

S_44 D 3G BL

The triple-glazed version reaches 47.350 kWh/m²y with 0.273 m of insulation, 11.8% below S_41. Façade emissions of 1.292 kgCO_2-eq/m²y and embodied carbon of 361.26 kgCO_2-eq/m² keep Rank B and Band A. Whole-life GWP is 929.460 kgCO_2-eq/m² (15.491 kgCO_2-eq/m²y), 7.6% below S_41 and 1.2% below S_43.

Parameters	Operational Energy	Embodied Carbon
Design Value	48.814	354.72
RIBA/LETI	Compliant 2030 Target	Band A
Carbon HEROES	N/A	Rank A

tab. 32

With Operational Energy in kWh/m²y, Embodied Carbon in kgCO_2-eq/m²y
N/A stands for Non Applicable

These two Scenarios share the sDa-ASE*Area/Total Area of 39.54%

Configuration 3: Aperture-Specific Parametric Shading Optimization

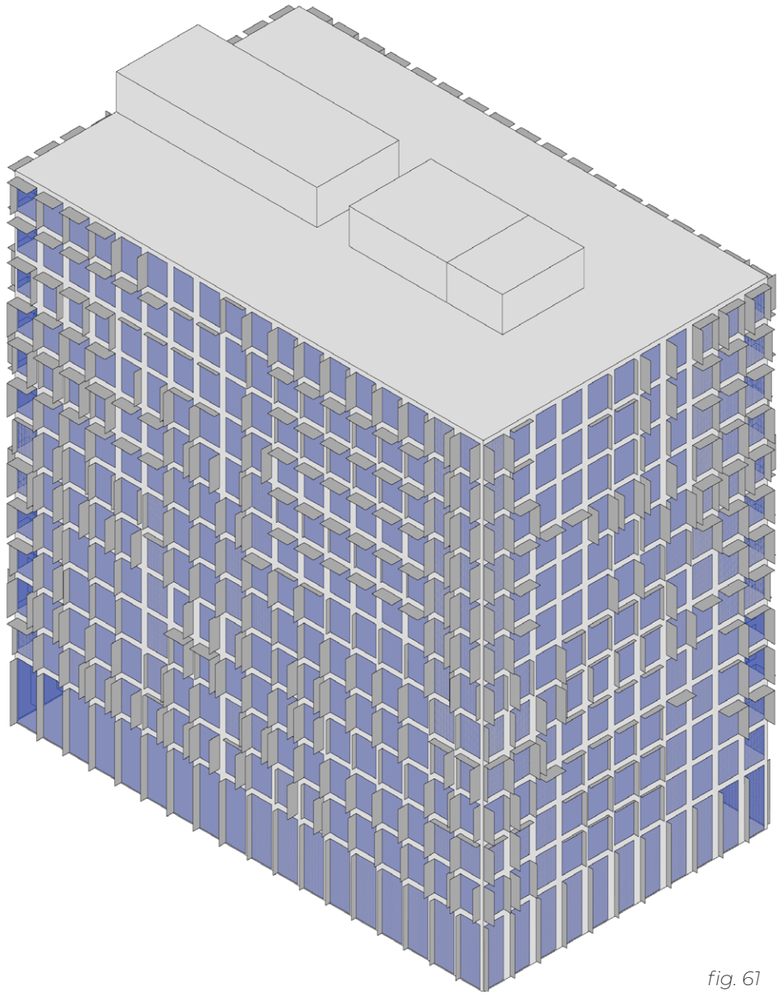

fig. 61

S_42 D 2G OS

With optimized shading, S_42 reaches 52.399 kWh/m²y at an optimal insulation thickness of 0.264 m, meeting the 2030 target.

Selective solar interception controls overheating in peak months while protecting daylit working conditions, and because the shading geometries carry no superfluous bulk, façade emissions stay at 1.102 $kgCO_2$-eq/m²y and embodied carbon at 349.86 $kgCO_2$-eq/m², preserving Band A and Rank A. Whole-life GWP contracts to 978.654 $kgCO_2$-eq/m² (16.311 $kgCO_2$-eq/m²y), the best of the double-glazed variants in this scenario and 3.8% below S_40.

Parameters	Operational Energy	Embodied Carbon
Design Value	52.399	349.86
RIBA/LETI	Compliant 2030 Target	Band A
Carbon HEROES	N/A	Rank A

tab. 33

S_45 D 3G OS

Triple glazing takes the EUI to 46.719 kWh/m²y and the optimum to 0.280 m. Façade emissions of 1.221 $kgCO_2$-eq/m²y and embodied carbon of 357.00 $kgCO_2$-eq/m² leave both ratings in place. Whole-life emissions fall to 917.640 $kgCO_2$-eq/m² (15.294 $kgCO_2$-eq/m²y), the lowest of the four configurations and 6.2% below S_42.

Parameters	Operational Energy	Embodied Carbon
Design Value	48.814	354.72
RIBA/LETI	Compliant 2030 Target	Band A
Carbon HEROES	N/A	Rank A

tab. 34

With Operational Energy in kWh/m²y, Embodied Carbon in $kgCO_2$-eq/m²y
N/A stands for Non Applicable

These two Scenarios share the sDa-ASE*Area/Total Area of 41.15%

Configuration 4: Modified Visual Transmittance

S_48 D 2G VT

The unshaded, modified-transparency opening has an EUI of 60.507 kWh/m²y at 0.243 m of insulation, 7.7% above S_40. Without shading, the altered optical properties admit more solar radiation, which places the design at the LETI/RIBA 2025 target rather than 2030. Façade emissions (0.982 $kgCO_2$-eq/m²y) and embodied carbon (342.60 $kgCO_2$-eq/m²) are identical to S_40, so Band A and Rank A hold. Whole-life emissions reach 1068.684 $kgCO_2$-eq/m² (17.811 $kgCO_2$-eq/m²y).

Parameters	Operational Energy	Embodied Carbon
Design Value	60.507	342.6
RIBA/LETI	Compliant 2025 Target	Band A
Carbon HEROES	N/A	Rank A

tab. 35

S_49 D 3G VT

Triple glazing cuts the EUI to 48.825 kWh/m²y, 19.3% below S_48, and moves the optimum to 0.268 m, reaching the 2030 target. Façade emissions of 1.180 $kgCO_2$-eq/m²y and embodied carbon of 354.60 $kgCO_2$-eq/m² leave the ratings unchanged. Whole-life GWP falls to 940.500 $kgCO_2$-eq/m² (15.675 $kgCO_2$-eq/m²y), a 12.0% saving that mirrors S_43.

Parameters	Operational Energy	Embodied Carbon
Design Value	48.825	354.6
RIBA/LETI	Compliant 2030 Target	Band A
Carbon HEROES	N/A	Rank A

tab. 36

With Operational Energy in kWh/m²y, Embodied Carbon in $kgCO_2$-eq/m²y
N/A stands for Non Applicable

These two Scenarios share the sDa-ASE*Area/Total Area of 38.18%

Cross-Performance Assessment of Top Daylight Candidates

This section deepens the envelope performance evaluation by focusing on the three design configurations that exhibited the most favorable daylighting metrics, identified strictly by their optimal balance between natural light availability and excessive solar exposure, specifically measured through the ratio between Spatial Daylight Autonomy (sDA) and Annual Sunlight Exposure (ASE).

Moving beyond a purely optical analysis, this investigation cross-examines these daylight-optimized candidates through an integrated environmental lens, evaluating both their operational energy use intensity (EUI) and upfront embodied carbon footprint. This multidimensional approach assesses whether envelopes tuned for peak visual autonomy remain energetically and ecologically competitive over a 60-year life cycle, verifying whether the operational savings gained from reduced electric lighting and passive solar gains justify the embodied carbon required to manufacture, assemble, and maintain their specific glazing, shading, and insulation assemblies.

S_51 B 2G OS VT

Leading the double-glazed candidates with the best sDA–ASE score (42.34%), S_51 layers optimized shading (OS) and then a modification of visual transmittance (VT). Even at the full 0.54 WWR, it reaches 54.071 kWh/m²y at 0.288 m of insulation, meeting the 2030 target. Relative to S_22, which has the same shading and insulation thickness (54.078 kWh/m²y), the glazing treatment leaves energy demand unchanged but trims façade emissions from 1.088 to 0.952 $kgCO_2$-eq/m²y and embodied carbon from 349.02 to 340.86 $kgCO_2$-eq/m². Whole-life emissions total 989.712 $kgCO_2$-eq/m² (16.495 $kgCO_2$-eq/m²y), with LETI Band A and Rank A secured.

Parameters	Operational Energy	Embodied Carbon
Design Value	54.071	340.86
RIBA/LETI	Compliant 2030 Target	Band A
Carbon HEROES	N/A	Rank A

tab. 37

S_61 B 3G OS VT

In triple glazing, S_61 lowers the EUI to 47.532 kWh/m²y and pushes the optimal insulation to 0.304 m, a 12.1% gain on S_51 achieved without compromising daylight. Façade carbon rises to 1.172 $kgCO_2$-eq/m²y and embodied carbon to 354.18 $kgCO_2$-eq/m², preserving both ratings, and whole-life emissions fall to 924.570 $kgCO_2$-eq/m² (15.409 $kgCO_2$-eq/m²y), 6.6% below S_51. Against S_25, which has the same shading and glazing without VT, the EUI is virtually unchanged (47.543 versus 47.532) but embodied carbon is 8 $kgCO_2$-eq/m² lower, enough to restore Rank A.

Parameters	Operational Energy	Embodied Carbon
Design Value	47.532	354.18
RIBA/LETI	Compliant 2030 Target	Band A
Carbon HEROES	N/A	Rank A

tab. 38

With Operational Energy in kWh/m²y, Embodied Carbon in $kgCO_2$-eq/m²y
N/A stands for Non Applicable

These two Scenarios share the sDa-ASE*Area/Total Area of 42.34%

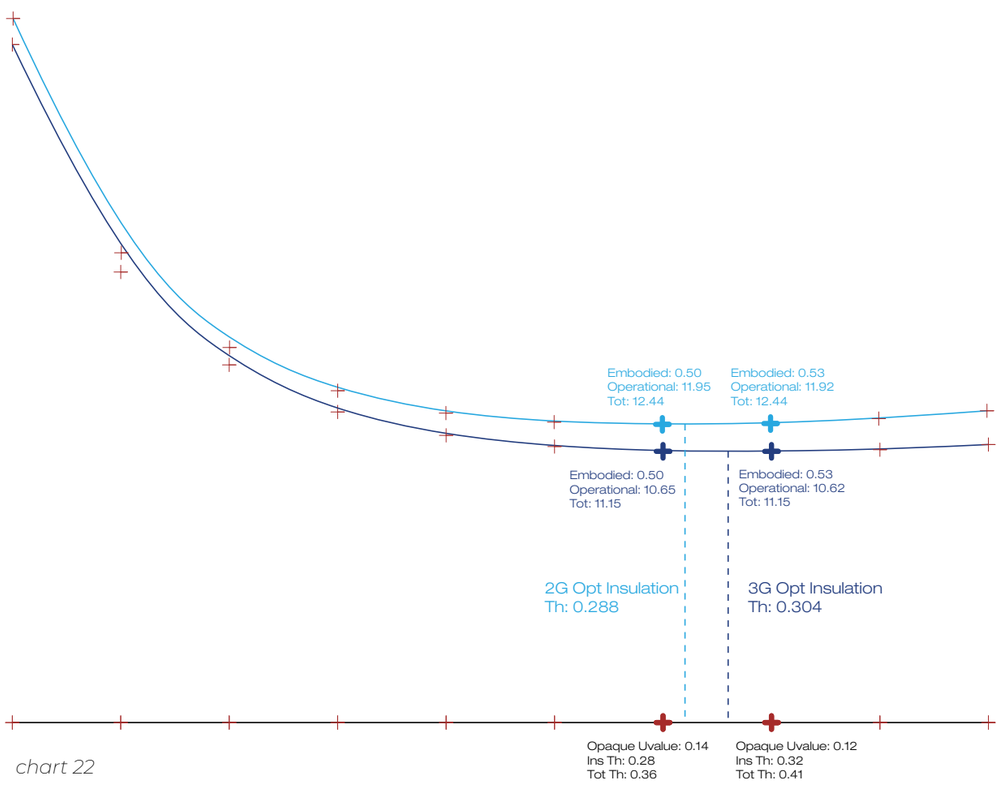

chart 22

S_52 B 2G VT OS

S_52 reverses the sequence, applying the VT modification first and the optimized shading afterwards. It reaches 54.635 kWh/m²y at 0.288 m, meeting the 2030 target. Façade emissions (0.952 $kgCO_2$-eq/m²y) and embodied carbon (340.86 $kgCO_2$-eq/m²) match S_51, and Band A and Rank A are kept. Whole-life emissions settle at 996.477 $kgCO_2$-eq/m² (16.608 $kgCO_2$-eq/m²y). The sDA–ASE score, 41.99%, is slightly below S_51's.

Parameters	Operational Energy	Embodied Carbon
Design Value	54.635	340.86
RIBA/LETI	Compliant 2030 Target	Band A
Carbon HEROES	N/A	Rank A

tab. 39

S_62 B 3G VT OS

In triple glazing, the order of application matters more. S_62 reaches an EUI of 47.808 kWh/m²y at 0.304 m, 12.5% below S_52 and close to S_61's 47.532, but its façade rises to 1.337 $kgCO_2$-eq/m²y and its embodied carbon to 364.02 $kgCO_2$-eq/m², against 1.172 and 354.18 for S_61, which moves Carbon HEROES to Rank B. Whole-life GWP falls to 937.710 $kgCO_2$-eq/m² (15.629 $kgCO_2$-eq/m²y), 5.9% below S_52 but 13 $kgCO_2$-eq/m² above S_61.

Parameters	Operational Energy	Embodied Carbon
Design Value	47.808	364.02
RIBA/LETI	Compliant 2030 Target	Band A
Carbon HEROES	N/A	Rank B

tab. 40

With Operational Energy in kWh/m²y, Embodied Carbon in $kgCO_2$-eq/m²y
N/A stands for Non Applicable

These two Scenarios share the sDa-ASE*Area/Total Area of 41.99%

S_53 D 2G OS VT

On the daylight-driven geometry (WWR 0.46), S_53 combines optimized shading with VT glazing and reaches 52.398 kWh/m²y at 0.264 m, level with S_42 (52.399) and within the 2030 target. Façade emissions of 1.002 $kgCO_2$-eq/m²y and embodied carbon of 343.86 $kgCO_2$-eq/m², 6 $kgCO_2$-eq/m² below S_42, keep Band A and Rank A. Whole-life emissions total 972.636 $kgCO_2$-eq/m² (16.211 $kgCO_2$-eq/m²y).

Parameters	Operational Energy	Embodied Carbon
Design Value	52.398	343.86
RIBA/LETI	Compliant 2030 Target	Band A
Carbon HEROES	N/A	Rank A

tab. 41

S_63 D 3G OS VT

With triple glazing, S_63 reduces the EUI to 46.720 kWh/m²y, 10.8% below S_53, and pushes the optimum to 0.280 m. Façade emissions rise to 1.192 $kgCO_2$-eq/m²y and embodied carbon to 355.26 $kgCO_2$-eq/m², still within Band A and Rank A. Whole-life emissions fall to 915.900 $kgCO_2$-eq/m² (15.265 $kgCO_2$-eq/m²y), 5.8% below S_53 and about 1.7 $kgCO_2$-eq/m² below S_45.

Parameters	Operational Energy	Embodied Carbon
Design Value	46.72	355.26
RIBA/LETI	Compliant 2030 Target	Band A
Carbon HEROES	N/A	Rank A

tab. 42

With Operational Energy in kWh/m²y, Embodied Carbon in $kgCO_2$-eq/m²y
N/A stands for Non Applicable

These two Scenarios share the sDa-ASE*Area/Total Area of 41.07%

S_54 H 2G OS VT

Included for completeness and benchmarking, S_54 brings the OS + VT combination to Horizon (WWR 0.24). It reaches 46.914 kWh/m²y at 0.249 m, identical to S_32, and meets the 2030 target. Façade emissions of 1.147 $kgCO_2$-eq/m²y and embodied carbon of 352.50 $kgCO_2$-eq/m² (S_32: 356.16) keep Band A and Rank A. Whole-life emissions settle at 915.462 $kgCO_2$-eq/m² (15.258 $kgCO_2$-eq/m²y).

Parameters	Operational Energy	Embodied Carbon
Design Value	46.914	352.5
RIBA/LETI	Compliant 2030 Target	Band A
Carbon HEROES	N/A	Rank A

tab. 43

S_64 H 3G OS VT

With triple glazing, S_64 lowers the EUI to 44.016 kWh/m²y and moves the optimum to 0.257 m. The façade reaches 1.250 $kgCO_2$-eq/m²y and embodied carbon 358.68 $kgCO_2$-eq/m², with both ratings retained. Whole-life emissions fall to 886.870 $kgCO_2$-eq/m² (14.781 $kgCO_2$-eq/m²y), 3.1% below S_54 and the lowest total of any configuration in the chapter, with 2.38 $kgCO_2$-eq/m²y of biogenic storage maintained.

Parameters	Operational Energy	Embodied Carbon
Design Value	44.016	358.68
RIBA/LETI	Compliant 2030 Target	Band A
Carbon HEROES	N/A	Rank A

tab. 44

With Operational Energy in kWh/m²y, Embodied Carbon in $kgCO_2$-eq/m²y
N/A stands for Non Applicable

These two Scenarios share the sDa-ASE*Area/Total Area of 32.07%

5

5. RESULTS AND CONCLUSIONS

5.1 Results
- 5.1.1 Elaboration of the results
- 5.1.2 Comparative Matrix between the Scenarios

5.2 Cross-Scenario Synthesis

5.3 Key-findings and Strategic Optimization Sequence

5.4 Future Developement
- 5.4.1 The Shifting Balance of Embodied and Operational Carbon
- 5.4.2 Dynamic Carbon Modeling and the Paradigm Shift in Desing

5.1 Results

This chapter presented a comprehensive visualization and analysis of the data derived from the preceding simulations. Initially, the evaluated configurations were ranked to identify the absolute minimum and maximum performance values across each target metric. Subsequently, a normalized comparative matrix was utilized to isolate the optimal design alternative, serving both as the ideal solution for this specific case study and as a broader template for similar architectural typologies.

The second section of the chapter conducted a cross-comparative analysis of the individual transformation scenarios. By isolating the "before and after" effects of each design intervention, the evaluation focused on the carbon efficiency and overall environmental impact of each strategy. This analysis culminated in the development of a sequential, step-by-step strategic design framework tailored for minimizing lifecycle emissions.

Finally, the chapter addressed future developments and the shifting equilibrium between embodied and operational carbon. As rapid grid decarbonization accelerates toward the 2050 net-zero targets, the carbon intensity of operational energy will drastically decline. This impending infrastructural shift threatens to render statically derived design strategies obsolete, highlighting the critical necessity for future research to adopt dynamic evaluation frameworks capable of adapting to a continuously evolving energy landscape.

5.1.1 Elaboration of the Results

The results derived from the analysis of the various options are presented in the table below. For each configuration and strategy applied, the table details the total, embodied, and operational Global Warming Potential (GWP) over both annual and 60-year timeframes. It also reports the corresponding daylighting performance, providing standards-compliant ratings for Spatial Daylight Autonomy (sDA), Annual Sunlight Exposure (ASE), and Net Useful Daylight Area (NUDA).”

ID	TOT GWP (kg CO2-eq/m2y)	TOT GWP 60y(kg CO2-eq/m2)	OP (kg CO2-eq/m2y)	OP 60y(kg CO2-eq/m2)	EMB (kg CO2-eq/m2y)	EMB 60y(kg CO2-eq/m2)	NUDA (%)	ASE (%)	sDA (%)
S_20 B 2G NS	17.495	1049.7	11.836	710.16	5.659	339.54	37.27	19.65	56.83
S_21 B 2G BL	17.211	1032.66	11.244	674.64	5.967	358.02	39.35	13.95	53.3
S_22 B 2G OS	16.633	997.98	10.816	648.96	5.817	349.02	41.79	11.26	53.05
S_28 B 2G TR	18.569	1114.14	12.91	774.6	5.659	339.54	38.67	16.4	55.08
S_23 B 3G NS	15.953	957.18	10.057	603.42	5.896	353.76	37.27	19.65	56.83
S_24 B 3G BL	15.916	954.96	9.719	583.14	6.197	371.82	39.35	13.95	53.3
S_25 B 3G OS	15.546	932.76	9.509	570.54	6.037	362.22	41.79	11.26	53.05
S_29 B 3G TR	15.951	957.06	10.056	603.36	5.895	353.7	38.67	16.4	55.08
S_30 H 2G NS	15.739	944.34	9.881	592.86	5.858	351.48	30.35	13.91	44.26
S_31 H 2G BL	15.784	947.04	9.624	577.44	6.16	369.6	31.34	9.59	40.93
S_32 H 2G OS	15.319	919.14	9.383	562.98	5.936	356.16	32.23	6.3	38.54
S_38 H 2G TR	16.083	964.98	10.224	613.44	5.859	351.54	30.59	11.99	42.58
S_33 H 3G NS	15.022	901.32	9.058	543.48	5.964	357.84	30.35	13.91	44.26
S_34 H 3G BL	15.185	911.1	8.918	535.08	6.267	376.02	31.34	9.59	40.93
S_35 H 3G OS	14.843	890.58	8.803	528.18	6.04	362.4	32.23	6.3	38.54
S_39 H 3G TR	15.021	901.26	9.059	543.54	5.962	357.72	30.59	11.99	42.58
S_40 D 2G NS	16.947	1016.82	11.237	674.22	5.71	342.6	37.8	17.73	55.54
S_41 D 2G BL	16.762	1005.72	10.737	644.22	6.025	361.5	39.54	12.23	51.77
S_42 D 2G OS	16.311	978.66	10.48	628.8	5.831	349.86	41.15	10.03	51.18
S_48 D 2G TR	17.811	1068.66	12.101	726.06	5.71	342.6	38.13	16.13	54.31
S_43 D 3G NS	15.675	940.5	9.763	585.78	5.912	354.72	37.8	17.73	55.54
S_44 D 3G BL	15.491	929.46	9.47	568.2	6.021	361.26	39.54	12.23	51.77
S_45 D 3G OS	15.294	917.64	9.344	560.64	5.95	357	41.15	10.03	51.18
S_49 D 3G TR	15.675	940.5	9.765	585.9	5.91	354.6	38.13	16.13	54.31
S_51 B 2G OS V	16.631	997.86	10.814	648.84	5.817	349.02	42.34	9.82	52.16
S_52 B 2G V OS	16.774	1006.44	10.927	655.62	5.847	350.82	41.99	9.26	51.26
S_53 D 2G OS V	16.311	978.66	10.48	628.8	5.831	349.86	41.07	9.56	50.63
S_61 B 3G OS V	15.543	932.58	9.506	570.36	6.037	362.22	42.34	9.82	52.16
S_62 B 3G V OS	15.629	937.74	9.562	573.72	6.067	364.02	41.99	9.26	51.26
S_63 D 3G OS V	15.294	917.64	9.344	560.64	5.95	357	41.07	9.56	50.63
S_54 H 2G OS V	15.319	919.14	9.383	562.98	5.936	356.16	32.07	5.79	37.86
S_64 H 3G OS V	14.843	890.58	8.803	528.18	6.04	362.4	32.07	5.79	37.86

tab. 45

Analysis of the data revealed that combining multiple design strategies, such as applying secondary modifications to an existing configuration, yields negligible performance variations compared to their primary baseline setups. Specifically, applying a secondary strategy, such as modifying the window's visual transmittance on a configuration that already incorporates a primary shading system, provides no significant benefit in terms of operational energy reduction. While minor variations in daylighting performance were observed, the lack of energy benefits renders these combinations redundant. Consequently, to maintain clarity and streamline the analysis, these combined alternatives were excluded from the final comparison matrix.
(e.g., S_61 B 3G OS V and S_25 B 3G OS)

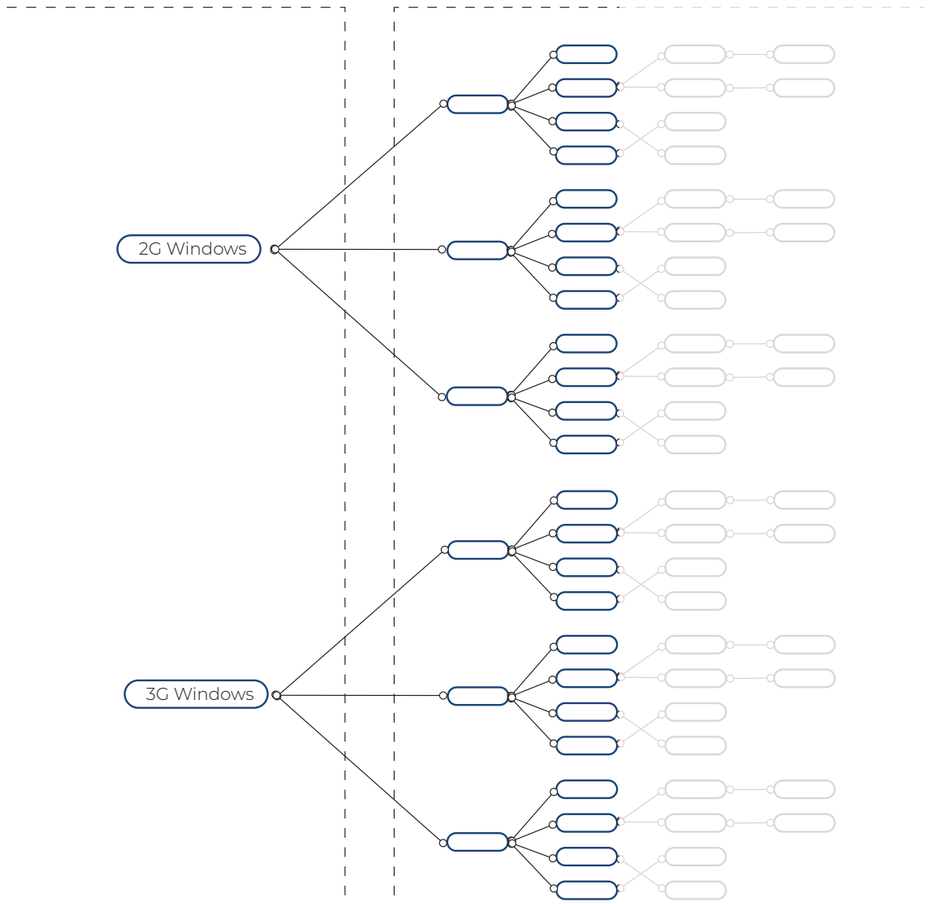

fig. 62

The tree graph diagrams below illustrate the analysis and ranking process for the evaluated design options. Expanding upon the previously established framework, the decision tree originates from the material-optimized baseline scenario. It then divides into two primary categories: double and triple glazing. The subsequent level defines the window configurations, namely, Maximum Glazing Ratio, Minimum Glazing Ratio, and Daylight-Driven designs, before the final branching, which represents the specific shading strategies applied to each alternative.

Desirability within these graphs is indicated by vertical placement, where higher positions denote superior overall performance. This optimal performance is defined by minimized values for Total, Operational, Embodied, and Heating Global Warming Potential (GWP) and Annual Sunlight Exposure (ASE), alongside maximized values for Spatial Daylight Autonomy (sDA) and Net Useful Daylight Area (NUDA). Consequently, the sequence of alternative codes listed on the right side of the graphs serves as a definitive ranking hierarchy.

Total GWP

chart 23

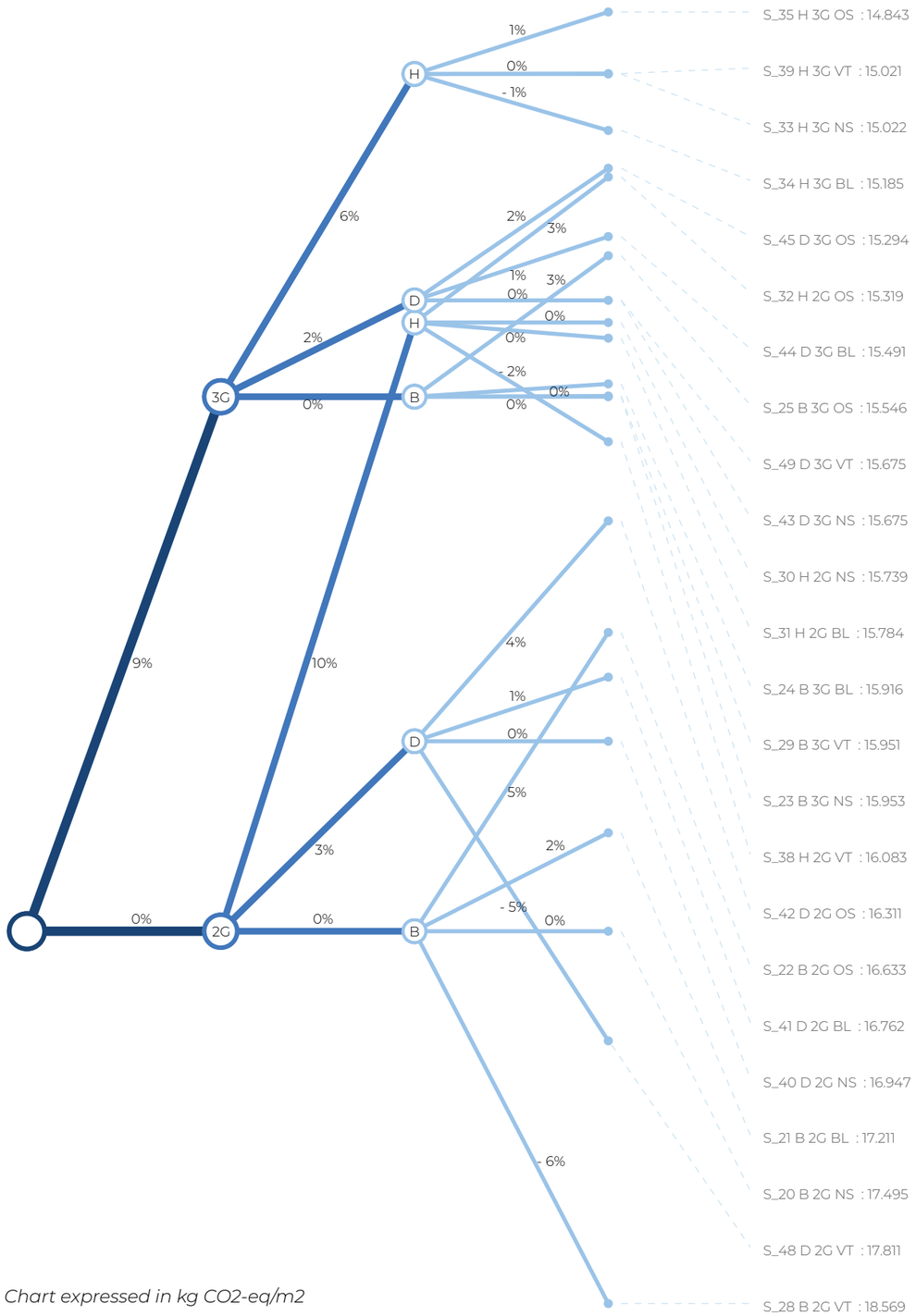

Chart expressed in kg CO2-eq/m2

An analysis of the Total GWP graph reveals that triple-glazed windows with a minimal glazing ratio yield the highest environmental performance. Within this specific category, the integration of optimized shading achieves the optimal result across all evaluated alternatives; specifically, configuration S_35 H 3G OS records the lowest total GWP at 14.84 kg CO_2eq/m²·y. Conversely, the least favorable performance is observed in the double-glazed, maximum glazing ratio configuration equipped with variable visual transmittance with 18.56 kg CO_2eq/m²·y (S_28 B 2G VT)

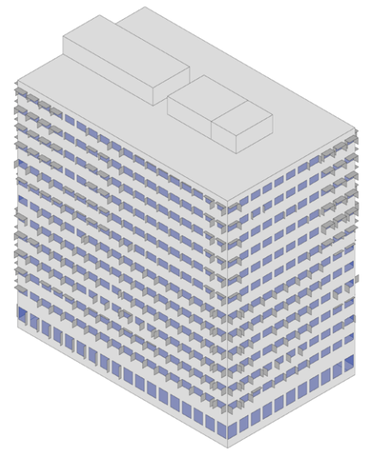

fig. 63

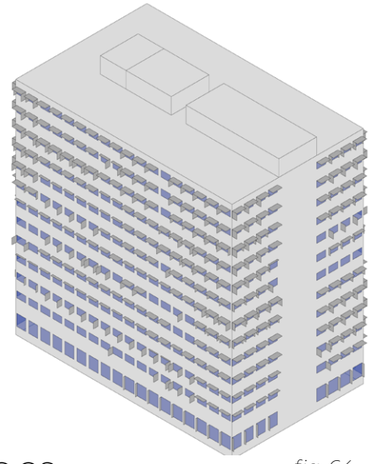

fig. 64

S_35 H 3G OS

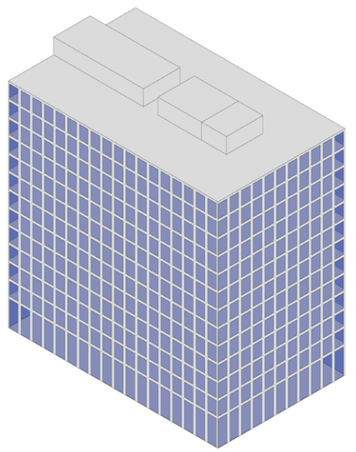

fig. 65

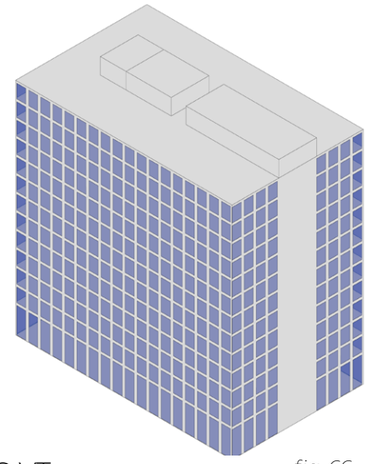

fig. 66

S_28 B 2G VT

Operational GWP

chart 24

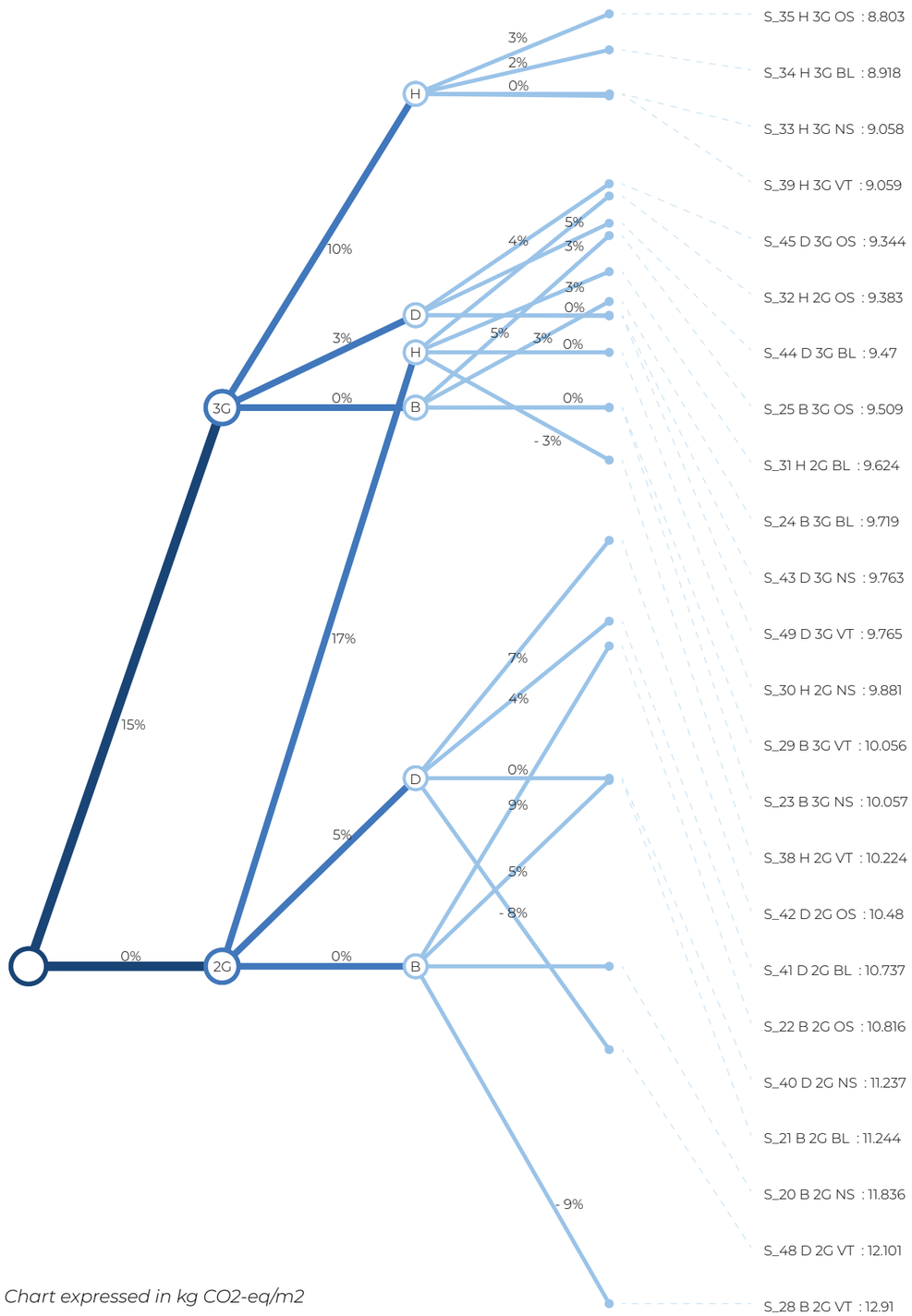

Chart expressed in kg CO2-eq/m2

The operational carbon graph closely mirrors the trends observed in the total GWP graph. This correlation is expected, given that operational carbon constitutes a significantly larger proportion of the total GWP compared to embodied carbon. Consequently, the optimal and least favorable design configurations remain identical across both metrics.

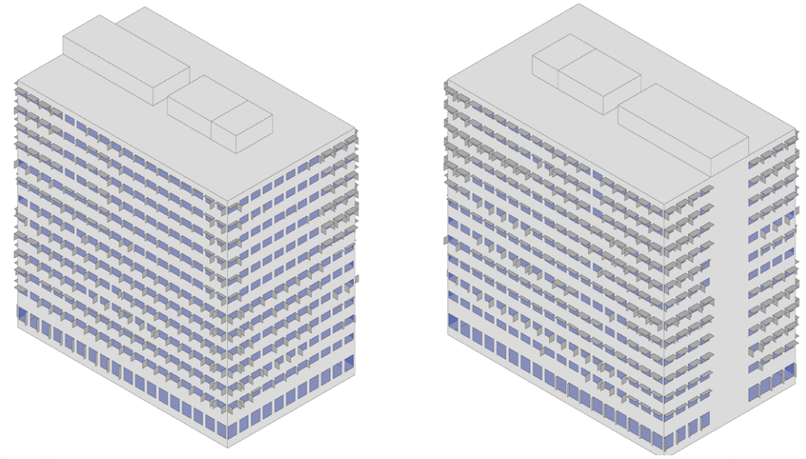

fig. 67 S_35 H 3G OS *fig. 68*

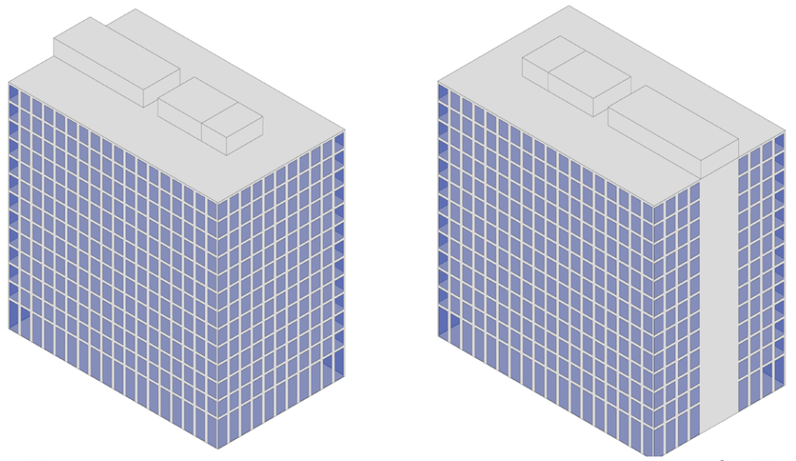

fig. 69 S_28 B 2G VT *fig. 70*

Embodied GWP

chart 25

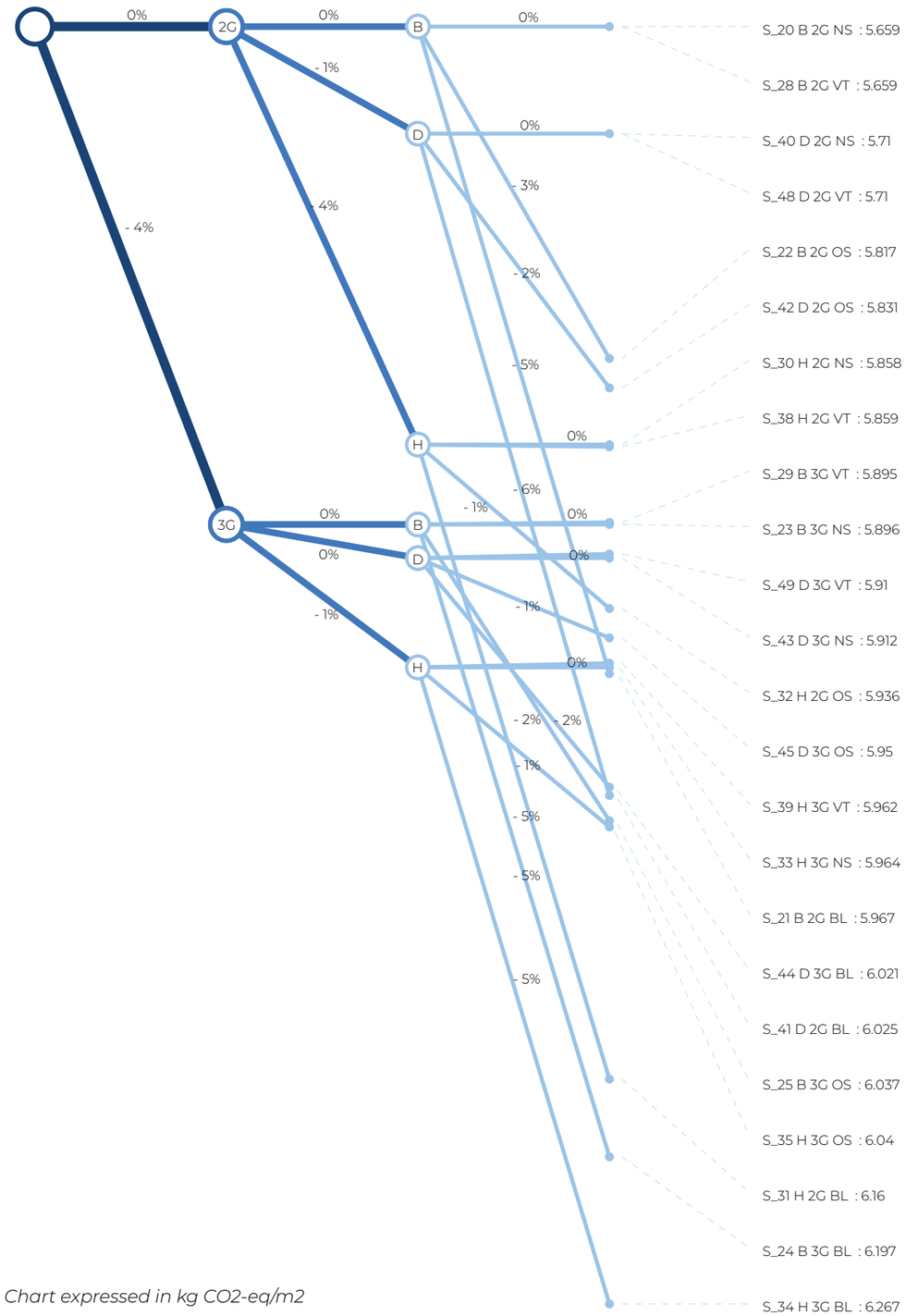

Chart expressed in kg CO2-eq/m2

In terms of embodied carbon, the unmodified baseline configuration featuring double glazing, a maximum glazing ratio, and no shading (S_20 B 2G NS) emerges as the most efficient option. This low environmental impact is primarily due to the reduced opaque wall area and the complete absence of supplementary shading structures, which minimize overall material usage. Conversely, the highest embodied carbon is associated with the minimal glazing ratio, triple-glazed configuration equipped with generalized shading (S_34 H 3G BL). This significant increase in embodied emissions is driven by three factors: the larger opaque area requiring more structural material and insulation, the higher manufacturing carbon footprint of triple glazing compared to double glazing, and the greater material volume demanded by generalized shading systems relative to optimized alternatives.

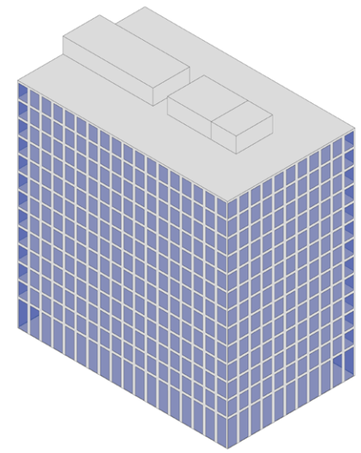

fig. 71

S_20 B 2G NS

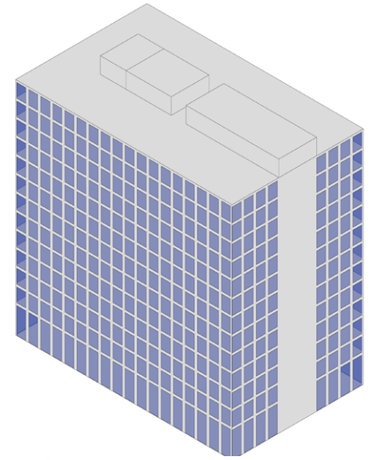

fig. 72

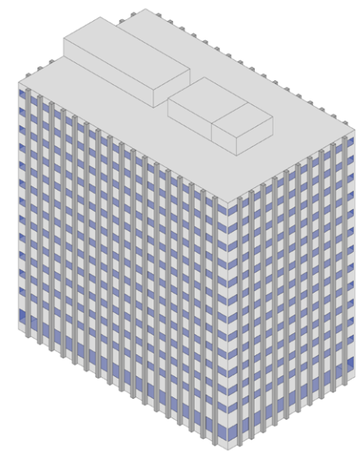

fig. 73

S_34 H 3G BL

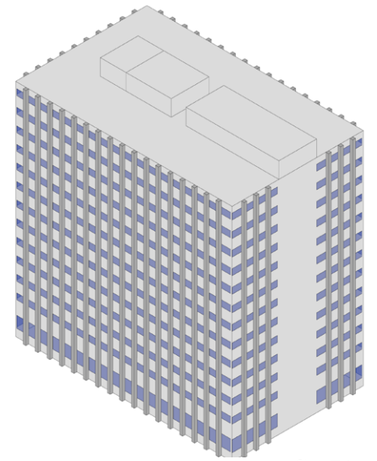

fig. 74

Heating EUI

chart 26

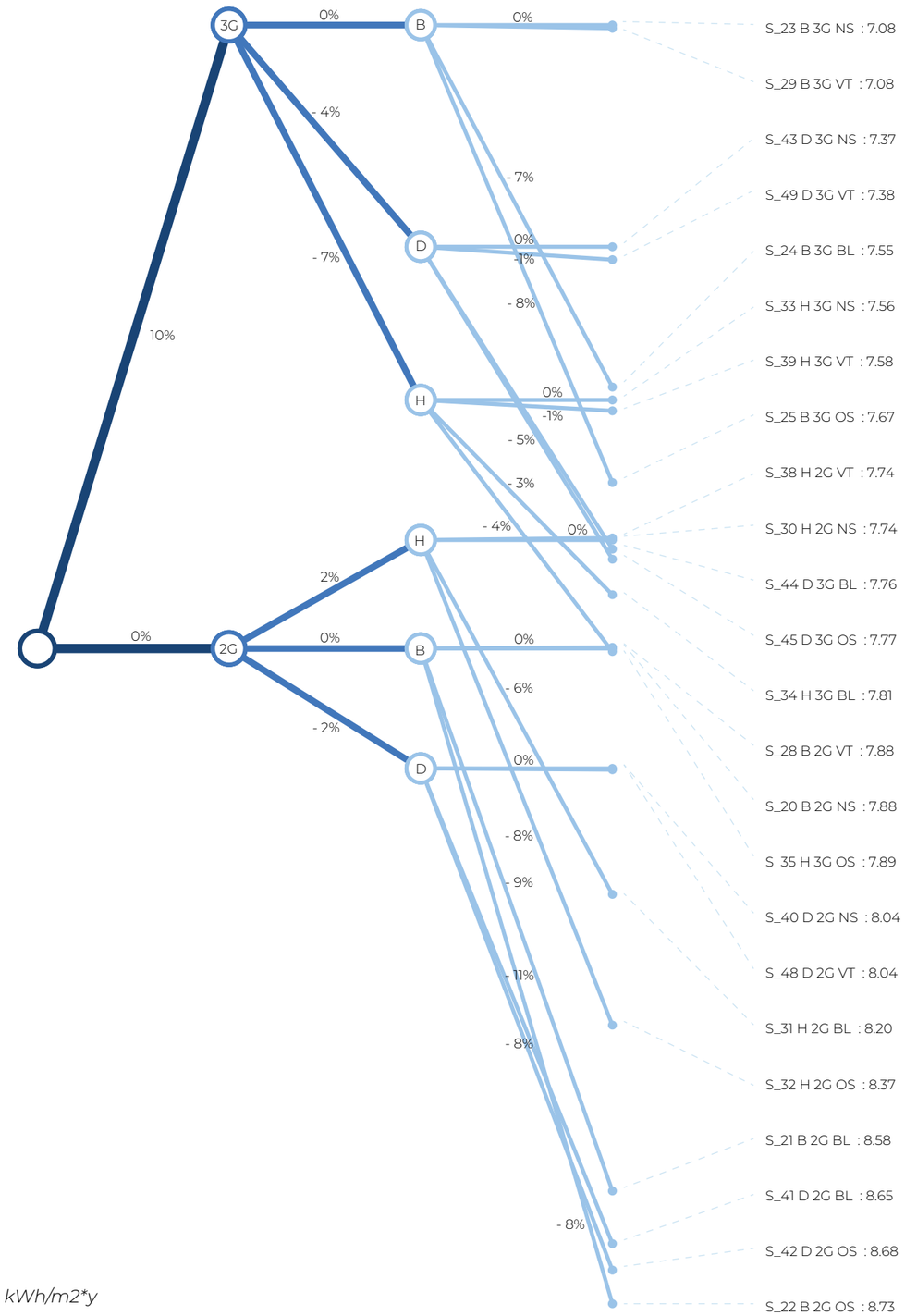

*kWh/m2*y*

Regarding Heating Energy Use Intensity (EUI), the configuration featuring triple glazing, a maximum glazing ratio, and no shading (S_23 B 3G NS) demonstrates the lowest energy demand. This optimal winter performance is driven by two combined factors: the unshaded, expansive glass area maximizes passive solar heat gains, while the superior thermal resistance of the triple glazing effectively traps this heat indoors. Conversely, the highest heating demand occurs within the same maximum glazing ratio category when utilizing double glazing and optimized shading (S_22 B 2G OS). In this scenario, the shading system intercepts direct solar radiation, depriving the space of natural warming, while the lower thermal efficiency of the double-glazed units allows for greater transmission heat losses to the exterior, thereby significantly increasing the reliance on active heating.

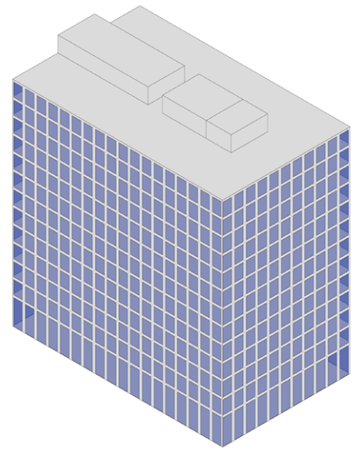

fig. 75

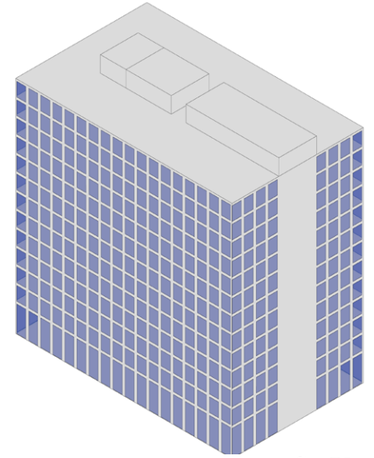

fig. 76

S_23 B 3G NS

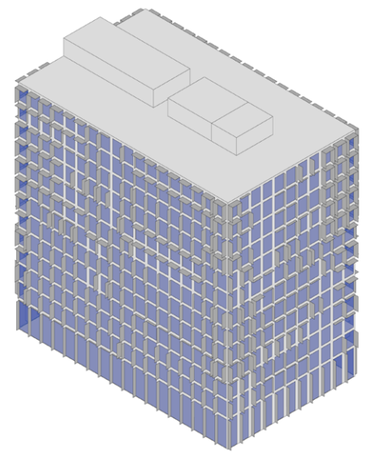

fig. 77

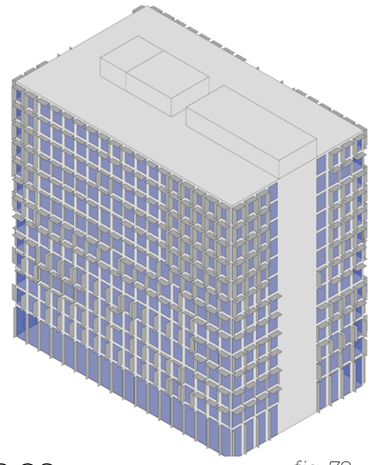

fig. 78

S_22 B 2G OS

Cooling EUI

chart 27

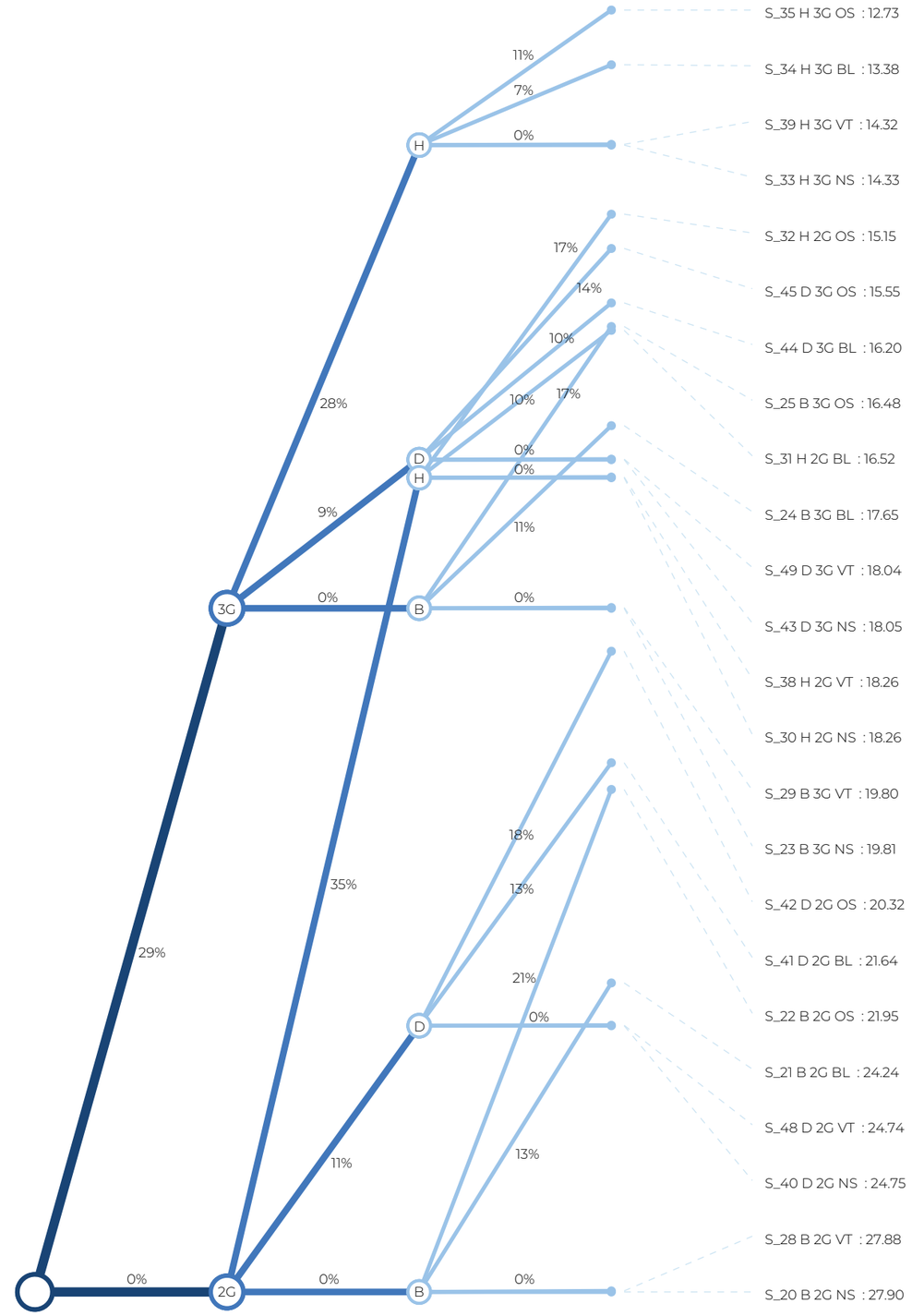

*kWh/m2*y*

Similar to the heating performance, the lowest cooling demand is achieved by configurations utilizing triple glazing, underscoring its overall effectiveness across diverse thermal scenarios. The optimal configuration for minimizing cooling loads is the triple-glazed, minimal glazing ratio setup equipped with optimized shading (S_35 H 3G OS). This design inherently minimizes the ingress of direct solar radiation, effectively mitigating the risk of summer overheating. Conversely, the highest cooling demand is observed in the unshaded, double-glazed baseline configuration with a maximum glazing ratio (S_20 B 2G NS), which allows unimpeded solar heat gain.

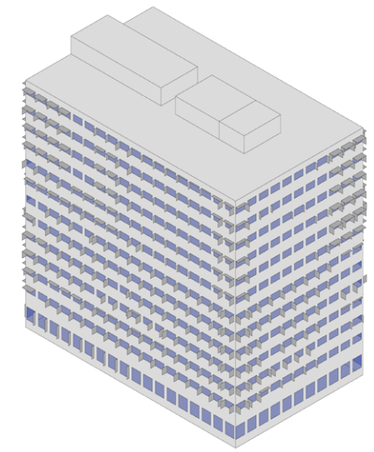

fig. 79

S_35 H 3G OS

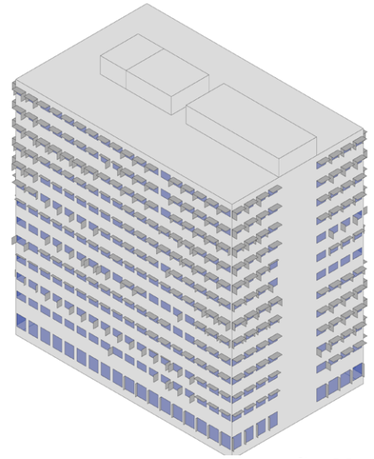

fig. 80

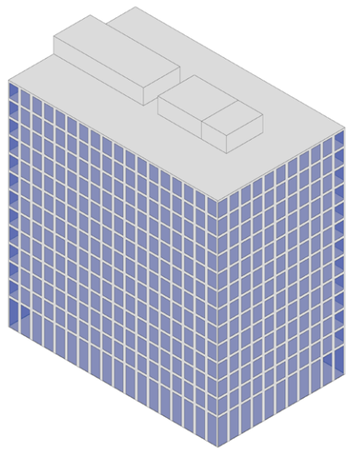

fig. 81

S_20 B 2G NS

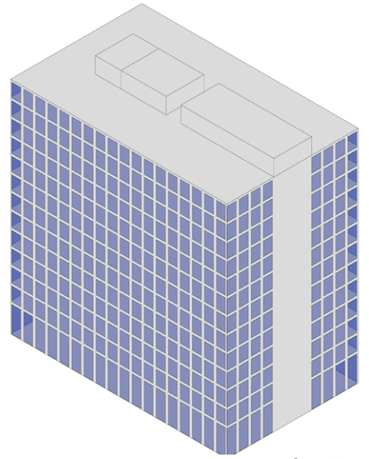

fig. 82

NUDA

chart 28

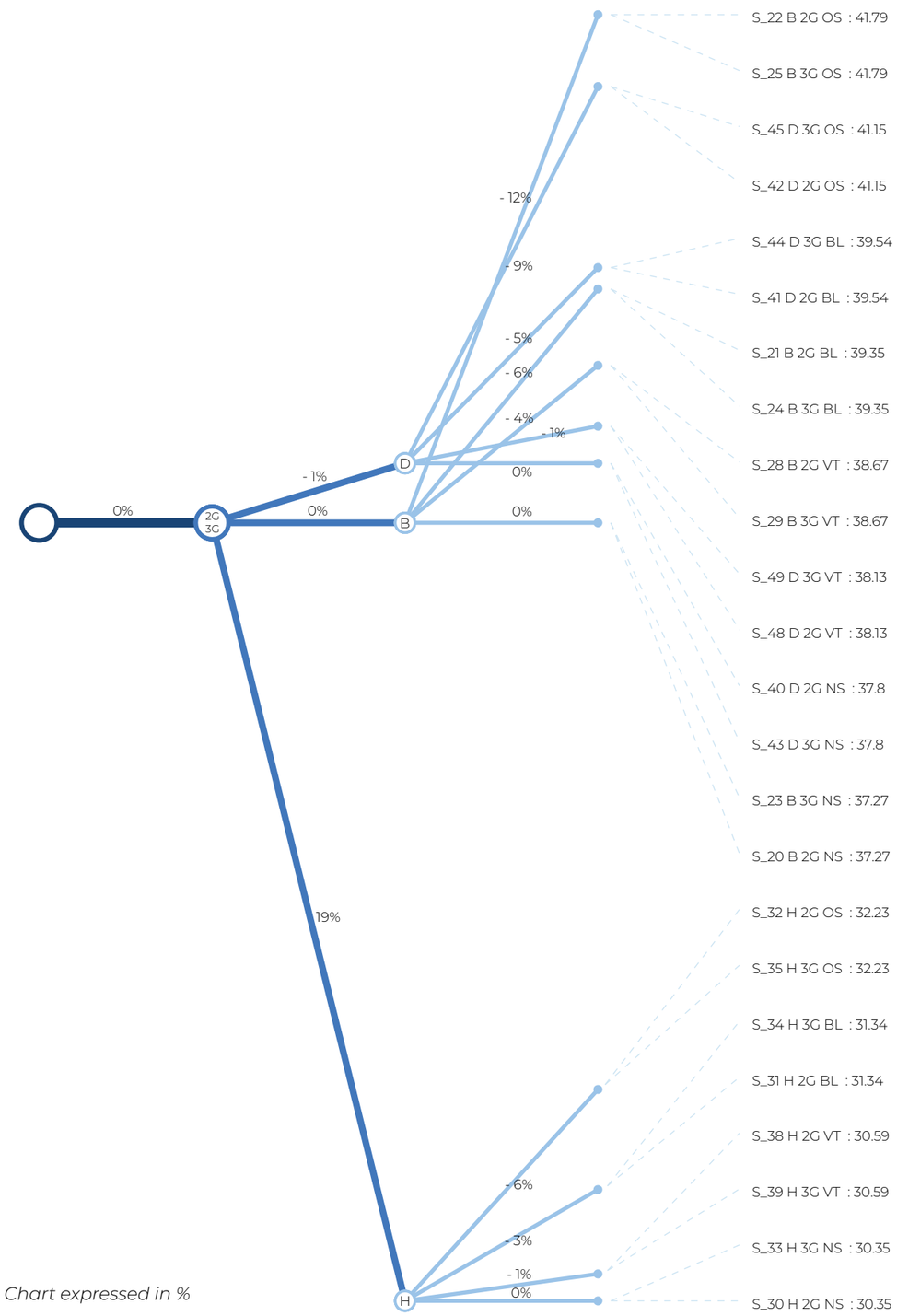

Chart expressed in %

The graph detailing Net Useful Daylight Area (NUDA) illustrates a clear performance division: configurations with maximum glazing ratios and Daylight-driven designs achieve significantly higher values, whereas minimum glazing alternatives fall into a markedly lower performance tier. Notably, there is no variance between the double and triple glazing variants within each configuration, as the visible light transmittance (VLT) was held constant across both glass types. The highest NUDA is achieved by the maximum glazing ratio configuration equipped with optimized shading (S_22 B 2G OS), closely followed by the Daylight-driven configuration with optimized shading (S_42 D 2G OS). This trend demonstrates that the excessive glare typically associated with extensive glazing can be effectively mitigated by appropriate shading systems without sacrificing overall daylight availability. Conversely, alternatives featuring a minimum glazing ratio, such as the unshaded S_30 H 2G NS, exhibit the lowest NUDA, a direct consequence of their inherently poor Spatial Daylight Autonomy (sDA).

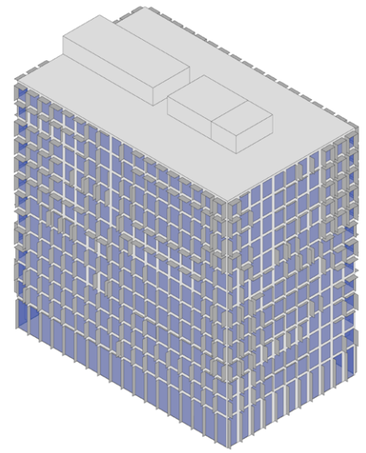

fig. 83

S_22 B 2G OS

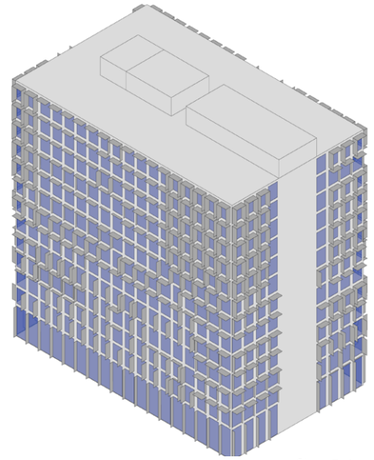

fig. 84

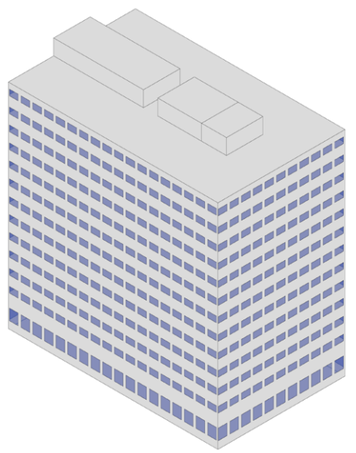

fig. 85

S_30 H 2G NS

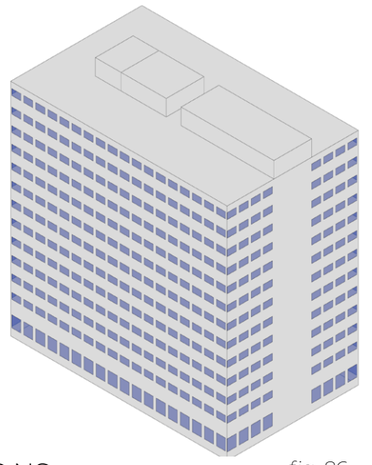

fig. 86

ASE

chart 29



Chart expressed in %

The Annual Sunlight Exposure (ASE) graph demonstrates that the lowest, and therefore most favorable, values are achieved by the configuration featuring a minimal glazing ratio coupled with optimized shading (S_32 H 2G OS). Conversely, the highest ASE, which indicates excessive direct solar penetration and a heightened risk of visual discomfort, is recorded in the baseline configuration utilizing a maximum glazing ratio with no shading elements installed (S_20 B 2G NS).

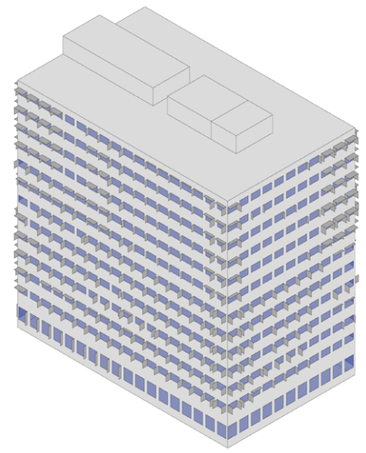

fig. 87

S_32 H 2G OS

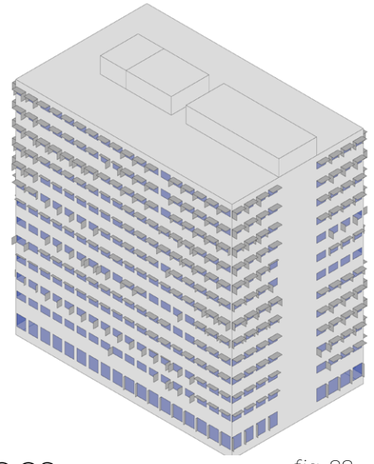

fig. 88

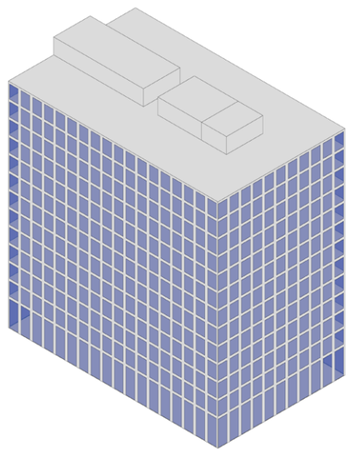

fig. 89

S_20 B 2G NS

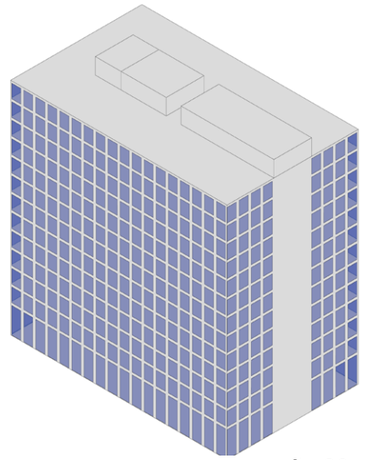

fig. 90

sDA

chart 30

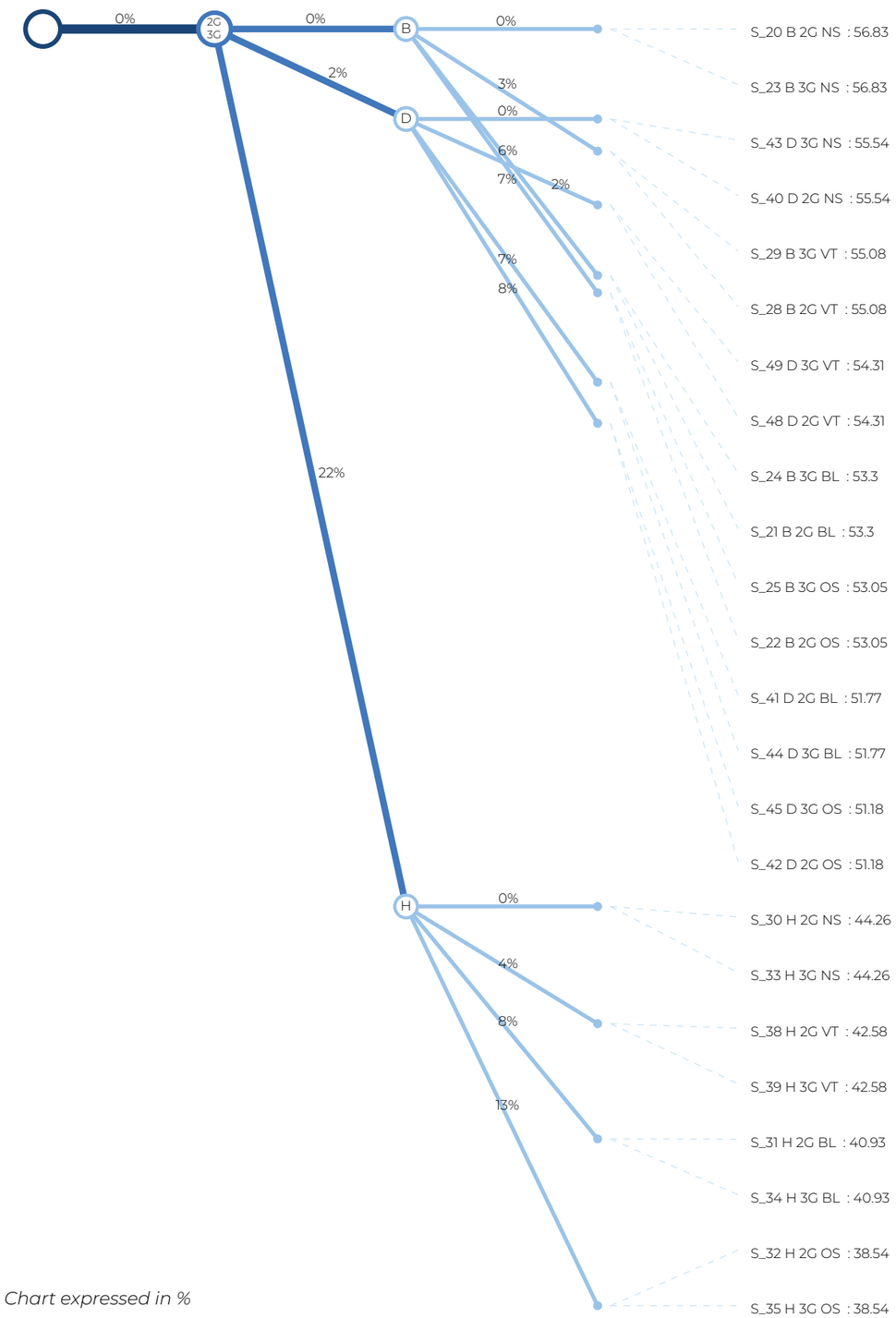

Chart expressed in %

The Spatial Daylight Autonomy (sDA) results demonstrate a direct proportional relationship with the ASE findings, highlighting a fundamental trade-off in daylighting design. Specifically, the configuration that generates the highest ASE also achieves the maximum sDA. Conversely, the heavily restricted configuration that successfully yielded the lowest ASE correspondingly records the lowest sDA.

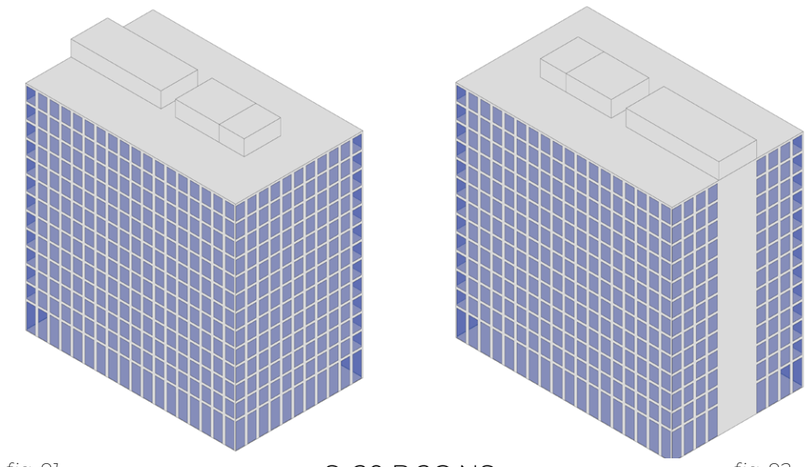

fig. 91

S_20 B 2G NS

fig. 92

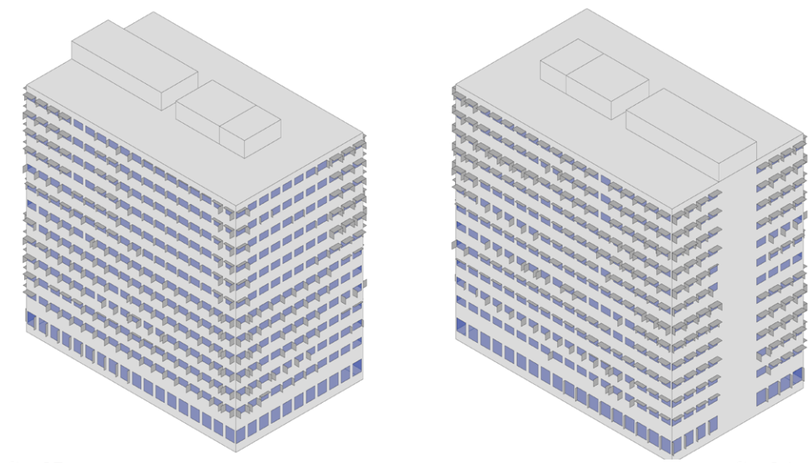

fig. 93

S_35 H 3G OS

fig. 94

5.1.2 Comparative Matrix between the Scenarios

The Comparative Matrix focuses exclusively on Total Global Warming Potential (GWP) and Net Useful Daylight Area (NUDA), as these two indices effectively synthesize the broader spectrum of evaluated parameters, including embodied and operational carbon, ASE, and sDA. To facilitate a comparative rather than strictly quantitative evaluation, the performance values for both Total GWP and NUDA were normalized and distributed across their respective domain bounds.

Among all evaluated alternatives, the configuration featuring triple glazing, a Daylight-driven design, and optimized shading (S_45 D 3G OS) demonstrates the most effective overall trade-off. This option achieves a NUDA of 41.15%, which is merely 1.5% below the absolute maximum recorded value of 41.79%. Concurrently, it yields a Total GWP of 15.29 kg CO_2eq/m²·y, sitting just 3% above the lowest possible carbon footprint of 14.84 kg CO_2eq/m²·y.

When compared to the baseline scenario, configuration S_45 D 3G OS reduces the total carbon footprint by 13% (from 17.49 to 15.29 kg CO_2eq/m²·y) while simultaneously improving daylighting performance, increasing NUDA by 10% (from 37.27% to 41.15%). This balanced performance is critical; by contrast, the alternative with the absolute lowest Total GWP achieves a 15% carbon reduction but severely compromises daylight availability, causing a 14% decline in NUDA (dropping from the baseline of 37.27% down to 32.23%)

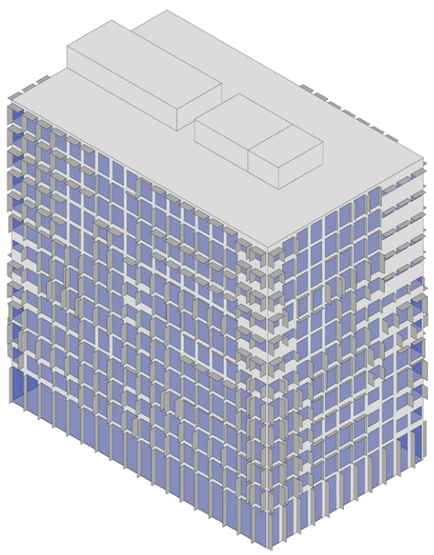

fig. 95

S_45 D 3G OS

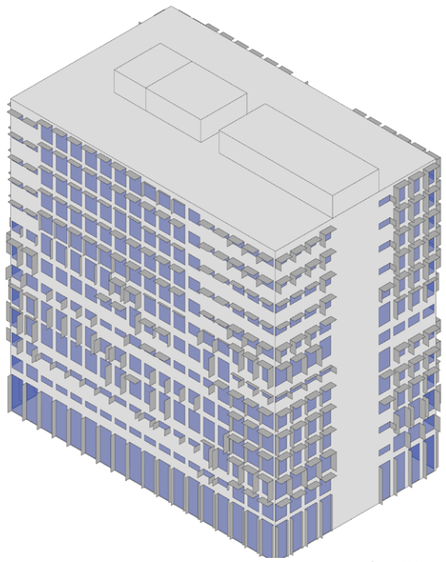

fig. 96

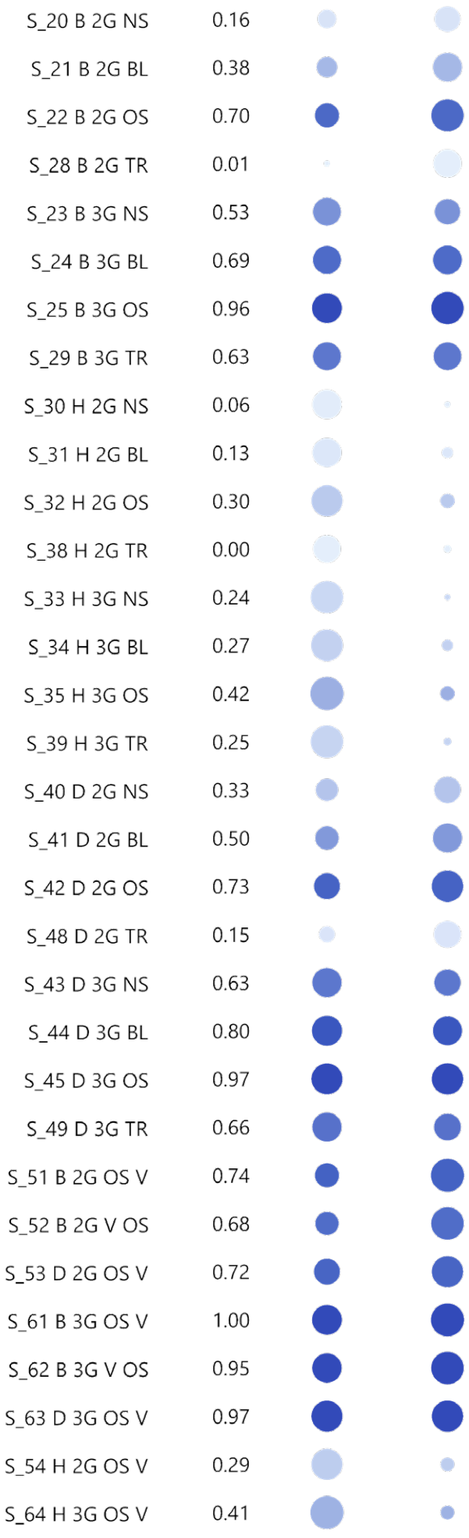

Comparative Matrix

chart 31

5.2 Cross-Scenario Synthesis and Cost-Benefit Analysis

Carbon Payback of the Double to Triple Glazing transformation

Upgrading from double to triple glazing inherently increases embodied carbon due to the additional glass pane and the heavier framing required. However, this initial carbon penalty is decisively offset by dramatic reductions in operational carbon. As demonstrated in the preceding heating and cooling load analyses, triple glazing consistently yields superior thermal performance across all seasonal scenarios. Over the building's lifecycle, the carbon efficiency of this upgrade ranges from 300% to 500%. This signifies a highly robust carbon return on investment, where every unit of additional embodied carbon yields roughly four units of operational carbon savings. Notably, this efficiency ratio is highly sensitive to the window-to-wall area; it is most pronounced in maximum glazing configurations, such as S_28 B 2G VT, and comparatively lower in minimal glazing alternatives, such as S_32 H 2G OS.

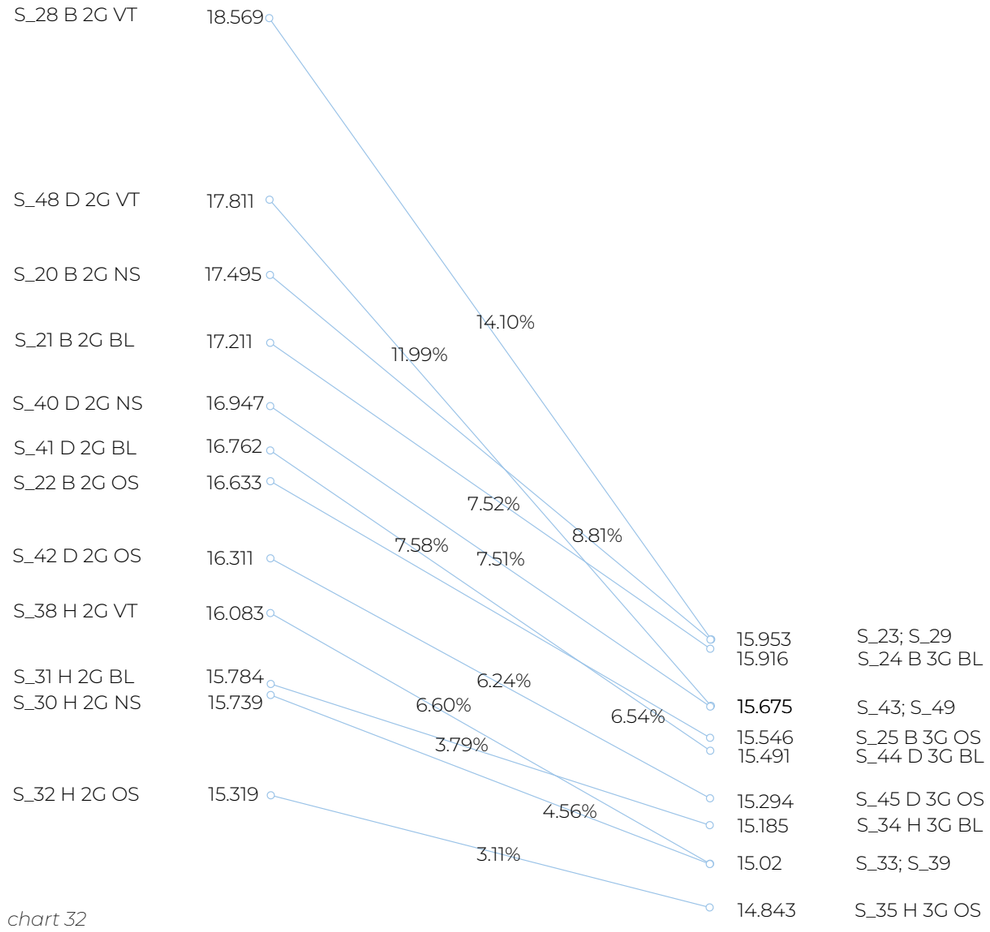

chart 32

Cost-Benefit of 2G to 3G Trasformation

chart 33

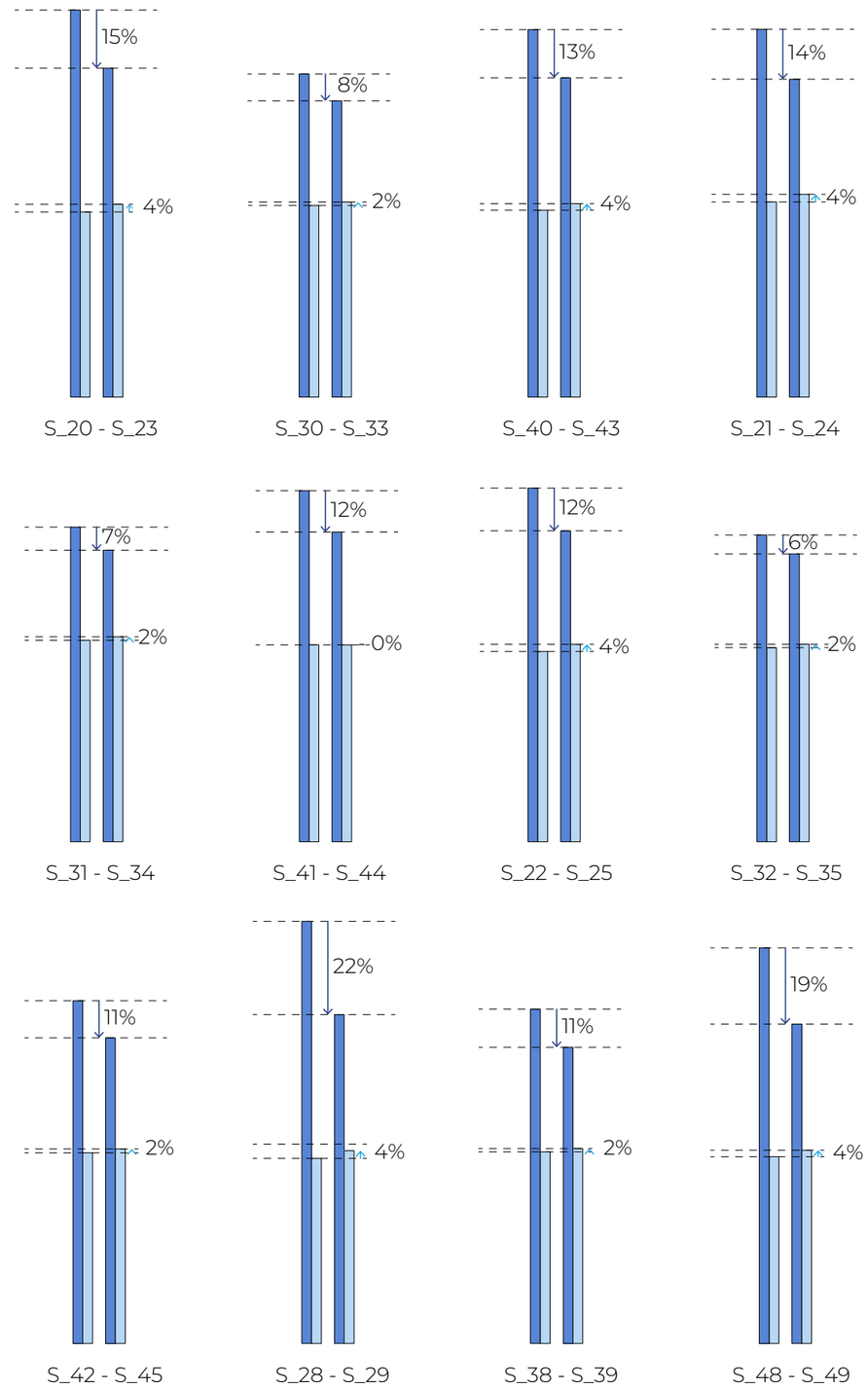

Impact of Minimizing the Glazing Ratio

Reducing the glazing ratio yields a significant decrease in the building's total carbon footprint. This reduction is primarily driven by a lowered cooling demand and the superior thermal insulation provided by a larger opaque wall area. The data indicates that this strategy is particularly impactful for configurations utilizing double-glazed windows, where the thermal vulnerability of the glass is highest. Conversely, in highly optimized configurations featuring efficient triple glazing and customized shading (e.g., S_25 B 3G OS), the marginal carbon savings of reducing the window area diminish to approximately 5%. Furthermore, this modest carbon reduction must be carefully weighed against its primary drawback: a notable decline in the availability of useful daylight (NUDA).

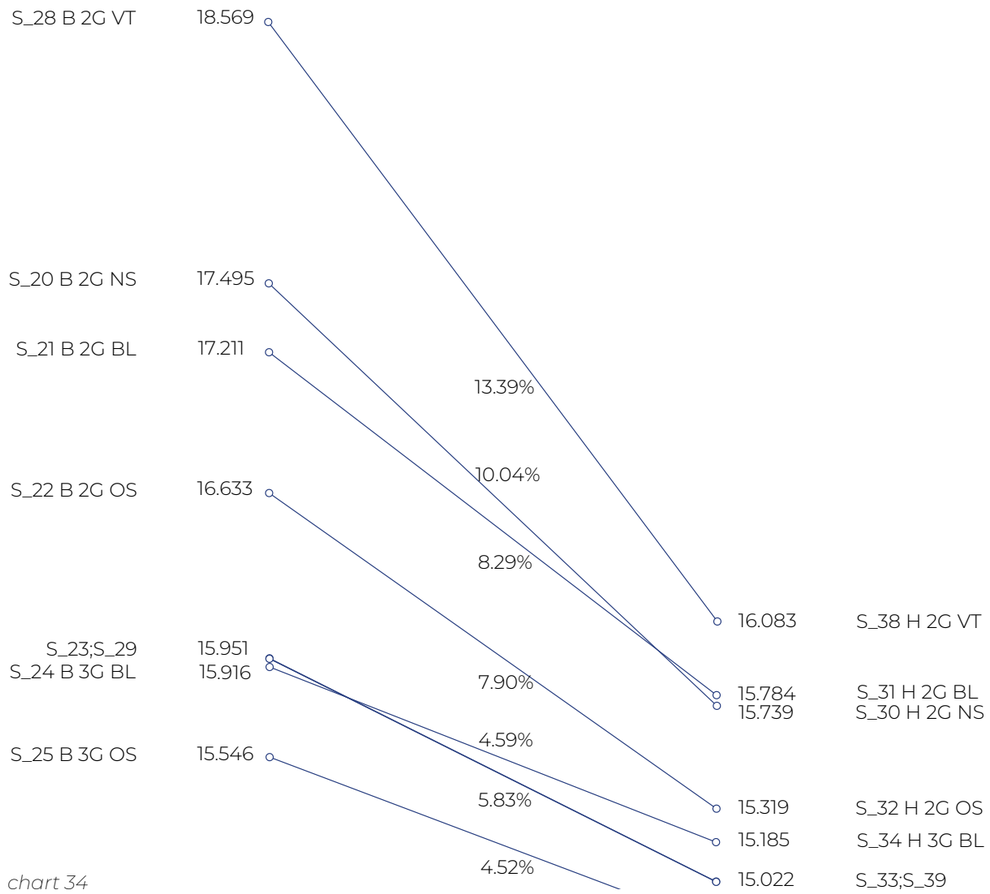

chart 34

Impact of the Daylight-Driven Glazing Configuration

Although adopting customized, daylight-driven window proportions successfully increases the Net Useful Daylight Area (NUDA), its influence on the building's overall emissions is comparatively subdued. Specifically, the magnitude of change in the total carbon footprint under this configuration is only about one-third of the variation observed when implementing the minimal glazing ratio strategy. This indicates that while optimizing window geometry for daylight is highly effective for visual comfort, it is a less potent lever for driving large-scale carbon reductions than simply minimizing the glass area.

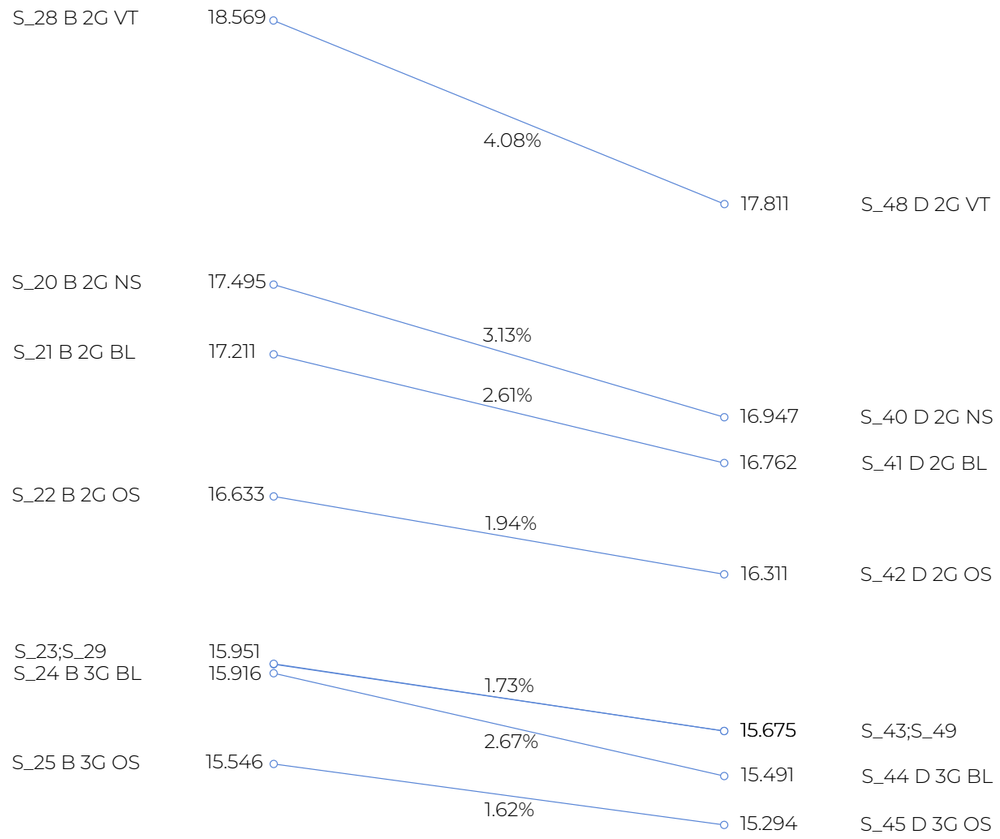

chart 35

Impact of Generalized Shading System

The implementation of a generalized shading strategy across the entire facade yields inconsistent results, producing both positive and negative performance impacts (as evidenced by cases [S_20 B 2G NS] and [S_33 H 3G NS]). This variability occurs because a uniform approach applies identical shading profiles across all zones, failing to account for localized parameters such as specific orientation, spatial location, programmatic function, and room geometry (area and height). Furthermore, because it requires extensive, untailored hardware, this monolithic approach imposes the highest embodied carbon penalty of any evaluated strategy.

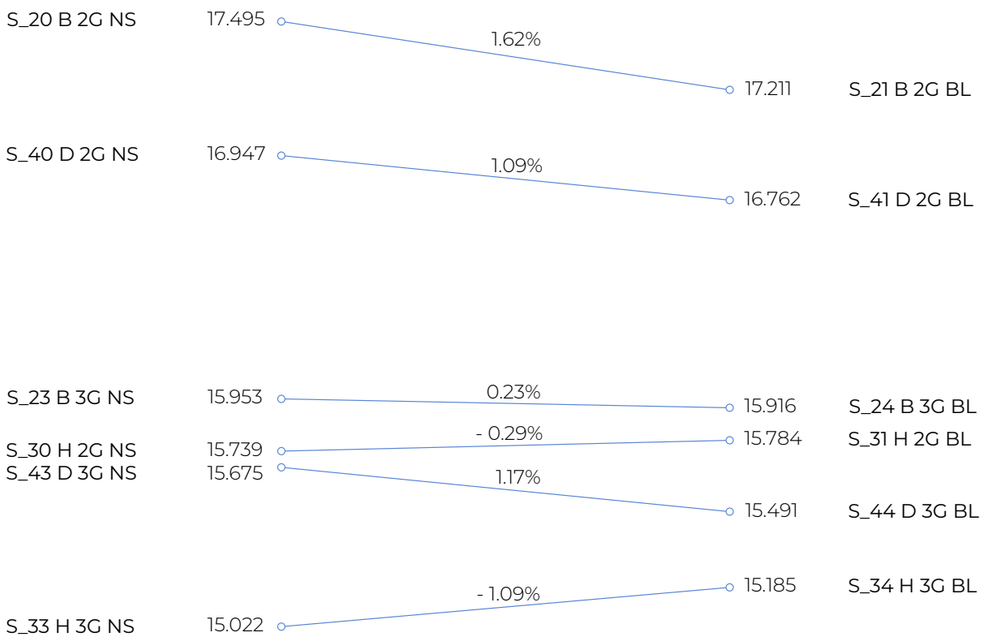

chart 36

Impact of Optimized Shading Systems

Among the evaluated shading strategies, optimized shading emerges as the optimal solution, consistently reducing the total carbon footprint across all configurations. This overarching improvement is primarily driven by a substantial reduction in cooling demand, which constitutes the main contributor to the building's operational carbon emissions. Furthermore, this strategy ensures that the embodied carbon penalty remains low. Because shading elements are selectively applied only where they yield a positive impact on daylighting performance, the required material surface area, and thus the embedded emissions, is kept to an absolute minimum.

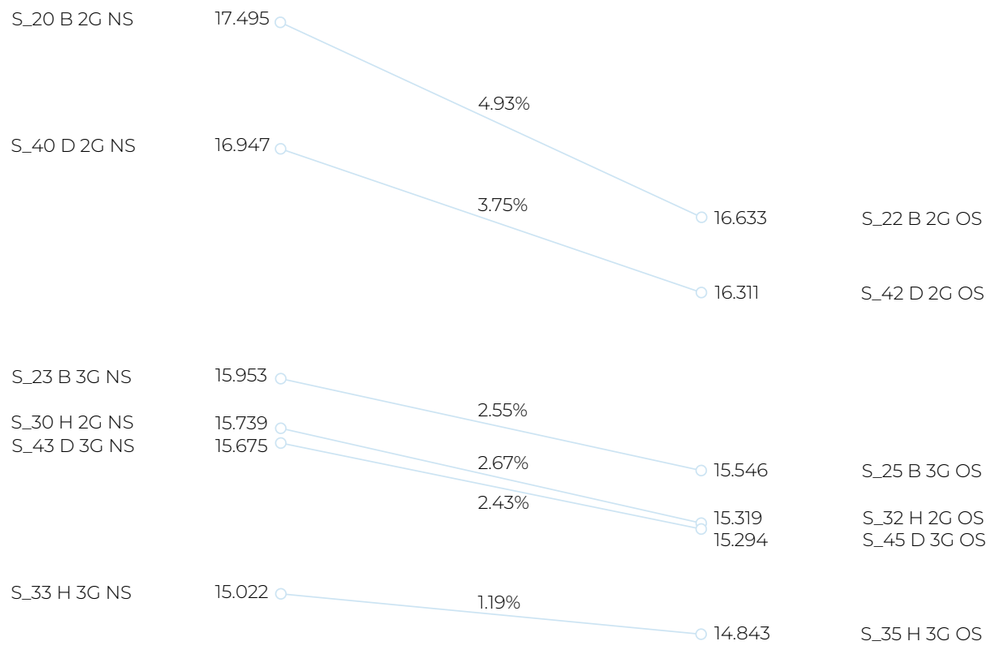

chart 37

Impact of Modifying Visual Transmittance

The embodied carbon penalty associated with altering the visual transmittance (VT) of the windows is minimal. This modification primarily relies on adjusting the physical properties of the glass, such as through the application of thin-film coatings, rather than installing material-intensive shading structures. However, while this strategy successfully increases the Net Useful Daylight Area (NUDA), it inadvertently yields a negative impact on operational energy performance. This operational penalty is driven by the intrinsic relationship between visual transmittance and the Solar Heat Gain Coefficient (SHGC). Altering the VT inherently fluctuates the SHGC, leading to undesirable localized increases in solar heat gain that drive up cooling demands. Notably, the data indicates that this SHGC variation is significantly less pronounced, and therefore less detrimental thermally, in triple-glazed configurations compared to double glazing.

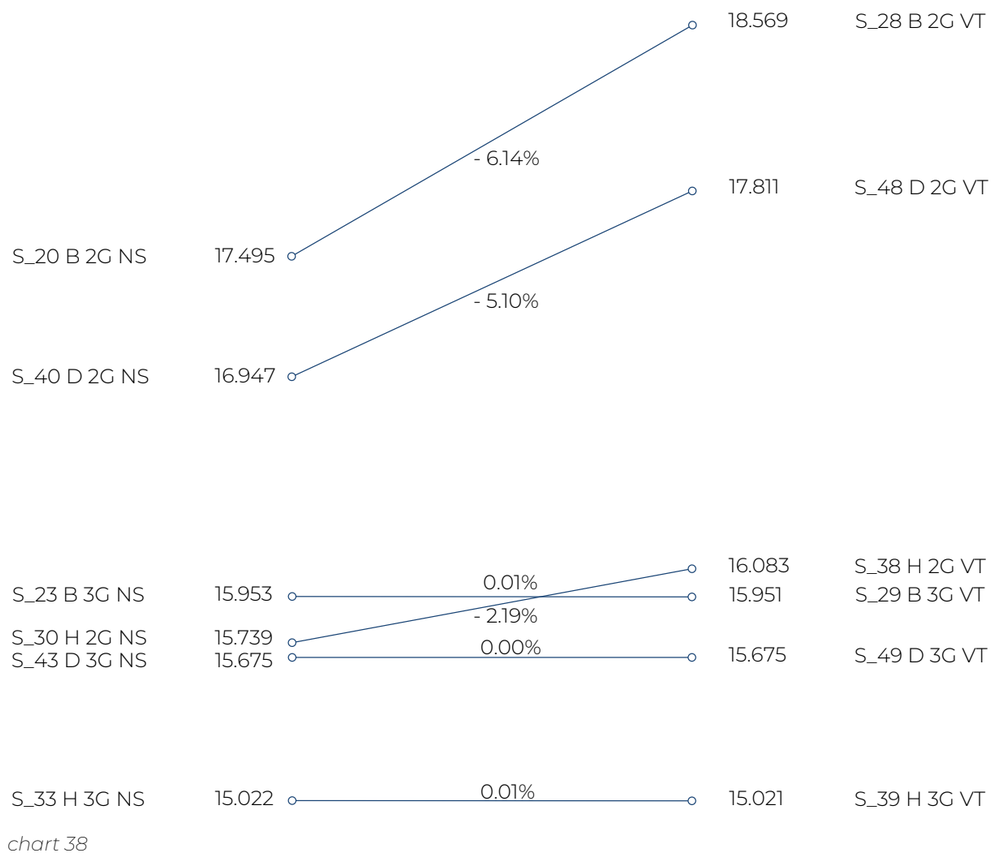

chart 38

5.3 Key-findings and Strategic Optimization Sequence

Based on the comparative analysis, achieving the optimal balance between daylighting and lifecycle carbon emissions requires a strict hierarchical approach to design interventions. The following sequential strategy is recommended:

1. Prioritize Envelope Thermal Resistance (Triple Glazing)
The foundational and most impactful intervention is upgrading from double to triple glazing. This strategy offers the most favorable holistic trade-offs by simultaneously suppressing both heating and cooling loads. The data demonstrates that improving window quality is more effective than installing shading systems, even in configurations with minimal glazing ratios. Furthermore, establishing a high-performance envelope via triple glazing inherently diminishes the thermal necessity of supplementary shading. While shading can still be added, its marginal efficiency regarding operational energy savings is significantly reduced once triple glazing is in place.

2. Optimize the Glazing Ratio
Following the glazing upgrade, the second strategic priority is calibrating the window-to-wall ratio. This step is critical as it inextricably links thermal performance with architectural geometry and daylight availability. In contexts where Spatial Daylight Autonomy (sDA) is already restricted (e.g., dense urban environments with severe contextual overshadowing), reducing the glazing ratio can lower the carbon footprint more significantly than other strategies. However, this architectural intervention is highly sensitive to the efficiency of the building's artificial lighting systems. If the interior lighting fixtures are inefficient, the increased electrical demand required to compensate for the loss of natural daylight may entirely negate the carbon savings achieved through reduced cooling loads.

3. Implement Optimized Shading
The final refinement step is the application of shading systems. Among the evaluated shading strategies, only customized, optimized shading universally improves performance across the modeled configurations. By strategically blocking direct solar radiation and preventing interior overheating, optimized shading significantly curbs cooling demands. Notably, the efficacy of this strategy is inversely proportional to the baseline envelope performance; it yields the highest operational savings in buildings characterized by high glazing ratios and lower-efficiency (double-glazed) windows.

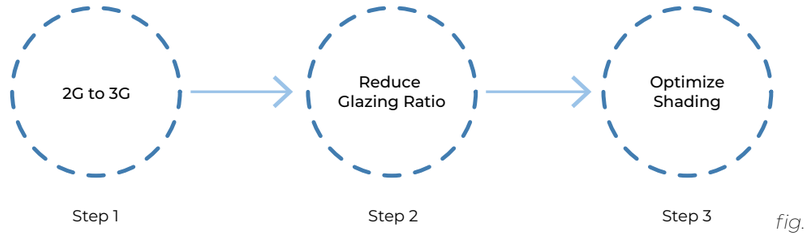

fig. 97

5.4 Future Developement

As the built environment transitions toward the global target of net-zero emissions by 2050, both operational and embodied carbon footprints are projected to decline. However, driven by rapid technological advancements in grid infrastructure and building systems, operational emissions are decreasing at a significantly accelerated rate. Consequently, while operational energy currently dictates the majority of a building's lifecycle carbon, embodied emissions from materials and construction will soon emerge as the dominant contributor. The design strategies derived in this study remain highly applicable for newly constructed office buildings in Milan or similar climates under present conditions. Nevertheless, architectural interventions optimized exclusively for today's energy landscape risk becoming environmental liabilities in the future. This shift underscores the necessity of evolving from static comparative analyses to dynamic modeling frameworks, ensuring that architectural design strategies remain resilient and forward-looking throughout a building's lifespan.

5.4.1 The Shifting Balance of Embodied and Operational Carbon

The accompanying pie charts illustrate the proportional distribution of embodied and operational carbon across all evaluated alternatives. On average, embodied carbon accounts for approximately 37% of the total lifecycle carbon footprint, equating to roughly 63% of the operational carbon share. In absolute terms, the mean embodied carbon stands at 355 kg CO_2eq/m², while the operational carbon averages 605 kg CO_2eq/m².

chart 39

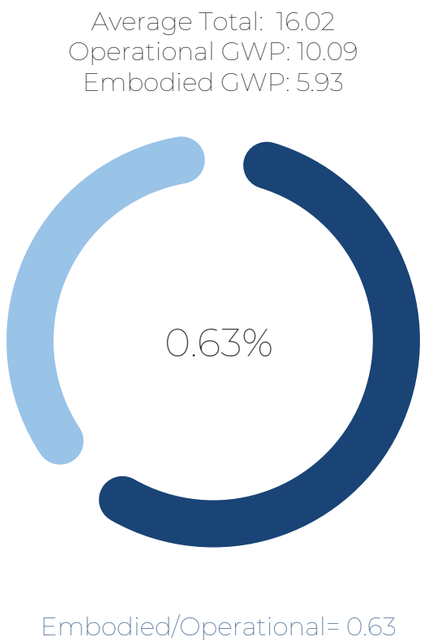



chart 40

However, looking ahead to future developments, this proportional relationship is expected to invert. According to the LETI Climate Emergency Design Guide (2020 edition) trajectory for 2030, embodied carbon will eventually dominate a building's total emission profile. This systemic shift is driven by the ongoing decarbonization of the national grid, the widespread integration of on-site renewable energy generation, and the transition to high-efficiency electrified systems, such as heat pumps. To align with this future, LETI's 2030 target suggests an embodied carbon limit of approximately 350 kg CO_2eq/m^2, emphasizing the necessity of building reuse and material efficiency.

Similarly, the RIBA 2030 Climate Challenge sets stringent benchmarks for non-domestic new-build offices. RIBA targets a lifecycle embodied carbon of less than 750 kg CO_2eq/m^2 and an operational energy use intensity of less than 55 kWh/m^2·y. Assuming a grid carbon intensity of 200 kg CO_2/MWh, this operational energy target translates to a lifecycle operational carbon footprint of strictly under 660 kg CO_2eq/m^2. Consequently, as operational emissions are aggressively curtailed to meet these 2030 targets.

While the evaluated office configurations successfully meet the rigorous embodied carbon targets set by both RIBA and LETI, and the majority achieve an operational energy demand below the 55 kWh/m^2·y threshold, the resulting ratio of embodied to operational carbon does not yet reflect anticipated future trajectories. Currently, the analysis assumes a baseline grid carbon intensity of 200 kg CO_2eq/MWh. However, for operational emissions to shrink to 28% of the total carbon footprint, as projected under future grid decarbonization scenarios, the carbon intensity of the energy supply must decrease by 80%, dropping to 40 kg CO_2eq/MWh an less.
This profound sensitivity to external electrical infrastructure underscores the limitation of static evaluations. Consequently, there is a clear need to develop a dynamic ranking framework that adapts to fluctuating grid carbon intensities, thereby enabling more resilient and forward-looking strategic decision-making in building design.

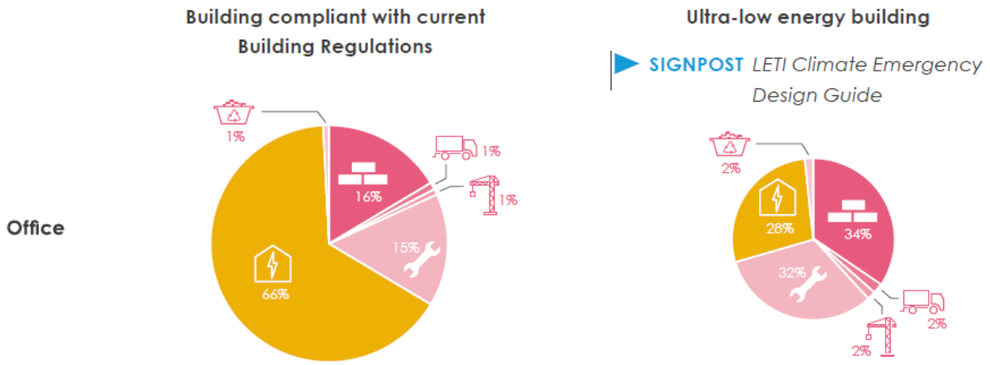

chart 41

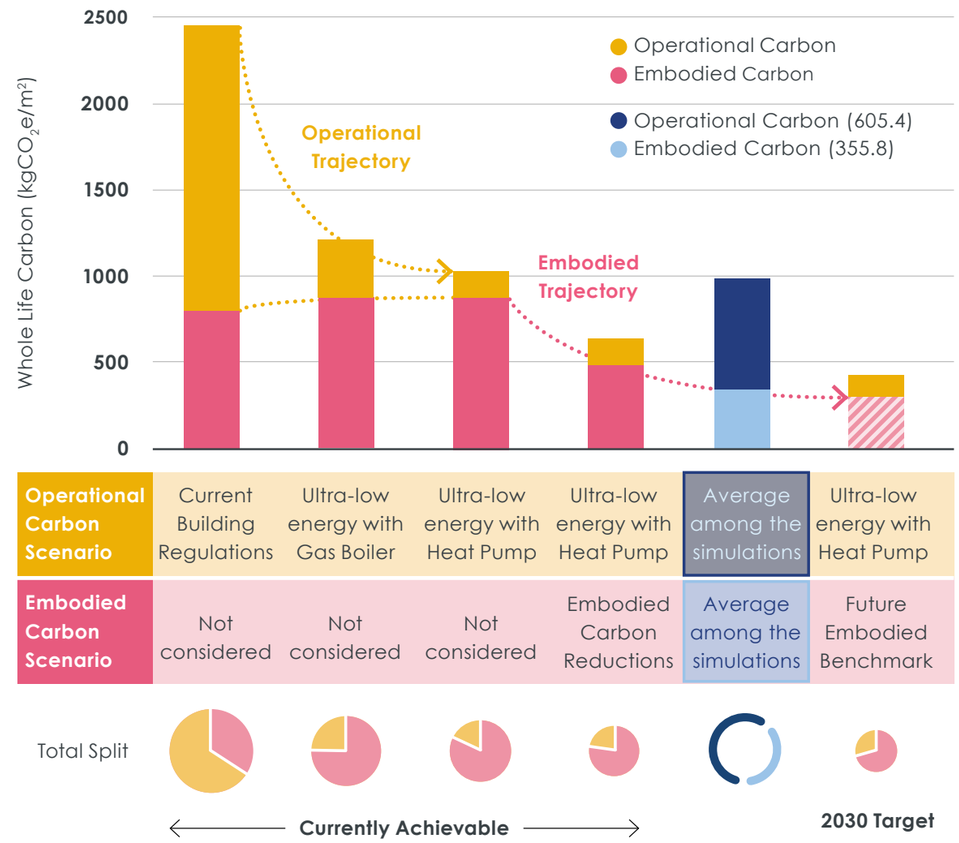

chart 42

5.4.2 Dynamic Carbon Modeling and the Paradigm Shift in Design

The subsequent diagram illustrates a dynamic model of the total carbon footprint, adjusted across a spectrum of grid carbon intensities. Starting from a baseline of 200 kg CO_2eq/MWh, the model projects decarbonization scenarios representing declines of 50%, 80%, and ultimately 90% (down to 20 kg CO_2eq/MWh). Observing these projections reveals a fundamental paradigm shift in architectural strategy: as grid energy becomes cleaner, the imperative shifts from minimizing operational energy to aggressively reducing embodied carbon. Consequently, alternatives previously identified as optimal under current grid conditions are no longer best practices, penalized heavily by their high initial emissions. For instance, the upgrade from double to triple glazing loses its environmental viability on a highly decarbonized grid, as the embodied carbon penalty of the extra glass far exceeds the now-marginal operational savings in heating and cooling.
This profound inversion in design priorities raises critical questions about long-term architectural resilience and opens the door for further exploration into low-embodied-carbon materials.

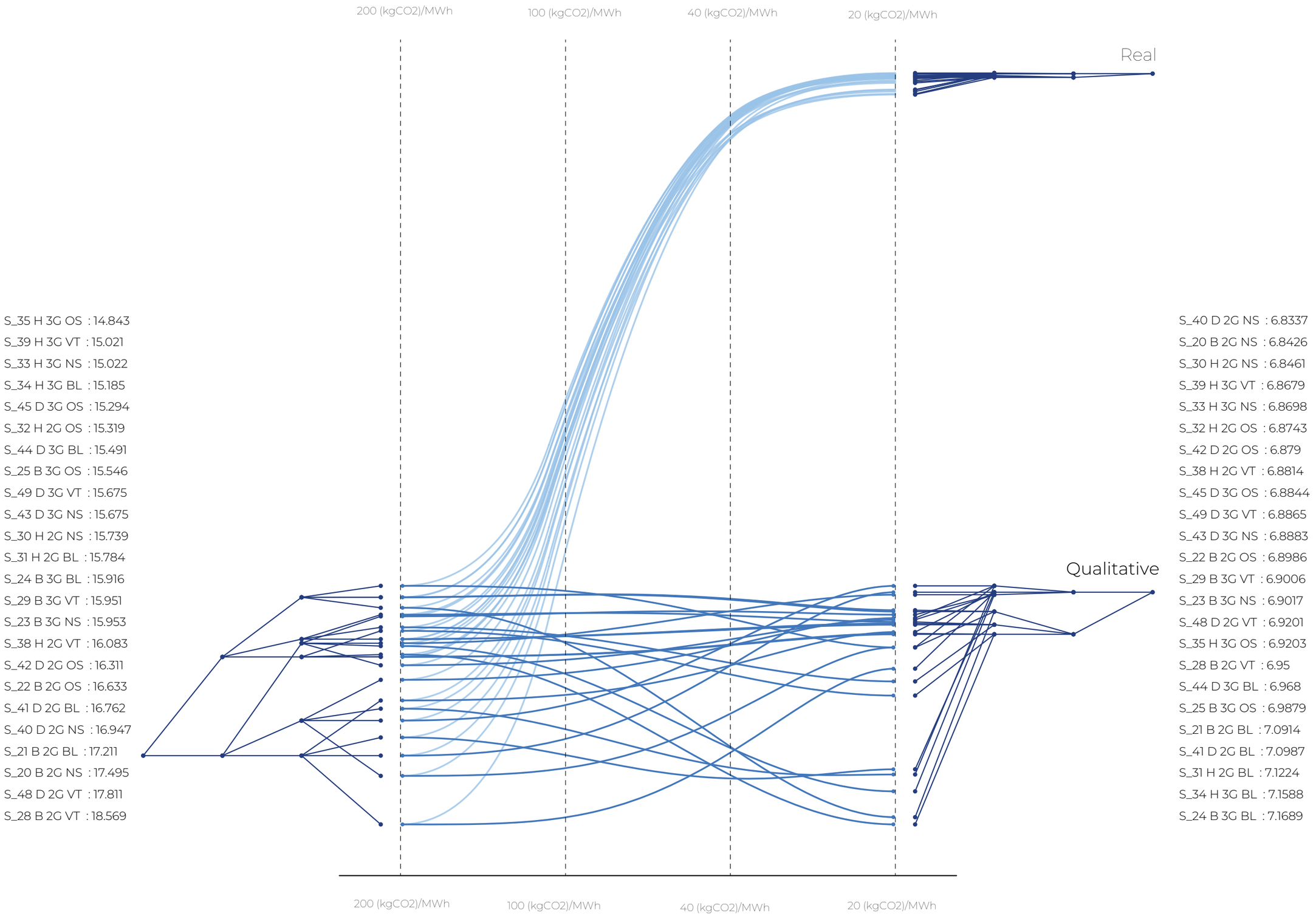
200 (kgCO2)/MWh
100 (kgCO2)/MWh
40 (kgCO2)/MWh
20 (kgCO2)/MWh
Real
Qualitative
S_35 H 3G OS : 14.843
S_39 H 3G VT : 15.021
S_33 H 3G NS : 15.022
S_34 H 3G BL : 15.185
S_45 D 3G OS : 15.294
S_32 H 2G OS : 15.319
S_44 D 3G BL : 15.491
S_25 B 3G OS : 15.546
S_49 D 3G VT : 15.675
S_43 D 3G NS : 15.675
S_30 H 2G NS : 15.739
S_31 H 2G BL : 15.784
S_24 B 3G BL : 15.916
S_29 B 3G VT : 15.951
S_23 B 3G NS : 15.953
S_38 H 2G VT : 16.083
S_42 D 2G OS : 16.311
S_22 B 2G OS : 16.633
S_41 D 2G BL : 16.762
S_40 D 2G NS : 16.947
S_21 B 2G BL : 17.211
S_20 B 2G NS : 17.495
S_48 D 2G VT : 17.811
S_28 B 2G VT : 18.569
S_40 D 2G NS : 6.8337
S_20 B 2G NS : 6.8426
S_30 H 2G NS : 6.8461
S_39 H 3G VT : 6.8679
S_33 H 3G NS : 6.8698
S_32 H 2G OS : 6.8743
S_42 D 2G OS : 6.879
S_38 H 2G VT : 6.8814
S_45 D 3G OS : 6.8844
S_49 D 3G VT : 6.8865
S_43 D 3G NS : 6.8883
S_22 B 2G OS : 6.8986
S_29 B 3G VT : 6.9006
S_23 B 3G NS : 6.9017
S_48 D 2G VT : 6.9201
S_35 H 3G OS : 6.9203
S_28 B 2G VT : 6.95
S_44 D 3G BL : 6.968
S_25 B 3G OS : 6.9879
S_21 B 2G BL : 7.0914
S_41 D 2G BL : 7.0987
S_31 H 2G BL : 7.1224
S_34 H 3G BL : 7.1588
S_24 B 3G BL : 7.1689
200 (kgCO2)/MWh
100 (kgCO2)/MWh
40 (kgCO2)/MWh
20 (kgCO2)/MWh

chart 43

References

[1] UN Environmental Program
https://www.unep.org/news-and-stories/press-release/emissions-building-sector-stopped-rising-first-time-2020-un-finds - *Accessed on 27 April 2026*

[2] UN Environmental Program
https://www.unep.org/news-and-stories/press-release/not-yet-built-purpose-global-building-sector-emissions-still-high - *Accessed on 27 April 2026*

[3] One Click LCA
https://oneclicklca.com/en-us/resources/articles/embodied-carbon-vs-operational-carbon - *Accessed on 27 April 2026*

[4] SDG Knowledge club
https://sdg.iisd.org/news/global-report-calls-for-accelerated-decarbonization-of-buildings-sector/ - *Accessed on 27 April 2026*

[5] **Wang, G., Luo, T., Luo, H.** et al. A comprehensive review of building lifecycle carbon emissions and reduction approaches. City Built Environment 2, 12 (2024).
https://link.springer.com/article/10.1007/s44213-024-00036-1 - *Accessed on 27 April 2026*

[6] UN Environmental Program
https://globalabc.org/buildingmaterialsandclimate/chapte-2-life-cycle-thinking/2-1-embodied-versus-operational-carbon-emissions-in-buildings.html
- *Accessed on 27 April 2026*

[7] **Lützkendorf, T., Balouktsi, M.** Embodied carbon emissions in buildings: explanations, interpretations, recommendations. Volume: 3 Issue: 1 (2022).
https://journal-buildingscities.org/articles/10.5334/bc.257 - *Accessed on 27 April 2026*

[8] **Zhong X., Hu M., Deetman S., Steubing B., Lin H.X., Hernandez G.A., Harpprecht C., Zhang C., Tukker A., Behrens P.** Global greenhouse gas emissions from residential and commercial building materials and mitigation strategies to 2060. Nat Commun. 2021 Oct 21; 12(1):6126
https://pmc.ncbi.nlm.nih.gov/articles/PMC8531392/ - *Accessed on 27 April 2026*

[9] **de Paula Filho, J.H.M., D'Antimo, M., Charlier, M., Vassart O.** Life-Cycle Assessment of an Office Building: Influence of the Structural Design on the Embodied Carbon Emissions. Modelling 2024, 5(1), 55-70
https://www.mdpi.com/2673-3951/5/1/4 - *Accessed on 27 April 2026*

[10] **Aquino, A., Bassetti, M., Martini, F., Martini C., Salvio, M.** Energy efficiency of the Italian office buildings: Highlights from mandatory energy audits. Energy and Buildings, Volume 347, Part A, 15 November 2025, 116275
https://www.sciencedirect.com/science/article/pii/S0378778825010059
- *Accessed on 27 April 2026*

[11] **Shi, Y., Cao, X., Yang, X.** Assessment and reduction of embodied carbon emissions in buildings: a systematic literature review of recent advances. Energy and Buildings Volume 345, 15 October 2025, 116058
https://www.sciencedirect.com/science/article/pii/S0378778825007881
- *Accessed on 28 April 2026*

[12] **Phillips, R., Troup. L., Fannon, D., Eckelman M.J.** (2020) Triple bottom line sustainability assessment of window-to-wall ratio in US office buildings. https://www.sciencedirect.com/science/article/abs/pii/S0360132320304376 - *Accessed on 07 September 2026*

[13] OneClick LCA
https://oneclicklca.com/en/resources/articles/life-cycle-assessment-examples-and-lca-defined/ - *Accessed on 28 April 2026*

[14] Ecochain
https://ecochain.com/blog/life-cycle-assessment-lca-guide/#h-3-the-4-phases-of-a-life-cycle-assessment - *Accessed on 28 April 2026*

[15] UN Environmental Program
https://globalabc.org/resources/publications/global-status-report-buildings-and-construction-beyond-foundations - *Accessed on 29 April 2026*

[16] **Magwood, C., Huynh, H., Olgyay, V.** (2023) The Hidden Climate Impact of Residential Construction
https://rmi.org/insight/hidden-climate-impact-of-residential-construction/ - *Accessed on 29 April 2026*

[17] UN Environmental Program
https://www.unep.org/resources/report/global-status-report-buildings-and-construction-20242025 - *Accessed on 29 April 2026*

[18] International Energy Agency
https://www.iea.org/policies/12766-european-commissions-renovation-wave-strategy - *Accessed on 29 April 2026*

[19] European Parliament WebSite
https://www.europarl.europa.eu/legislative-train/theme-a-european-green-deal/file-renovation-wave - *Accessed on 29 April 2026*

[20] Buildings Performance Institute Europe (BPIE)
https://imt.org/wp-content/uploads/2022/02/SPIPA_EU_rev6_508.pdf
- *Accessed on 29 April 2026*

[21] European Commission: BUILD UP
https://build-up.ec.europa.eu/en/news-and-events/news/renovation-wave-and-transformation-eu-building-stock - *Accessed on 29 April 2026*

[22] MIND
https://www.mindmilano.it/ - *Accessed on 30 April 2026*

[23] **Hollberg, A., Kaushal, D., Basic, S., Galimshina, A., Habert, G.** (2020) A data-driven parametric tool for under-specified LCA in the design phase. IOP Conf. Ser.: Earth Environ.
https://iopscience.iop.org/article/10.1088/1755-1315/588/5/052018/meta
- *Accessed on 30 April 2026*

[24] EPDItaly
Beton Lana GmbH/S.r.l.
https://www.epditaly.it/epd/miscele-di-calcestruzzo-riciclato-3/
- *Accessed on 22 May 2026*

[25] EPDItaly
Pittini Group
https://www.pittini.it/documentazione/dichiarazione-ambientale-epd/
- *Accessed on 22 May 2026*

[26] EPDItaly
Pittini Group
https://www.pittini.it/documentazione/dichiarazione-ambientale-epd/
- *Accessed on 22 May 2026*

[27] ÖKOBAUDAT
Rubner Holding AG - S.p.A.
https://www.oekobaudat.de/OEKOBAU.DAT/datasetdetail/process.xhtml?uuid=efa55966-4f29-4f15-bfec-8c08b3945923&version=00.03.000
- *Accessed on 23 May 2026*

[27] ÖKOBAUDAT
SWISS KRONO TEX GmbH & Co. KG
https://www.oekobaudat.de/OEKOBAU.DAT/datasetdetail/process.xhtml?uuid=1cb94463-8401-44cf-8d36-d49c3b82a72b&version=00.02.000
- *Accessed on 23 May 2026*

[28] One Click LCA
https://oneclicklca.com/en/resources/articles/carbon-benchmark-join-the-carbon-heroes-program-for-green-buildings
- *Accessed on 25 May 2026*

[29] **Alsukkar, M., Ibrahim, A., Eltaweel, A.** (2026) Multi-objective optimization of daylighting systems for energy efficiency and thermal-visual comfort in buildings: a review.
https://www.sciencedirect.com/science/article/pii/S2950156325000065
- *Accessed on 07 September 2026*

[30] EPD International AB
LONGi Green Energy Technology Co., Ltd.
https://www.environdec.com/library/epd9079
- *Accessed on 25 August 2026*

[31] **Heschong Mahone Group.** (2012) Daylight Metrics: PIER Program Final Project Report. California Energy Commission.
https://www.researchgate.net/publication/328965606_DAYLIGHT_METRICS_REPORT_for_the_CEC_PIER_Daylighting_Plus_Research_Program
- *Accessed on 23 September 20267*

[32] **Konis,K., Gamas, A., Kensek, K.** (2016) Passive performance and building form: An optimization framework for early-stage design support
https://www.sciencedirect.com/science/article/pii/S0038092X15006933
- *Accessed on 23 September 2026*

[33] **Carlucci, S., Cattarin, G., Causone, F., Pagliano, L.** (2015) Multi-objective optimization of a nearly zero-energy building based on thermal and visual discomfort minimization using a non-dominated sorting genetic algorithm (NSGA-II)
https://www.sciencedirect.com/science/article/pii/S0378778815301080?via%3Dihub
- *Accessed on 23 September 2026*

[34] **Mardaljevic, J., Nabil, A.** (2005) Useful daylight illuminance: a new paradigm for assessing daylight in buildings
https://www.researchgate.net/publication/245385301_Useful_daylight_illuminance_a_new_paradigm_for_assessing_daylight_in_buildings
- *Accessed on 23 September 2026*

[35] Carbon Alignment LETI
https://www.leti.uk/carbonalignment
- Accessed on 24 September 2026

[36] Embodied Carbon Primer LETI
https://www.leti.uk/ecp
- Accessed on 24 September 2026

[37] 2030 Climate Challenge - RIBA
https://www.riba.org/campaigns/climate-action/2030-climate-challenge/
- Accessed on 24 September 2026

ANNEX A

Daylight-Driven Optimization for Glazing and Shadings simulations results

Annex A from page 2 to page 6: Optimization process explanatations
Annex A from page 7 to page 36: Daylight Simulations Results

Window Size Optimisation

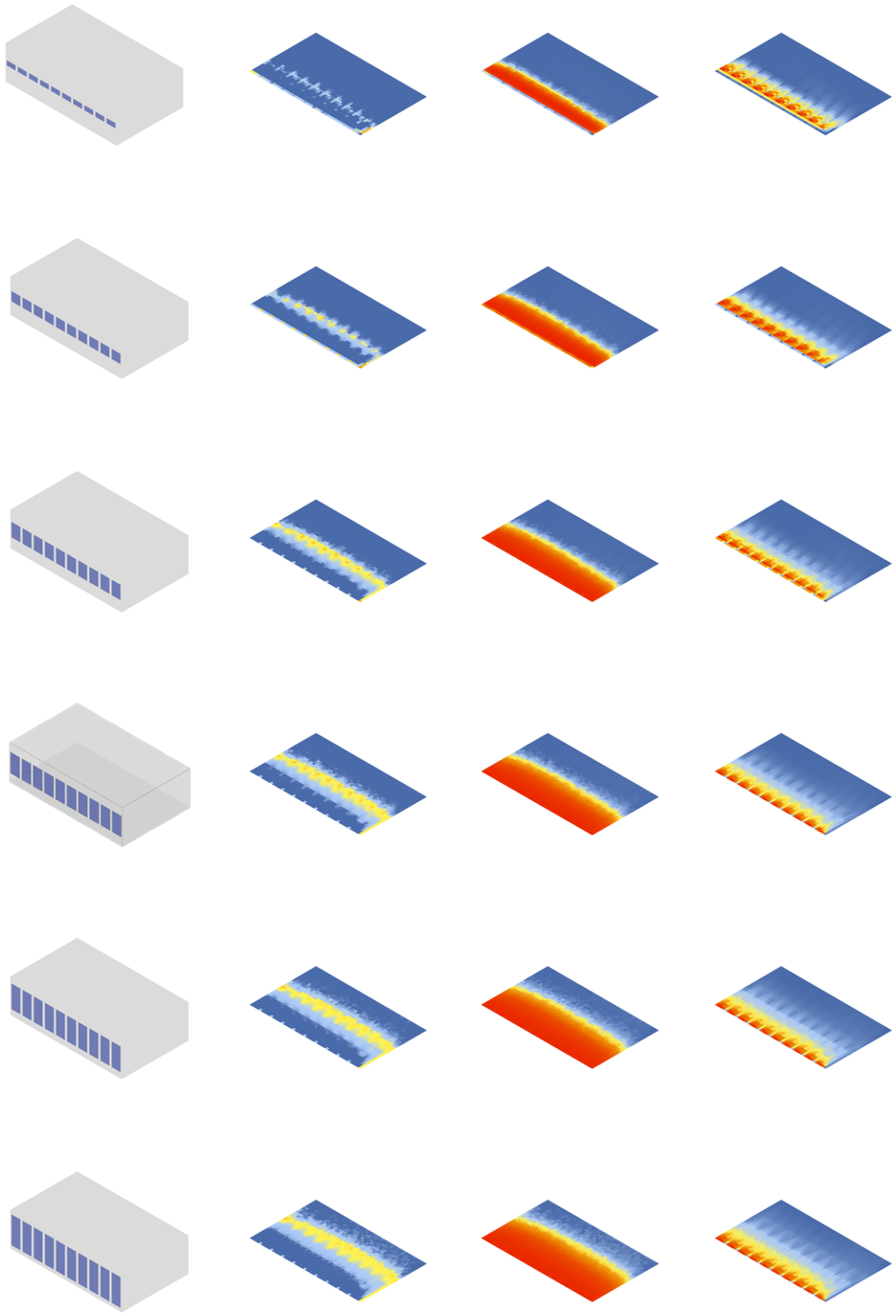

Static Shading Optimization

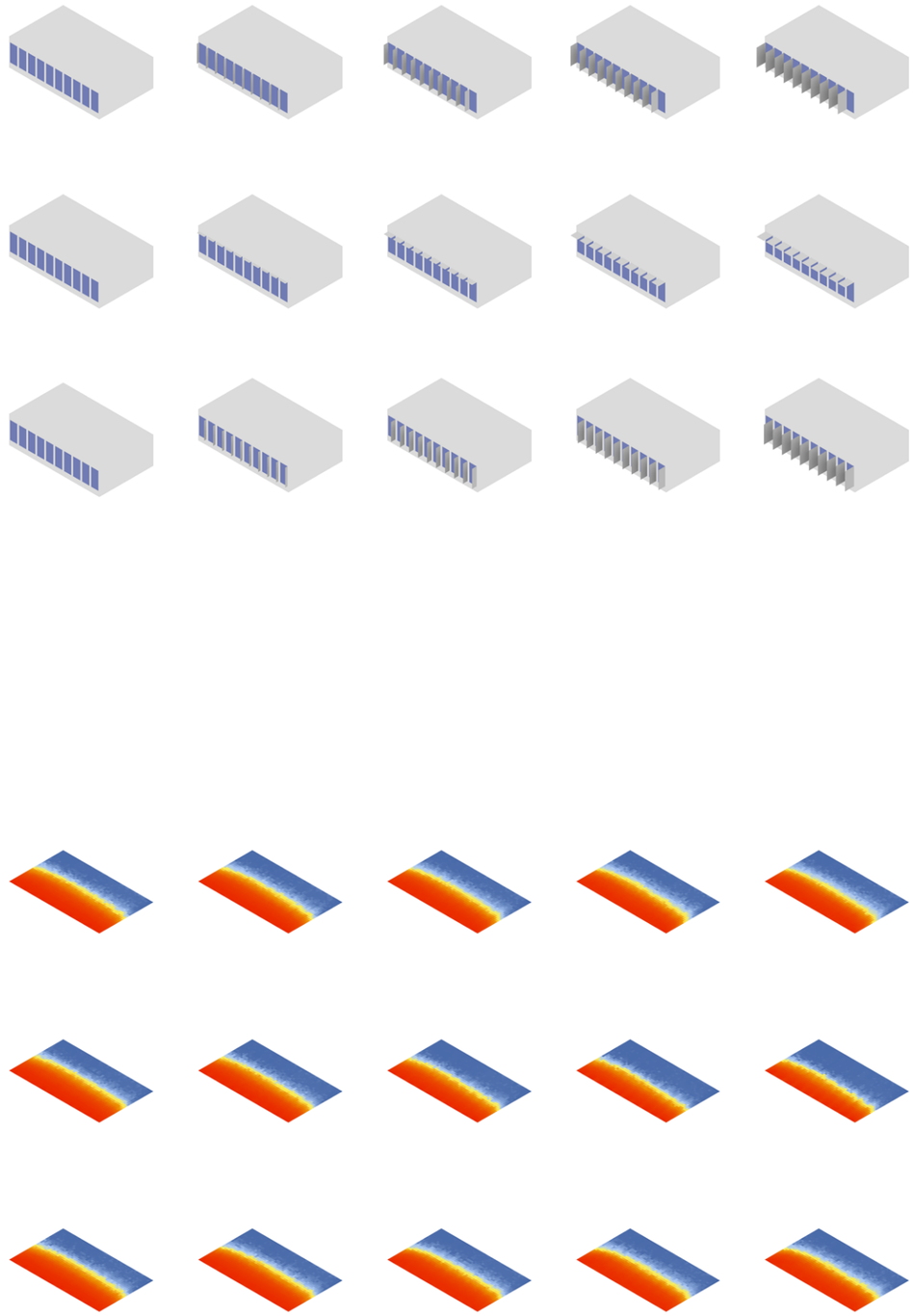

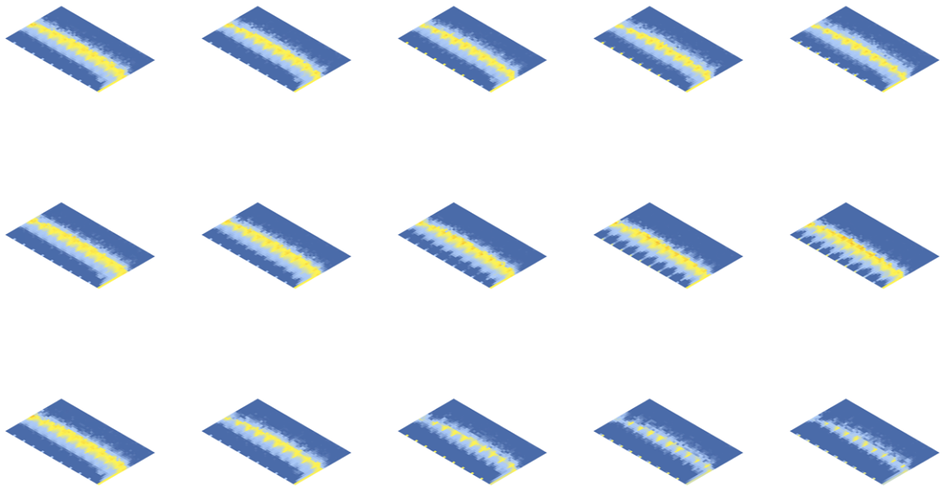

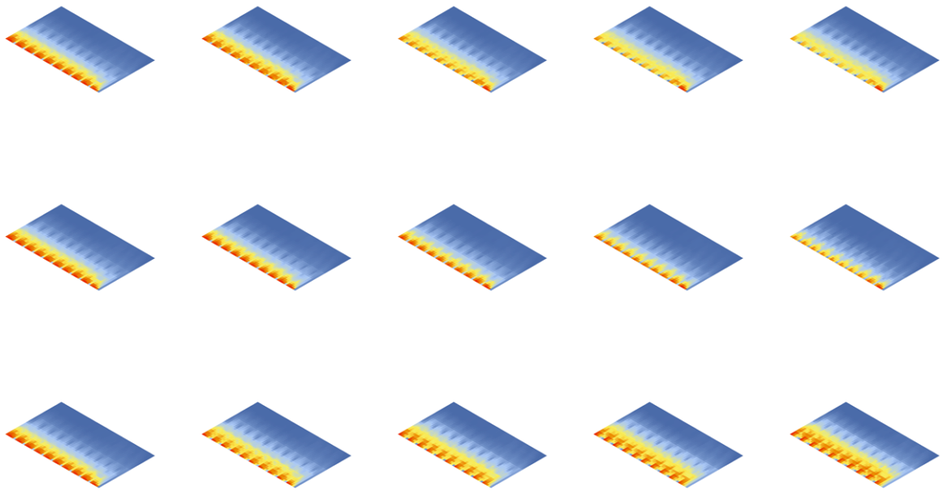

Second Step Optimization

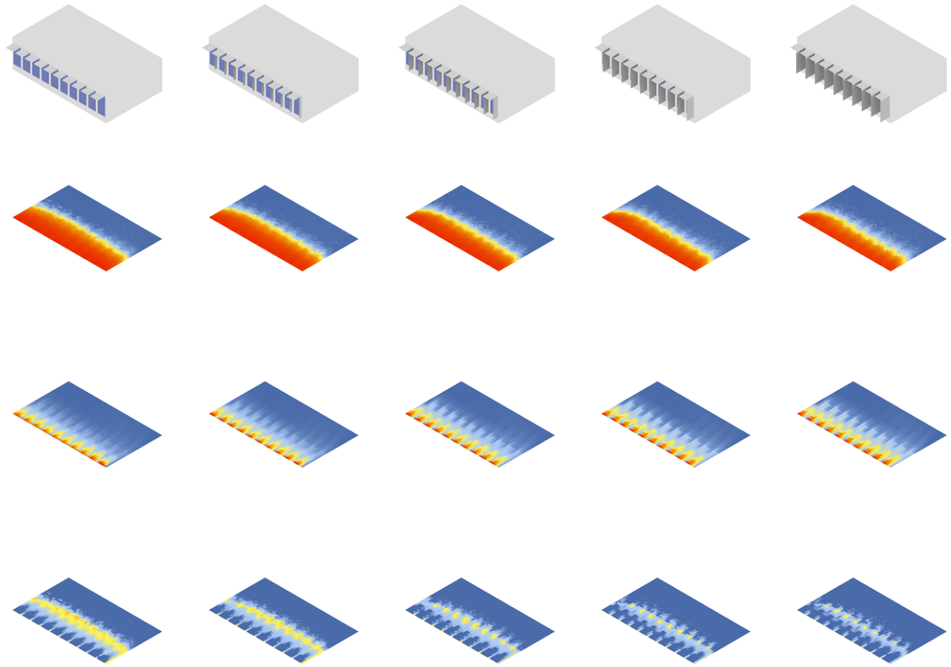

Third Step Optimization

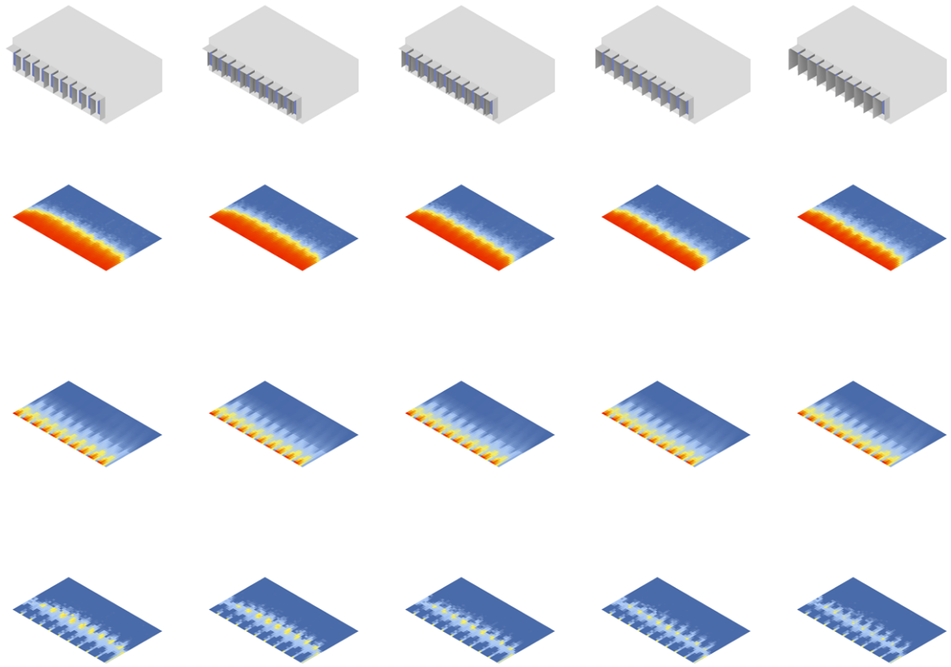

Visible Transmittance Optimization:

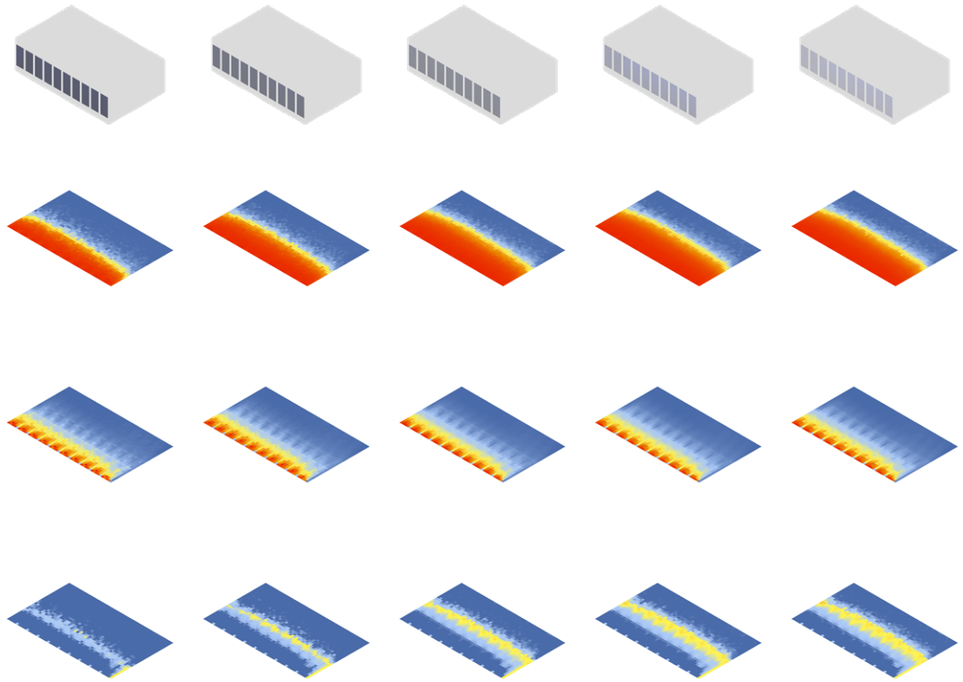

S_20,23 B NS
ASE * Area/Total Area : 19.56%
sDA * Area / Total Area : 56.83%
(sDa-ASE)* Area / Total Area : 37.27%

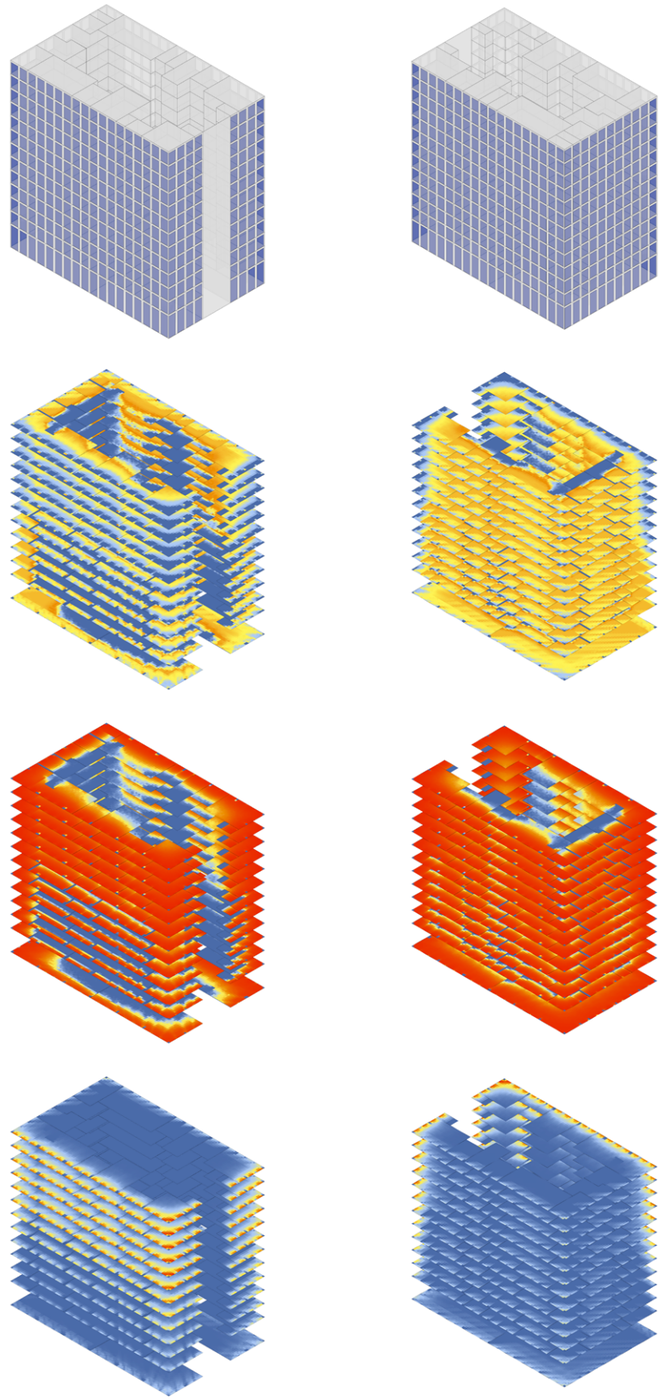

S_30,33 H NS
ASE * Area / Total Area : 13.91%
sDA * Area / Total Area : 44.26%
(sDa-ASE)* Area / Total Area : 30.35%

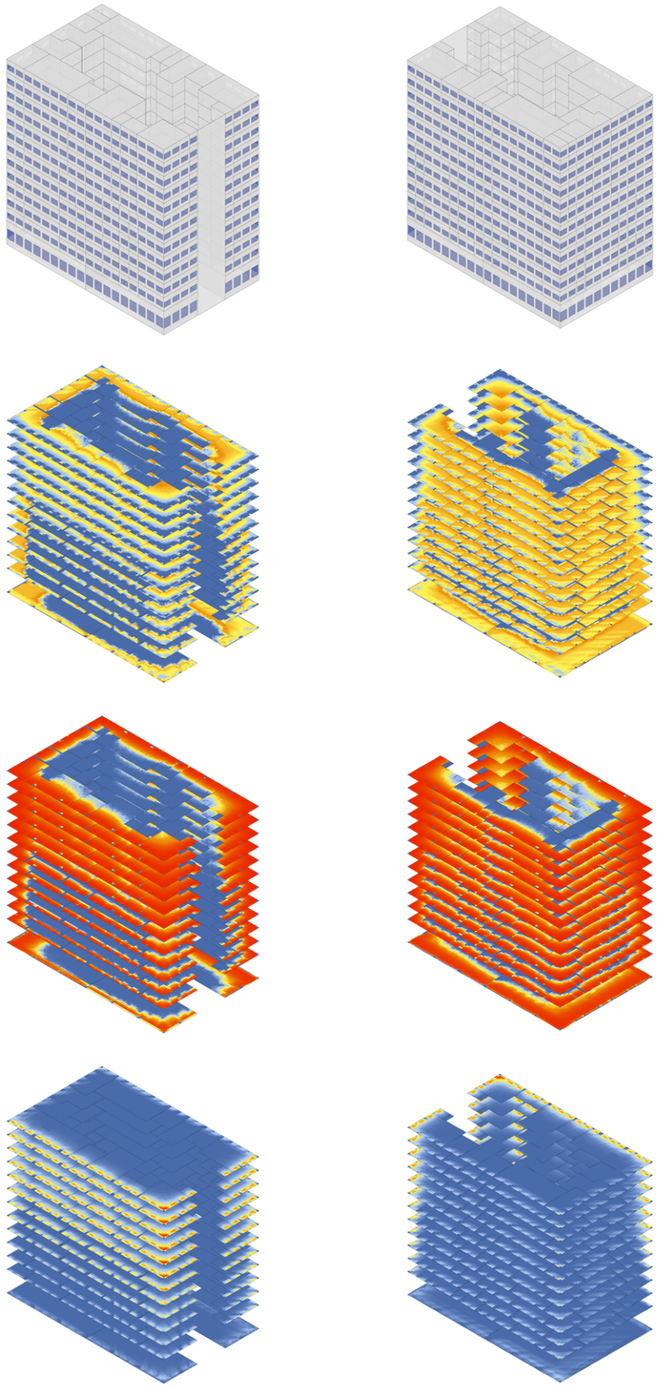

S_40,43 D NS
ASE * Area / Total Area : 17.73%
sDA * Area / Total Area : 55.54%
(sDa-ASE)* Area / Total Area : 37.80%

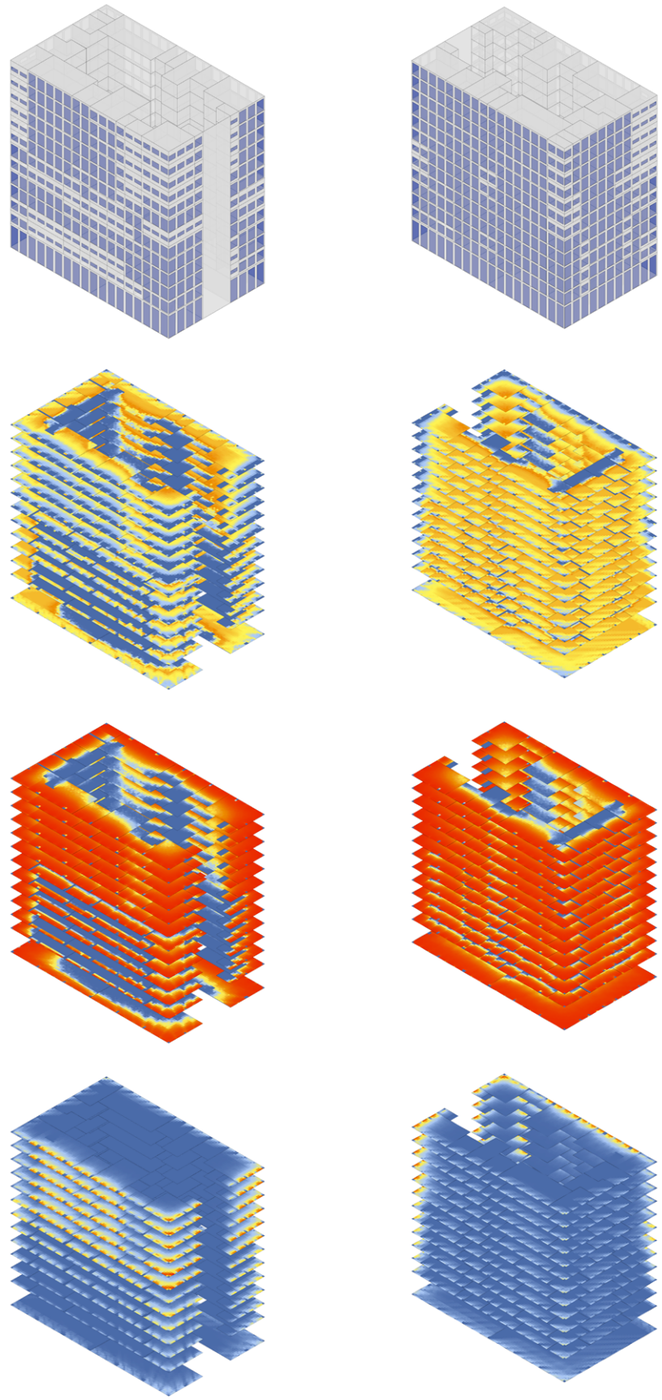

S_21,24 B BL
ASE * Area / Total Area : 13.95%
sDA * Area / Total Area : 53.30%
(sDa-ASE)* Area / Total Area : 39.35%

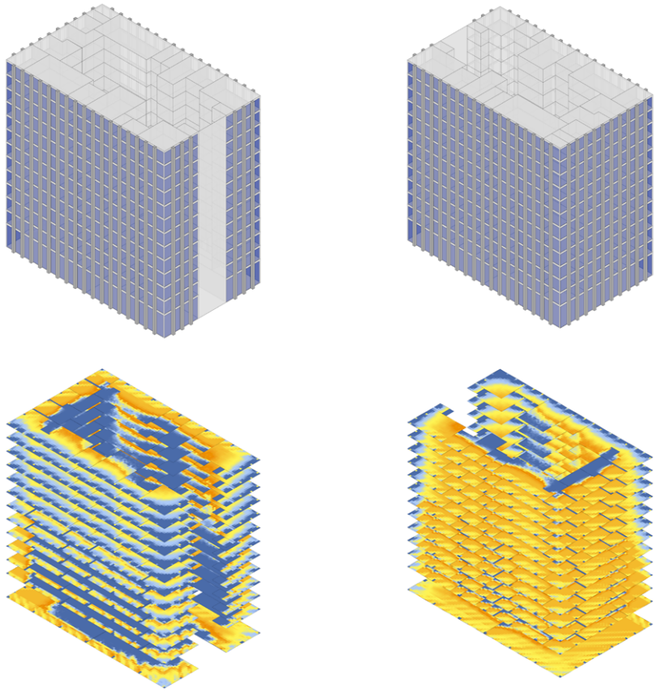

S_31,34 H BL
ASE * Area / Total Area : 9.59%
sDA * Area / Total Area : 40.93%
(sDa-ASE)* Area / Total Area : 31.34%

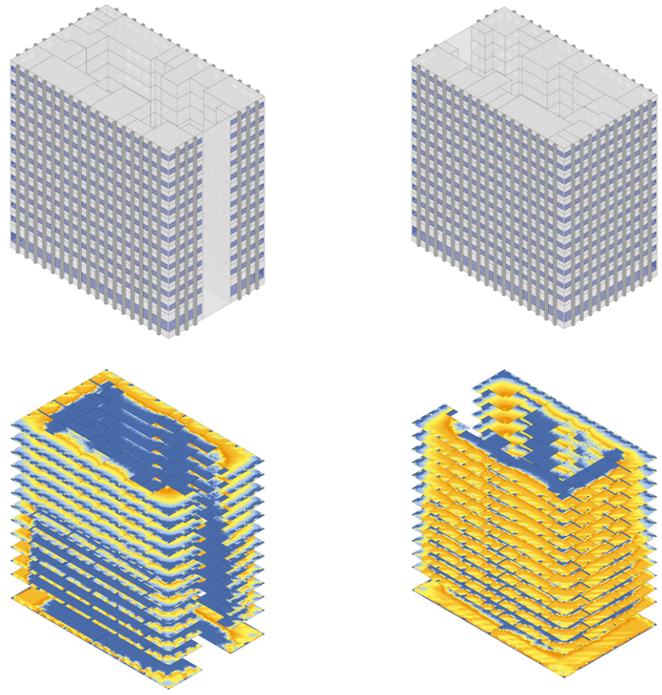

S_41,44 D BL
ASE * Area / Total Area : 12.23%
sDA * Area / Total Area : 51.77%
(sDa-ASE)* Area / Total Area : 39.54%

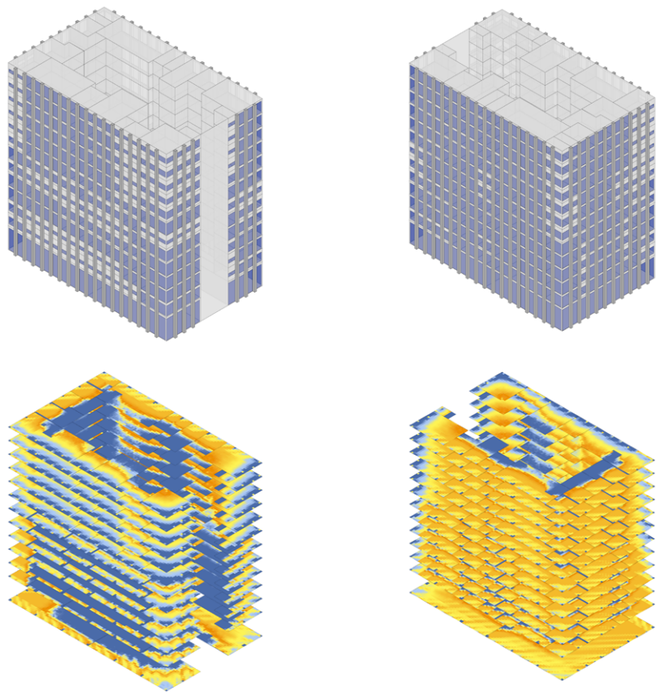

S_22,25 B OS
ASE * Area / Total Area : 11.26%
sDA * Area / Total Area : 53.05%
(sDa-ASE)* Area / Total Area : 41.79%

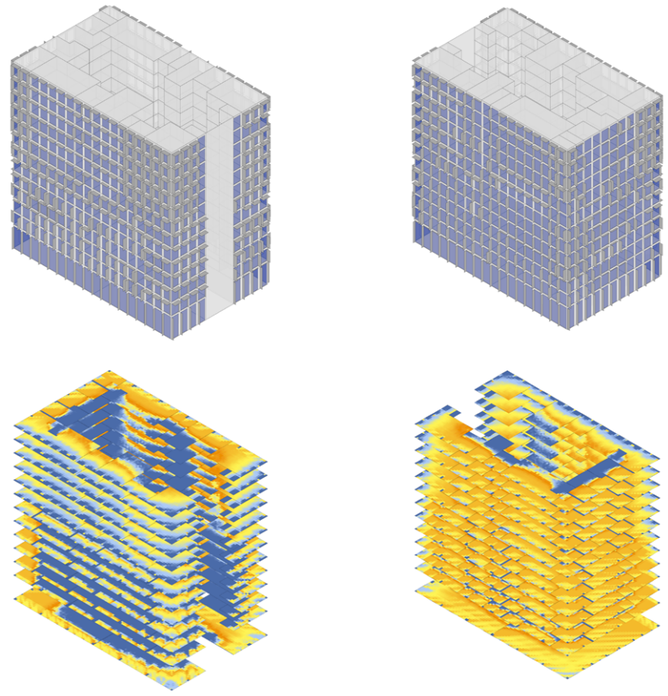

S_32,35 H OS
ASE * Area / Total Area : 6.30%
sDA * Area / Total Area : 38.54%
(sDa-ASE)* Area / Total Area : 32.23%

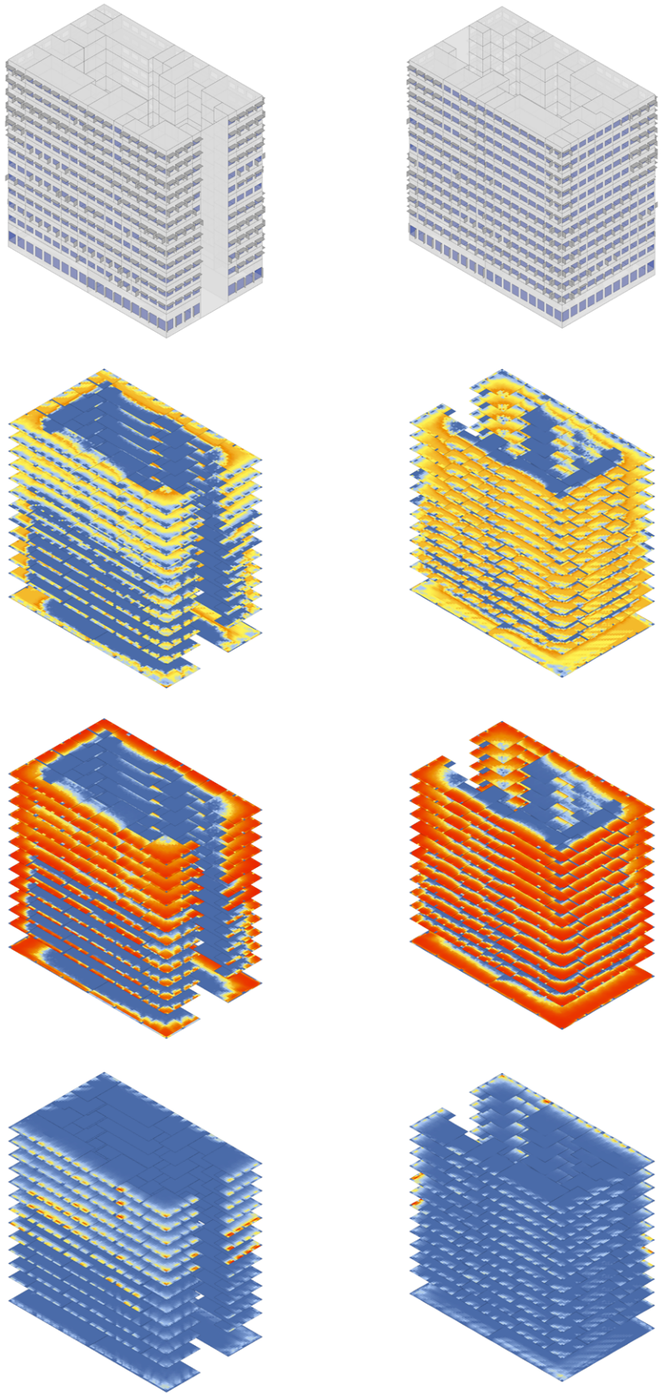

S_42,45 D OS
ASE * Area / Total Area : 10.03%
sDA * Area / Total Area : 51.18%
(sDa-ASE)* Area / Total Area : 41.15%

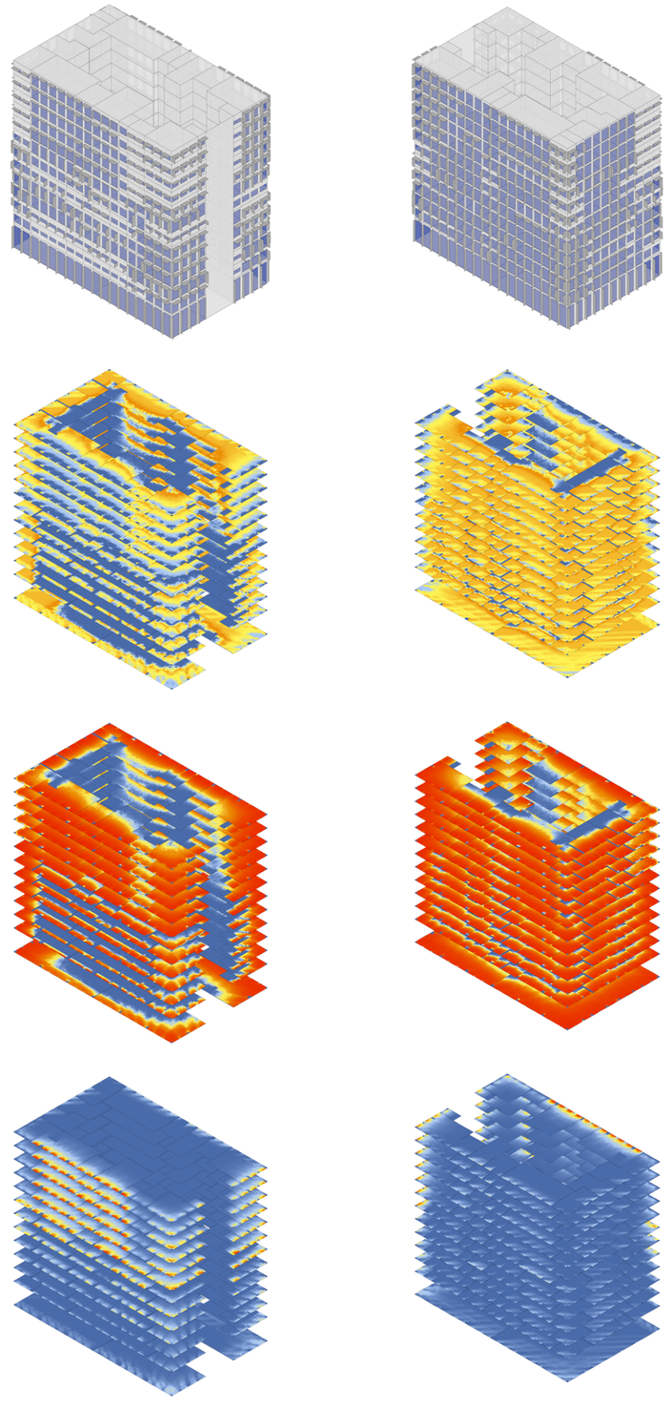

S_28,29 B VT
ASE * Area / Total Area : 16.40%
sDA * Area / Total Area : 55.08%
(sDa-ASE)* Area / Total Area : 38.67%

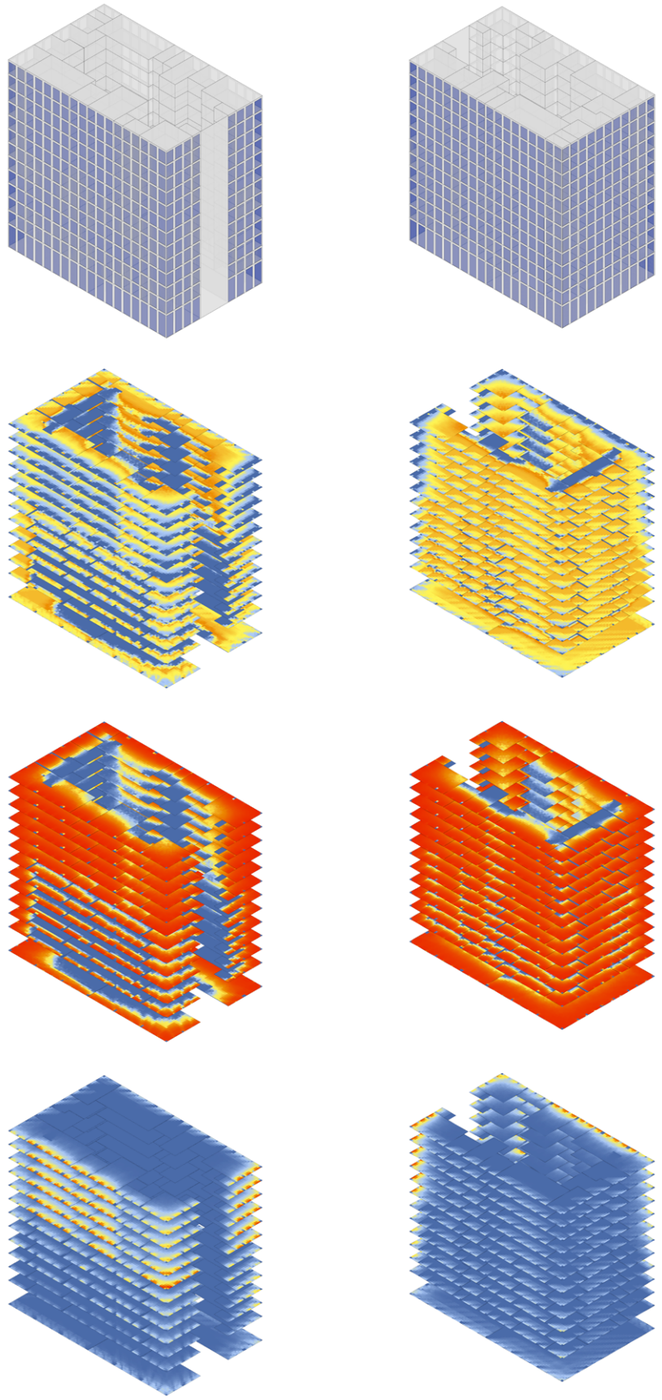

S_38,39 H VT
ASE * Area / Total Area : 11.99%
sDA * Area / Total Area : 42.58%
(sDa-ASE)* Area / Total Area : 30.59%

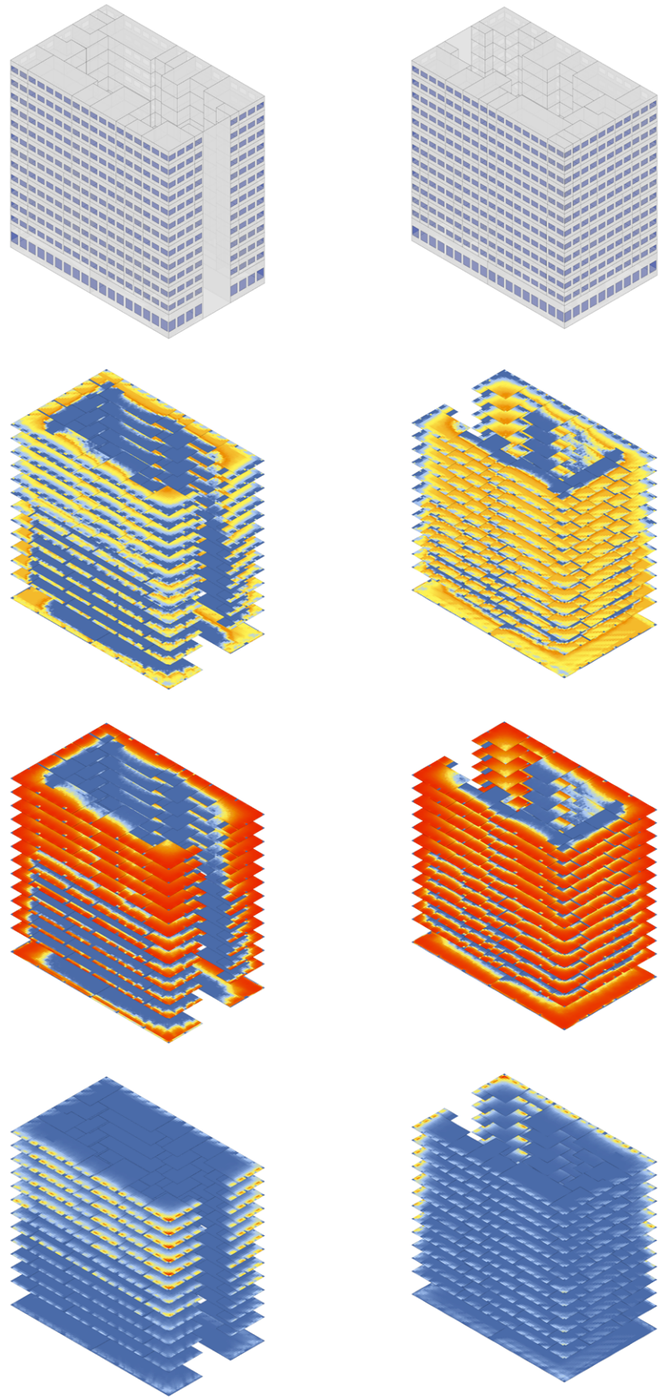

S_48,49 D VT
ASE * Area / Total Area : 16.13%
sDA * Area / Total Area : 54.31%
(sDa-ASE)* Area / Total Area : 38.18%

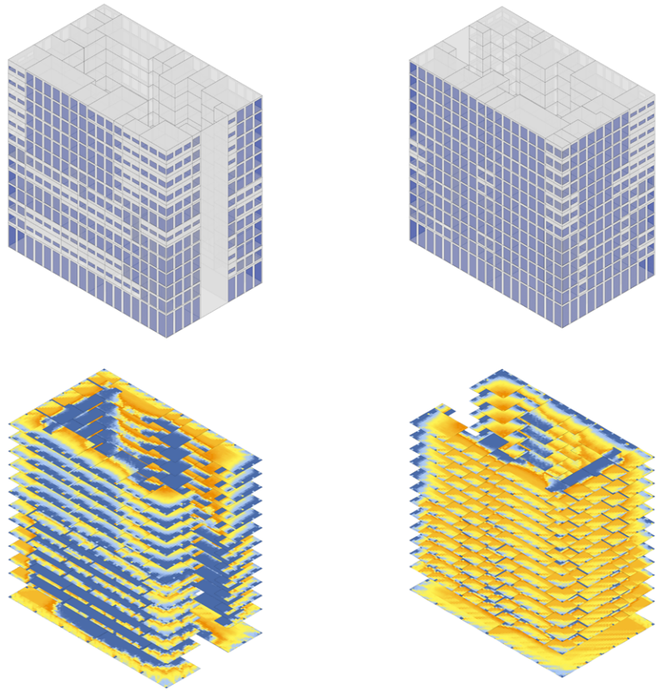

S_51,61 B OS V
ASE * Area / Total Area : 9.82%
sDA * Area / Total Area : 52.16%
(sDa-ASE)* Area / Total Area : 42.34%

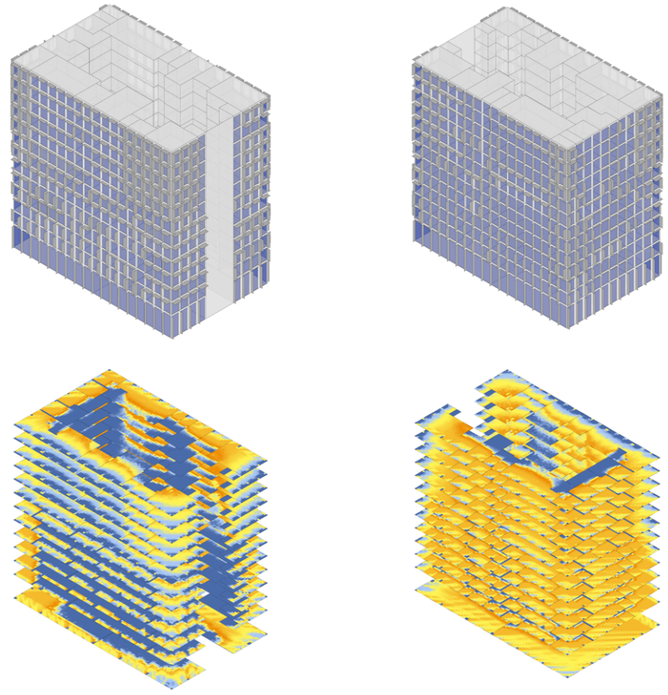

S_54,64 H OS V
ASE * Area / Total Area : 5.79%
sDA * Area / Total Area : 37.86%
(sDa-ASE)* Area / Total Area : 32.07%

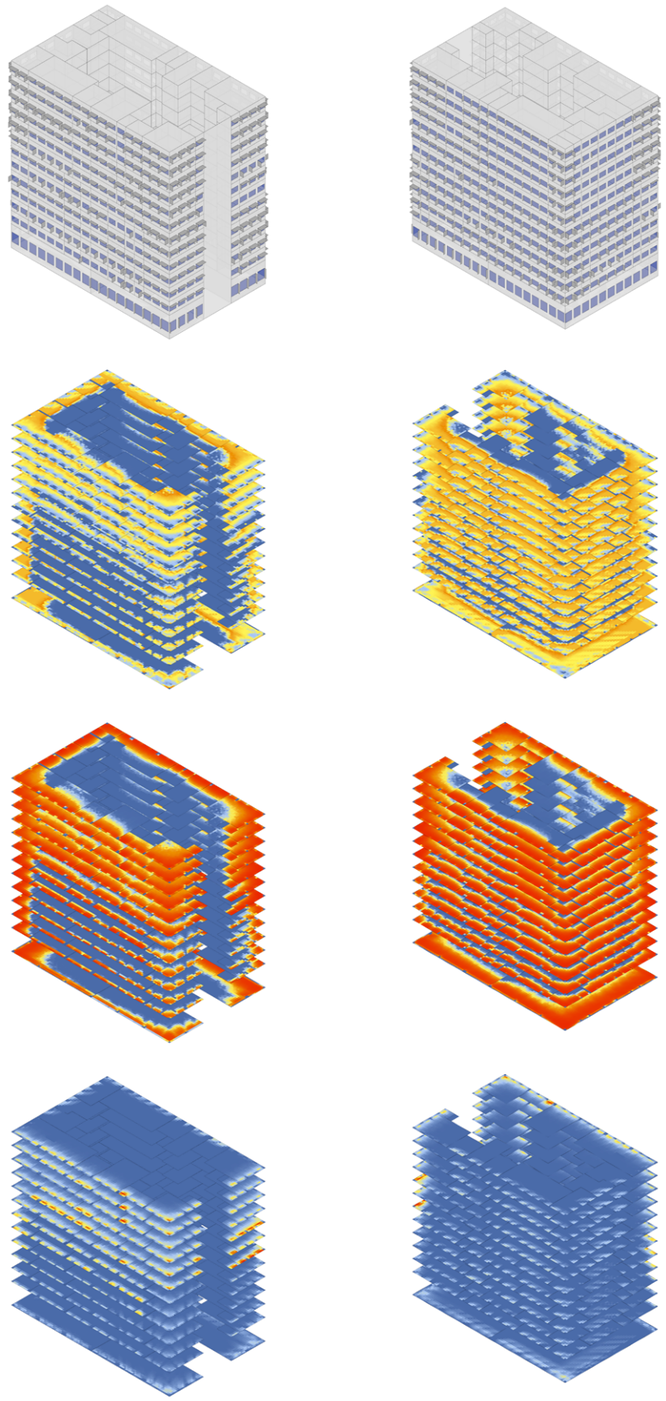

S_53,63 D OS VT
ASE * Area / Total Area : 9.56%
sDA * Area / Total Area : 50.63%
(sDa-ASE)* Area / Total Area : 41.07%

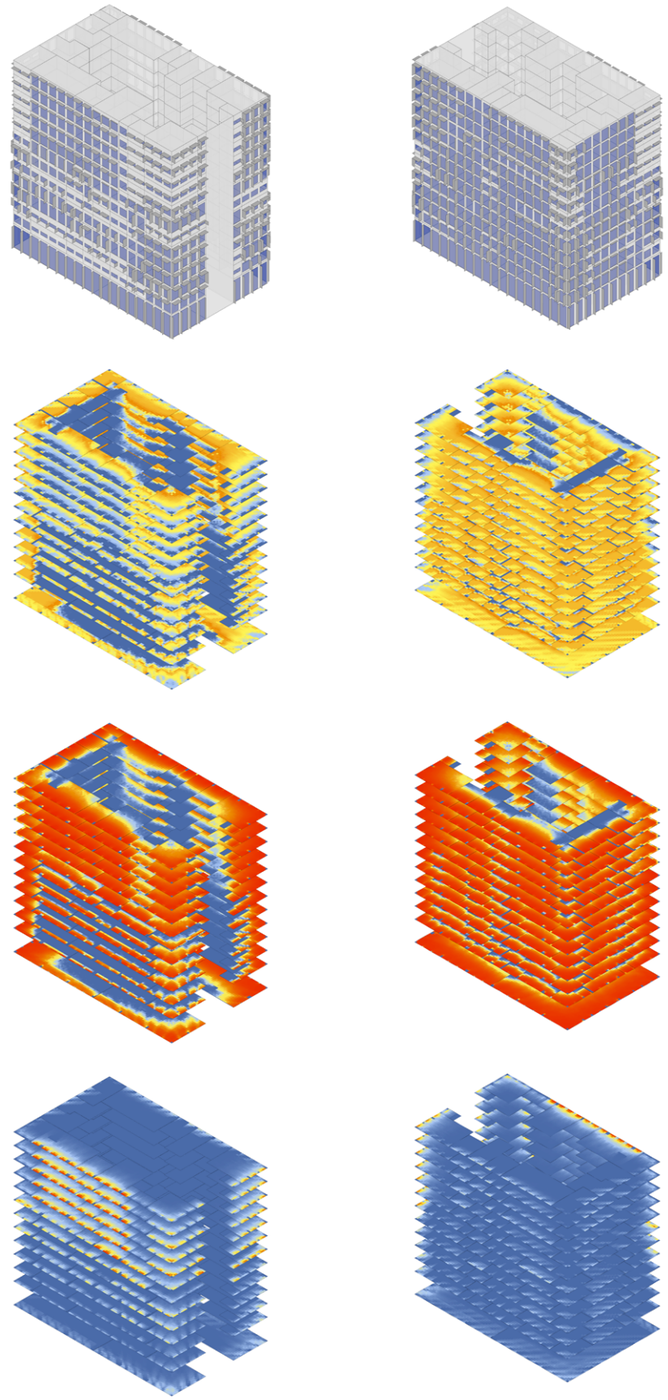

B BL VT
ASE * Area / Total Area : 11.00%
sDA * Area / Total Area : 51.38%
(sDa-ASE)* Area / Total Area : 40.37%

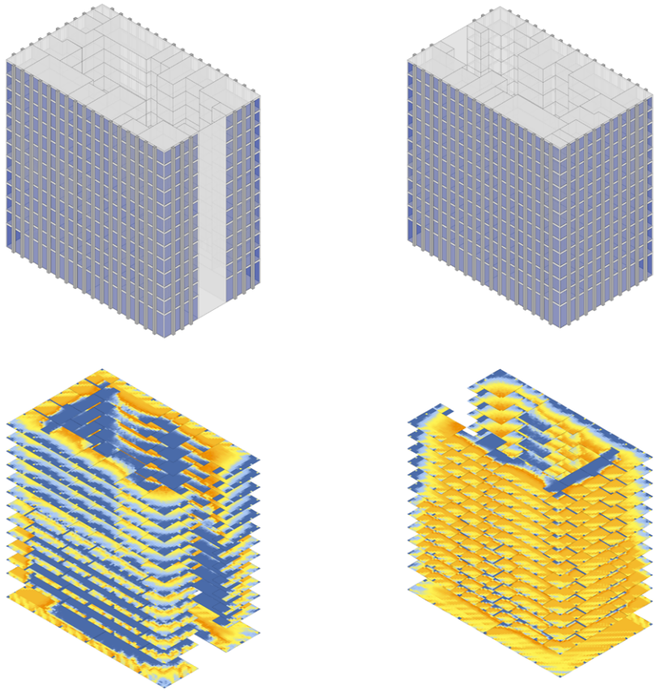

H BL VT
ASE * Area / Total Area : 7.86%
sDA * Area / Total Area : 38.96%
(sDa-ASE)* Area / Total Area : 31.10%

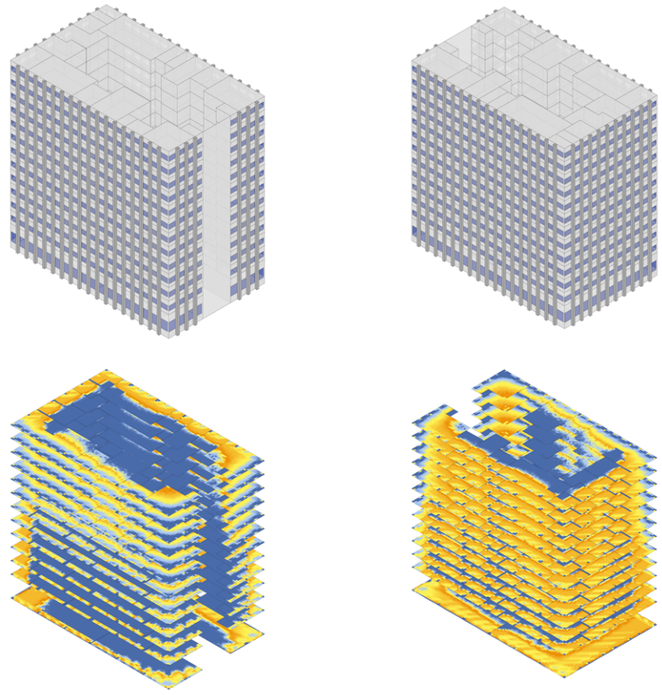

D BL VT
ASE * Area / Total Area : 10.36%
sDA * Area / Total Area : 49.95%
(sDa-ASE)* Area / Total Area : 39.59%

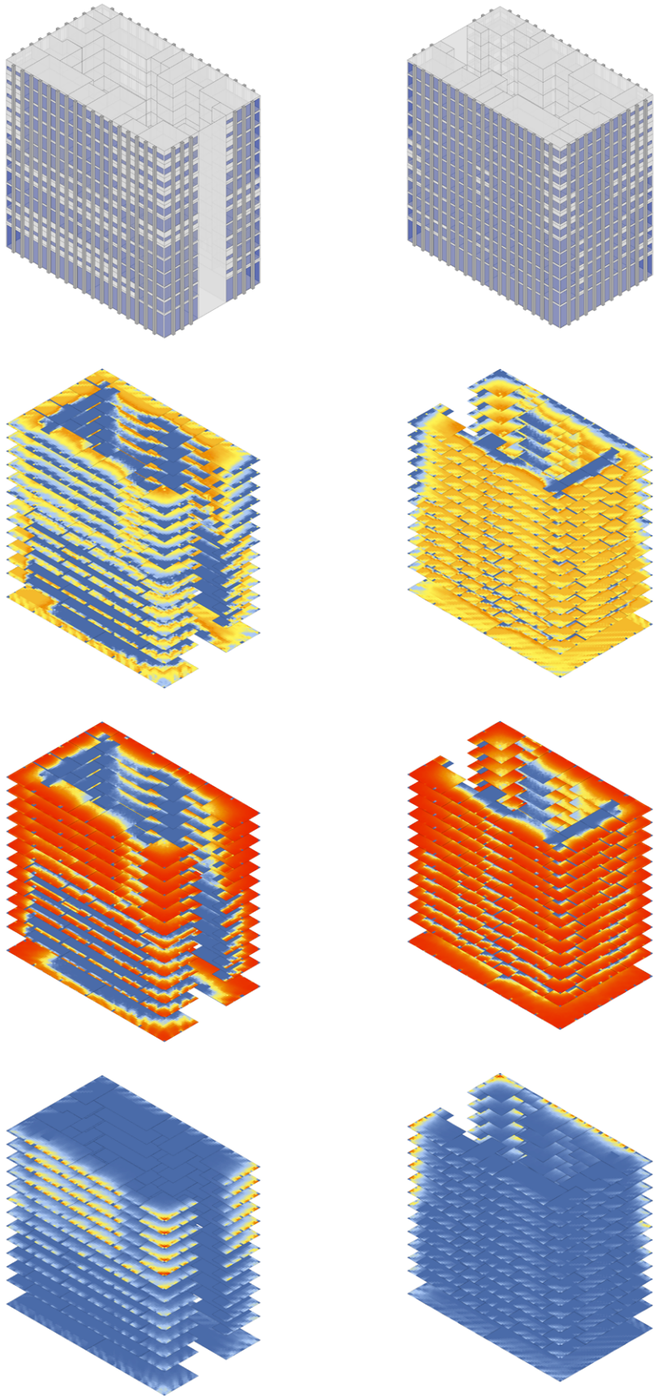

B BL OS
ASE * Area / Total Area : 11.48%
sDA * Area / Total Area : 51.63%
(sDa-ASE)* Area / Total Area : 40.15%

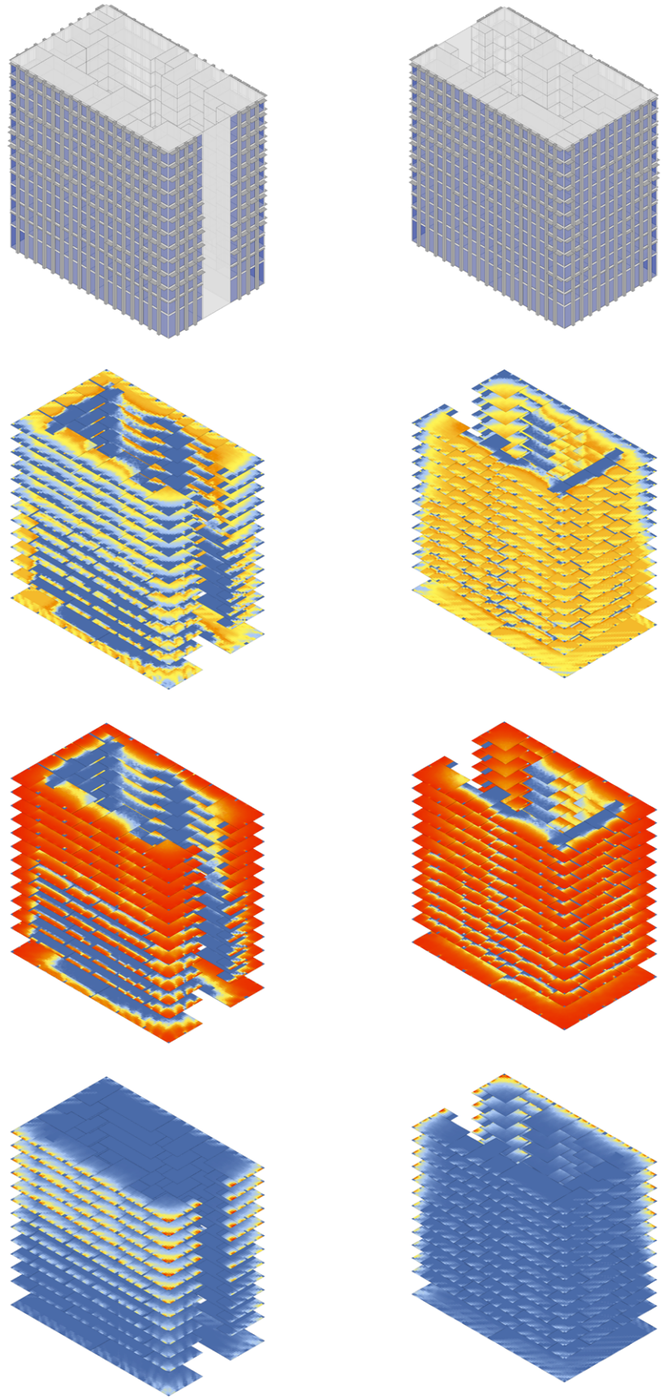

H BL OS
ASE * Area / Total Area : 4.65%
sDA * Area / Total Area : 34.74%
(sDa-ASE)* Area / Total Area : 30.10%

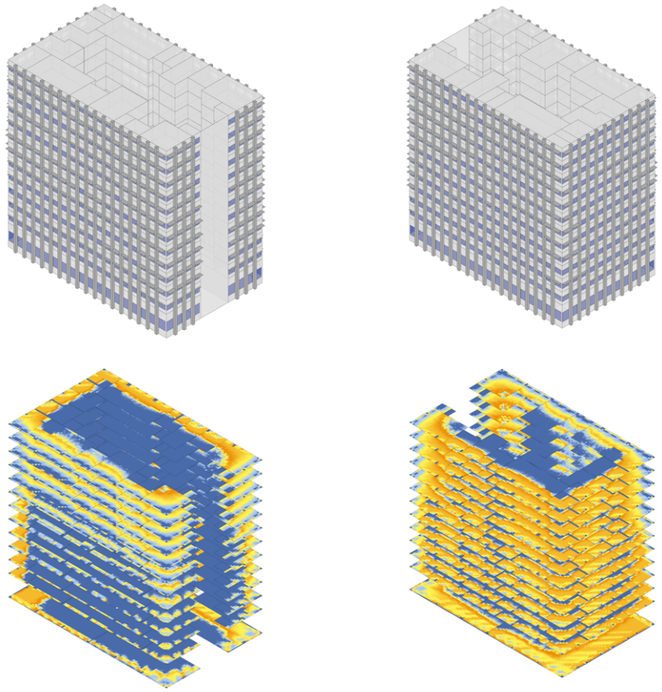

D BL OS
ASE * Area / Total Area : 9.05%
sDA * Area / Total Area : 48.95%
(sDa-ASE)* Area / Total Area : 39.90%

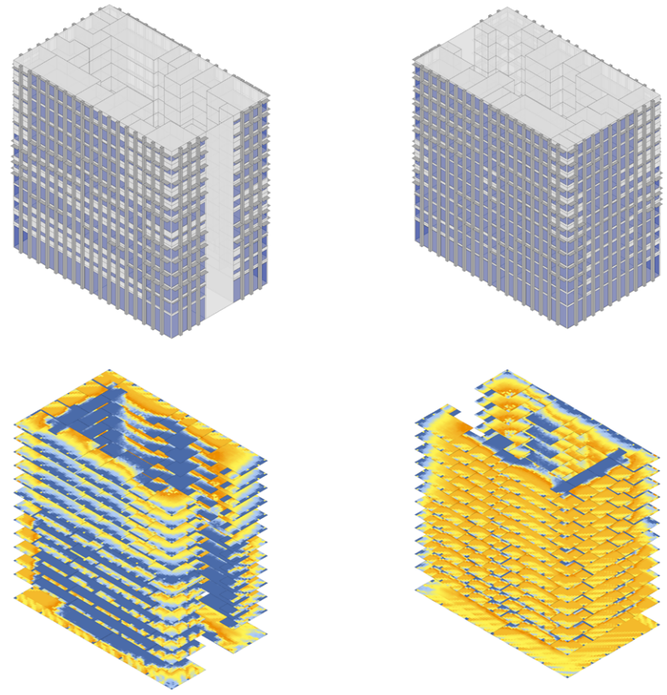

S_52,62 B VT OS
ASE * Area / Total Area : 9.26%
sDA * Area / Total Area : 51.26%
(sDa-ASE)* Area / Total Area : 41.99%

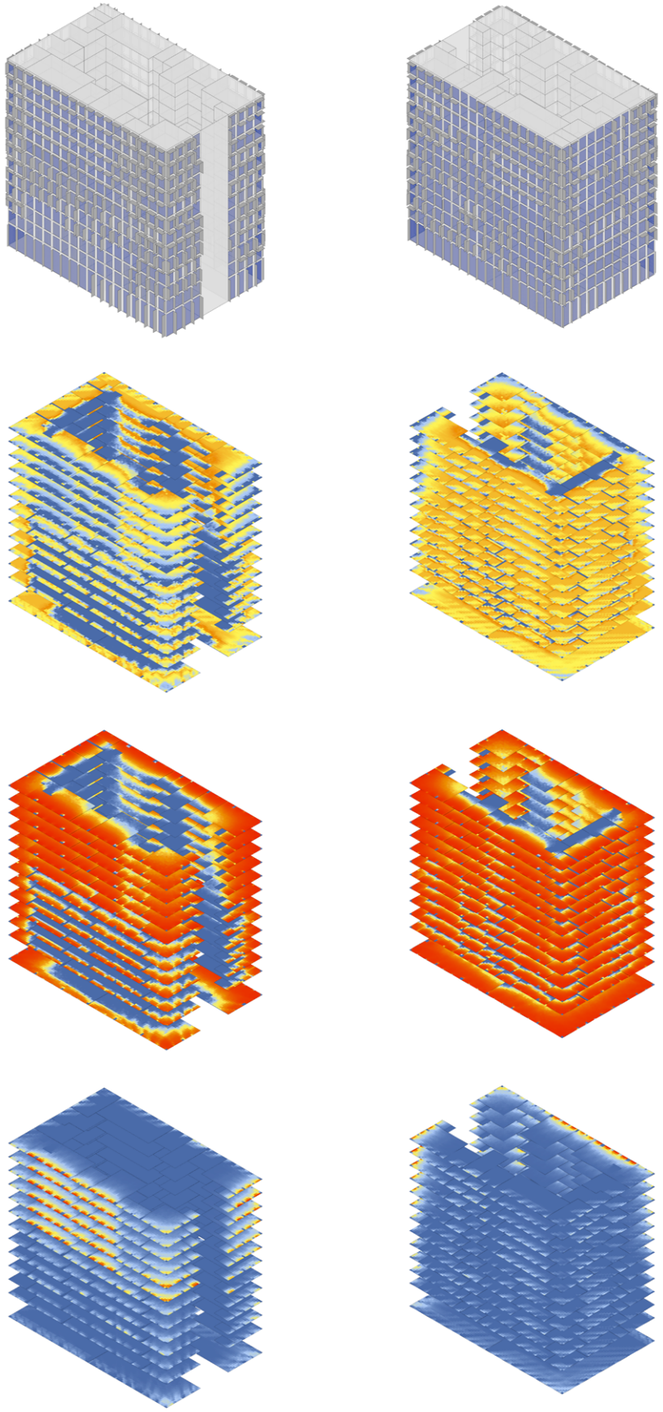

H VT OS
ASE * Area / Total Area : 5.68%
sDA * Area / Total Area : 37.72%
(sDa-ASE)* Area / Total Area : 32.04%

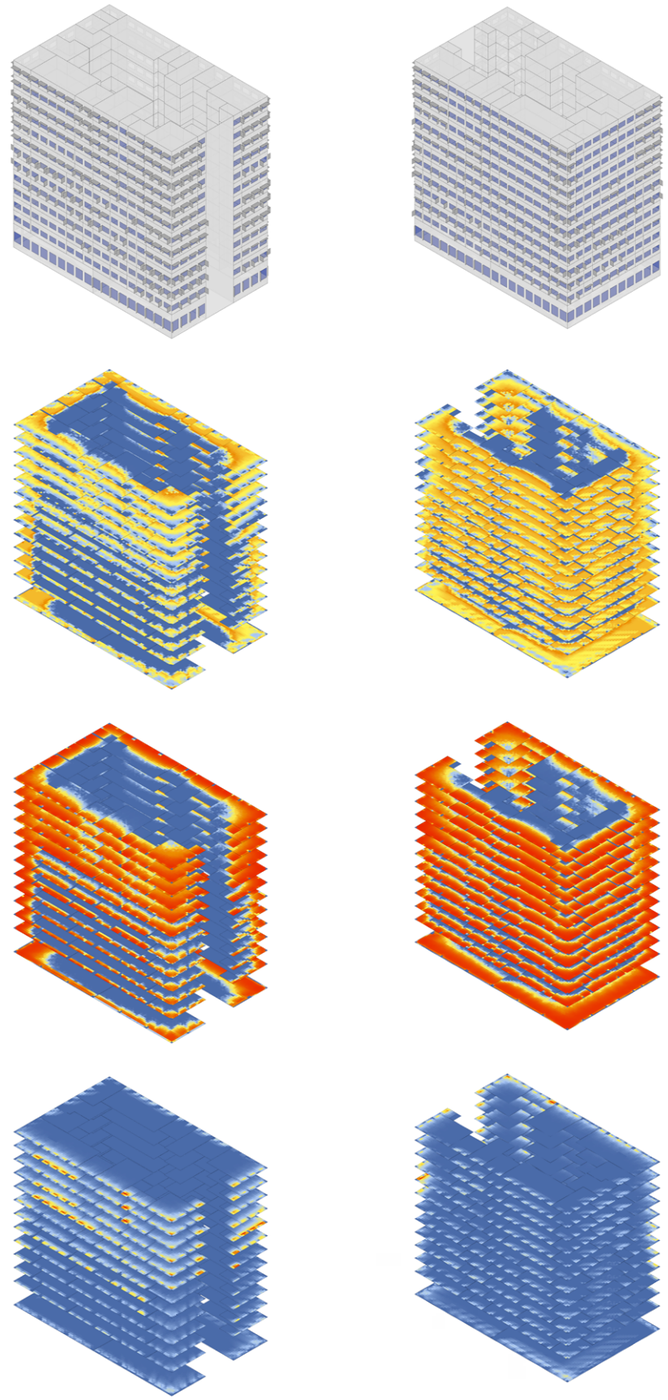

D VT OS
ASE * Area / Total Area : 9.34%
sDA * Area / Total Area : 49.97%
(sDa-ASE)* Area / Total Area : 40.63%

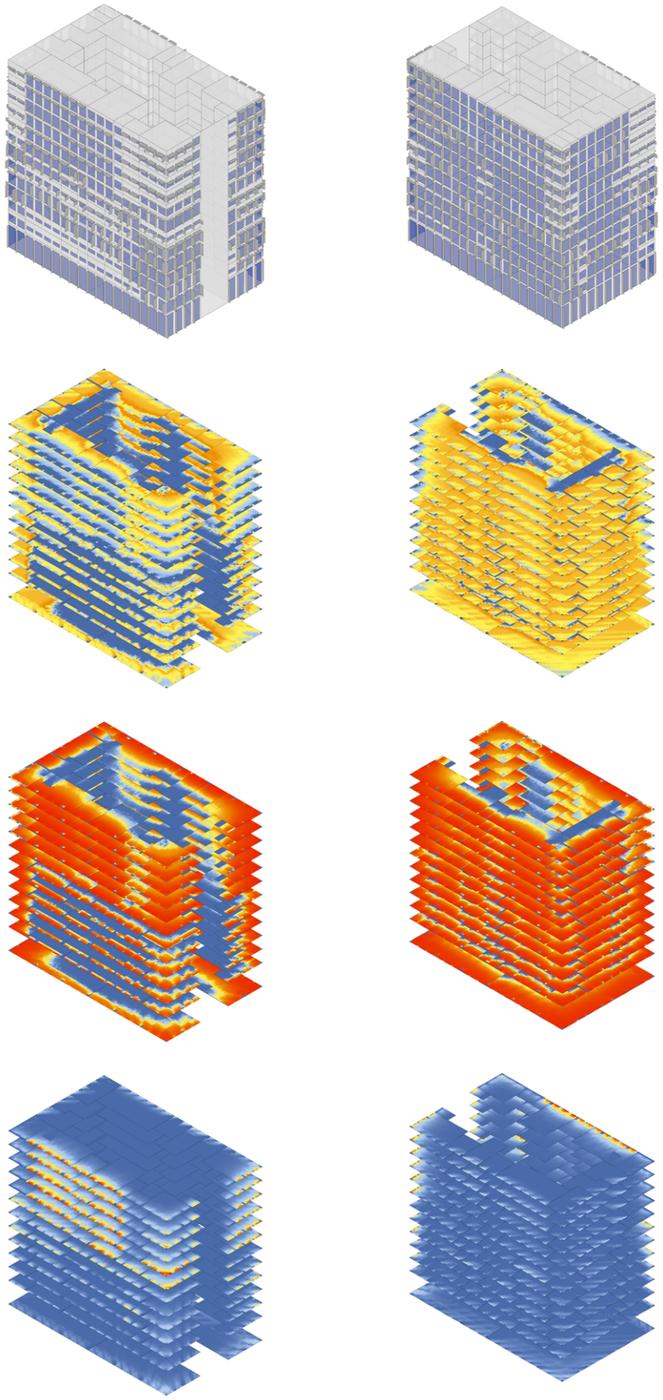

B BL OS VT
ASE * Area / Total Area : 10.31%
sDA * Area / Total Area : 51.15%
(sDa-ASE)* Area / Total Area : 40.84%

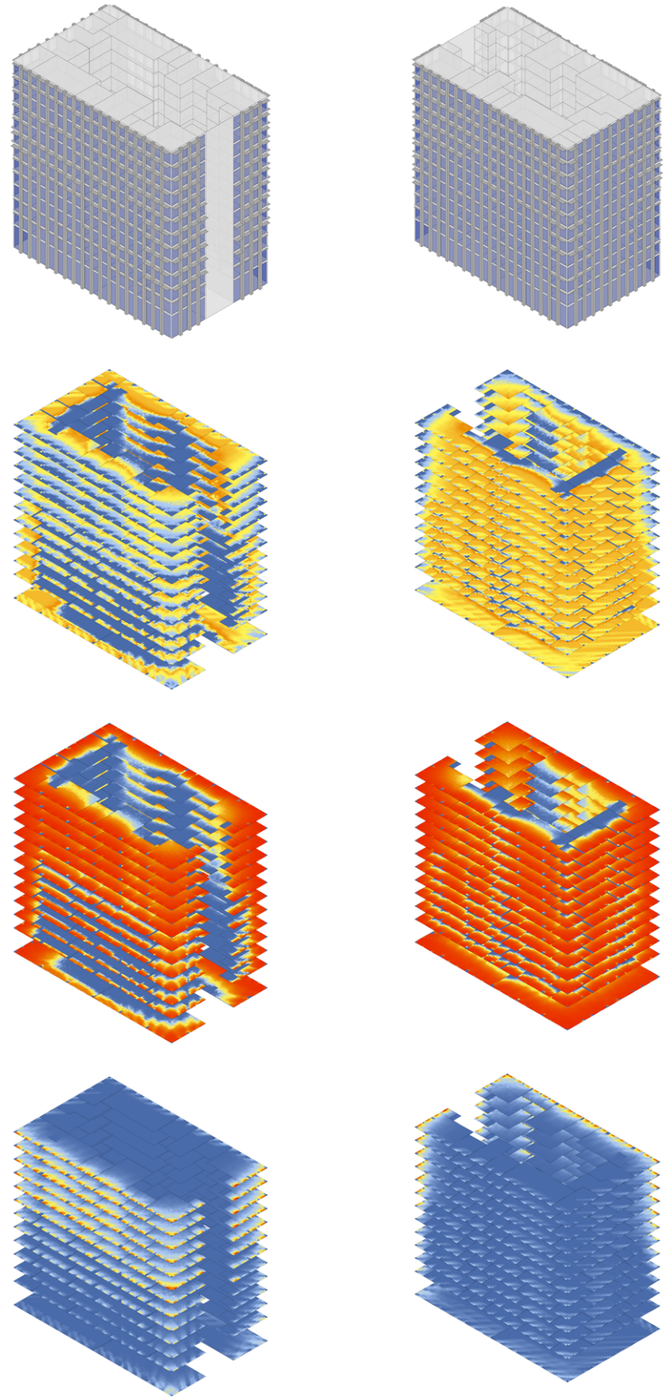

H BL OS VT
ASE * Area / Total Area : 3.75%
sDA * Area / Total Area : 33.28%
(sDa-ASE)* Area / Total Area : 29.53%

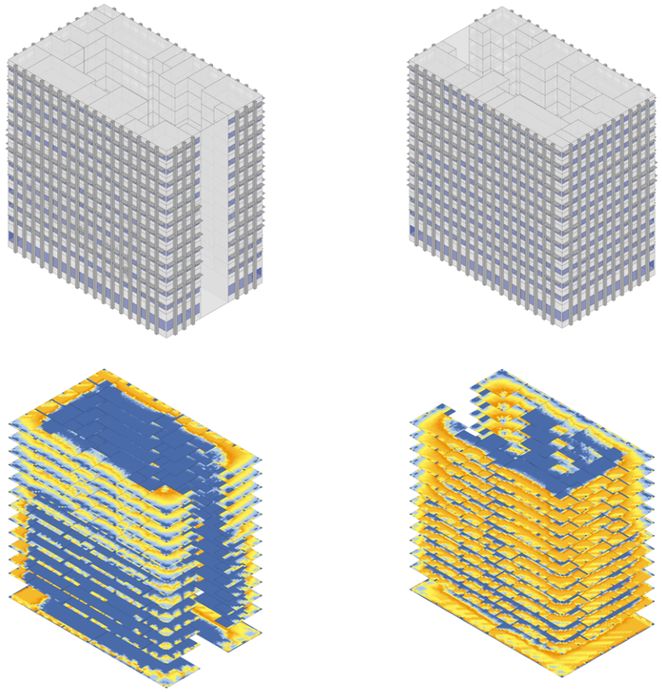

D BL OS VT
ASE * Area / Total Area : 8.61%
sDA * Area / Total Area : 48.24%
(sDa-ASE)* Area / Total Area : 39.63%

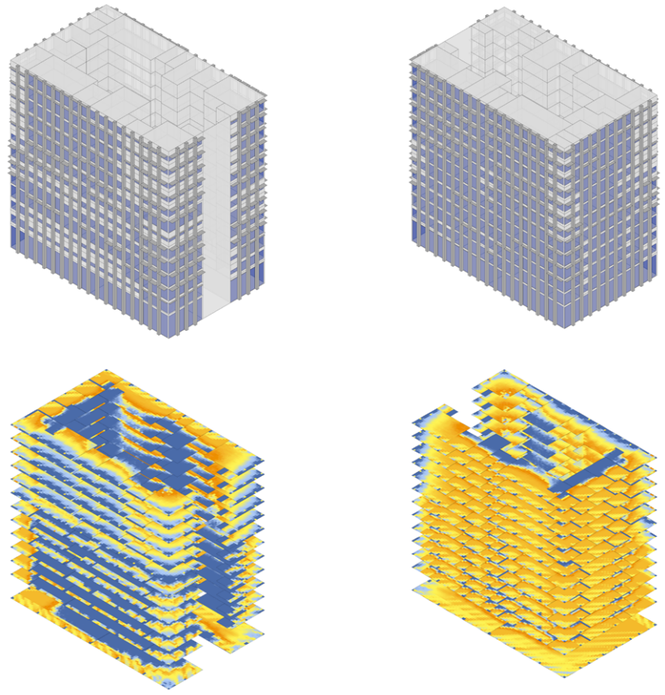

B BL VT OS
ASE * Area / Total Area : 9.04%
sDA * Area / Total Area : 50.14%
(sDa-ASE)* Area / Total Area : 41.10%

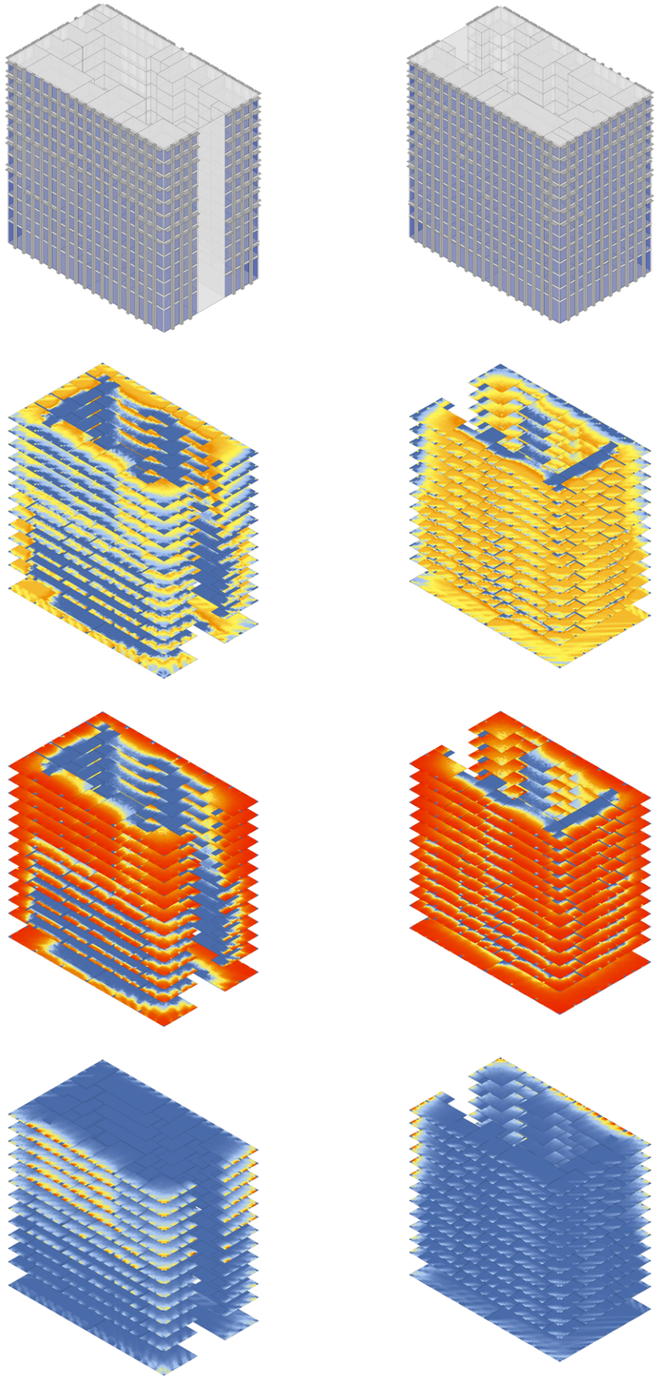

H BL VT OS
ASE * Area / Total Area : 4.58%
sDA * Area / Total Area : 36.23%
(sDa-ASE)* Area / Total Area : 31.65%

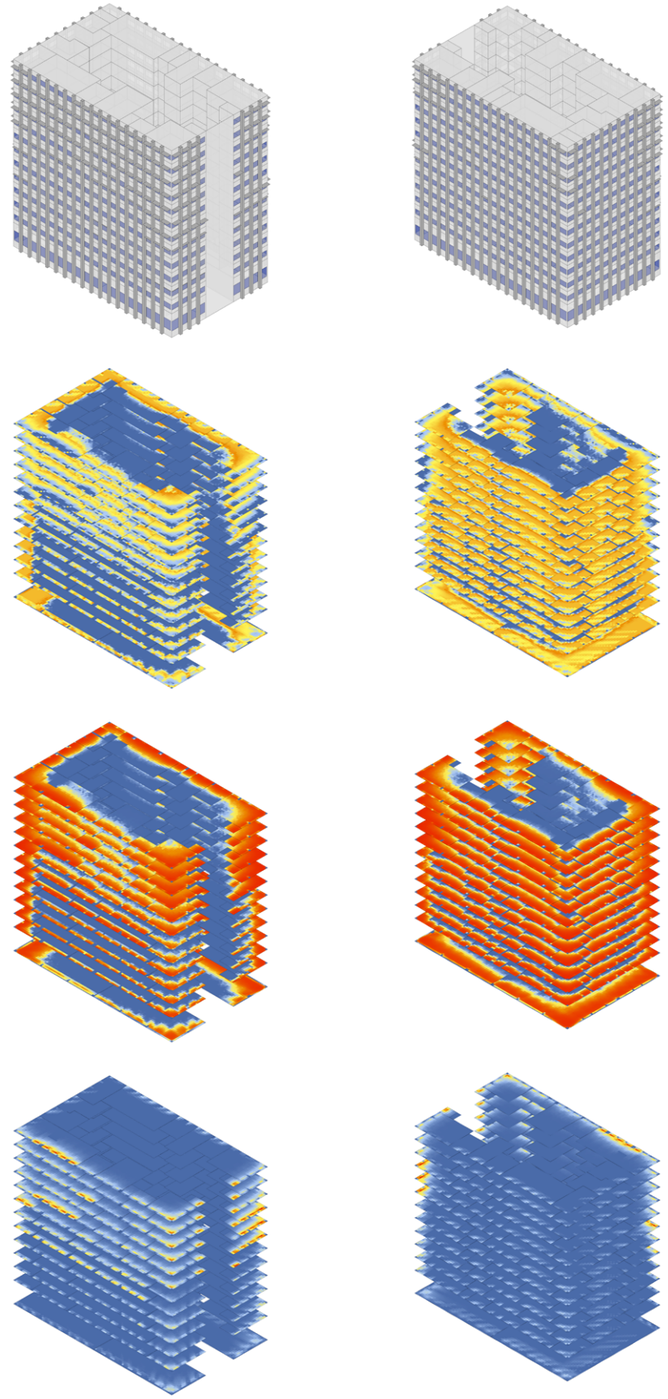

D BL VT OS
ASE * Area / Total Area : 8.03%
sDA * Area / Total Area : 47.71%
(sDa-ASE)* Area / Total Area : 39.68%

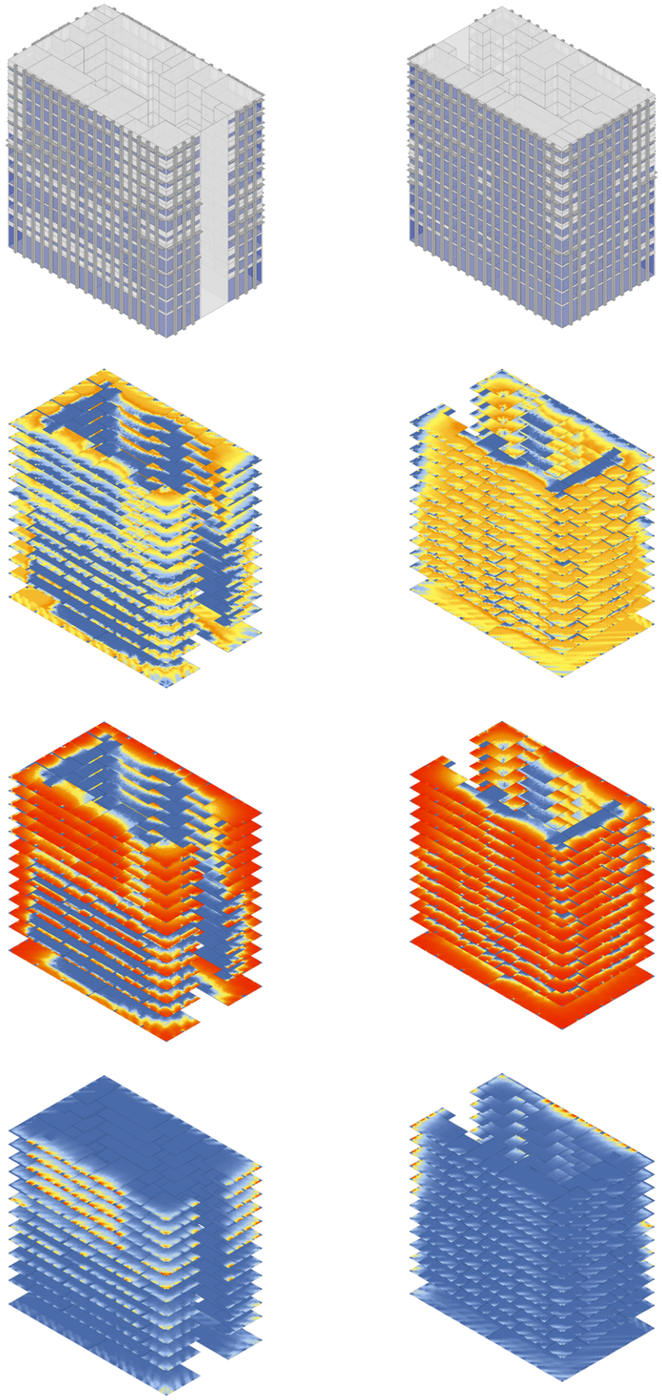

ANNEX B

Operational Energy and Embodied Carbon Simulations results for each Scenario investigated along the research

Annex B from page 2 to page 17: Simulations results organized in tables
Annex B from page 18 to page 24: Thickness optimization charts
Annex B from page 25 to page 35: Energy Balance charts

S_20 B 2G NS

S_20	Values	Units
EUI	59.178	kWh/m2y
Opt insulation Thickness	0.259	m
Embodied GWP	5.659	kg CO2-eq/m2y
Embodied GWP Total (60y)	339.54	kg CO2-eq/m2
Operational GWP	11.836	kg CO2-eq/m2y
Operational GWP Total (60y)	710.139	kg CO2-eq/m2
GWP Embodied + Operational	17.495	kg CO2-eq/m2y
GWP Embodied + Operational Total (60y)	1049.679	kg CO2-eq/m2
Biogenic carbon Storage	2.29	kg CO2-eq/m2y
GWP Structure	2.56	kg CO2-eq/m2y
GWP Partition	0.315	kg CO2-eq/m2y
GWP Façade	0.93	kg CO2-eq/m2y
GWP Doors	0.061	kg CO2-eq/m2y
GWP Systems	1.3	kg CO2-eq/m2y
GWP Others	0.13	kg CO2-eq/m2y
GWP PV panels	0.112	kg CO2-eq/m2y
Window/Wall ratio	0.54	/

S_23 B 3G NS

S_23	Values	Units
EUI	50.286	kWh/m2y
Opt insulation Thickness	0.295	m
Embodied GWP	5.896	kg CO2-eq/m2y
Embodied GWP Total (60y)	353.76	kg CO2-eq/m2
Operational GWP	10.057	kg CO2-eq/m2y
Operational GWP Total (60y)	603.433	kg CO2-eq/m2
GWP Embodied + Operational	15.953	kg CO2-eq/m2y
GWP Embodied + Operational Total (60y)	957.193	kg CO2-eq/m2
Biogenic carbon Storage	2.29	kg CO2-eq/m2y
GWP Structure	2.56	kg CO2-eq/m2y
GWP Partition	0.315	kg CO2-eq/m2y
GWP Façade	1.166	kg CO2-eq/m2y
GWP Doors	0.061	kg CO2-eq/m2y
GWP Systems	1.3	kg CO2-eq/m2y
GWP Others	0.13	kg CO2-eq/m2y
GWP PV panels	0.112	kg CO2-eq/m2y
Window/Wall ratio	0.54	/

S_21 B 2G BL

S_21	Values	Units
EUI	56.222	kWh/m2y
Opt insulation Thickness	0.268	m
Embodied GWP	5.967	kg CO2-eq/m2y
Embodied GWP Total (60y)	358.02	kg CO2-eq/m2
Operational GWP	11.244	kg CO2-eq/m2y
Operational GWP Total (60y)	674.667	kg CO2-eq/m2
GWP Embodied + Operational	17.211	kg CO2-eq/m2y
GWP Embodied + Operational Total (60y)	1032.69	kg CO2-eq/m2
Biogenic carbon Storage	2.29	kg CO2-eq/m2y
GWP Structure	2.56	kg CO2-eq/m2y
GWP Partition	0.315	kg CO2-eq/m2y
GWP Façade	1.238	kg CO2-eq/m2y
GWP Doors	0.061	kg CO2-eq/m2y
GWP Systems	1.3	kg CO2-eq/m2y
GWP Others	0.13	kg CO2-eq/m2y
GWP PV panels	0.112	kg CO2-eq/m2y
Window/Wall ratio	0.54	/

S_24 B 3G BL

S_24	Values	Units
EUI	48.593	kWh/m2y
Opt insulation Thickness	0.295	m
Embodied GWP	6.197	kg CO2-eq/m2y
Embodied GWP Total (60y)	371.82	kg CO2-eq/m2
Operational GWP	9.719	kg CO2-eq/m2y
Operational GWP Total (60y)	583.117	kg CO2-eq/m2
GWP Embodied + Operational	15.916	kg CO2-eq/m2y
GWP Embodied + Operational Total (60y)	954.937	kg CO2-eq/m2
Biogenic carbon Storage	2.29	kg CO2-eq/m2y
GWP Structure	2.56	kg CO2-eq/m2y
GWP Partition	0.315	kg CO2-eq/m2y
GWP Façade	1.467	kg CO2-eq/m2y
GWP Doors	0.061	kg CO2-eq/m2y
GWP Systems	1.3	kg CO2-eq/m2y
GWP Others	0.13	kg CO2-eq/m2y
GWP PV panels	0.112	kg CO2-eq/m2y
Window/Wall ratio	0.54	/

S_22 B 2G OS

S_22	Values	Units
EUI	54.078	kWh/m2y
Opt insulation Thickness	0.288	m
Embodied GWP	5.817	kg CO2-eq/m2y
Embodied GWP Total (60y)	349.02	kg CO2-eq/m2
Operational GWP	10.816	kg CO2-eq/m2y
Operational GWP Total (60y)	648.939	kg CO2-eq/m2
GWP Embodied + Operational	16.633	kg CO2-eq/m2y
GWP Embodied + Operational Total (60y)	997.959	kg CO2-eq/m2
Biogenic carbon Storage	2.29	kg CO2-eq/m2y
GWP Structure	2.56	kg CO2-eq/m2y
GWP Partition	0.315	kg CO2-eq/m2y
GWP Façade	1.088	kg CO2-eq/m2y
GWP Doors	0.061	kg CO2-eq/m2y
GWP Systems	1.3	kg CO2-eq/m2y
GWP Others	0.13	kg CO2-eq/m2y
GWP PV panels	0.112	kg CO2-eq/m2y
Window/Wall ratio	0.54	/

S_25 B 3G OS

S_25	Values	Units
EUI	47.543	kWh/m2y
Opt insulation Thickness	0.302	m
Embodied GWP	6.037	kg CO2-eq/m2y
Embodied GWP Total (60y)	362.22	kg CO2-eq/m2
Operational GWP	9.509	kg CO2-eq/m2y
Operational GWP Total (60y)	570.516	kg CO2-eq/m2
GWP Embodied + Operational	15.953	kg CO2-eq/m2y
GWP Embodied + Operational Total (60y)	932.736	kg CO2-eq/m2
Biogenic carbon Storage	2.29	kg CO2-eq/m2y
GWP Structure	2.56	kg CO2-eq/m2y
GWP Partition	0.315	kg CO2-eq/m2y
GWP Façade	1.307	kg CO2-eq/m2y
GWP Doors	0.061	kg CO2-eq/m2y
GWP Systems	1.3	kg CO2-eq/m2y
GWP Others	0.13	kg CO2-eq/m2y
GWP PV panels	0.112	kg CO2-eq/m2y
Window/Wall ratio	0.54	/

S_28 B 2G VT

S_28	Values	Units
EUI	64.548	kWh/m2y
Opt insulation Thickness	0.26	m
Embodied GWP	5.659	kg CO2-eq/m2y
Embodied GWP Total (60y)	339.54	kg CO2-eq/m2
Operational GWP	12.91	kg CO2-eq/m2y
Operational GWP Total (60y)	774.58	kg CO2-eq/m2
GWP Embodied + Operational	18.569	kg CO2-eq/m2y
GWP Embodied + Operational Total (60y)	1114.12	kg CO2-eq/m2
Biogenic carbon Storage	2.29	kg CO2-eq/m2y
GWP Structure	2.56	kg CO2-eq/m2y
GWP Partition	0.315	kg CO2-eq/m2y
GWP Façade	0.931	kg CO2-eq/m2y
GWP Doors	0.061	kg CO2-eq/m2y
GWP Systems	1.3	kg CO2-eq/m2y
GWP Others	0.13	kg CO2-eq/m2y
GWP PV panels	0.112	kg CO2-eq/m2y
Window/Wall ratio	0.54	/

S_29 B 3G VT

S_29	Values	Units
EUI	50.282	kWh/m2y
Opt insulation Thickness	0.295	m
Embodied GWP	5.895	kg CO2-eq/m2y
Embodied GWP Total (60y)	353.7	kg CO2-eq/m2
Operational GWP	10.056	kg CO2-eq/m2y
Operational GWP Total (60y)	603.381	kg CO2-eq/m2
GWP Embodied + Operational	15.951	kg CO2-eq/m2y
GWP Embodied + Operational Total (60y)	957.081	kg CO2-eq/m2
Biogenic carbon Storage	2.29	kg CO2-eq/m2y
GWP Structure	2.56	kg CO2-eq/m2y
GWP Partition	0.315	kg CO2-eq/m2y
GWP Façade	1.165	kg CO2-eq/m2y
GWP Doors	0.061	kg CO2-eq/m2y
GWP Systems	1.3	kg CO2-eq/m2y
GWP Others	0.13	kg CO2-eq/m2y
GWP PV panels	0.112	kg CO2-eq/m2y
Window/Wall ratio	0.54	/

S_30 H 2G NS

S_30	Values	Units
EUI	49.406	kWh/m2y
Opt insulation Thickness	0.238	m
Embodied GWP	5.858	kg CO2-eq/m2y
Embodied GWP Total (60y)	351.48	kg CO2-eq/m2
Operational GWP	9.881	kg CO2-eq/m2y
Operational GWP Total (60y)	592.872	kg CO2-eq/m2
GWP Embodied + Operational	15.739	kg CO2-eq/m2y
GWP Embodied + Operational Total (60y)	944.352	kg CO2-eq/m2
Biogenic carbon Storage	2.37	kg CO2-eq/m2y
GWP Structure	2.56	kg CO2-eq/m2y
GWP Partition	0.315	kg CO2-eq/m2y
GWP Façade	1.13	kg CO2-eq/m2y
GWP Doors	0.061	kg CO2-eq/m2y
GWP Systems	1.3	kg CO2-eq/m2y
GWP Others	0.13	kg CO2-eq/m2y
GWP PV panels	0.112	kg CO2-eq/m2y
Window/Wall ratio	0.24	/

S_33 H 3G NS

S_33	Values	Units
EUI	45.29	kWh/m2y
Opt insulation Thickness	0.247	m
Embodied GWP	5.964	kg CO2-eq/m2y
Embodied GWP Total (60y)	357.84	kg CO2-eq/m2
Operational GWP	9.058	kg CO2-eq/m2y
Operational GWP Total (60y)	543.482	kg CO2-eq/m2
GWP Embodied + Operational	15.022	kg CO2-eq/m2y
GWP Embodied + Operational Total (60y)	901.322	kg CO2-eq/m2
Biogenic carbon Storage	2.38	kg CO2-eq/m2y
GWP Structure	2.56	kg CO2-eq/m2y
GWP Partition	0.315	kg CO2-eq/m2y
GWP Façade	1.236	kg CO2-eq/m2y
GWP Doors	0.061	kg CO2-eq/m2y
GWP Systems	1.3	kg CO2-eq/m2y
GWP Others	0.13	kg CO2-eq/m2y
GWP PV panels	0.112	kg CO2-eq/m2y
Window/Wall ratio	0.24	/

S_31 H 2G BL

S_31	Values	Units
EUI	48.12	kWh/m2y
Opt insulation Thickness	0.238	m
Embodied GWP	6.16	kg CO2-eq/m2y
Embodied GWP Total (60y)	369.6	kg CO2-eq/m2
Operational GWP	9.624	kg CO2-eq/m2y
Operational GWP Total (60y)	577.437	kg CO2-eq/m2
GWP Embodied + Operational	15.784	kg CO2-eq/m2y
GWP Embodied + Operational Total (60y)	947.037	kg CO2-eq/m2
Biogenic carbon Storage	2.37	kg CO2-eq/m2y
GWP Structure	2.56	kg CO2-eq/m2y
GWP Partition	0.315	kg CO2-eq/m2y
GWP Façade	1.432	kg CO2-eq/m2y
GWP Doors	0.061	kg CO2-eq/m2y
GWP Systems	1.3	kg CO2-eq/m2y
GWP Others	0.13	kg CO2-eq/m2y
GWP PV panels	0.112	kg CO2-eq/m2y
Window/Wall ratio	0.24	/

S_34 H 3G BL

S_34	Values	Units
EUI	44.592	kWh/m2y
Opt insulation Thickness	0.248	m
Embodied GWP	6.267	kg CO2-eq/m2y
Embodied GWP Total (60y)	376.02	kg CO2-eq/m2
Operational GWP	8.918	kg CO2-eq/m2y
Operational GWP Total (60y)	535.099	kg CO2-eq/m2
GWP Embodied + Operational	15.185	kg CO2-eq/m2y
GWP Embodied + Operational Total (60y)	911.119	kg CO2-eq/m2
Biogenic carbon Storage	2.38	kg CO2-eq/m2y
GWP Structure	2.56	kg CO2-eq/m2y
GWP Partition	0.315	kg CO2-eq/m2y
GWP Façade	1.539	kg CO2-eq/m2y
GWP Doors	0.061	kg CO2-eq/m2y
GWP Systems	1.3	kg CO2-eq/m2y
GWP Others	0.13	kg CO2-eq/m2y
GWP PV panels	0.112	kg CO2-eq/m2y
Window/Wall ratio	0.24	/

S_32 H 2G OS

S_32	Values	Units
EUI	46.914	kWh/m2y
Opt insulation Thickness	0.249	m
Embodied GWP	5.936	kg CO2-eq/m2y
Embodied GWP Total (60y)	356.16	kg CO2-eq/m2
Operational GWP	9.383	kg CO2-eq/m2y
Operational GWP Total (60y)	562.964	kg CO2-eq/m2
GWP Embodied + Operational	15.319	kg CO2-eq/m2y
GWP Embodied + Operational Total (60y)	919.124	kg CO2-eq/m2
Biogenic carbon Storage	2.38	kg CO2-eq/m2y
GWP Structure	2.56	kg CO2-eq/m2y
GWP Partition	0.315	kg CO2-eq/m2y
GWP Façade	1.208	kg CO2-eq/m2y
GWP Doors	0.061	kg CO2-eq/m2y
GWP Systems	1.3	kg CO2-eq/m2y
GWP Others	0.13	kg CO2-eq/m2y
GWP PV panels	0.112	kg CO2-eq/m2y
Window/Wall ratio	0.24	/

S_35 H 3G OS

S_35	Values	Units
EUI	44.017	kWh/m2y
Opt insulation Thickness	0.257	m
Embodied GWP	6.04	kg CO2-eq/m2y
Embodied GWP Total (60y)	362.4	kg CO2-eq/m2
Operational GWP	8.803	kg CO2-eq/m2y
Operational GWP Total (60y)	528.203	kg CO2-eq/m2
GWP Embodied + Operational	14.843	kg CO2-eq/m2y
GWP Embodied + Operational Total (60y)	890.603	kg CO2-eq/m2
Biogenic carbon Storage	2.38	kg CO2-eq/m2y
GWP Structure	2.56	kg CO2-eq/m2y
GWP Partition	0.315	kg CO2-eq/m2y
GWP Façade	1.312	kg CO2-eq/m2y
GWP Doors	0.061	kg CO2-eq/m2y
GWP Systems	1.3	kg CO2-eq/m2y
GWP Others	0.13	kg CO2-eq/m2y
GWP PV panels	0.112	kg CO2-eq/m2y
Window/Wall ratio	0.24	/

S_38 H 2G TR

S_38	Values	Units
EUI	51.12	kWh/m2y
Opt insulation Thickness	0.238	m
Embodied GWP	5.859	kg CO2-eq/m2y
Embodied GWP Total (60y)	351.54	kg CO2-eq/m2
Operational GWP	10.224	kg CO2-eq/m2y
Operational GWP Total (60y)	613.439	kg CO2-eq/m2
GWP Embodied + Operational	16.083	kg CO2-eq/m2y
GWP Embodied + Operational Total (60y)	964.979	kg CO2-eq/m2
Biogenic carbon Storage	2.37	kg CO2-eq/m2y
GWP Structure	2.56	kg CO2-eq/m2y
GWP Partition	0.315	kg CO2-eq/m2y
GWP Façade	1.131	kg CO2-eq/m2y
GWP Doors	0.061	kg CO2-eq/m2y
GWP Systems	1.3	kg CO2-eq/m2y
GWP Others	0.13	kg CO2-eq/m2y
GWP PV panels	0.112	kg CO2-eq/m2y
Window/Wall ratio	0.24	/

S_39 H 3G TR

S_39	Values	Units
EUI	45.296	kWh/m2y
Opt insulation Thickness	0.245	m
Embodied GWP	5.962	kg CO2-eq/m2y
Embodied GWP Total (60y)	357.72	kg CO2-eq/m2
Operational GWP	9.059	kg CO2-eq/m2y
Operational GWP Total (60y)	543.552	kg CO2-eq/m2
GWP Embodied + Operational	15.021	kg CO2-eq/m2y
GWP Embodied + Operational Total (60y)	901.272	kg CO2-eq/m2
Biogenic carbon Storage	2.37	kg CO2-eq/m2y
GWP Structure	2.56	kg CO2-eq/m2y
GWP Partition	0.315	kg CO2-eq/m2y
GWP Façade	1.233	kg CO2-eq/m2y
GWP Doors	0.061	kg CO2-eq/m2y
GWP Systems	1.3	kg CO2-eq/m2y
GWP Others	0.13	kg CO2-eq/m2y
GWP PV panels	0.112	kg CO2-eq/m2y
Window/Wall ratio	0.24	/

S_40 D 2G NS

S_40	Values	Units
EUI	56.183	kWh/m2y
Opt insulation Thickness	0.243	m
Embodied GWP	5.71	kg CO2-eq/m2y
Embodied GWP Total (60y)	342.6	kg CO2-eq/m2
Operational GWP	11.237	kg CO2-eq/m2y
Operational GWP Total (60y)	674.2	kg CO2-eq/m2
GWP Embodied + Operational	16.947	kg CO2-eq/m2y
GWP Embodied + Operational Total (60y)	1016.8	kg CO2-eq/m2
Biogenic carbon Storage	2.31	kg CO2-eq/m2y
GWP Structure	2.56	kg CO2-eq/m2y
GWP Partition	0.315	kg CO2-eq/m2y
GWP Façade	0.982	kg CO2-eq/m2y
GWP Doors	0.061	kg CO2-eq/m2y
GWP Systems	1.3	kg CO2-eq/m2y
GWP Others	0.13	kg CO2-eq/m2y
GWP PV panels	0.112	kg CO2-eq/m2y
Window/Wall ratio	0.46	/

S_41 D 2G BL

S_41	Values	Units
EUI	53.685	kWh/m2y
Opt insulation Thickness	0.255	m
Embodied GWP	6.025	kg CO2-eq/m2y
Embodied GWP Total (60y)	361.5	kg CO2-eq/m2
Operational GWP	10.737	kg CO2-eq/m2y
Operational GWP Total (60y)	644.224	kg CO2-eq/m2
GWP Embodied + Operational	16.762	kg CO2-eq/m2y
GWP Embodied + Operational Total (60y)	1005.724	kg CO2-eq/m2
Biogenic carbon Storage	2.31	kg CO2-eq/m2y
GWP Structure	2.56	kg CO2-eq/m2y
GWP Partition	0.315	kg CO2-eq/m2y
GWP Façade	1.296	kg CO2-eq/m2y
GWP Doors	0.061	kg CO2-eq/m2y
GWP Systems	1.3	kg CO2-eq/m2y
GWP Others	0.13	kg CO2-eq/m2y
GWP PV panels	0.112	kg CO2-eq/m2y
Window/Wall ratio	0.46	/

S_43 D 3G NS

S_43	Values	Units
EUI	48.814	kWh/m2y
Opt insulation Thickness	0.271	m
Embodied GWP	5.912	kg CO2-eq/m2y
Embodied GWP Total (60y)	354.72	kg CO2-eq/m2
Operational GWP	9.763	kg CO2-eq/m2y
Operational GWP Total (60y)	585.77	kg CO2-eq/m2
GWP Embodied + Operational	15.675	kg CO2-eq/m2y
GWP Embodied + Operational Total (60y)	940.49	kg CO2-eq/m2
Biogenic carbon Storage	2.32	kg CO2-eq/m2y
GWP Structure	2.56	kg CO2-eq/m2y
GWP Partition	0.315	kg CO2-eq/m2y
GWP Façade	1.183	kg CO2-eq/m2y
GWP Doors	0.061	kg CO2-eq/m2y
GWP Systems	1.3	kg CO2-eq/m2y
GWP Others	0.13	kg CO2-eq/m2y
GWP PV panels	0.112	kg CO2-eq/m2y
Window/Wall ratio	0.46	/

S_44 D 3G BL

S_44	Values	Units
EUI	47.35	kWh/m2y
Opt insulation Thickness	0.273	m
Embodied GWP	6.021	kg CO2-eq/m2y
Embodied GWP Total (60y)	361.26	kg CO2-eq/m2
Operational GWP	9.47	kg CO2-eq/m2y
Operational GWP Total (60y)	568.202	kg CO2-eq/m2
GWP Embodied + Operational	15.491	kg CO2-eq/m2y
GWP Embodied + Operational Total (60y)	929.46	kg CO2-eq/m2
Biogenic carbon Storage	2.32	kg CO2-eq/m2y
GWP Structure	2.56	kg CO2-eq/m2y
GWP Partition	0.315	kg CO2-eq/m2y
GWP Façade	1.292	kg CO2-eq/m2y
GWP Doors	0.061	kg CO2-eq/m2y
GWP Systems	1.3	kg CO2-eq/m2y
GWP Others	0.13	kg CO2-eq/m2y
GWP PV panels	0.112	kg CO2-eq/m2y
Window/Wall ratio	0.46	/

S_42 D 2G OS

S_42	Values	Units
EUI	52.399	kWh/m2y
Opt insulation Thickness	0.264	m
Embodied GWP	5.831	kg CO2-eq/m2y
Embodied GWP Total (60y)	349.86	kg CO2-eq/m2
Operational GWP	10.48	kg CO2-eq/m2y
Operational GWP Total (60y)	628.794	kg CO2-eq/m2
GWP Embodied + Operational	16.311	kg CO2-eq/m2y
GWP Embodied + Operational Total (60y)	978.654	kg CO2-eq/m2
Biogenic carbon Storage	2.31	kg CO2-eq/m2y
GWP Structure	2.56	kg CO2-eq/m2y
GWP Partition	0.315	kg CO2-eq/m2y
GWP Façade	1.102	kg CO2-eq/m2y
GWP Doors	0.061	kg CO2-eq/m2y
GWP Systems	1.3	kg CO2-eq/m2y
GWP Others	0.13	kg CO2-eq/m2y
GWP PV panels	0.112	kg CO2-eq/m2y
Window/Wall ratio	0.46	/

S_45 D 3G OS

S_45	Values	Units
EUI	46.719	kWh/m2y
Opt insulation Thickness	0.28	m
Embodied GWP	5.95	kg CO2-eq/m2y
Embodied GWP Total (60y)	357	kg CO2-eq/m2
Operational GWP	9.344	kg CO2-eq/m2y
Operational GWP Total (60y)	560.625	kg CO2-eq/m2
GWP Embodied + Operational	15.294	kg CO2-eq/m2y
GWP Embodied + Operational Total (60y)	917.64	kg CO2-eq/m2
Biogenic carbon Storage	2.25	kg CO2-eq/m2y
GWP Structure	2.56	kg CO2-eq/m2y
GWP Partition	0.315	kg CO2-eq/m2y
GWP Façade	1.221	kg CO2-eq/m2y
GWP Doors	0.061	kg CO2-eq/m2y
GWP Systems	1.3	kg CO2-eq/m2y
GWP Others	0.13	kg CO2-eq/m2y
GWP PV panels	0.112	kg CO2-eq/m2y
Window/Wall ratio	0.46	/

S_48 D 2G TR

S_48	Values	Units
EUI	60.507	kWh/m2y
Opt insulation Thickness	0.243	m
Embodied GWP	5.71	kg CO2-eq/m2y
Embodied GWP Total (60y)	342.6	kg CO2-eq/m2
Operational GWP	12.101	kg CO2-eq/m2y
Operational GWP Total (60y)	726.084	kg CO2-eq/m2
GWP Embodied + Operational	17.811	kg CO2-eq/m2y
GWP Embodied + Operational Total (60y)	1068.684	kg CO2-eq/m2
Biogenic carbon Storage	2.31	kg CO2-eq/m2y
GWP Structure	2.56	kg CO2-eq/m2y
GWP Partition	0.315	kg CO2-eq/m2y
GWP Façade	0.982	kg CO2-eq/m2y
GWP Doors	0.061	kg CO2-eq/m2y
GWP Systems	1.3	kg CO2-eq/m2y
GWP Others	0.13	kg CO2-eq/m2y
GWP PV panels	0.112	kg CO2-eq/m2y
Window/Wall ratio	0.46	/

S_49 D 3G TR

S_49	Values	Units
EUI	48.825	kWh/m2y
Opt insulation Thickness	0.268	m
Embodied GWP	5.91	kg CO2-eq/m2y
Embodied GWP Total (60y)	354.6	kg CO2-eq/m2
Operational GWP	9.765	kg CO2-eq/m2y
Operational GWP Total (60y)	585.9	kg CO2-eq/m2
GWP Embodied + Operational	15.675	kg CO2-eq/m2y
GWP Embodied + Operational Total (60y)	940.5	kg CO2-eq/m2
Biogenic carbon Storage	2.32	kg CO2-eq/m2y
GWP Structure	2.56	kg CO2-eq/m2y
GWP Partition	0.315	kg CO2-eq/m2y
GWP Façade	1.18	kg CO2-eq/m2y
GWP Doors	0.061	kg CO2-eq/m2y
GWP Systems	1.3	kg CO2-eq/m2y
GWP Others	0.13	kg CO2-eq/m2y
GWP PV panels	0.112	kg CO2-eq/m2y
Window/Wall ratio	0.46	/

S_51 B 2G OS VT

S_51 B 2G OS VT	Values	Units
EUI	54.071	kWh/m2y
Opt insulation Thickness	0.288	m
Embodied GWP	5.681	kg CO2-eq/m2y
Embodied GWP Total (60y)	340.86	kg CO2-eq/m2
Operational GWP	10.814	kg CO2-eq/m2y
Operational GWP Total (60y)	648.852	kg CO2-eq/m2
GWP Embodied + Operational	16.495	kg CO2-eq/m2y
GWP Embodied + Operational Total (60y)	989.712	kg CO2-eq/m2
Biogenic carbon Storage	2.29	kg CO2-eq/m2y
GWP Structure	2.56	kg CO2-eq/m2y
GWP Partition	0.315	kg CO2-eq/m2y
GWP Façade	0.952	kg CO2-eq/m2y
GWP Doors	0.061	kg CO2-eq/m2y
GWP Systems	1.3	kg CO2-eq/m2y
GWP Others	0.13	kg CO2-eq/m2y
GWP PV panels	0.112	kg CO2-eq/m2y
Window/Wall ratio	0.54	/

S_61 B 3G OS VT

S_61 B 3G OS VT	Values	Units
EUI	47.532	kWh/m2y
Opt insulation Thickness	0.304	m
Embodied GWP	5.903	kg CO2-eq/m2y
Embodied GWP Total (60y)	354.18	kg CO2-eq/m2
Operational GWP	9.506	kg CO2-eq/m2y
Operational GWP Total (60y)	570.39	kg CO2-eq/m2
GWP Embodied + Operational	15.409	kg CO2-eq/m2y
GWP Embodied + Operational Total (60y)	924.57	kg CO2-eq/m2
Biogenic carbon Storage	2.29	kg CO2-eq/m2y
GWP Structure	2.56	kg CO2-eq/m2y
GWP Partition	0.315	kg CO2-eq/m2y
GWP Façade	1.172	kg CO2-eq/m2y
GWP Doors	0.061	kg CO2-eq/m2y
GWP Systems	1.3	kg CO2-eq/m2y
GWP Others	0.13	kg CO2-eq/m2y
GWP PV panels	0.112	kg CO2-eq/m2y
Window/Wall ratio	0.54	/

S_52 B 2G VT OS

S_52 B 2G VT OS	Values	Units
EUI	54.635	kWh/m2y
Opt insulation Thickness	0.288	m
Embodied GWP	5.681	kg CO2-eq/m2y
Embodied GWP Total (60y)	340.86	kg CO2-eq/m2
Operational GWP	10.927	kg CO2-eq/m2y
Operational GWP Total (60y)	655.617	kg CO2-eq/m2
GWP Embodied + Operational	16.608	kg CO2-eq/m2y
GWP Embodied + Operational Total (60y)	996.477	kg CO2-eq/m2
Biogenic carbon Storage	2.29	kg CO2-eq/m2y
GWP Structure	2.56	kg CO2-eq/m2y
GWP Partition	0.315	kg CO2-eq/m2y
GWP Façade	0.952	kg CO2-eq/m2y
GWP Doors	0.061	kg CO2-eq/m2y
GWP Systems	1.3	kg CO2-eq/m2y
GWP Others	0.13	kg CO2-eq/m2y
GWP PV panels	0.112	kg CO2-eq/m2y
Window/Wall ratio	0.54	/

S_62 B 3G VT OS

S_62 B 3G VT OS	Values	Units
EUI	47.808	kWh/m2y
Opt insulation Thickness	0.304	m
Embodied GWP	6.067	kg CO2-eq/m2y
Embodied GWP Total (60y)	364.02	kg CO2-eq/m2
Operational GWP	9.562	kg CO2-eq/m2y
Operational GWP Total (60y)	573.691	kg CO2-eq/m2
GWP Embodied + Operational	15.629	kg CO2-eq/m2y
GWP Embodied + Operational Total (60y)	937.711	kg CO2-eq/m2
Biogenic carbon Storage	2.29	kg CO2-eq/m2y
GWP Structure	2.56	kg CO2-eq/m2y
GWP Partition	0.315	kg CO2-eq/m2y
GWP Façade	1.337	kg CO2-eq/m2y
GWP Doors	0.061	kg CO2-eq/m2y
GWP Systems	1.3	kg CO2-eq/m2y
GWP Others	0.13	kg CO2-eq/m2y
GWP PV panels	0.112	kg CO2-eq/m2y
Window/Wall ratio	0.54	/

S_53 D 2G OS VT

S_53 D 2G OS VT	Values	Units
EUI	52.398	kWh/m2y
Opt insulation Thickness	0.264	m
Embodied GWP	5.731	kg CO2-eq/m2y
Embodied GWP Total (60y)	343.86	kg CO2-eq/m2
Operational GWP	10.48	kg CO2-eq/m2y
Operational GWP Total (60y)	628.776	kg CO2-eq/m2
GWP Embodied + Operational	16.211	kg CO2-eq/m2y
GWP Embodied + Operational Total (60y)	972.636	kg CO2-eq/m2
Biogenic carbon Storage	2.31	kg CO2-eq/m2y
GWP Structure	2.56	kg CO2-eq/m2y
GWP Partition	0.315	kg CO2-eq/m2y
GWP Façade	1.002	kg CO2-eq/m2y
GWP Doors	0.061	kg CO2-eq/m2y
GWP Systems	1.3	kg CO2-eq/m2y
GWP Others	0.13	kg CO2-eq/m2y
GWP PV panels	0.112	kg CO2-eq/m2y
Window/Wall ratio	0.46	/

S_63 D 3G OS VT

S_63 D 3G OS VT	Values	Units
EUI	46.72	kWh/m2y
Opt insulation Thickness	0.28	m
Embodied GWP	5.921	kg CO2-eq/m2y
Embodied GWP Total (60y)	355.26	kg CO2-eq/m2
Operational GWP	9.344	kg CO2-eq/m2y
Operational GWP Total (60y)	560.637	kg CO2-eq/m2
GWP Embodied + Operational	15.265	kg CO2-eq/m2y
GWP Embodied + Operational Total (60y)	915.897	kg CO2-eq/m2
Biogenic carbon Storage	2.32	kg CO2-eq/m2y
GWP Structure	2.56	kg CO2-eq/m2y
GWP Partition	0.315	kg CO2-eq/m2y
GWP Façade	1.192	kg CO2-eq/m2y
GWP Doors	0.061	kg CO2-eq/m2y
GWP Systems	1.3	kg CO2-eq/m2y
GWP Others	0.13	kg CO2-eq/m2y
GWP PV panels	0.112	kg CO2-eq/m2y
Window/Wall ratio	0.46	/

S_54 H 2G OS V

S_54 H 2G OS VT	Values	Units
EUI	46.914	kWh/m2y
Opt insulation Thickness	0.249	m
Embodied GWP	5.875	kg CO2-eq/m2y
Embodied GWP Total (60y)	352.5	kg CO2-eq/m2
Operational GWP	9.383	kg CO2-eq/m2y
Operational GWP Total (60y)	562.962	kg CO2-eq/m2
GWP Embodied + Operational	15.258	kg CO2-eq/m2y
GWP Embodied + Operational Total (60y)	915.462	kg CO2-eq/m2
Biogenic carbon Storage	2.38	kg CO2-eq/m2y
GWP Structure	2.56	kg CO2-eq/m2y
GWP Partition	0.315	kg CO2-eq/m2y
GWP Façade	1.147	kg CO2-eq/m2y
GWP Doors	0.061	kg CO2-eq/m2y
GWP Systems	1.3	kg CO2-eq/m2y
GWP Others	0.13	kg CO2-eq/m2y
GWP PV panels	0.112	kg CO2-eq/m2y
Window/Wall ratio	0.24	/

S_64 H 3G OS V

S_64 H 3G OS VT	Values	Units
EUI	44.016	kWh/m2y
Opt insulation Thickness	0.257	m
Embodied GWP	5.978	kg CO2-eq/m2y
Embodied GWP Total (60y)	358.68	kg CO2-eq/m2
Operational GWP	8.803	kg CO2-eq/m2y
Operational GWP Total (60y)	528.187	kg CO2-eq/m2
GWP Embodied + Operational	14.781	kg CO2-eq/m2y
GWP Embodied + Operational Total (60y)	886.867	kg CO2-eq/m2
Biogenic carbon Storage	2.38	kg CO2-eq/m2y
GWP Structure	2.56	kg CO2-eq/m2y
GWP Partition	0.315	kg CO2-eq/m2y
GWP Façade	1.25	kg CO2-eq/m2y
GWP Doors	0.061	kg CO2-eq/m2y
GWP Systems	1.3	kg CO2-eq/m2y
GWP Others	0.13	kg CO2-eq/m2y
GWP PV panels	0.112	kg CO2-eq/m2y
Window/Wall ratio	0.24	/

S_21 and S_24 thickness optimization

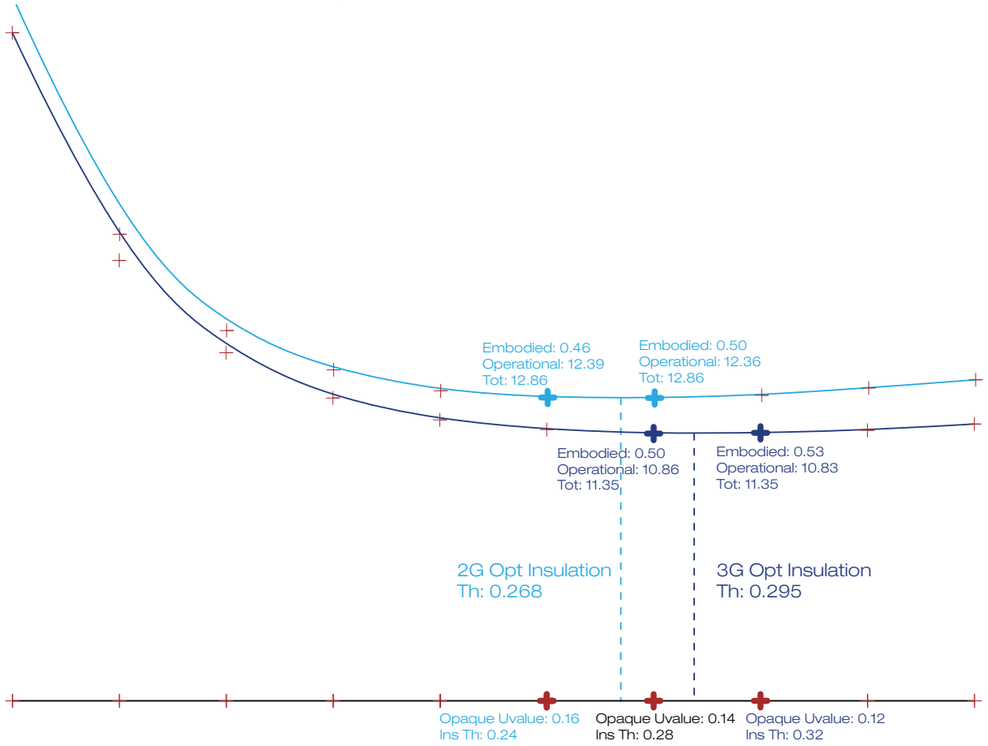

S_22 and S_25 thickness optimization

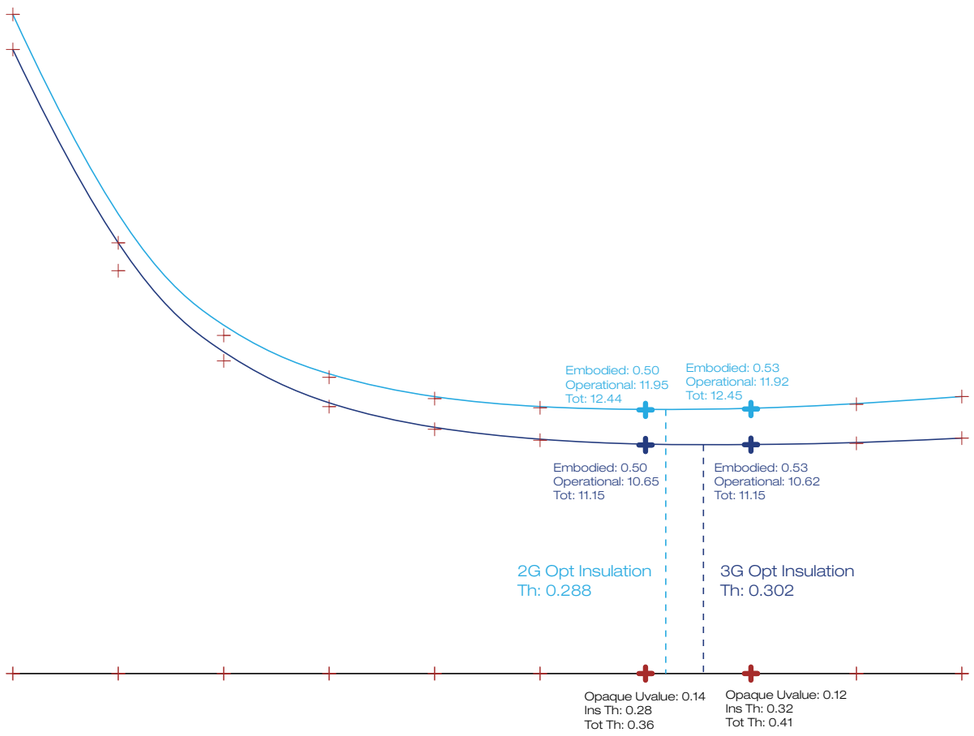

S_28 and S_29 thickness optimization

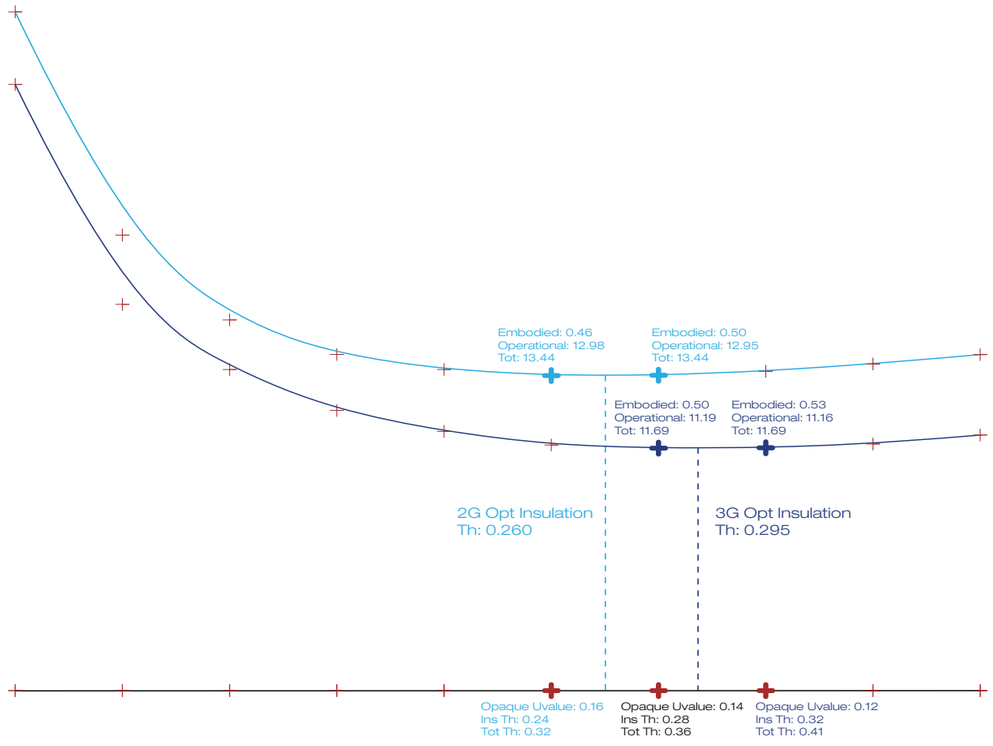

S_30 and S_33 thickness optimization

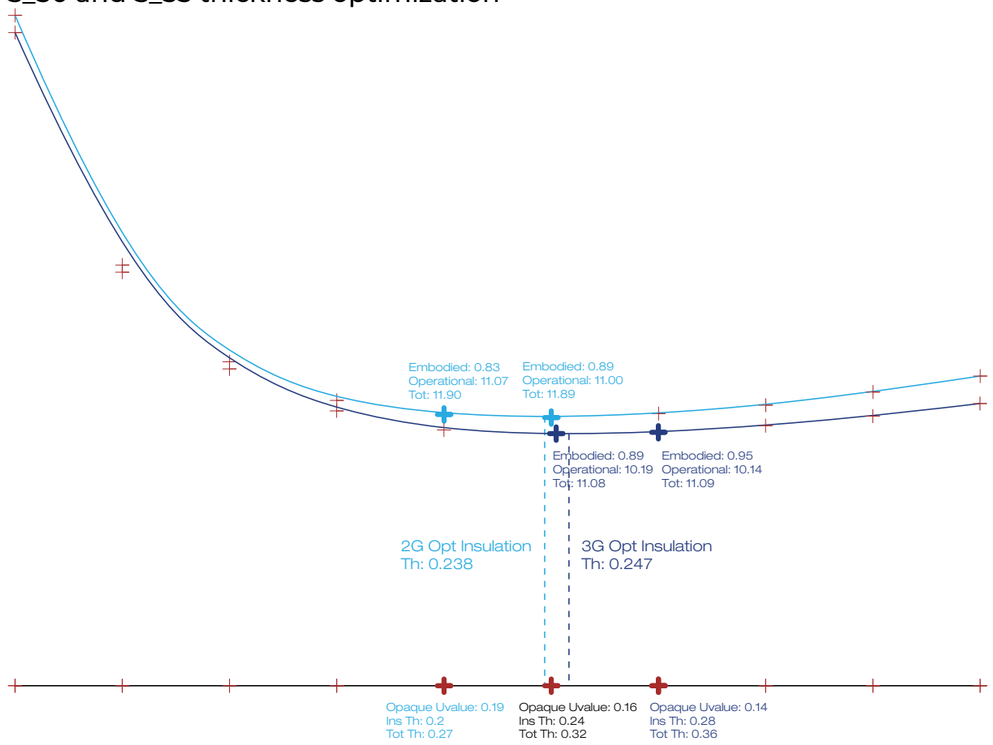

S_31 and S_34 thickness optimization

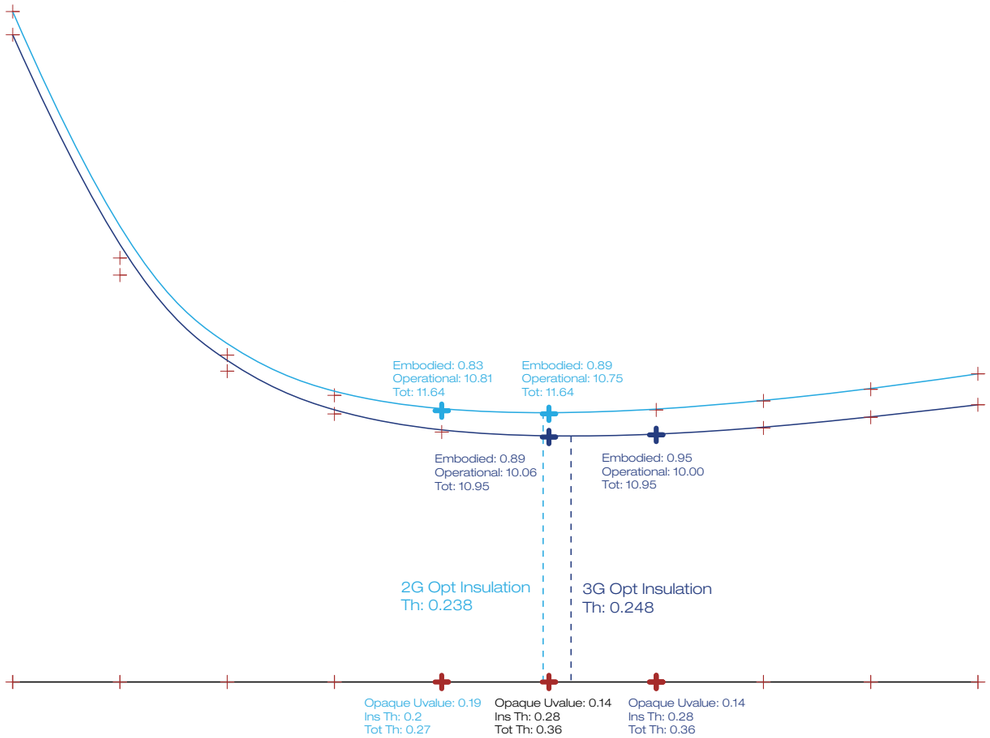

S_32 and S_35 thickness optimization

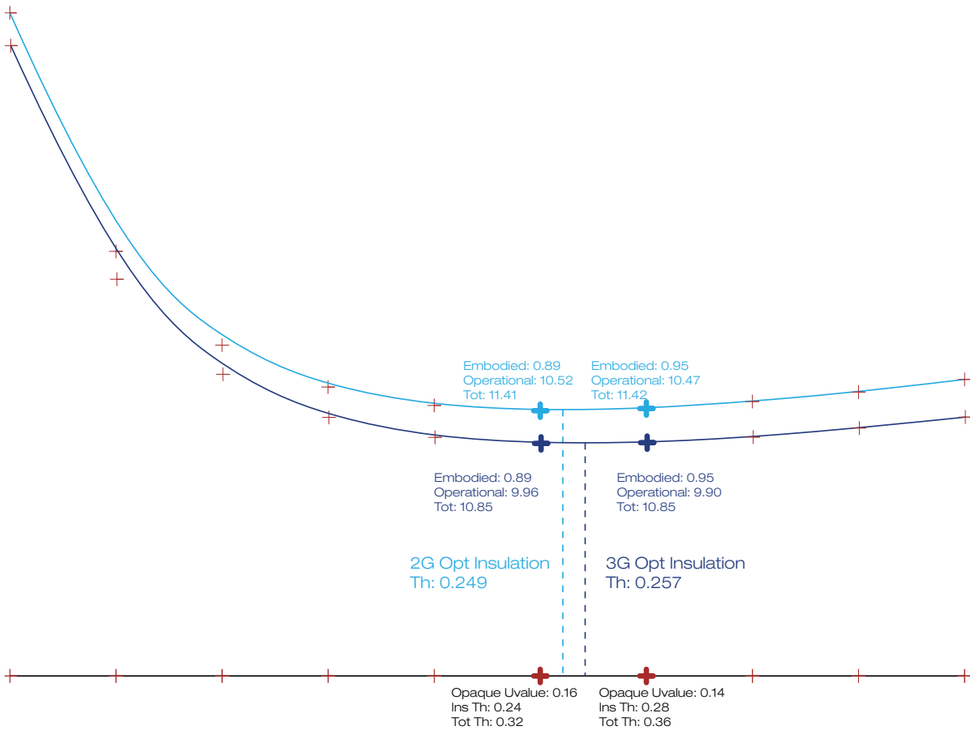

S_38 and S_39 thickness optimization

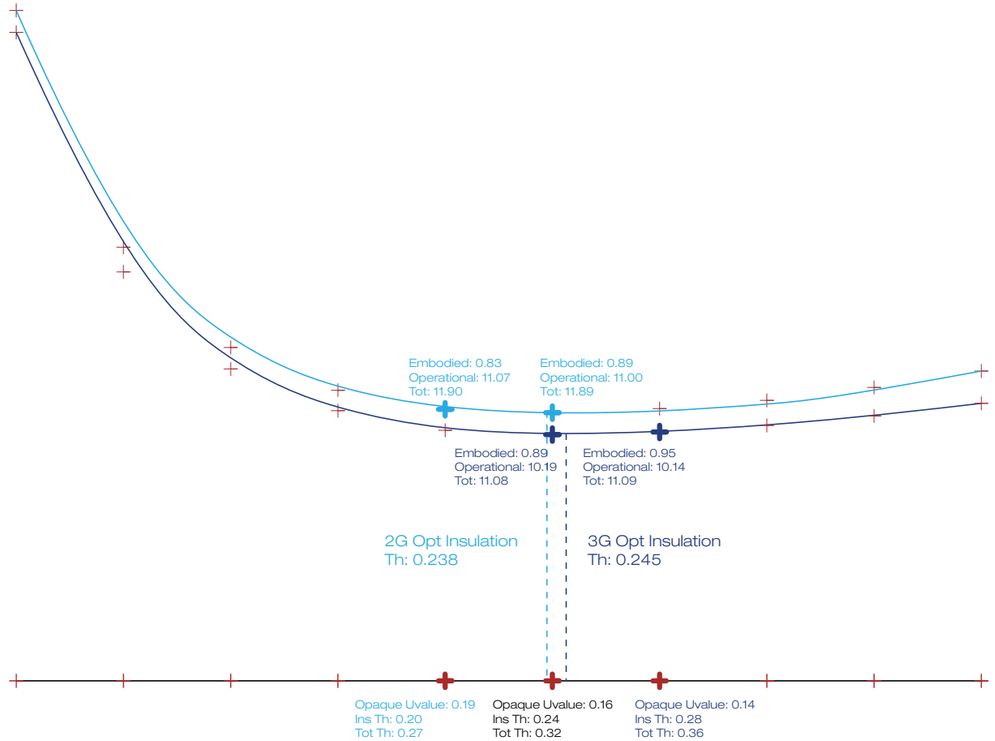

S_40 and S_43 thickness optimization

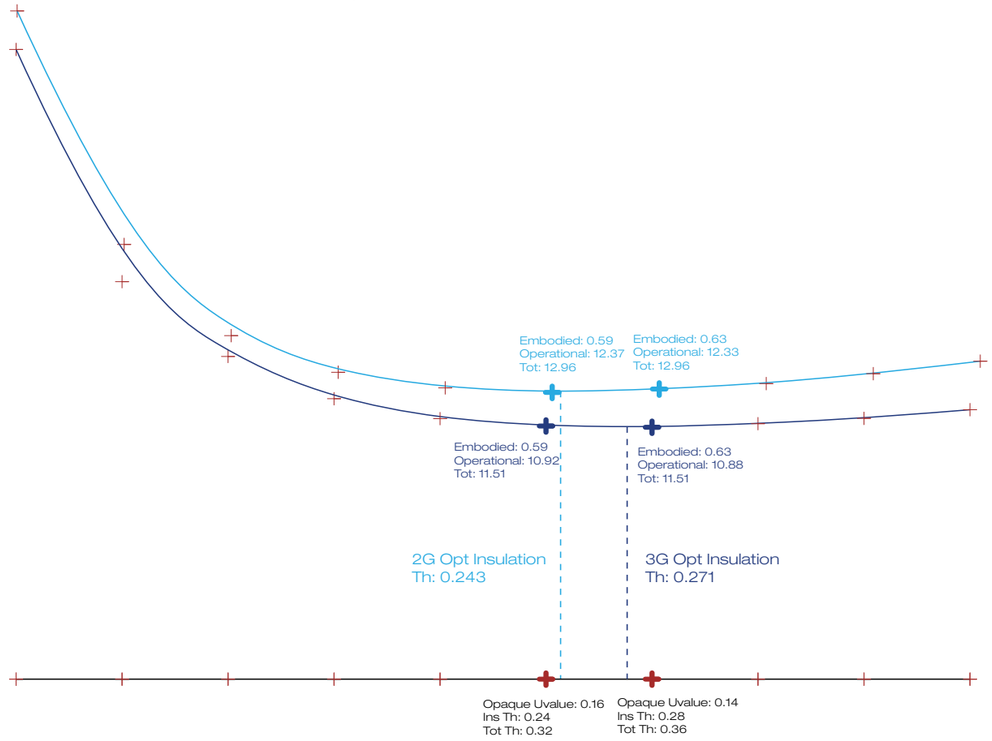

S_41 and S_44 thickness optimization

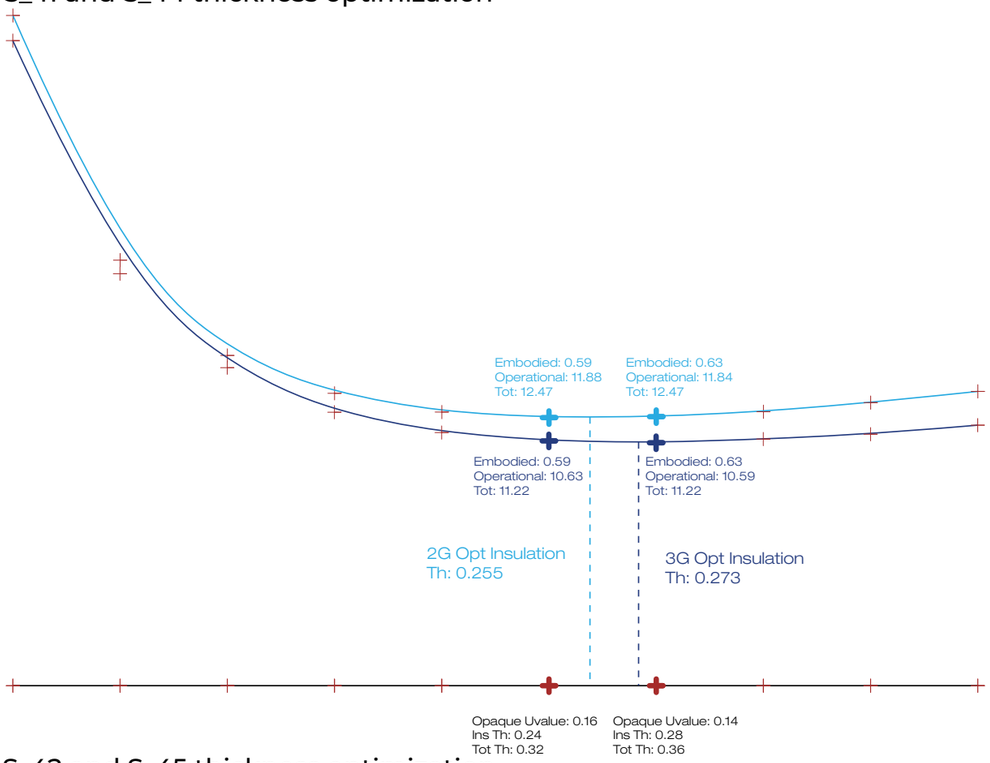

S_42 and S_45 thickness optimization

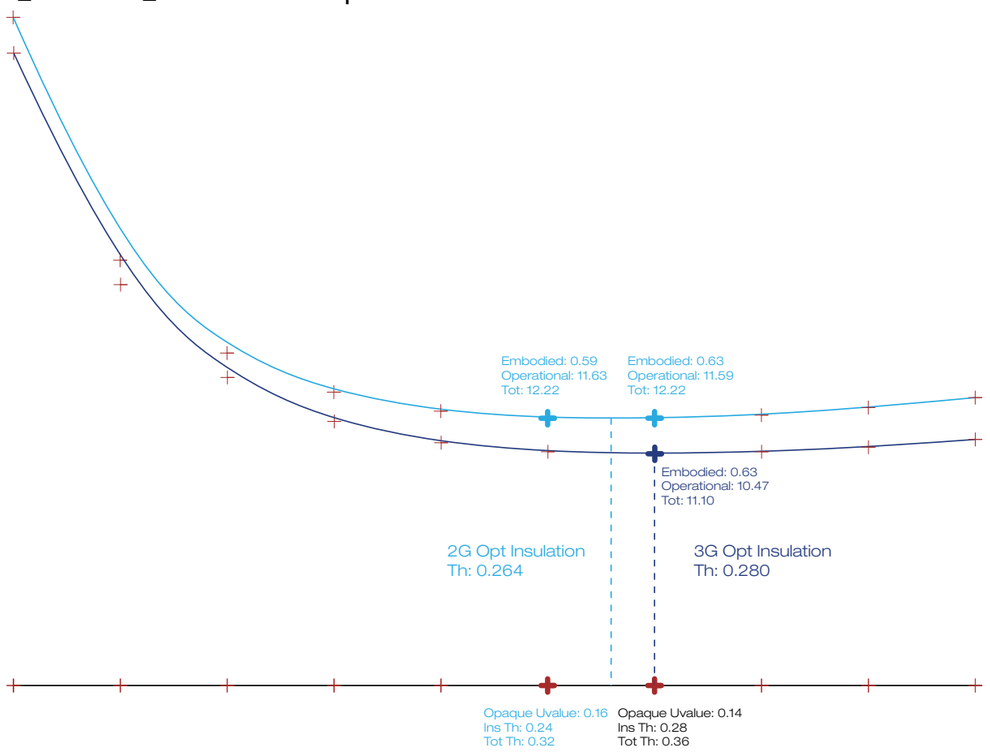

S_48 and S_49 thickness optimization

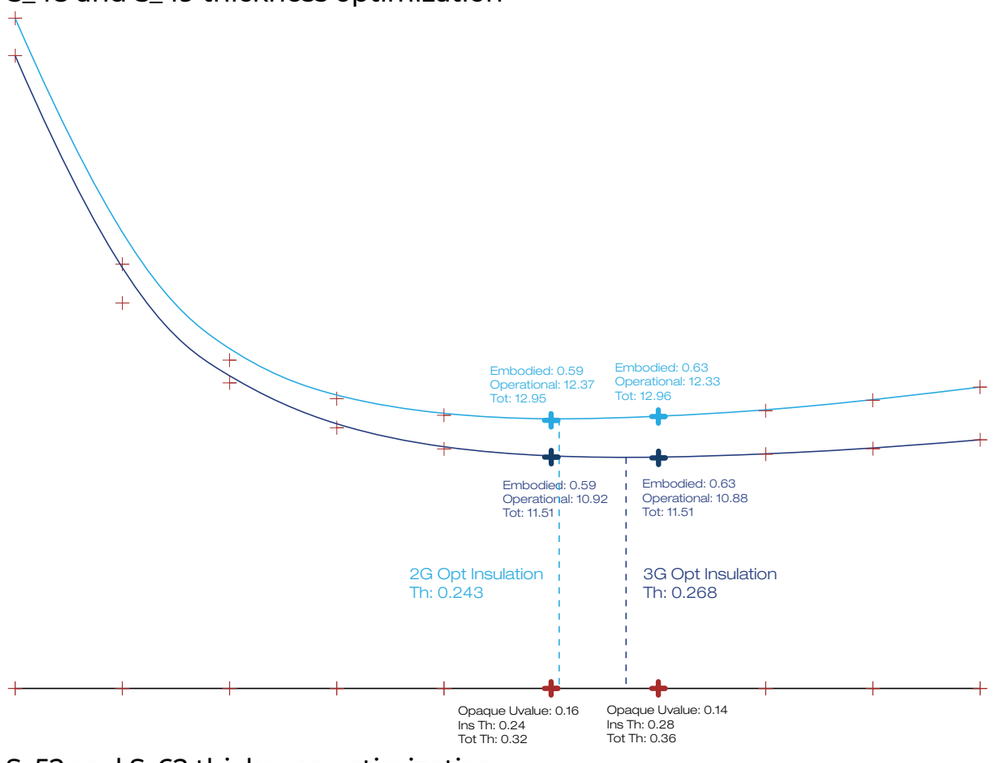

S_52 and S_62 thickness optimization

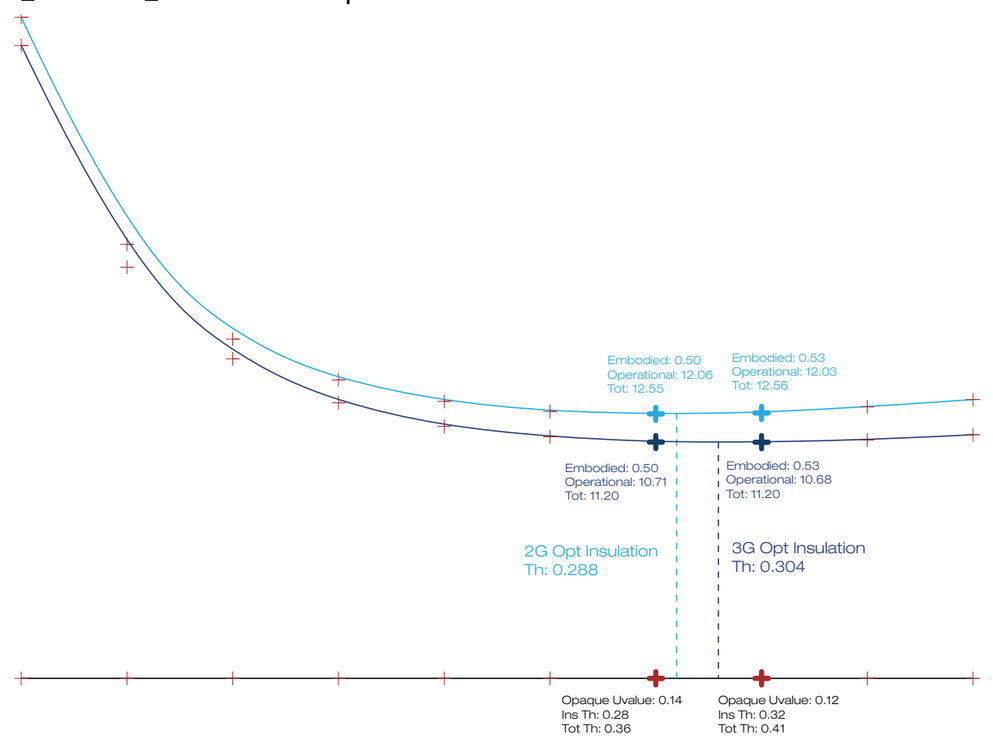

S_53 and S_63 thickness optimization

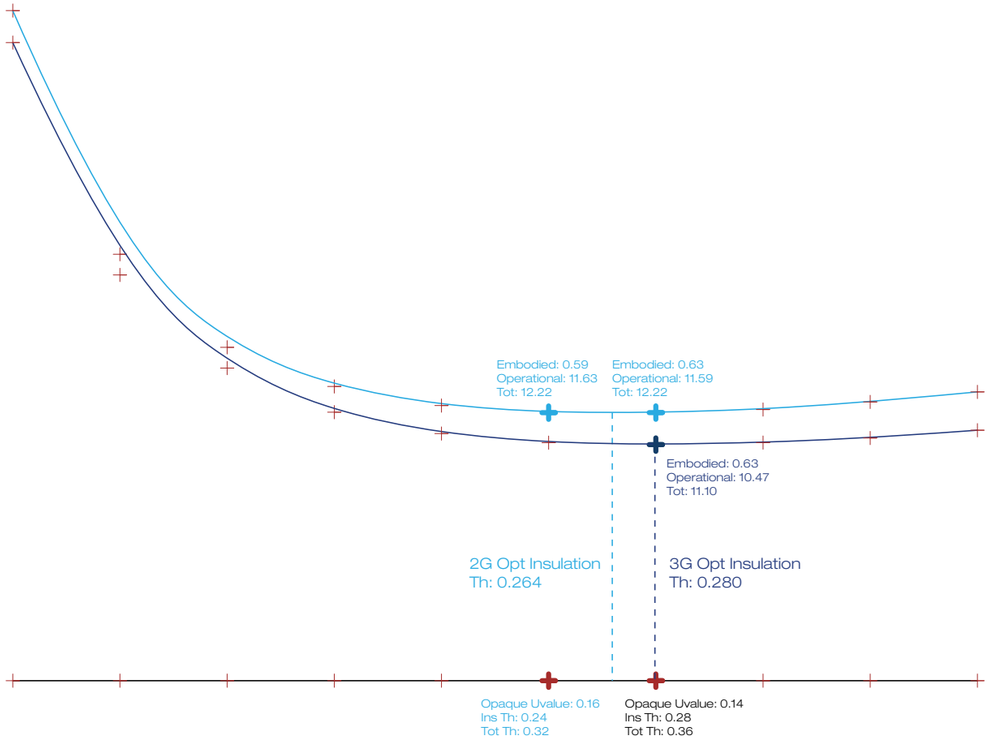

S_54 and S_64 thickness optimization

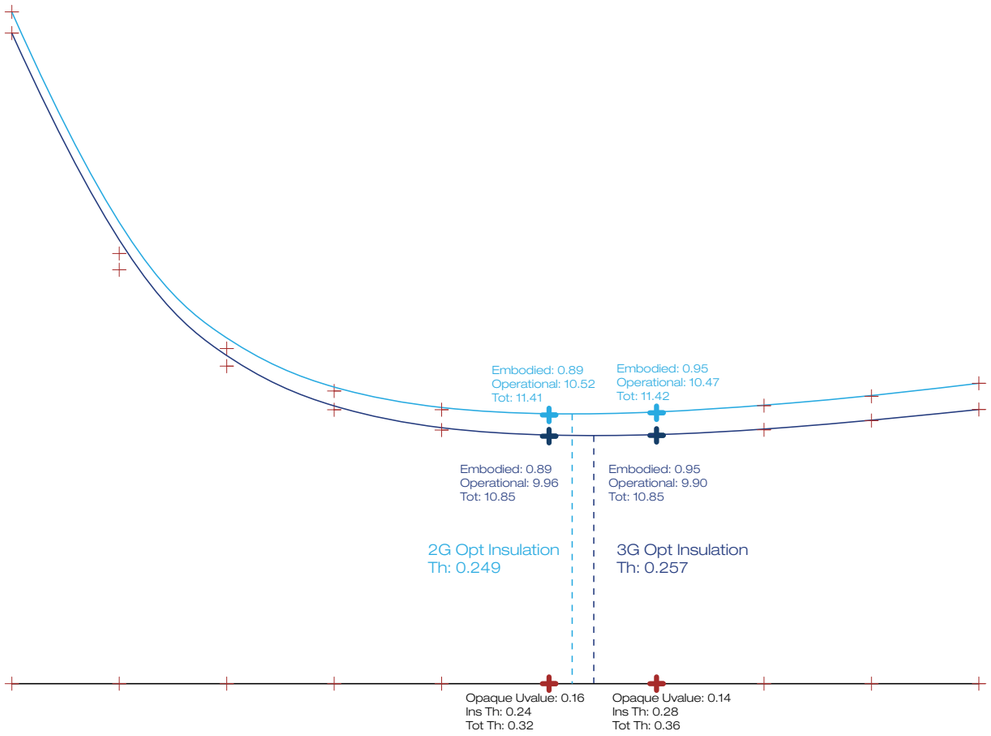

S_20 B 2G NS

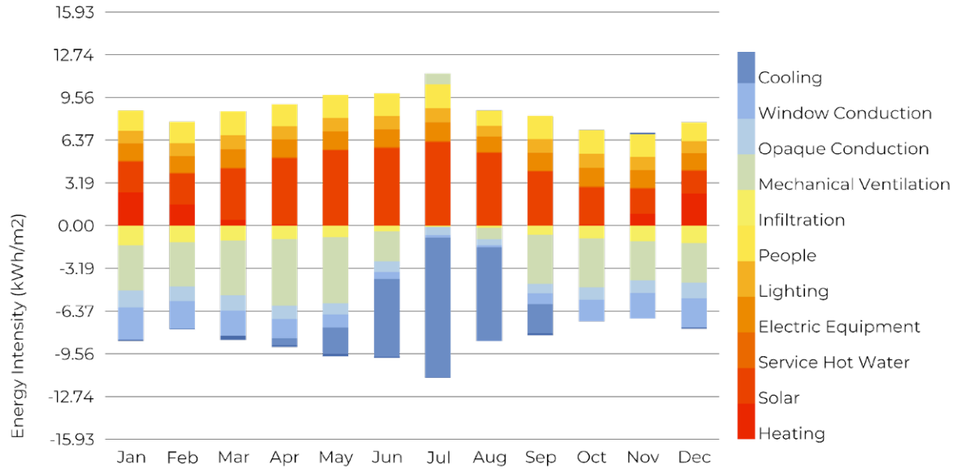

S_21 B 2G BL

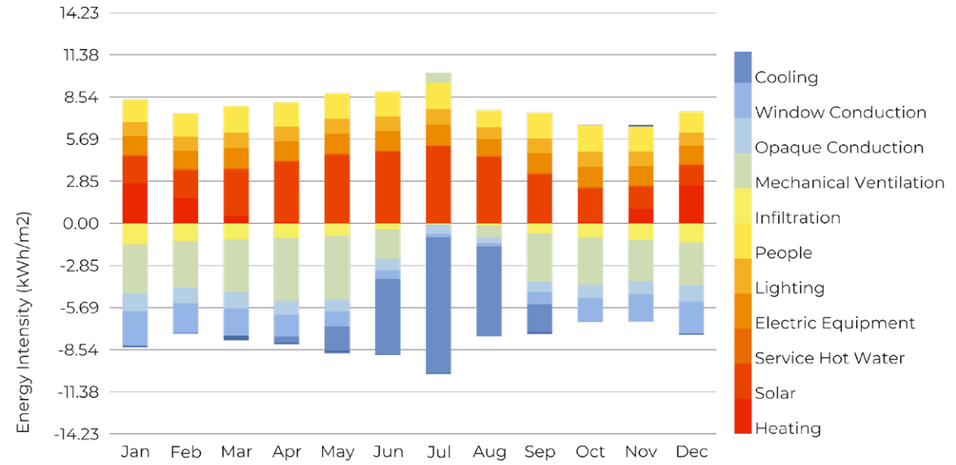

S_22 B 2G OS

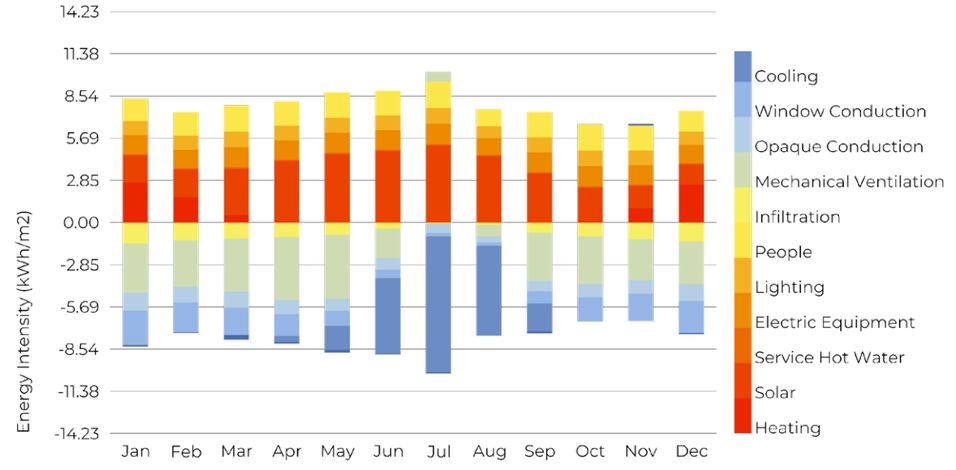

S_28 B 2G VT

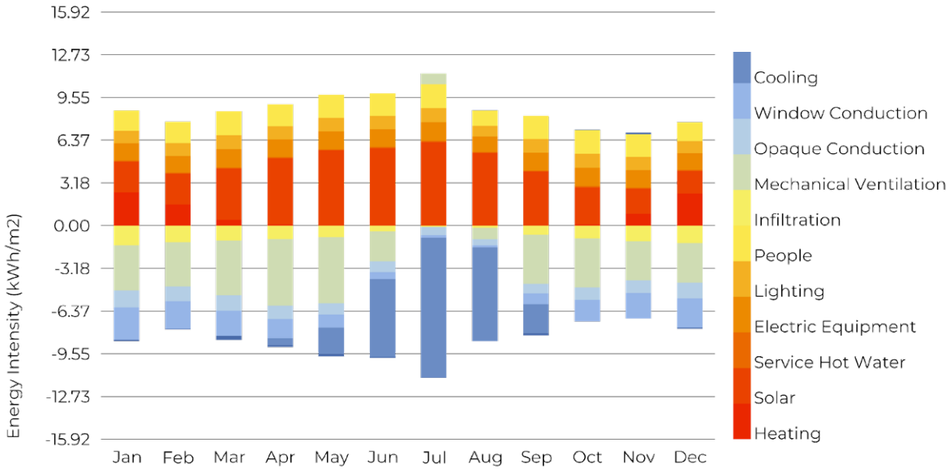

S_23 B 3G NS

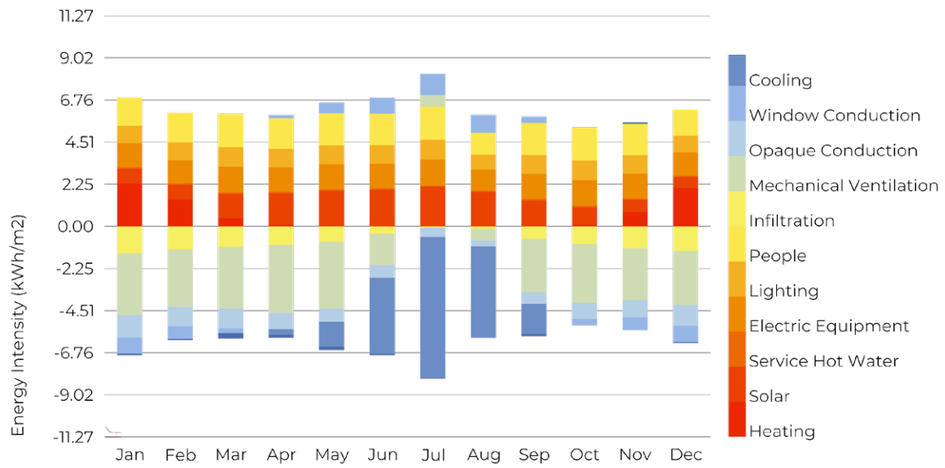

S_24 B 3G BL

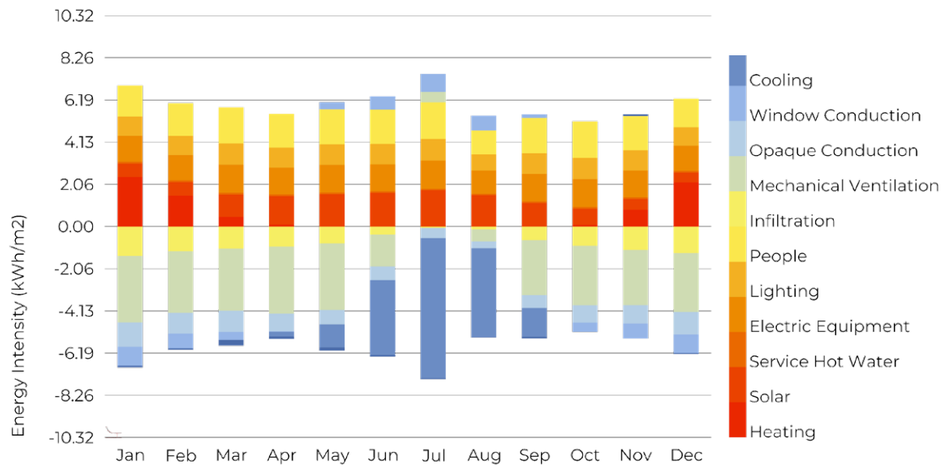

S_25 B 3G OS

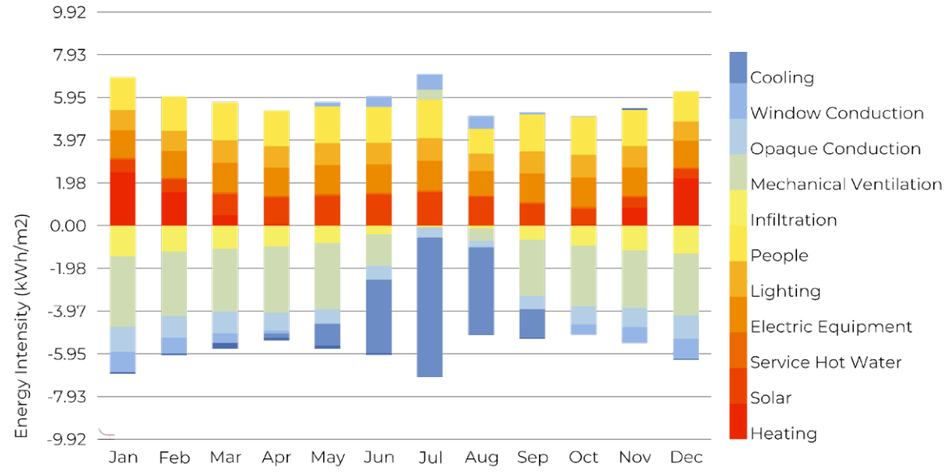

S_29 B 3G VT

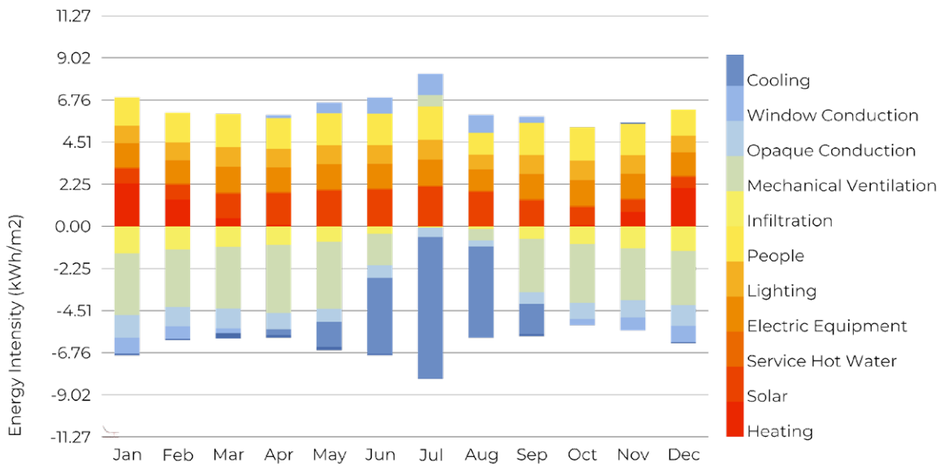

S_30 H 2G NS

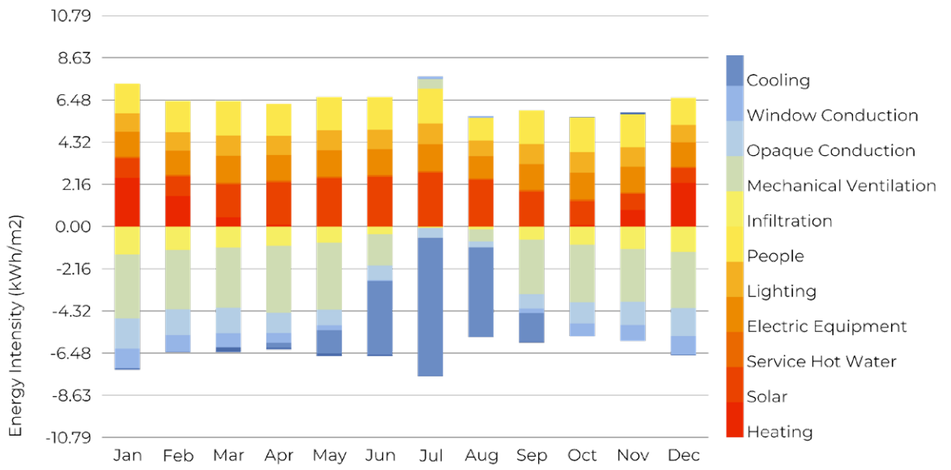

S_31 H 2G BL

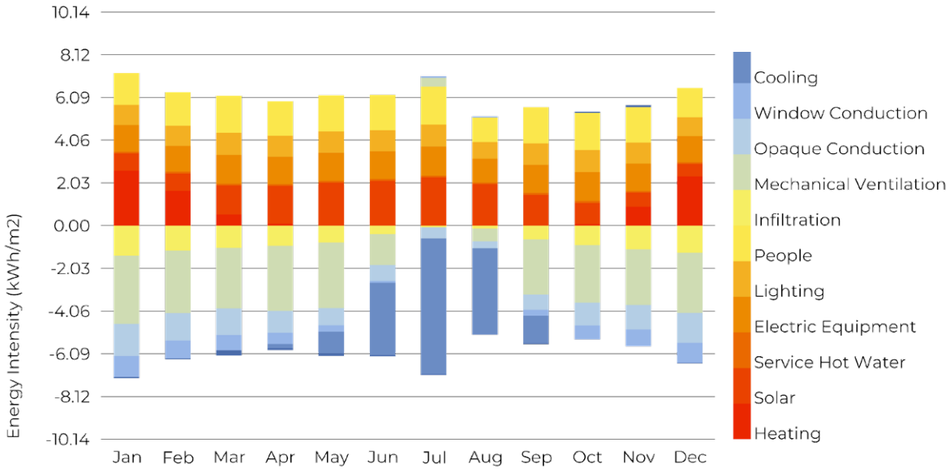

S_32 H 2G OS

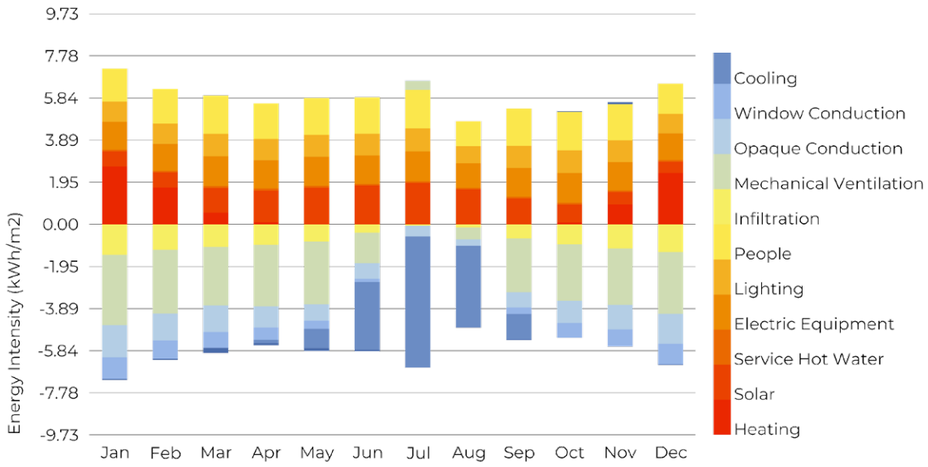

S_38 H 2G VT

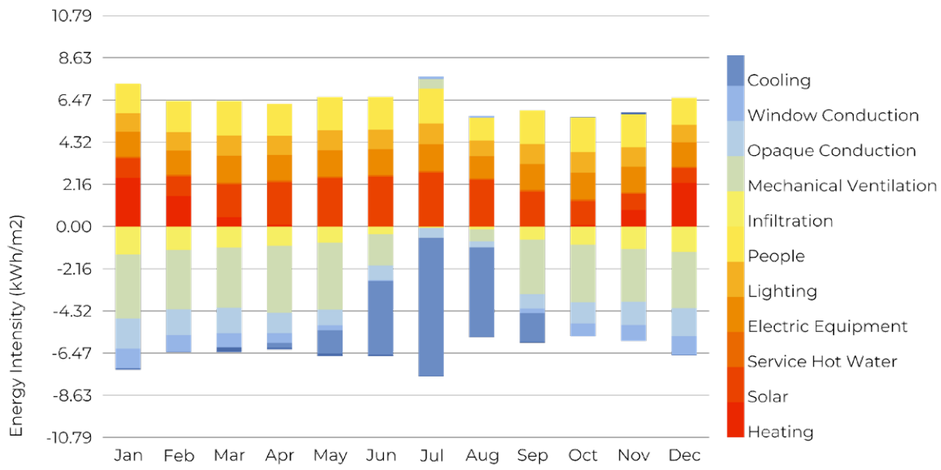

S_33 H 3G NS

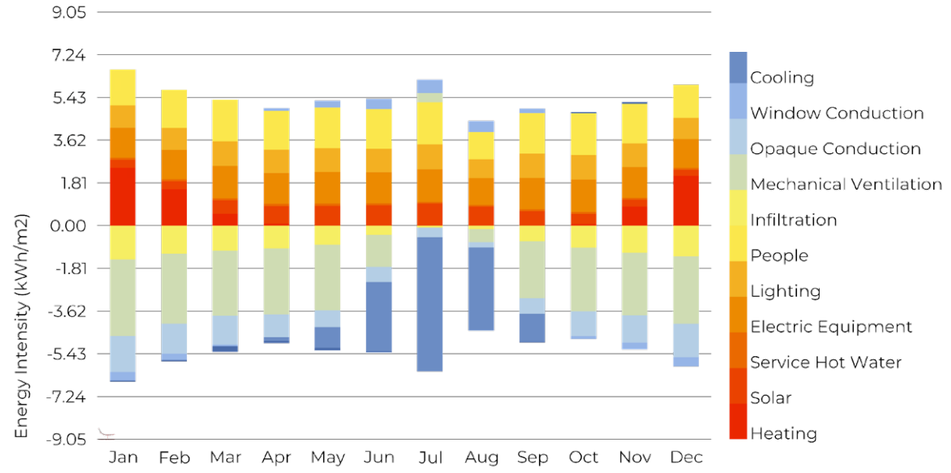

S_34 H 3G BL

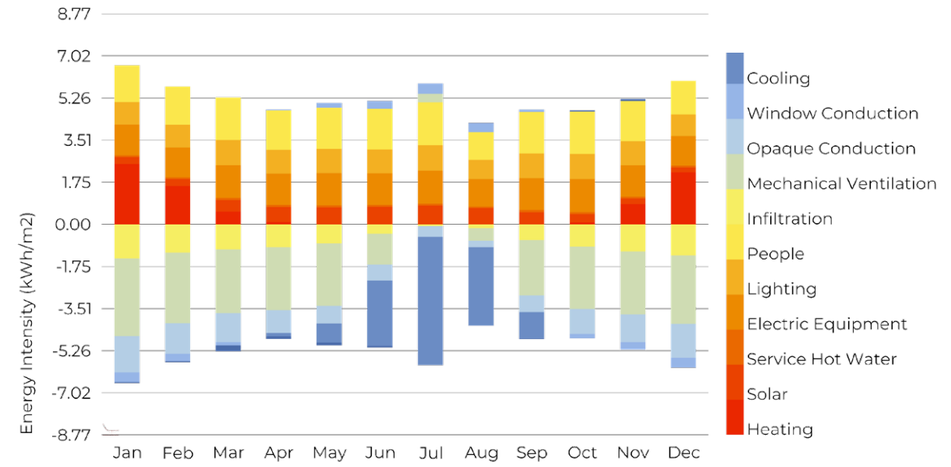

S_35 H 3G OS

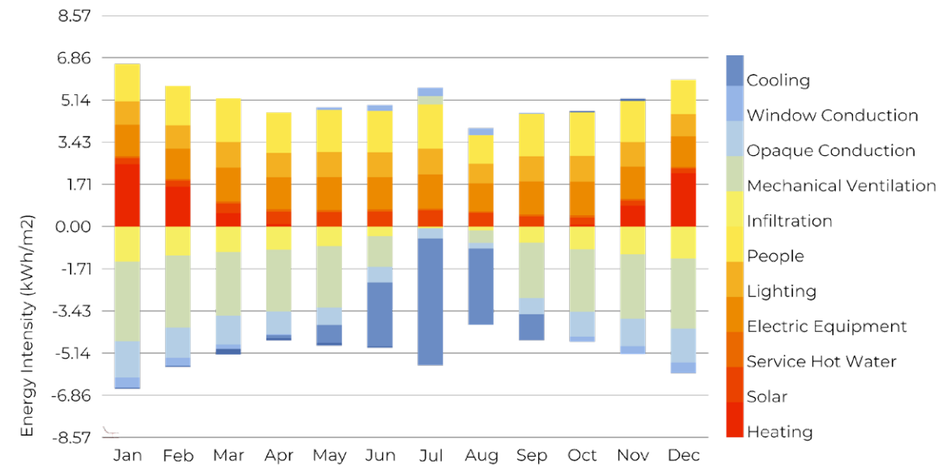

S_39 H 3G VT

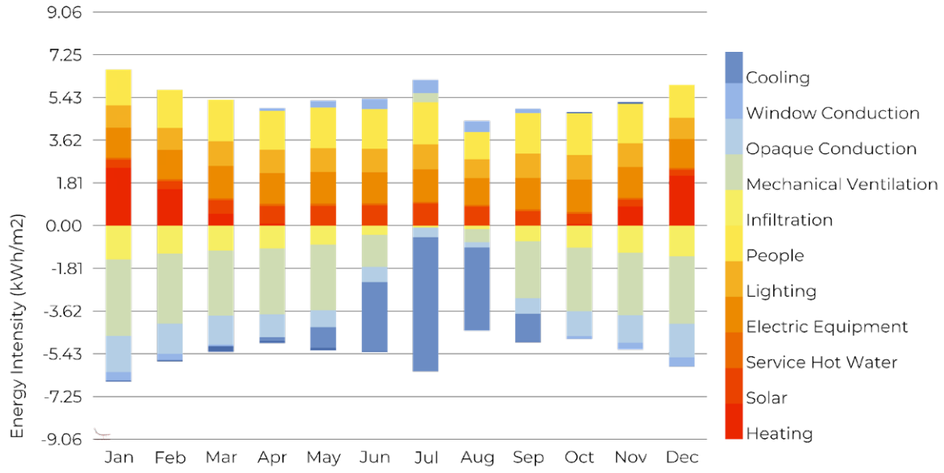

S_40 D 2G NS

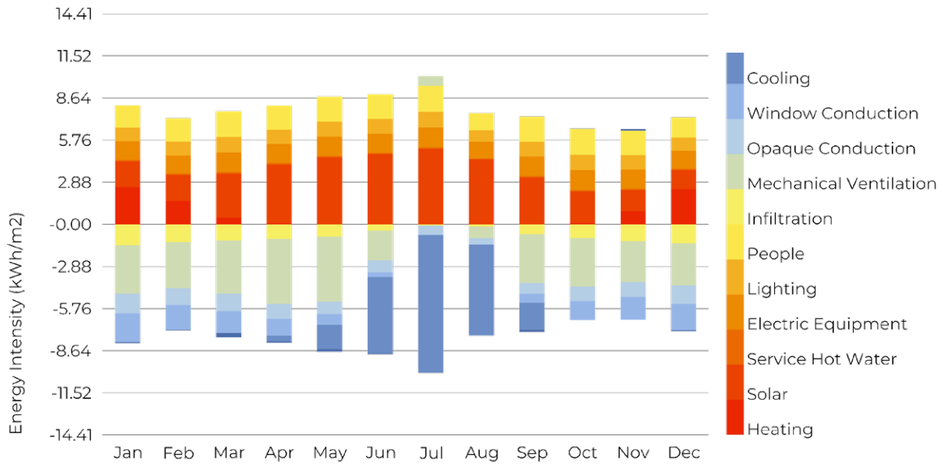

S_41 D 2G BL

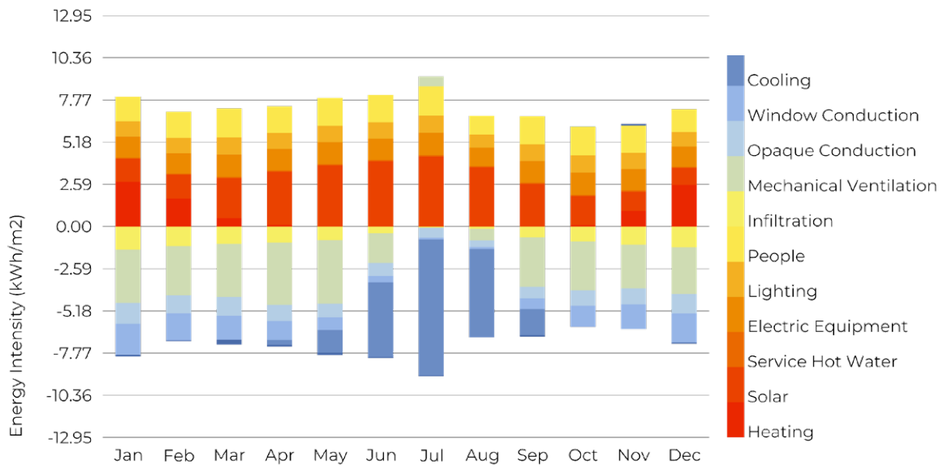

S_42 D 2G OS

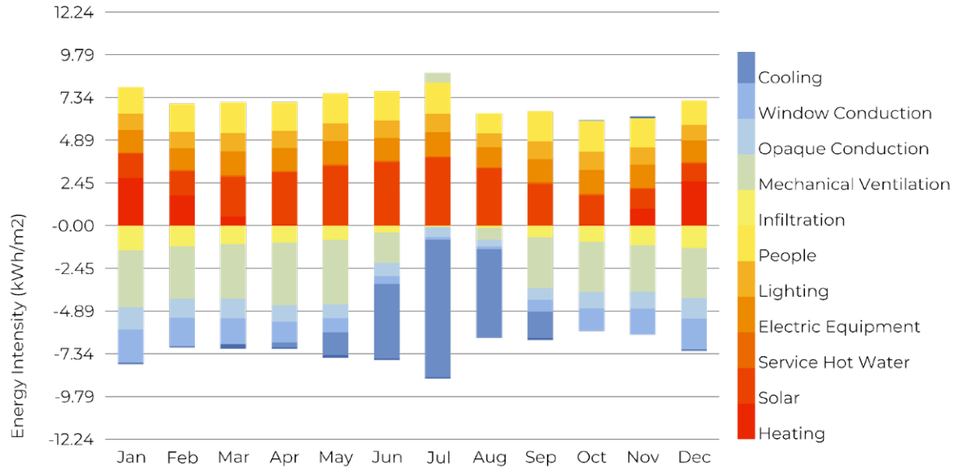

S_48 D 2G VT

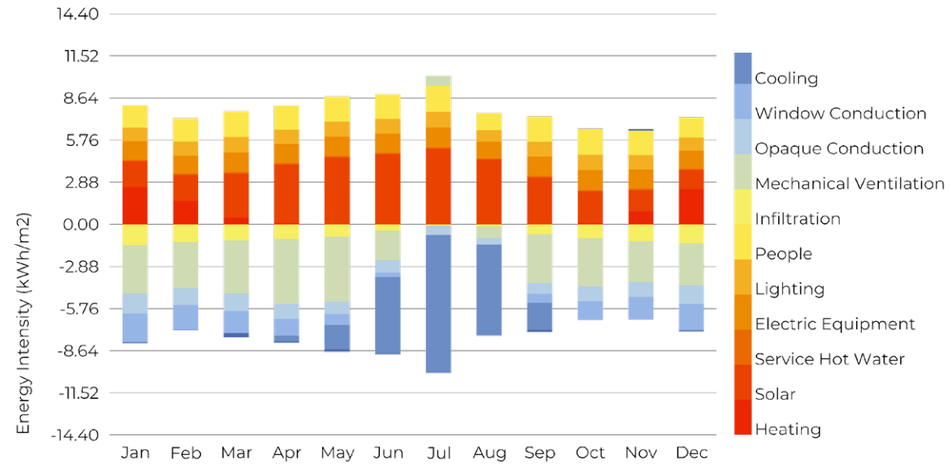

S_43 D 3G NS

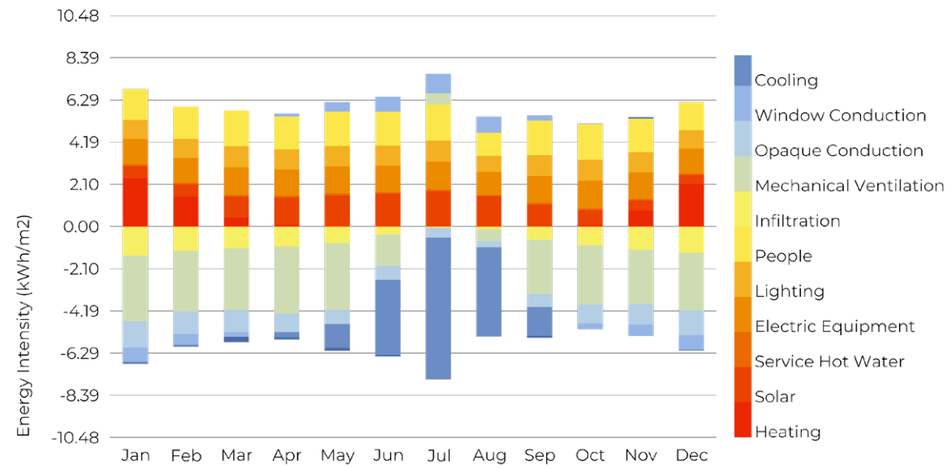

S_44 D 3G BL

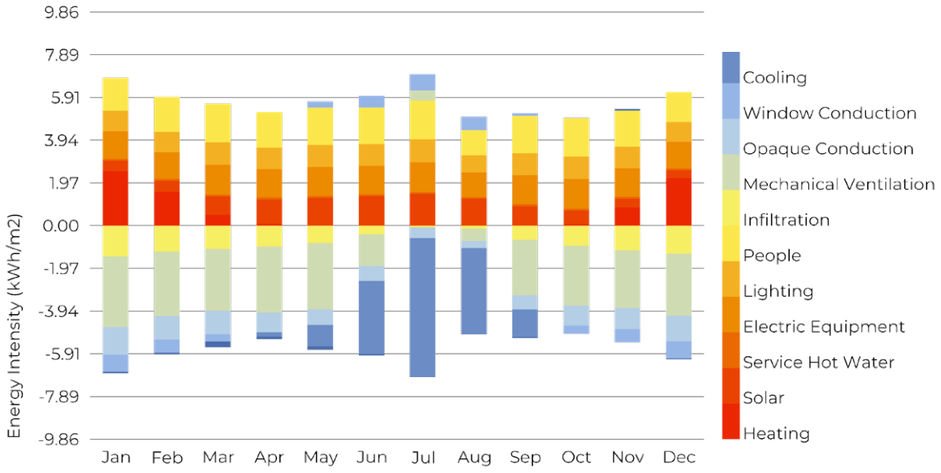

S_45 D 3G OS

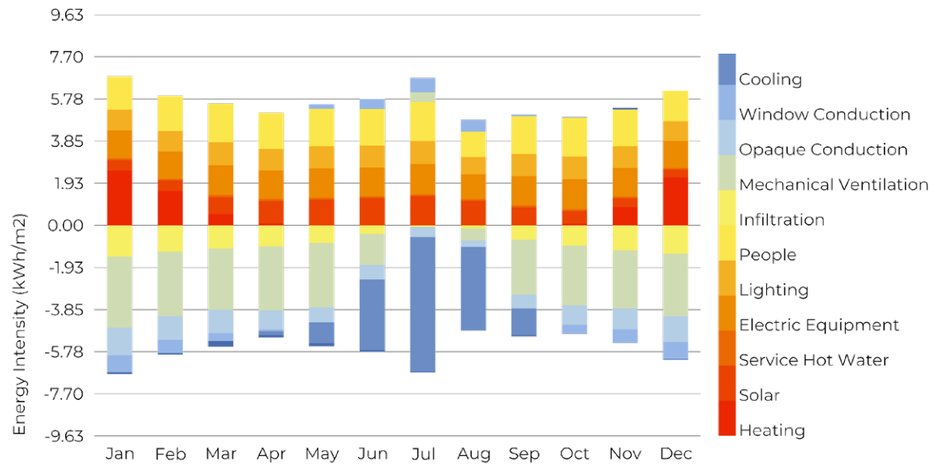

S_49 D 3G TR

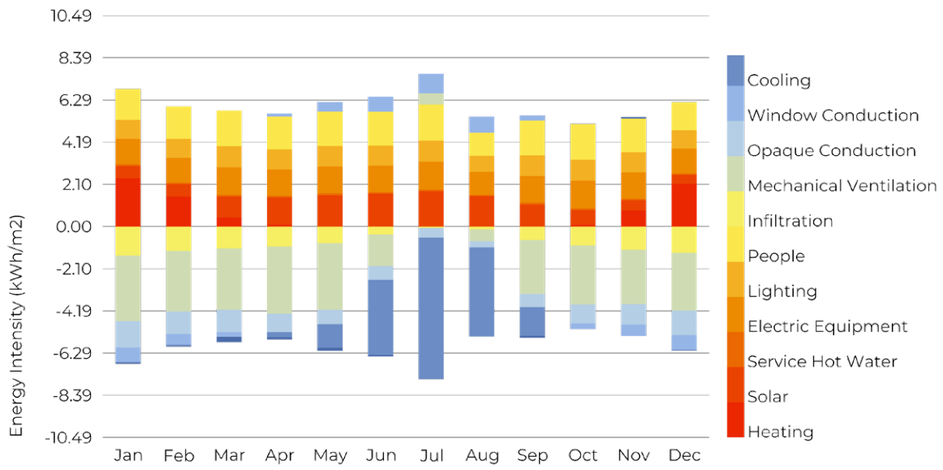

S_51 B 2G OS VT

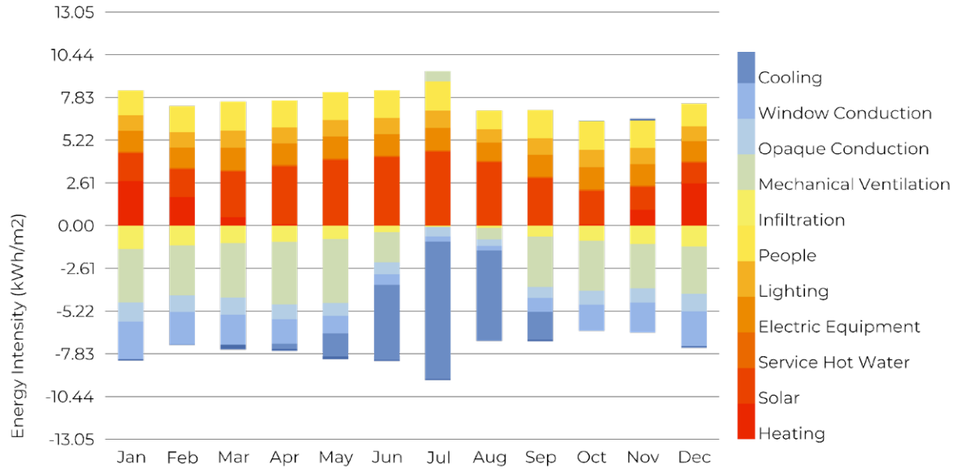

S_52 B 2G VT OS

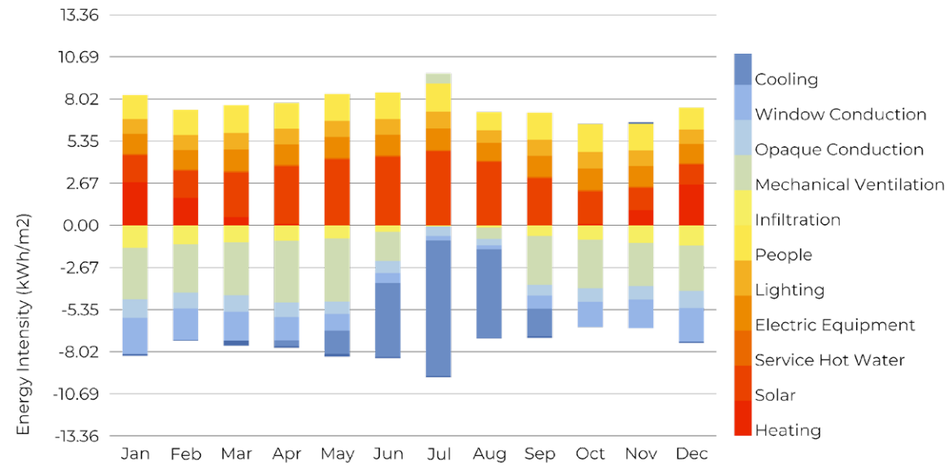

S_53 D 2G OS VT

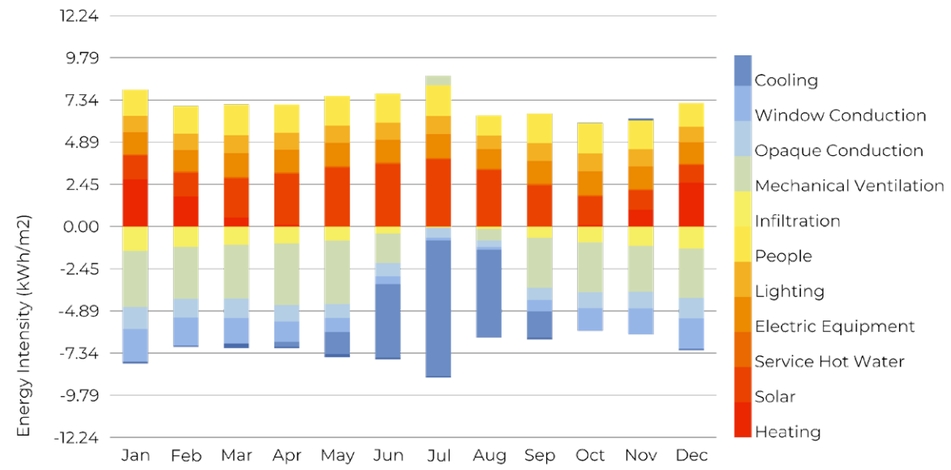

S_54 H 2G OS VT

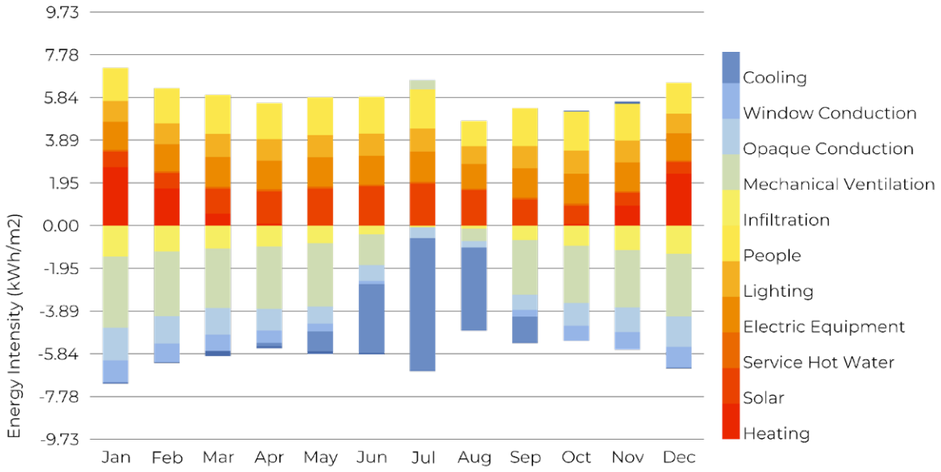

S_61 B 3G OS VT

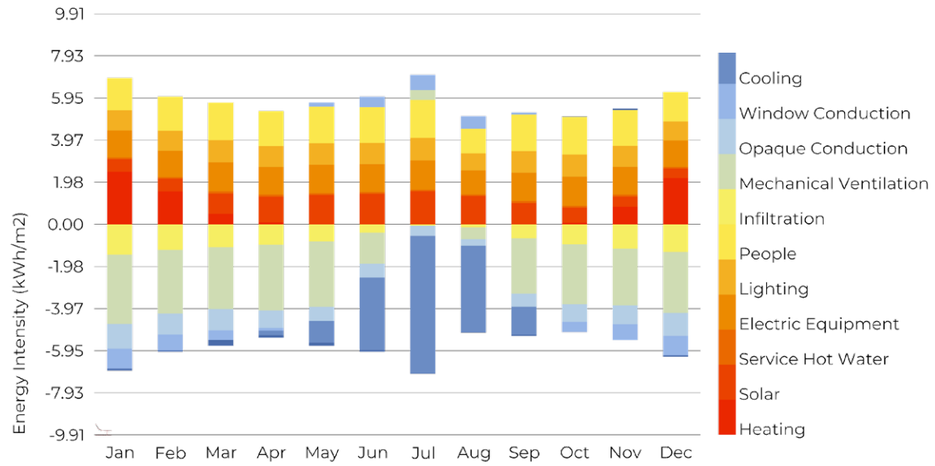

S_62 B 3G VT OS

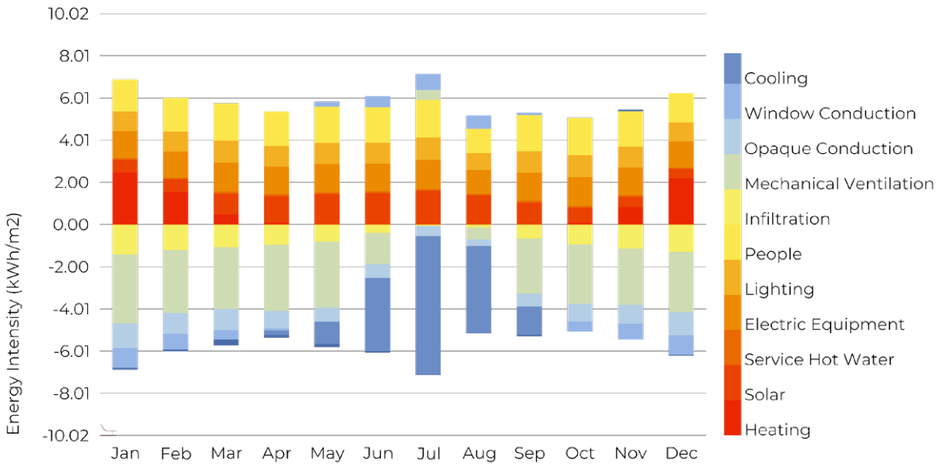

S_63 D 3G OS VT

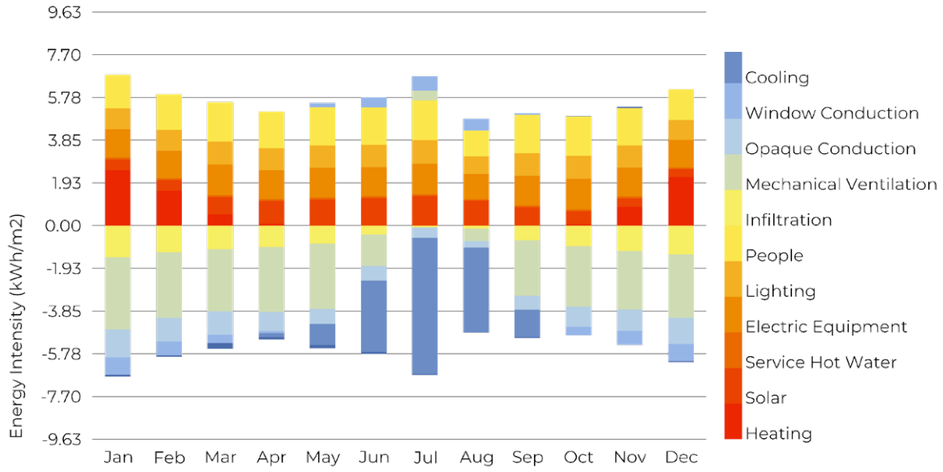

S_64 H 3G OS VT

